Modeling and Compensation of Rate-Dependent Asymmetric Hysteresis Nonlinearities of Magnetostrictive Actuators

Omar Farhan Aljanaideh

A Thesis

in

The Department

of

Mechanical and Industrial Engineering

Presented in Partial Fulfillment of the Requirements
For the Degree of Doctor of Philosophy (Mechanical Engineering) at
Concordia University
Montreal, Quebec, Canada

December 2013

CONCORDIA UNIVERSITY
SCHOOL OF GRADUATE STUDIES

This is to certify that the thesis prepared

By: **Omar Farhan Aljanaideh**

Entitled: **Modeling and Compensation of Rate-Dependent Asymmetric Hysteresis Nonlinearities of Magnetostrictive Actuators**

and submitted in partial fulfillment of the requirements for the degree of

DOCTOR OF PHILOSOPHY (Mechanical Engineering)

complies with the regulations of the University and meets the accepted standards with respect to originality and quality.
Signed by the final examining committee:

_____ Chair
Dr. D. Qiu

_____ External Examiner
Dr. D. Zhang

_____ External to Program
Dr. A. Aghdam

_____ Examiner
Dr. Y. Zhang

_____ Examiner
Dr. R. Sedaghati

_____ Thesis Co-Supervisor
Dr. S. Rakheja

_____ Thesis Co-Supervisor
Dr. C.Y. Su

Approved by _____
Dr. A. Dolatabadi, Graduate Program Director

February 11, 2014

_____
Dr. C. Trueman, Interim Dean
Faculty of Engineering and Computer Science

ABSTRACT

Omar Farhan Aljanaideh
Concordia University, 2013

Smart material actuators are increasingly being explored for various micropositioning applications. Magnetostrictive actuators, in particular, are considered attractive for micro/nano positioning and high speed precision machining due to their high energy density, resolution and force capacity. The magnetostrictive actuators, similar to other smart material actuators, however, exhibit considerable hysteresis and output saturation nonlinearities that tend to become far more significant under high rates of input. Such nonlinearities cause response oscillations and errors in the positioning tasks. Reliable compensation of such nonlinearities is thus highly desirable to enhance micro/nano positioning performance of the actuator over a wide range of operating conditions.

This dissertation research is concerned with characterization of output-input nonlinearities of a magnetostrictive actuator and control of hysteresis nonlinearities under a wide range of inputs. A comprehensive experimental study was performed to characterize output-input characteristics of a magnetostrictive actuator under a wide range of excitation conditions include amplitude, frequency, and bias of the input and the mechanical loading of the actuator. The measured data were analyzed to characterize output-input properties and to formulate a hysteresis model, to describe the hysteresis properties of these actuators. A Prandtl-Ishlinskii model was considered due to its continuous nature and thereby the invertability to seek hysteresis compensation. A rate-dependent threshold function was proposed to describe hysteresis properties of the actuator over a wide range of input frequencies. The inverse of the

proposed rate-dependent hysteresis model was subsequently formulated for compensation of rate-dependent symmetric hysteresis nonlinearities. The effectiveness of the inverse model was investigated through simulations and hardware-in-the-loop test methods considering a 100 μm magnetostrictive actuator acquired from Etrema Inc. The results clearly illustrated effective compensation of symmetric hysteresis nonlinearities under low magnitude excitation currents over the entire frequency range. The method, however, revealed substantial errors under medium to high amplitude excitation, which was attributed to output saturation and asymmetry. The concept of a stop-operator based Prandtl-Ishlinskii model was proposed to achieve compensation of hysteresis nonlinearities described by the play-operator based hysteresis model on the basis of the initial loading curve, it was shown that the complementary properties of stop operators can be effectively applied for compensation of actuator hysteresis described by the Prandtl-Ishlinskii model.

The inverse rate-dependent Prandtl-Ishlinskii model and the stop-operator based Prandtl-Ishlinskii model, however, are applicable only for compensation rate-dependent symmetric hysteresis and rate-independent hysteresis nonlinearities, respectively. The proposed rate-Prandtl-Ishlinskii model was refined to describe the rate-dependent asymmetric hysteresis nonlinearities together with output saturation by integrating a memoryless function to the rate-dependent Prandtl-Ishlinskii model. The resulting integrated model could accurately describe the asymmetric hysteresis nonlinearities and output saturation of the magnetostrictive actuator. The inverse of the integrated model was obtained by integrating the inverse of the rate-dependent Prandtl-Ishlinskii model with that of the memoryless function. The effectiveness of the integrated inverse model in compensating for hysteresis nonlinearities was investigated through simulations and experimentally using hardware-in-the-loop test method. The results

suggested that the proposed integrated model and its inverse could effectively characterize and compensate for rate-dependent asymmetric hysteresis nonlinearities of magnetostrictive actuator. Both the experimental and simulation results showed that the peak hysteresis observed under high magnitude excitation could be reduced from 49.1 % to 3.7 % in the 1-250 Hz range when the integrated model inverse is applied.

ACKNOWLEDGMENTS

I am sincerely grateful to my supervisors, prof. S. Rakheja and prof. C. Y. Su for their constant guidance and support throughout my thesis work. I would like to thank my mother *Faridah Mahmoud* and my father *Farhan Aljanaideh* who have been encouraging and supporting me in my whole life, and for them I would like to dedicate this thesis.

LIST OF CONTENTS

ABSTRACT ..... **ii**

List of Figures ..... **vi**

1 CHAPTER 1 ..... **1**

1.1 Introduction 1

1.2 Literature review 3

1.2.1 Characterization of hysteresis in magnetostrictive actuators 3

1.2.2 Rate-independent hysteresis models 5

1.2.3 Preisach model 7

1.2.4 Krasnosel'skii-Pokrovskii model 11

1.2.5 Prandtl-Ishlinskii model 13

1.2.6 Modified and generalized Prandtl-Ishlinskii models 17

1.3 Rate-dependent hysteresis models 21

1.3.1 Operator-based rate-dependent hysteresis models 21

1.3.2 Differential equation-based hysteresis models 23

1.4 Hysteresis compensation 24

1.5 Scope and objectives 30

1.5.1 Objectives of the dissertation research 31

1.5.2 Organization of the manuscript-based thesis 32

2 CHAPTER 2 ..... **37**

2.1 General 37

2.2 Magnetostriction and magnetostrictive actuators 38

2.3 Characterization of output-input properties of a magnetostrictive actuator 41

2.3.1 Experimental set-up 41

2.3.2 Experiment design 43

2.4 Measured output-input characteristics 46

2.4.1 Input current amplitude and rate effects 46

2.4.2 Minor and major hysteresis loops 51

2.4.3 Input Magnetic Bias and rate Effects 55

2.4.4 Mechanical load effect 56
2.5 Summary and conclusions 64

3 CHAPTER 3 65

3.1 Introduction 65
3.2 The Prandtl-Ishlinskii model 67
3.2.1 The PPI model 67
3.2.2 The SPI model 68
3.3 Compensation of hysteresis via SPI model 70
3.3.1 Feedforward compensation 70
3.3.2 Analytical implementation of the feedforward compensator by using SPI model . 71
3.4 Experimental verification 76
3.4.1 Experimental setup 76
3.4.2 Hysteresis modeling 77
3.4.3 Compensation of hysteresis nonlinearity using SPI model 78
3.5 Conclusions 80

4 CHAPTER 4 81

4.1 Introduction 81
4.2 Output-input characteristics of a magnetostrictive actuator 86
4.2.1 Experimental setup and methods 86
4.2.2 Influence of input amplitude 88
4.2.3 Influence of rate of input 90
4.2.4 Influence of input bias 92
4.3 Minor hysteresis loops 95
4.4 Formulation of an integrated hysteresis model 97
4.4.1 Parameters identification 101
4.4.2 Relative significance of the proposed integrated hysteresis model 105
4.5 Conclusions 107

5 CHAPTER 5 108

5.1 Introduction 108

5.2 Rate-dependent Prandtl-Ishlinskii model and its inverse 110
5.3 Characterization of hysteresis of a magnetostrictive actuator 113
5.3.1 Model parameters identification 116
5.4 Feedforward compensation of rate-dependent hysteresis nonlinearities 121
5.4.1 Simulation results 122
5.4.2 Experimental results 125
5.5 Conclusions 128

6 CHAPTER 6 129

6.1 Introduction 129
6.2 An integrated Prandtl-Ishlinskii model and its inverse 132
6.2.1 Inverse of the integrated Prandtl-Ishlinskii model 134
6.3 Characterization of hysteresis of a magnetostrictive actuator 137
6.4 Compensation of rate-dependent asymmetric Hysteresis 146
6.4.1 Simulation results 146
6.4.2 Hardware-in-the-loop implementation of the inverse compensator 149
6.5 Conclusions 153

7 CHAPTER 7 154

7.1 Major contributions of the dissertation research 154
7.2 Major conclusions 155
7.3 Recommendations for future work 157

8 REFERENCES 158

LIST OF FIGURES

Figure 1.1: Measured hysteresis properties of magnetostrictive actuators reported in different studies: (a) Major and minor hysteresis loops [12]; (b) Saturation in output displacement [17]; (c) Minor loops at identical amplitude but different bias levels [13]; and (d) Influence of rate of input [7]. 6

Figure 1.2: The input-output relationship of the relay operator used in the Preisach hysteresis model [24]. 8

Figure 1.3: The input-output relationship of the KP operator [1]. 12

Figure 1.4: The input-output relationship of the stop operator [26]. 14

Figure 1.5: Input-output relationship of the play operator [26]. 16

Figure 1.6: Input-output relationship of a deadzone operator for input $v(t)$ [12]. 18

Figure 1.7: Output-input characteristics of a generalized play operator [26]. 19

Figure 1.8: Open-loop hysteresis compensation using inverse hysteresis model. 26

Figure 2.1: Magnetic domain orientations: (a) in the absence of a magnetic field, H=0 [1]; and (b) in the presence of a magnetic field [1]. 40

Figure 2.2: Pictorial views of the magnetostrictive actuator and sensor support fixture. 45

Figure 2.3: Experimental platform. 45

Figure 2.4: Measured output-input characteristics of the magnetostrictive actuator, displaying hysteresis, and output asymmetry ad saturation (I_o=7 A, f=10 Hz, H_{bias}=44.1 kA/m). 46

Figure 2.5: Measured output-input characteristics of the magnetostrictive actuator under a harmonic current excitation with linearly increasing current (f=10 Hz). 47

Figure 2.6: Time histories of: (a) Excitation current; and (b) Actuator displacement (f=10 Hz). 47

Figure 2.7: Measured hysteresis loops illustrating output asymmetry and saturation nonlinearities of the magnetostrictive actuator under different current amplitudes ranging from 1 to 9 A. 49

Figure 2.8: Time histories of output displacement measured under different amplitudes of applied current at frequency of 10 Hz (H_{bias}=44.1 kA/m). 49

Figure 2.9: Measured hysteresis loops relating output displacement response of the magnetostrictive actuator to the harmonic input current at different frequencies in the 10 to 250 Hz range: (a) I_o=2 A; (b) I_o = 4 A; (c) I_o = 5 A; (d) I_o = 6; and (e) I_o = 8 A (H_{Bias}=44.1 kA/m). . 51

Figure 2.10: Area bounded by the hysteresis loops of the magnetostrictive actuator under harmonic excitations at different frequencies in the 10 to 250 Hz range: (a) I_o =2 A; and (b) I_o = 8 A (Bias=44.1 kA/m). 51

Figure 2.11: Measured output-input characteristics under the complex harmonic input current of the form, $I(t) = 4 \sin(2\pi f_o t) + 3 \sin(6\pi f_o t)$, illustrating major and minor hysteresis loops. 52

Figure 2.12: Output-input characteristics of the magnetostrictive actuator illustrating different minor hysteresis loops under three different complex harmonic inputs of the form: $I(t)= I_{AC1}\sin(2\pi f_o t)+ I_{AC2} \sin(6\pi f_o t)$, with ($I_{AC1}$, I_{AC2} = 3, 4 A), (I_{AC1}, I_{AC2} = 5, 2 A) and (I_{AC1}, I_{AC2} = 4, 3 A). 53

Figure 2.13: Measured hysteresis loops relating output displacement response of a magnetostrictive actuator with the complex harmonic input current, $I(t)=I_{AC1} \sin(2\pi f_o t)+ I_{AC2} \sin(6\pi f_o t)$, with three different amplitudes, (I_{AC1}, I_{AC2})=(5, 2), (4, 3), and (3, 4), and fundamental frequency f_o=20 Hz. 54

Figure 2.14: (a) Measured output-input characteristics of the actuator under complex harmonic input at different fundamental frequencies (f_o=20, 50 and 100 Hz) illustrating two sets of minor hysteresis loops 'A' and 'B'; and (b) The peak percent hysteresis of the minor hysteresis loops as a function of the fundamental frequency, f_o (-set A; - set B)..... 55

Figure 2.15: Influence of variations in the excitation frequency *f* on the output-input characteristics of the magnetostrictive actuator under different levels of magnetic bias (H_{bias}): (a) 30 kA/m; (b) 45 kA/m; (c) 60 kA/m; and (d) Comparison of the measured responses under three bias levels..... 57

Figure 2.16: Variations in peak percent hysteresis in the displacement responses as a function of frequency of the applied input at three different levels of magnetic bias. 58

Figure 2.17: A pictorial view of magnetostrictive actuator with the mechanical loads. 59

Figure 2.18: Static load-deflection characteristic of the magnetostrictive actuator..... 60

Figure 2.19: Time history of the displacement response of the unloaded actuator to 1 A step current. 61

Figure 2.20: The output-input characteristics of the unloaded and the loaded actuator under 1.0 A harmonic current at different frequencies. 63

Figure 2.21: The normalized output displacement of the unloaded and loaded actuator under 1.0 A harmonic current at different frequencies. 63

Figure 3.1: Input-output relationship of the play hysteresis operator. 68

Figure 3.2: Input-output relationship of the play hysteresis operator. 69

Figure 3.3: Open-loop control system. 71

Figure 3.4: Inner structure of the stop-operator based Prandtl-Ishlinskii model (SPI) and play-operator based Prandtl-Ishlinskii model (PPI). 71

Figure 3.5: (a) Initial loading curve of the stop operator based Prandtl-Ishlinskii (SPI) model SPI, (b) Initial loading curves of the stop operator based Prandtl-Ishlinskii (PPI) model, (c) Composition of the initial loading curves of the SPI and PPI models to achieve perfect compensation. 73

Figure 3.6: The initial loading curves of the SPI and PPI models. 74

Figure 3.7: The experimental platform. 77

Figure 3.8: Comparisons between the measured displacement responses with the results derived from the PPI model under two selected inputs, (a) sinusoidal excitation (b) complex harmonic excitation. 79

Figure 3.9: The outputs of the SPI model under two selected inputs, (a) sinusoidal excitation (b) complex harmonic excitation. 79

Figure 3.10: Input-output characteristics of the piezoceramic stage with the SPI model compensator under two selected inputs, (a) sinusoidal excitation (b) complex harmonic excitation. 80

Figure 4.1: Schematic of the (a) Terfenol-D magnetostrictive actuator used in the study; and (b) experimental setup. 88

Figure 4.2: Variations in the actuator displacement response under different amplitudes of harmonic current excitation: (a) 1, 2 and 3 A; (b) 4, 5 and 6 A; and (c) 7, 8 and 9 A (f= 10 Hz; magnetic bias= 44.1 kA/m). 89

Figure 4.3: Influence of variations in the applied current amplitude on: (a) peak-peak output displacement and rate of change of the peak-peak displacement with respect to peak-peak current; and (b) the area bounded by the hysteresis loop (f=10 Hz). 90

Figure 4.4: Measured hysteresis loops relating output displacement response of the magnetostrictive actuator under harmonic excitations at different frequencies in the 10-200 Hz range: (a) input current=3 A; and (b) input current = 7 A (Bias=44.1 kA/m). 91

Figure 4.5: Effects of excitation frequency on: (a) the peak-peak displacement response; and (b) the area bounded by the hysteresis loop. 92

Figure 4.6: Influence of variations in the magnetic bias (H_{bias}) on: (a) the output-input characteristics of the magnetostrictive actuator, (b) peak-peak output displacement; and (c) area of the hysteresis loop (harmonic magnetic field amplitude = 15 kA/m and f=25 Hz). 95

Figure 4.7: (a) The output-input characteristics of the actuator illustrating minor as well as major hysteresis loops (f_o=20 Hz; magnetic bias = 44.1 kA/m); and (b) time history of the complex

harmonic input, $I(t)=2\sin(2.5\times2\pi f_o t)+3\sin(2\pi f_o t)$ applied to characterize minor hysteresis loops. 96

Figure 4.8: Output-input characteristics of the actuator zoomed around the minor hysteresis loops under a complex harmonic input current $I(t)=2\sin(2.5\times2\pi f_o t)+3\sin(2\pi f_o t)$ (where , f_o= 20 Hz; and and the f_o=40 Hz. 97

Figure 4.9: (a) A memoryless function Λ_d introduced to the output of the rate-dependent Prandtl-Ishlinskii Π model to observe saturation and asymmetry effects; and (b) structure of the memoryless function Λ_d, as a superposition of weighted deadband operators. 100

Figure 4.10: Variations in the norm of error with the number of the rate-dependent play operators (n). 103

Figure 4.11: Comparisons of measured responses of the magnetostrictive actuator with those of the integrated Prandtl-Ishlinskii model Ω under: (a) I_o=3 A at 10 Hz; (b) I_o=3 A at 100; (c) I_o=3 A at 200 Hz; (d) I_o=7 A at 10 Hz; (e) I_o=7 A at 100 Hz; and (f) I_o=7 A at 200 Hz..... 104

Figure 4.12: Comparisons of measured responses of the magnetostrictive actuator with those of the integrated Prandtl-Ishlinskii model under: (a) current of 3, 5 and 7 A at 10 Hz excitation frequency; and (b) complex harmonic input $I(t)=2\sin(2.5\times2\pi f_o t)+3\sin(2\pi f_o t)$ (f_o=20 Hz; magnetic bias = 44.1 kA/m). 104

Figure 4.13: Measured responses at amplitudes of 5 and 7 A under 10, 50 and 200 Hz compared with those predicted from the: (a)-(c) rate-dependent symmetric Prandtl-Ishlinskii model, (d)-(f) asymmetric rate-independent Prandtl-Ishlinskii model [12]; and (g)-(i) the integrated Prandtl-Ishlinskii model Ω. 106

Figure 4.14: Comparisons of percent peak displacement error between the measured response from the actuator and the observed from the rate-dependent symmetric model Π, rate-independent asymmetric model [12], and the integrated Prandtl-Ishlinskii model Ω at 10, 50 and 200 Hz applied under: (a) 5 A; and (b) 7 A..... 106

Figure 5.1: A cascade arrangement of the rate–dependent inverse Prandtl-Ishlinskii model Π^{-1} and the hysteresis model Π. 113

Figure 5.2: Construction of a Terfenol-D magnetostrictive actuator..... 114

Figure 5.3: Experimental setup for characterization of hysteresis nonlinearities of a magnetostrictive actuator. 115

Figure 5.4: Measured hysteresis nonlinearities of the magnetostrictive actuator under different inputs: (a) $v(t) = 2.3\sin(2\pi f\, t)$, f=1 Hz, 50 Hz and 200 Hz; and (b) $v(t) = 1.0\sin(100\pi t) + 1.3\sin(90\pi t)$ A. 116

Figure 5.5: Percent peak normalized hysteresis of current-to-displacement loops of the magnetostrictive actuator at different excitation frequencies. 116

Figure 5.6: Comparisons of measured responses of the magnetostrictive actuator with those of the Prandtl-Ishlinskii model Π, formulated using *4* rate-dependent play operators, under 2.3 A harmonic input at different frequencies: (a) 1 Hz, (b) 50 Hz, (c) 200 Hz; and (d) the complex harmonic input, $v(t) = 1.0 \sin(100\pi t) + 1.3 \sin(90\pi t)$ A. 120

Figure 5.7: Comparisons of the percent peak normalized hysteresis obtained from the Prandtl-Ishlinskii model, formulated using *4* rate-dependent play operators, with the measured data under harmonic excitations at different frequencies. 120

Figure 5.8: Comparisons of measured responses of the magnetostrictive actuator with those of the Prandtl-Ishlinskii model Π, formulated using *25* rate-dependent play operators, under 2.3 A harmonic input at different frequencies: (a) 1 Hz, (b) 50 Hz, (c) 200 Hz; and (d) the complex harmonic input, $v(t) = 1.0 \sin(100\pi t) + 1.3 \sin(90\pi t)$ A. 122

Figure 5.9: The output-input characteristics of the inverse Prandtl-Ishlinskii model, formulated using 4 rate-dependent play operators, under harmonic and complex harmonic inputs: (a) $v(t) = 2.3 \sin(2\pi f t)$, $f = 1$, 50 and 200 Hz ; and (b) $v(t) = 1.0\sin(100\pi t) + 1.3 \sin(90\pi t)$..... 123

Figure 5.10: Output-input characteristics of the inverse rate-dependent Prandtl-Ishlinskii model Π^{-1}, rate-dependent Prandtl-Ishlinskii model Π, and the compensated output $u = \Pi \circ \Pi^{-1}$, where $v(t) = 2.3\sin(2\pi f t)$, (a) $f = 1$ Hz, (b) $f = 50$ Hz, and (c) $f = 200$ Hz, and (d) $v(t) = 1.0 \sin(100\pi t) + 1.3 \sin(90\pi t)$. 124

Figure 5.11: The output-input characteristics of the magnetostrictive actuator employing the inverse rate-dependent Prandtl-Ishlinskii model as a feedforward compensator under different inputs: (a) $v(t) = 2.3\sin(2\pi f t)$ A, $f = 1$, 25, 50, 75, 100, 125, 150, 175 and 200 Hz; and (b) $v(t) = 1.0 \sin(100\pi t) + 1.3 \sin(90\pi t)$ A. 126

Figure 5.12: (a) The time-history of the error with the inverse rate-dependent Prandtl-Ishlinskii model under the harmonic excitation at 100 Hz, (b) Percent peak normalized hysteresis of current-to-displacement loops of the magnetostrictive actuator with the inverse rate-dependent Prandtl-Ishlinskii model at different excitation frequencies. 127

Figure 6.1: Feedforward Compensation using the cascade arrangement of inverse model Ω^{-1} and the hysteresis model Ω 134

Figure 6.2: Experimental setup for characterization of hysteresis nonlinearities of a magnetostrictive actuator. 138

Figure 6.3: Output displacement-input current of the magnetostrictive actuator under different inputs: (a) $v(t) = 6.0 \sin(2\pi f t)$, $f = 10$, 50, 150 and 250 Hz; and $v(t) = 1.0 \sin(2\pi \times 50 f_o t) + 5.0 \sin(2\pi \times 100 f_o t)$ A, (b) $f_o = 1$ and, (c) $f_o = 2$. 139

Figure 6.4: Area bounded by hysteresis of displacement-to-current loops of the magnetostrictive actuator under 6 A harmonic excitation at different frequencies. 140

Figure 6.5: Comparisons of measured responses of the magnetostrictive actuator with those of the integrated rate-dependent Prandtl-Ishlinskii model Ω formulated using 12 rate-dependent play

operators and 17 deadband operators, at different frequencies 10, 150 and 250 Hz applied under amplitudes of : (a) 3 A, (b) 5 A, and (c) 6 A..... 143

Figure 6.6: Comparisons of measured responses of the magnetostrictive actuator with those of the integrated rate-dependent Prandtl-Ishlinskii model Ω formulated using 12 rate-dependent play operators and 17 deadband operators, under the complex harmonic inputs: (a) 1.0 sin(100πt) +5.0 sin(200πt) A, and (b) 1.0 sin(200πt) +5.0 sin(400πt)..... 144

Figure 6.7: Comparisons of the area bounded by the hysteresis loops obtained from the integrated rate-dependent Prandtl-Ishlinskii model, with the measured data under 3 and 6 A harmonic excitations at different frequencies. 144

Figure 6.8: Comparisons of measured responses of the magnetostrictive actuator with those of the integrated rate-dependent Prandtl-Ishlinskii model Ω formulated using 36 rate-dependent play operators and 17 deadband operators: 6 A harmonic input at different frequencies-(a) 10 Hz, (b) 150 Hz and (c) 250 Hz; 3 A harmonic input at different frequencies-(d) 10 Hz, (e) 150 Hz, (f) 250 Hz; (g) sin(100πt) +5 sin(200πt) A; and (h) sin(200πt) +5 sin(400πt). 145

Figure 6.9: Output-input characteristics of the inverse of the integrated rate-dependent Prandtl-Ishlinskii model Π^{-1} formulated using 12 rate-dependent play operators and 17 deadband operators, the integrated rate-dependent Prandtl-Ishlinskii model Ω, and the composition $u = (\Omega \circ \Omega^{-1})$, under 3 A excitation at different frequencies (10, 150, 250 Hz). 147

Figure 6.10: Output-input characteristics of the inverse of the integrated rate-dependent Prandtl-Ishlinskii model Ω^{-1} formulated using 12 rate-dependent play operators and 17 deadband operators, the integrated rate-dependent Prandtl-Ishlinskii model Ω, and the composition $u = \Omega \circ \Omega^{-1}$, under 6 A excitation at different frequencies (10, 150, 250 Hz). 148

Figure 6.11: Output-input characteristics of the inverse of the integrated rate-dependent Prandtl-Ishlinskii model Ω^{-1} formulated using 12 rate-dependent play operators and 17 deadband operators, the integrated rate-dependent Prandtl-Ishlinskii model Ω, and the composition $u = \Omega \circ \Omega^{-1}$, under complex harmonic excitations: (a) $v(t)$ = sin(100πt)+5 sin(200πt) A; and (b) $v(t)$ = sin(200πt)+5 sin(400πt). 148

Figure 6.12: The output-input characteristics of the magnetostrictive actuator with the inverse of the integrated rate-dependent Prandtl-Ishlinskii model Ω^{-1} under different inputs: (a) $v(t)$=6.0 sin(2πft) A, f =1, 10, 50, 150, and 250 Hz; (b) $v(t)$=1.0 sin(100π t)+5.0 sin(100πt) A; and (c) $v(t)$=1.0 sin(200π t)+5.0 sin(400πt) A..... 151

Figure 6.13: (a) The time-history of desired output and the achieved output displacement of the magnetostrictive actuator with the inverse model Ω^{-1} under the harmonic input $v(t)$=1.0 sin(100πt)+5.0 sin(100πt) A; (b) The time-history of error between the desired and the achieved output displacement under the harmonic input $v(t)$=1.0 sin(100πt)+5.0 sin(100πt) A; and (c) percent peak normalized hysteresis of displacement-to-current loops of the magnetostrictive actuator with the inverse model Ω^{-1} at different excitations of frequency under amplitude of 6 A. 152

NOMENCLATURE

a	Weights of the rate-dependent Prandtl-Ishlinskii model
$\hat{a}$	Weights of the inverse rate-dependent Prandtl-Ishlinskii model
a_{KP}	Krasnosel'skii-Pokrovskii model constant
a_D, b_D, c_D	Duhem model constants
B	Magnetic induction
d	Threshold of the deadband function
$\hat{d}$	Threshold of the inverse deadband function
E_s	Rate-independent Stop operator
F_r	Rate-independent play operator
f	Frequency of the input
f_o	Fundamental frequency of the complex harmonic input
g, $\hat{g}$	Weights of the deadband function and its inverse
$\overline{g}_s$	Density function of the stop operator based Prandtl-Ishlinskii model
g_s	Weighting function of the stop model
g_d	Weighting function of the deadband function
$\overline{p}_G(r)$	Density function of the generalized Prandtl-Ishlinskii model
$\overline{h}(t)$	Output of the rate-dependent play operator

H_P	Peak hysteresis
H	Magnetic field
H_{PM}	Magnetic bias due to permanent magnets
H_{bias}	Total magnetic bias
I_o	Amplitude of input current
I_{bias}	Input current bias
I_{AC1}, I_{AC2}	Amplitudes of complex harmonic input
$I(t)$	Input current
i, j, k, l	Indices
J_d	Deadband operators
J_s	Number of stop operators
J_p	Number of play operators
J_G	Number of generalized play operators
k_o	Coil factor
L_o	Length of the Terfenol-D rods
m	Number of data points
$\overline{m}(t)$	Output of inverse rate-dependent Prandtl-Ishlinskii model
M	Magnetization
M_{KP}	Krasnosel'skii-Pokrovskii operator

M_P	Peak-peak output displacement
n_p	Number of the play operators
n_Q	Number of deadzone operators
n_s	Number of stop operators
n_G	Number of generalized play operators
n_c	Number of the turns in the coil
n_{BW}	Positive integer of the Bouc-Wen model
p	Weights of the rate-independent play operator based Prandtl-Ishlinskii model
$\hat{p}$	Weights of inverse rate-independent play operator based Prandtl-Ishlinskii model
$\overline{p}_r$	Density function of the rate-independent play operator based Prandtl-Ishlinskii model
p_r	Weighting function of the rate-independent play operator based Prandtl-Ishlinskii model
q	Constant corresponding to the linear part of the play operator based Prandtl-Ishlinskii model
r	Threshold of the rate-independent Prandtl-Ishlinskii model
$\hat{r}$	Threshold of inverse rate-independent Prandtl-Ishlinskii model
$r\,(\dot{v}(t))$	Rate-dependent threshold function of rate-dependent Prandtl-Ishlinskii model
$\hat{r}\,(\dot{v}(t))$	Rate-dependent threshold function of inverse rate-dependent Prandtl-Ishlinskii model
s	Threshold of stop operator based Prandtl-Ishlinskii
S_r	Generalized play operator

s_0	Large positive real number $s_0 > \max(v(t))$ corresponds to the threshold of stop compensator.
t	Time
$v(t)$	Input
$v_0(t)$	Excitation input signal generated from dSpace ControlDesk
$\dot{v}(t)$	Derivative of the input
w	Weights of the stop operator based Prandtl-Ishlinskii model
$\overline{w}_s(s)$	Density function of the stop operator based Prandtl-Ishlinskii model
$\mathrm{Y}(t)$	Measured output displacement of the actuator
$z_{\_BW}$	Bouc-Wen model constants
$\alpha_{\_BW}, \beta_{\_BW}, \gamma_{\_BW}$	Bouc-Wen model constant
α	Rate-independent constant of the rate-dependent threshold function $r(\dot{v}(t))$
$\alpha_P,\ \beta_P$	Thresholds of relay operator
$\gamma_{\alpha_P\beta_P}[v](t)$	Relay operator
γ	Rate-dependent constant of the rate-dependent threshold function $r(\dot{v}(t))$
$\gamma_l,\ \gamma_r$	Envelope functions of generalized play operator
Γ	Rate-dependent play operator
δ	Output of the rate-dependent Prandtl-Ishlinskii
δ_{KP}	Ridge function of the Krasnosel'skii-Pokrovskii model

ζ_1 , ζ_2	Thresholds of the generalized play operator
λ	Magnetostriction
Λ	Memoryless function
Λ^{-1}	Inverse memoryless function
Π	Rate-dependent Prandtl-Ishlinskii model
Π^{-1}	Inverse rate-dependent Prandtl-Ishlinskii model
ρ	Output of integrated model
ρ_{KP}	Density function of the Krasnosel'skii-Pokrovskii model
ϕ_s	Initial loading curve of the stop operator based Prandtl-Ishlinskii model
ϕ_r	Initial loading curve of the play operator based Prandtl-Ishlinskii model
Φ	Rate-independent the play operator based Prandtl-Ishlinskii model
$\overline{\Phi}$	Continuous form of the play operator based Prandtl-Ishlinskii model
$\overline{\Phi}_G$	Continuous form of the generalized Prandtl-Ishlinskii model
ψ	A hysteresis model
ψ^{-1}	An inverse hysteresis model
Ψ_{KP}	Krasnosel'skii-Pokrovskii model
Ψ	Rate-independent stop operator based Prandtl-Ishlinskii model
$\omega_P(\alpha_P, \beta_P)$	Density function of Preisach model

Ω	Integrated Prandtl-Ishlinskii model
Ω^{-1}	Inverse integrated Prandtl-Ishlinskii model
Ω_P	Preisach model

CHAPTER 1

LITERATURE REVIEW AND SCOPE OF THE DISSERTATION

2.1 Introduction

Smart materials are new technologies that have emerged during the past two decades to replace the classic type of actuators such as (electromagnetic, hydraulic and pneumatic) for applications requiring miniaturization, micropositioning, fast response and high resolution. These materials are able to change their physical properties in response to external cues like electric or magnetic fields. Such materials are considered attractive for micro-positioning actuation and sensing purposes. Magnetostrictive materials are among the most widely used materials in micro-actuators requiring high force capacity and rapid response [1]. These actuators have been used in high accuracy milling, hydraulic valves and vibration attenuation devices [1-4]. The positioning and tracking performance of smart material actuators is strongly limited due to the presence of hysteresis nonlinearities between the input and the output. These nonlinearities are known to cause oscillations in the open-loop system's responses, as well as poor tracking performance and potential instabilities in the closed-loop system [5,6]. The nonlinearities in the Terfenol-D type magnetostrictive actuators are particularly significant due to their asymmetric output-input relationship and output saturation effect.

The tracking performance of such actuators could be significantly enhanced through compensation of hysteresis effects. Considerable efforts have thus been made towards compensation of hysteresis effects through various controller designs. Compared to the controller-based compensation methods, the model-based methods may be considered more effective in realizing hysteresis compensation over a wider range of operating conditions. However, the

available inverse-model based compensation methods lack adequate considerations of strong effects of the input rate on the hysteresis nonlinearities of smart actuators. The hysteresis nonlinearities of magnetostrictive actuators, similar to the other smart material actuators, invariably, increase with increasing excitation frequency of the applied input [7-9], which limits the application of these models to a narrow range of excitation frequency. Furthermore, unlike the other smart material actuators, the magnetostrictive actuators exhibit substantial asymmetry in the output and output saturation.

The proposed dissertation research concerns the characterization and compensation of hysteresis of magnetostrictive actuators that invariably exhibit symmetric as well as asymmetric input-output properties with output saturation nonlinearity. Since the hysteresis properties of magnetostrictive actuators are strongly dependent upon the rate of applied input current, a rate-dependent Prandtl-Ishlinskii model is proposed to characterize the symmetric output-input hysteresis as a function of the input rate. The suggested model is subsequently enhanced by integrating a memoryless function of deadband operators to describe asymmetric output-input hysteresis nonlinearities. The model parameters are identified on the basis of comprehensive measured data acquired for a Terfenol-D magnetostrictive actuator under a wide range of operating conditions, involving various current amplitude, rate of input, input bias and mechanical load. An inverse of the rate-dependent Prandtl-Ishlinskii model is subsequently formulated and implemented in a feedforward manner to seek compensation for rate-dependent hysteresis and output saturation nonlinearities. The validity of the rate-dependent hysteresis model is demonstrated on the basis of the measured data. The inverse model is implemented in the laboratory with a Terfenol-D magnetostrictive actuator in a hardware-in-the-loop configuration to illustrate effectiveness of the model based hysteresis compensator.

2.2 Literature review

Compensation of hysteresis in smart material actuators involves hysteresis characterization, modeling and development of compensation algorithms and controllers. The reported relevant studies in each of these domains are reviewed to build essential background knowledge and to select effective methods for characterization and compensation of hysteresis as well as output saturation nonlinearities. The reviewed studies are systematically grouped under different relevant topics and summarized in the following subsections.

2.2.1 Characterization of hysteresis in magnetostrictive actuators

Magnetostrictive materials, generally, exhibit rate-dependent, saturated, major and minor hysteresis loops in the output-input characteristics. The measured hysteresis relations between the input current (magnetic field) and the output displacement (magnetization) of magnetostrictive actuators have been reported in different studies [7,10,11,12]. Although the output displacement of a magnetostrictive actuator depends on several operating conditions like bias level, and magnitude and frequency of the input current, the reported experimental studies on hysteresis phenomenon in magnetostrictive actuators have been mostly limited to only some of these influencing operating conditions.

Calkiens et al. [11] characterized the hysteresis nonlinearities of a magnetostrictive actuator comprising a 115 mm long and 12.7 mm diameter Terfenol-D rod. Two different coils encapsulated the rod providing a magnetic field of up to 5.6 kA/m. An LVDT was coupled to the system to measure the output displacement of the rod. The device was actuated at both high and low input levels to generate major and minor hysteresis loops. Ignoring the effect of the input rate, the study concluded that excitations at different input levels yield different hysteresis properties.

Furthermore, the displacement responses of the magnetostrictive actuators invariably reveal significant saturation nonlinearity under large amplitude excitations. Stuebner et al. [13] investigated the hysteresis properties of a magnetostrictive actuator under identical current amplitudes but different bias levels in the magnetic field. The experiment considered a sinusoidal magnetic field of amplitude 12.5 kA/m, applied with three different bias fields (25.0, 50.0, 75.0 kA/m). The peak displacement responses under inputs with 50.0 and 75.0 kA/m bias were 50% and 75% lower, respectively, compared to that measured under lower bias of 25 kA/m. In an attempt to investigate the effect of input rate, Tan and Baras [7] characterized the hysteresis of a magnetostrictive actuator under inputs over the 10-300 Hz frequency range. The actuator employed a Terfenol-D rod of length of 51.3 mm and coil factor of 1.54×10^4/m. As in the previous studies, the output displacement of the driving rod was measured using an LVDT, which typically showed a drift and affected the accuracy of measurements under higher operating frequencies. The results demonstrated hysteresis nonlinearities that are strongly rate-dependent beyond the excitation frequency of 10 Hz, and relatively rate-independent at frequencies below 10 Hz.

The studies reporting the measured output-input characteristics of magnetostrictive actuators have generally shown consistent effects of different operating factors, which are summarized below [1,7,10,11,13,14,15,17]:

- The instantaneous displacement response of the actuator depends on the value of the instantaneous input current in addition to the displacement at the previous instant;

- The displacement amplitude response of the actuator increases and tends to saturate as the input current increases, and decreases as the input current decreases [11,17];

- The major hysteresis loop can be formed by decreasing and increasing the input current between the extreme minimum and maximum amplitudes of the input current (magnetic field) [16];

- The minor hysteresis loops in the output-input characteristics of the magnetostrictive actuators, generated at identical amplitudes of harmonic inputs and different bias levels, showed notable differences in the displacement response. Moreover, regardless of the output level, the minor loops generated under same input level were non-congruent [1];

- The hysteresis loops were relatively rate-independent at low frequencies (for example: 1, 5, 10 Hz), but effect of the input rate increased significantly at frequencies above 10 Hz [18].

Figure 1.1 illustrates the measured output-input characteristics of magnetostrictive actuators reported in the some of the above-mentioned studies. The majority of the reported studies have focused on synthesizing a rate-independent model and a compensator on the basis of the experimental results attained under limited ranges of operating conditions, while the influences of both the frequency and amplitude of excitation current have been generally ignored.

2.2.2 Rate-independent hysteresis models

A large number of analytical models have been proposed to characterize the hysteresis properties of smart actuators. The primary goal of these models is to predict the hysteresis behaviour of materials and smart actuators in order to study the effects of hysteresis on the system output response and facilitate the design of controllers and hysteresis compensation. These models may be generally classified into physics-based models [1,14,19,20,21] and phenomenological models [8,22,23,24,25]. The phenomenological models can be further classified into differential equation-based models such as Duhem model [24] and Bouc-Wen model [24], and the operator-based hysteresis models such as Preisach model [1,22,23], Prandtl-Ishlinskii model [26] and Kransnosel'skii-Pokrovskii model [1,28,29]. The differential equation-based models comprise nonlinear differential equations for describing the input-output relations. These models, however,

exhibit several limitations for control system design applications, and pose considerable challenges in parameters identification. Moreover, these models are not invertible and cannot be applied for model-based hysteresis compensation [1,17,21,27].

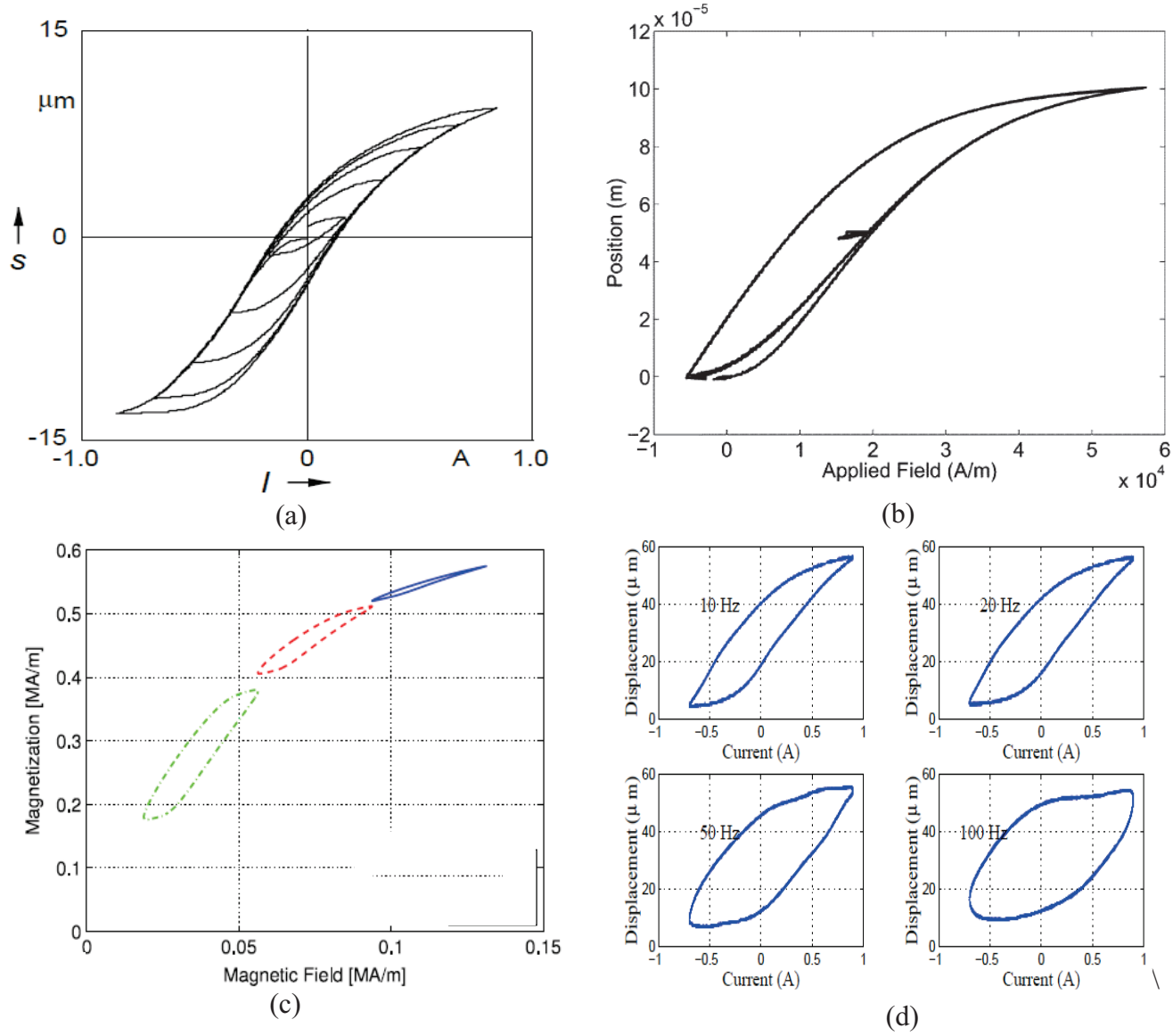

Figure 1.1: Measured hysteresis properties of magnetostrictive actuators reported in different studies: (a) Major and minor hysteresis loops [12]; (b) Saturation in output displacement [17]; (c) Minor loops at identical amplitude but different bias levels [13]; and (d) Influence of rate of input [7].

The phenomenological models such as Preisach, Krasnosel'skii-Pokrovskii and Prandtl-Ishlinskii models have been widely employed to characterize hysteresis behaviour of smart

material actuators. These models are described below in details together with their implementation for smart material actuators.

2.2.3 Preisach model

The hysteresis in magnetic materials was first studied by James A. Ewing in 1881, where hysteresis loops between the magnetic field H and the magnetic flux density B in soft-iron ring were observed. The first attempt to characterize this phenomenon, however, was carried out nearly 60 years later by Ferenc Preisach, where it was suggested to use an aggregate of superposition of weighted blocks "relays" to represent the H-B hysteresis in an iron compound material [1,22,30,31]. The Preisach model exhibits flexibility and desirable mathematical properties to quantify hysteresis nonlinearities in several hysteretic systems. Consequently, this model has been extensively used for modeling hysteresis of electromagnetic materials and smart actuators. Mayergoyz in [22] assigned the congruency and the wiping out properties as the necessary conditions for any hysteretic systems to be described by the Preisach model. These properties have been validated in for piezoceramic and shape memory alloy (SMA) actuators [32]. The Preisach model employs an infinite set of relay operators $\gamma_{\alpha_P\beta_P}$, while the output of the model is derived from a superposition of a set of the weighted relay operators. For a given input $v(t)$ in each interval $[t_{j-1}, t_j]$ of a partition $C[0, T]$, the output $\gamma_{\alpha_P\beta_P}[v](t)$ of the relay operator is given by:

$$\gamma_{\alpha_P\beta_P}[v](t_j) = \begin{cases} +1 & for \quad v(t_j) \geq \alpha_P \\ -1 & for \quad v(t_j) \leq \beta_P \\ \gamma_{\alpha_P\beta_P}[v](t_{j-1}) & for \quad v(t_j) < \alpha_P \,\&\, v(t_j) > \beta_P \end{cases} \tag{1.1}$$

for $t \in [t_{j-1}, t_j]$.

where $v(t)$ is the input, and the constants α_P and β_P define the switching or the threshold values of the input corresponding to upward and downward shifting of the output, respectively, as shown in Figure 1.2.

The above operator forms the building block for the Preisach model, where the output of the relay operator is either +1 or -1 depending on the value of the input. The output switches from -1 to +1 when the input approaches or exceeds α_P, and from +1 to -1 when the input is less than and β_P. The operator thus exhibits strong discontinuities near $v(t)= \alpha_P$ and $v(t)= \beta_P$, while the output is limited to either +1 or -1.

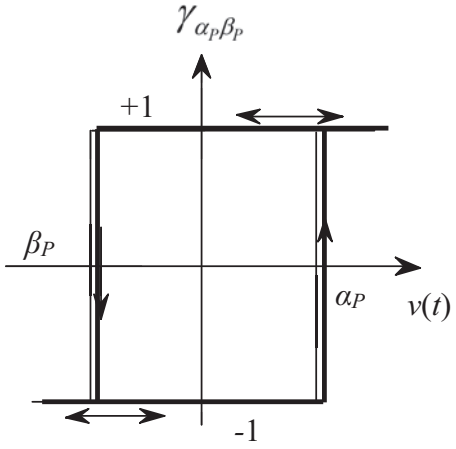

Figure 1.2: The input-output relationship of the relay operator used in the Preisach hysteresis model [24].

The output of the Preisach model $\Omega_P[v](t)$ is obtained from superposition of weighted outputs of the relay operators such that [22]:

$$\Omega_P[v](t) = \iint_{\alpha_P \geq \beta_P} \omega_P(\alpha_P, \beta_P)\gamma_{\alpha_P\beta_P}[v](t)d\alpha_P d\beta_P \tag{1.2}$$

where $\omega_P(\alpha_P, \beta_P)$ is the density function, which is integrable and positive, and is generally identified from the measured data of a particular material or actuator.

Properties of the Preisach model and its applications to smart material actuators hysteresis

In [22], Mayergoyz defined two essential properties of the Preisach model: (i) the wiping out property; and (ii) the congruent minor loop property. These are the necessary and sufficient conditions for the existence of a Preisach model. The wiping out property states that the extrema of the input can remove the effects of a previous extrema, essentially, the memory of the model will be wiped out. The congruent minor-loop property states that, at any point on the minor loop, the output variation will be identical under two inputs and the minor loops will thus have the same shape. Furthermore, the result two minor loops are considered to be equivalent only if they are generated by identical monotonically varying inputs. These two properties have also been verified by Hughes and Wen [32] for piezoceramic and SMA actuators. Furthermore, the Preisach model has been applied in the same study to characterize hysteresis properties of the piezoceramic and SMA actuators by integrating the classical relay operator and a density function in the form of a second-order polynomial in thresholds. Several studies have proposed different modified Preisach models for characterizing hysteresis in various materials and smart actuators such as piezoceramic [33], magnetostrictive [16,18] and SMA actuators [34,35,36]. Ge and Jouaneh [33] modified the classical relay operator with the output threshold of either '-1' or '+1' to an alternate Preisach operator with a threshold or switching values of '0' or '+1', considering the unidirectional dipole polarization of the piezoceramic materials. Subsequently, a model was formulated to characterize hysteresis of a piezoceramic actuator subject to inputs at 0.5 Hz. Modifying the output switching values to '0' and '+1' instead of '-1' and '+1' does not, however, address the asymmetric hysteresis loops observed in magnetostrictive actuators, which could be achieved by employing a density function with different weights for the increasing and decreasing inputs. Such an approach has been applied to characterize hysteresis of magnetostrictive actuators in [7,8,16,38].

Hughes and Wen [32] measured the hysteresis properties of piezoceramic patches and SMA wires coupled with a cantilever beam. Since the Preisach model is characterized by two properties, wiping out and minor loops congruency, the study was performed to validate the applicability of the Preisach model to describe the hysteresis nonlinearities of these actuators. Consequently, the measurements were performed in order to characterize the congruency of minor hysteresis loops and the wiping out property of the beam coupled with the selected actuator, while the deflections of the beam were measured using strain gauges. The piezoceramic patches showed a high degree of congruency in the comparable minor loops and the wiping out property was largely satisfied. The effects of different preloads on the actuators' hysteresis were also investigated by applying a high magnitude static force to the tip of the beam.

The modeling of magnetic field (H)-magnetic induction (B) hysteresis in magnetic materials is a classic problem that goes back to 1935 [1], when Ferenc Preisach suggested analytical mathematical formulas, referred to as the "Preisach model", to characterize H-B hysteresis loops in a magnetic material. Since magnetic materials exhibit similar hysteresis behaviour, several studies have employed Preisach model to characterize H-B hysteretic curves in various magnetic materials such as cobalt and iron compounds [8,29,37]. The application of Preisach model to characterize magnetic field (H)-magnetization (M) curves observed in magnetostrictive materials began in the early 1990s [38], where a variation of magnetic field H due to an input current was applied to attain an elongation (magnetostriction) λ of a Terfenol-D specimen due to change in the magnetization M.

The Preisach model has been used in numerous studies to describe hysteresis nonlinearities of magnetostrictive actuators employing Terfenol-D rods along with permanent magnetic field that provides constant bias level in the magnetic field (H_{bias}) [7,8,16,37]. The classic Preisach model

was employed by Natale et al. [10] to characterize rate-independent hysteresis of a magnetostrictive actuator. A Preisach density function identified using a fuzzy-logic algorithm and the model showed good agreements with the experimental data acquired under an excitation at 5 Hz. Preisach model was also applied in an attempt to characterize the hysteresis nonlinearities of a magnetostrictive actuator from Etrema Inc. that provided 50 μm output stroke [16]. The study employed the classic relay operator with a density function identified based on the least square optimization method to characterize major hysteresis loops measured at a frequency of 1 Hz.

Cavallo et al. [37] tested the performance of a magnetostrictive actuator from Energen Company that was designed with variable prestress level on the Terfenol-D rod using a compression bolt. The output displacement of the actuator was measured under different prestress levels (80, 160 N), using an eddy current proximity sensor. The actuator showed relatively higher displacement under the higher prestress. The results were employed to formulate a Preisach model to account for the prestress level effect, which showed good agreement with the experimental data acquired at an excitation frequency of 2 Hz.

2.2.4 Krasnosel'skii-Pokrovskii model

The Krasnosel'skii-Pokrovskii (KP) model employs hysteresis operator derived from the Preisach operator [1,28,29]. This operator is constructed from two different functions bounded by two piecewise Lipschitz continuous functions. A ridge function, $\delta_{KP}(v)$, is used to formulate the Krasnosel'skii-Pokrovskii operator, expressed as:

$$\delta_{KP}(v(t)) = \begin{cases} -1 & for \quad v(t) < 0 \\ -1 + \dfrac{2v(t)}{a_{KP}} & for \quad 0 \le v(t) \le a_{KP} \\ 1 & for \quad v(t) > a_{KP} \end{cases} \tag{1.3}$$

where a_{KP} is a positive constant for a given input $v(t) \in C[0, T]$. The output of the Krasnosel'skii-Pokrovskii operator $M_{KP}[v](t)$ for input $v(t)$ in each interval $[t_{j-1}, t_j]$ of a partition $C[0, T]$ is expressed as (Figure 1.3):

$$M_{KP}[v](t) = \begin{cases} \max(\ M_{KP}[v](t_{j-1}), \delta_{KP}(v(t) - \alpha_P)) & for \quad \dot{v}(t) > 0 \\ \min(\ M_{KP}[v](t_{j-1}), \delta_{KP}(v(t) - \beta_P)) & for \quad \dot{v}(t) < 0 \\ M_{KP}(t_{j-1}) & for \quad \dot{v}(t) = 0 \end{cases} \tag{1.4}$$

for $t \in [t_{j-1}, t_j]$, where α_P and β_P are constant thresholds of the Preisach relay operator, as shown in Figure 1.3.

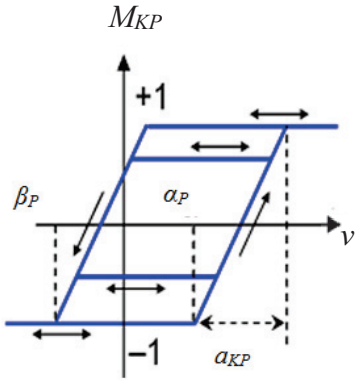

Figure 1.3: The input-output relationship of the KP operator [1].

The KP operator is Lipschitz continuous, the input-output curve exhibits a finite slope. The output of the Krasnosel'skii-Pokrovskii model is derived upon integration of the weighted KP operators as [28,29]:

$$\Psi_{KP}[v](t) = \iint_{\alpha_P \geq \beta_P} \rho_{KP}(\alpha_P, \beta_P)\ M_{KP}[v](t) d\alpha_P d\beta_P \tag{1.5}$$

where $\Psi_{KP}(t)$ is the output and $\rho_{KP}(\alpha_P, \beta_P)$ is a density function.

A few studies have also employed the KP operator in the Preisach model to characterize hysteresis of smart actuators. Banks et al. [39] investigated the properties of the Krasnosel'skii-

Pokrovskii model for characterizing hysteresis nonlinearities in smart actuators, particularly the SMA actuators. Galinaitis [28] employed Krasnosel'skii-Pokrovskii operator, instead of the Preisach relay operator, in the Preisach model to characterize hysteresis nonlinearities of a piezoceramic actuator at an excitation frequency of 0.01 Hz. In a similar manner, Smith [1] suggested this model for characterization of hysteresis nonlinearities in magnetostrictive actuators.

2.2.5 Prandtl-Ishlinskii model

The Prandtl-Ishlinskii model is a subclass of the Preisach model that quantifies hysteresis nonlinearities by summation of weighted play or stop operators [26]. The one dimensional play and stop operators provide continuity, and are characterized by the input $v(t)$ and the threshold s. Figures 1.3 and 1.4 depict the input-output characteristics of the stop and play operators, respectively. The attributes of the stop operator match the linear stress-strain relationship described by the Hooke's law, when the stress is below the yield threshold stress s. As the stress approaches the yield value of s, the stress remains constant under further increase in the strain. The output of the stop operator $E_s[v](t)$ for an input $v(t)$ in each interval $[t_{j-1}, t_j]$ of a partition $C[0, T]$ can be expressed as [26]:

$$E_s[v](t) = \min\{\ \max\{\ -s,\ \ v(t) - v(t_{j-1}) + E_s[v](t_{j-1})\},\ \ s\} \tag{1.6}$$

for $t \in [t_{j-1}, t_j]$.

E_s

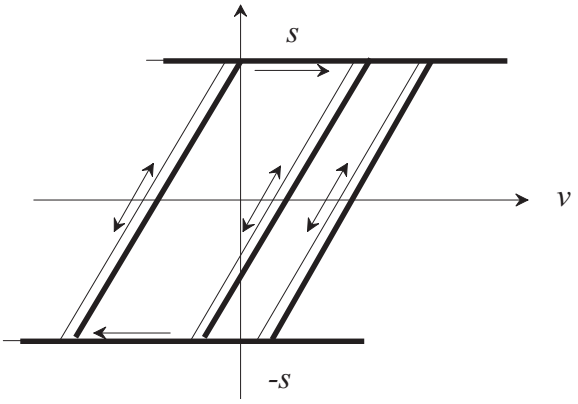

Figure 1.4: The input-output relationship of the stop operator [26].

The output of the stop operator-based Prandtl-Ishlinskii (SPI) model $\overline{\Psi}[v](t)$ is obtained from summation of the weighted operators in a similar manner:

$$\overline{\Psi}[v](t) = \int_0^S \overline{w}_s(s) E_s[v](t) dr \tag{1.7}$$

where $\overline{w}_s(s)$ is the density function. The output of the SPI model may be numerically expressed as [26]:

$$\Psi[v](t) = \sum_{i=1}^{n_s} w_s(s_i) E_{s_i}[v](t) \tag{1.8}$$

where n_s is a positive integer that represents the number of stop operators used and the weights $w_s(s_i)$ are defined as:

$$w_s(s_i) = \overline{w}_s(s_i)[s_{i+1} - s_i] \tag{1.9}$$

Figure 1.5 illustrates the input-output characteristics of the play operator which is characterized by the threshold r and the input $v(t)$. Analytically, for an input $v(t)$ in each interval $[t_{j-1}, t_j]$ of a partition $AC[0, T]$, the output of the play operator $F_r[v](t)$ can be expressed as [26]:

$$F_r[v](t) = \max\{v(t) - r, \min\{v(t) + r, F_r[v](t_{j-1})\}\} \tag{1.10}$$

for $t \in [t_{j-1}, t_j]$.

The output of the classical Prandtl-Ishlinskii model $\overline{\Phi}[v](t)$ employing the play operators F_r and the density function $\overline{p}_r(r)$ can be expressed as [26]:

$$\overline{\Phi}[v](t) = \int_0^R \overline{p}_r(r) F_r[v](t) dr \tag{1.11}$$

where q is a positive constant. The output of the play operator-based Prandtl-Ishlinskii (PPI) model can also be numerically expressed as [26]:

$$\Phi[v](t) = qv(t) + \sum_{i=1}^{n_p} p_r(r_i) F_{r_i}[v](t) \tag{1.12}$$

where n_p is a positive integer representing the number of the play operators considered and $p_r(r_i)$ are the weights, expressed as:

$$p_r(r_i) = \overline{p}_r(r_i)[r_{i+1} - r_i] \tag{1.13}$$

F_r

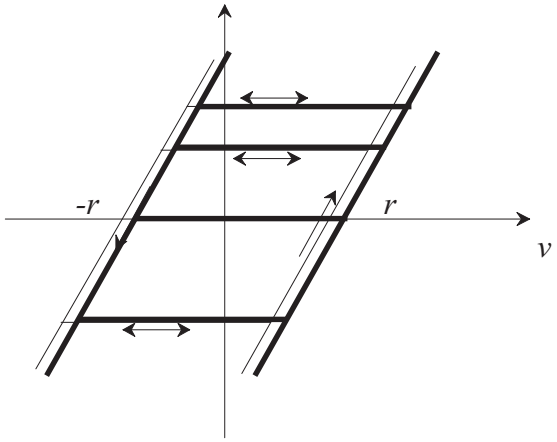

Figure 1.5: Input-output relationship of the play operator [26].

The classical Prandtl-Ishlinskii model cannot accurately characterize the hysteresis properties of magnetic materials and smart actuators, which invariably exhibit nonlinear output saturation and asymmetry in the output-input characteristics. However, the model can effectively describe the hysteresis properties of piezoceramic actuators subjected to excitations at low frequencies (below 5 Hz), which are known to be symmetric [25,33,42,40]. Consequently, the model has been employed to characterize hysteresis in actuators that show symmetric, unsaturated hysteresis nonlinearities such as piezoceramic actuators. Janocha and Kuhnen [41] employed classic play operators to characterize hysteresis in a piezoceramic actuator subjected to triangular input at a frequency of 0.5 Hz. Due to the continuous nature, the use of only 10 play operators resulted in accurate characterization of the hysteresis nonlinearities of the actuator. In a similar manner, Krejci and Kuhnen [42] proposed the classical play operator to characterize hysteresis nonlinearities of a piezoceramic actuator subjected to harmonic inputs applied at a low frequency, while the output displacement was measured using high-precision laser interferometer.

2.2.6 Modified and generalized Prandtl-Ishlinskii models

The continuity in time and space makes the play operator-based Prandtl-Ishlinskii (PPI) model an attractive choice for generating input-output hysteresis loops using only a few play operators, which reduces the computational demand compared to the Preisach and KP models. However, the classic PPI model shows unsaturated and symmetric hysteresis loops, and is thus limited to characterization of hysteresis nonlinearities of piezoceramic actuators, which show unsaturated and symmetric hysteresis loops [9,42]. Consequently, a few modifications have been proposed to relax the symmetry of the model in order to utilize its attractive continuity property to characterize hysteresis of range of smart actuators. These modifications may be grouped into two method-based categories, namely: (i) those based on integration of a deadzone operator together with the PPI model, and (ii) those employing dissimilar envelope functions under increasing and decreasing inputs to formulate generalized play operators.

The modified Prandtl-Ishlinskii model employs the classic Prandtl-Ishlinskii model coupled with a summation of weighted deadband operators, which are nonlinear and memoryless operators. This approach can relax the symmetry of the classical model and provide saturation of the output, as observed in magnetostrictive actuators. Figure 1.6 illustrates the output-input characteristics of the deadzone operator $J_d[v](t)$, as a function of the threshold d and the input $v(t)$. The input-output characteristics of the deadzone operator have been related to physical phenomena in motors, attributed to frictional torques [43]. The Prandtl-Ishlinskii model coupled with the deadband operators can be employed to characterize both asymmetric as well as saturated hysteresis nonlinearities [44]. The output of the resulting modified Prandtl-Ishlinskii model $Z[v](t)$ is a composition of the deadband operators output, Λ, and the classical Prandtl-Ishlinskii model output, Φ, as [44]:

$$Z[v](t) = (\Lambda \circ \Phi)[v](t) \tag{1.14}$$

For an input $v(t)$, the output of the deadband memoryless function, $\Lambda[v](t)$ is obtained from weighted summation of the deadband operators, J_{d_i} :

$$\Lambda[v](t) = \sum_{i=1}^{n_Q} g_{di} J_{d_i}[v](t) \tag{1.15}$$

where g_{d_i} defines the weights and n_Q is a positive integer representing the number of deadzone operators. The deadband operator, described in Figure 1.6, can be expressed as:

$$J_{d_i}[\Phi](t) = \begin{cases} \max\{\Phi(t) - d_i, 0\} & for \quad d_i > 0, \\ \Phi(t) & for \quad d_i = 0, \\ \min\{\Phi(t) - d_i, 0\} & for \quad d_i < 0. \end{cases} \tag{1.16}$$

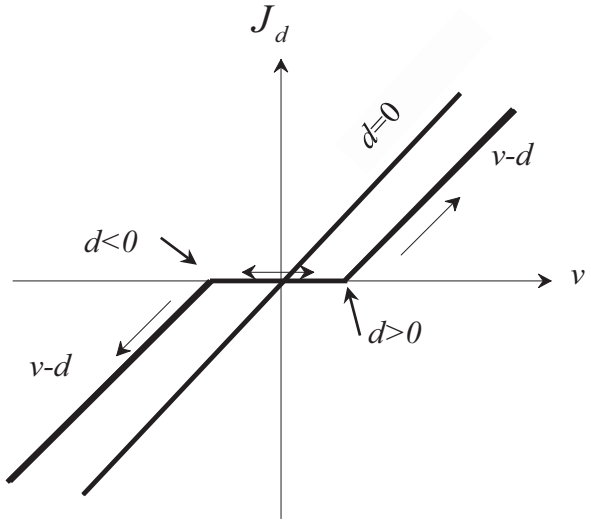

Figure 1.6: Input-output relationship of a deadzone operator for input $v(t)$ [12].

Since the relay operator of the Preisach model yields either +1 or -1, it does not relax the symmetry of the model without using a density function with different weights for increasing and decreasing inputs. Alternatively, a generalized play operator has been defined to yield either

increasing or decreasing output $S_r[v](t)$ with increasing or decreasing inputs, in an asymmetric manner along the continuous envelope curves γ_l and γ_r, as shown in Figure 1.7 [26]. The output of the generalized play operator for any input $v(t)$ in each interval $t \in [t_{j-1}, t_j]$ of a partition $C[0,T]$ is analytically defined as:

$$S_r[v](t_j) = \max\left(\gamma_l(v(t_j)) - r, \min(\gamma_r(v(t_j)) + r, S_r[v](t_{j-1})\right) \tag{1.17}$$

In the above formulation, r refers to the threshold value of the classical play operator. Unlike the classical play operator, the generalized play operator yields zero output, $S_r[v](t)=0$, at two different threshold values, ζ_1 and ζ_2, of the increasing and decreasing input $v(t)$, as shown in Figure 1.7. The difference in the magnitudes of constants ζ_1 and ζ_2 allows for describing asymmetric hysteresis loops. These constants, corresponding to increasing and decreasing inputs, have been related to the envelope functions and the threshold in the following manner [45]:

$$\begin{aligned} \zeta_1 &= \gamma_l^{-1}(r) \ \textit{for} \ \dot{v}(t) > 0 \\ \zeta_2 &= \gamma_r^{-1}(-r) \ \textit{for} \ \dot{v}(t) < 0 \end{aligned} \tag{1.18}$$

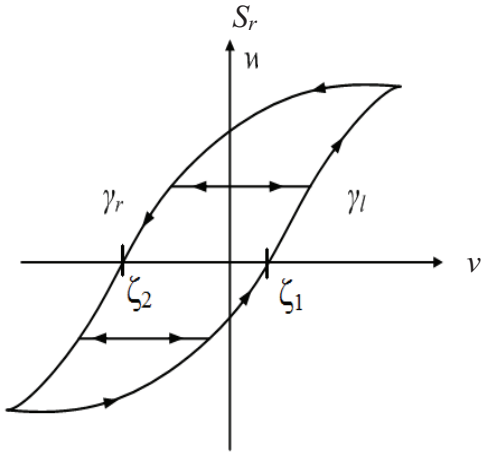

Figure 1.7: Output-input characteristics of a generalized play operator [26].

The output of generalized Prandtl-Ishlinskii model is subsequently formulated upon integrating the generalized play operator and the density function as [61]:

$$\overline{\Phi}_G[v](t) = \int_0^R \overline{p}_G(r) S_r[v](t) dr \tag{1.19}$$

where $\overline{\Phi}_G[v](t)$ is the output of generalized Prandtl-Ishlinskii model, and $\overline{p}_G(r)$ is the density function.

This model integrates the generalized play operator with appropriate envelope and density functions to describe minor and major hysteresis loops of smart actuators and materials with asymmetry and saturation properties. The output of the generalized play operator-based Prandtl-Ishlinskii (GPPI) model can be numerically expressed as [26]:

$$\Phi_G[v](t) = \sum_{j=0}^{J_G} p_G(r_j) S_{r_j}[v](t) \tag{1.20}$$

Kuhnen [12] characterized asymmetric hysteresis nonlinearity of a magnetostrictive actuator using the rate-independent Prandtl-Ishlinskii model coupled with a superposition of weighted deadband operators. In another study, Kuhnen and Krejci [44] proposed a play operator with deadzone operator in order to characterize and compensate for complex hysteresis and creep effects in a piezoceramic stack-actuated system, with an extended operating range. A recent study has proposed a generalized Prandtl-Ishlinskii model to characterize asymmetric hysteresis nonlinearities observed in several smart material actuators [45]. The proposed method showed effectiveness of the model for describing both asymmetric and saturated hysteresis loops of magnetostrictive and SMA actuators using a few generalized play operators.

2.3 Rate-dependent hysteresis models

2.3.1 Operator-based rate-dependent hysteresis models

Although smart material actuators generally exhibit strong rate-dependency of hysteresis under high rates of inputs, only a few attempts have been made towards models that can account for the rate effect. A few operator-based hysteresis models have been proposed for characterization of rate-dependent hysteresis effects in smart material actuators [8,7,22,37,46]. Many of these were derived from the classical rate-independent models. The most common approach to account for rate-dependent hysteresis effects in Preisach model is to apply a dynamic density function in to classical model. Mayergoyz [22,30] proposed a rate-dependent Preisach model by introducing the time rate of the output in the density function to characterize rate-dependent hysteresis nonlinearities of magnetic materials. In a similar manner, Ben Mrad and Hu [47] employed a dynamic density function in the Preisach model, where the input was replaced by the average rate of the input. The model results obtained under sinusoidal inputs at six distinct frequencies in the 0.1 to 800 Hz range showed agreement with the measured responses of a piezoceramic actuator. The measured data in this study, however, was limited to only six distinct data points in the major hysteresis loop. Furthermore, piezoceramic actuators generally exhibit decreasing actuator output with increasing rate of input [9]

The above-reported studies were mostly based on the Preisach model coupled with a dynamic density function comprising the rate of either input or the output. Inserting the rate of the measured output in the density function yields a complex nonlinear differential equation with memory effects. Alternatively, the output of the model can simply be computed by employing the rate of the applied input in the density function, instead of the rate of the measured output. The

effectiveness of the dynamic density function for characterizing hysteresis under higher rate of inputs, however, has not been demonstrated.

Alternatively, Tan and Baras [7], in an attempt to characterize rate-dependent hysteresis nonlinearities in a magnetostrictive actuator, assumed a second order linear differential equation coupled with the classical Preisach model to describe major hysteresis loops under excitations in the 10 and 300 Hz range. The model, however, showed greater characterization error at excitation frequencies beyond 50 Hz. For example, the maximum characterization error between the output of the model and the measured displacement at an excitation frequency of 150 Hz was greater than 25%. Moreover, the proposed model could not be employed to characterize hysteresis nonlinearities acquired at frequencies below 5 Hz, where the hysteresis of the magnetostrictive actuator is rate-independent. Ang et al. [46] proposed a density function in conjunction with the Prandtl-Ishlinskii model and deadzone operators to characterize rate-dependent hysteresis in a piezoceramic actuator. The validity of this model was demonstrated under sinusoidal inputs in the 1 and 19 Hz frequency range. The proposed dynamic model resulted in substantially lower, hysteresis error, nearly 50 % lower, compared to that attained from the rate-independent hysteresis model.

Rate-dependent play operators together with a rate-dependent density function have been proposed and integrated to the Prandtl-Ishlinskii model to describe rate-dependent hysteresis behaviour of a piezoceramic actuator [9,45]. This model employed a density function formulated as a nonlinear function of the rate of input. The model was observed to be very effective in characterizing hysteresis nonlinearities of a piezoceramic actuator under different inputs in the frequency range of 5 to 500 Hz.

2.3.2 *Differential equation-based hysteresis models*

Differential equation-based hysteresis models such as Duhem and the Bouc–Wen models have been widely used for characterizing hysteresis nonlinearities in different materials and actuators. The Bouc–Wen model is a differential equation-based model, which originates from the Bouc model presented in [24,48]. This model has been extensively used to describe hysteretic behaviour between the applied displacement and the output force in a wide range of mechanical systems. The relationship between the output of the model $z(t)$ and the input $v(t)$ is expressed by the following differential equation:

$$\dot{z}_{BW}(t) = \alpha_{\_BW}\dot{v}(t) + \beta_{\_BW}\left|\dot{v}(t)\right| \; z(t) \; \left|z(t)\right|^{n_{BW}-1} + \gamma_{BW}\dot{v}(t) \; \left|z(t)\right|^{n_{BW}} \tag{1.21}$$

where n_{BW} is a positive integer. The positive constants, $\alpha_{\_BW}$, $\beta_{\_BW}$ and $\gamma_{\_BW}$, govern the shape of the hysteresis loops. Different forms of Bouc-Wen model have been proposed to suit hysteresis properties of different systems, materials, and actuators [48,49]. Hysteretic systems, piezoceramic actuators [50], polyurethane foams and magneto-rheological fluid dampers [51] are some of the examples. The major limitations of the Bouc-Wen model are associated with parameter identification necessary to formulate the model. Moreover, the model, as an equation-based hysteresis model, is not invertible and thus cannot be applied to inverse model-based hysteresis compensation methods.

Hodgdon and Coleman [52] proposed the Duhem model for describing relationship between the input magnetic field $H(t)$ and the output flux density $B(t)$ and thereby the hysteresis in ferromagnetic materials. The model is described by the following differential equation:

$$\dot{B}(t) = a\_D\left|\dot{H}(t)\right|\left(b\_D H(t) - B\_D(t)\right) + c\_D\dot{H}(t) \tag{1.22}$$

where a_D, b_D, and c_D are positive constants that control the shape of the hysteresis loop. The output of the Duhem model yields symmetric hysteresis loops. Furthermore, the output of the model may exhibit unstable minor hysteresis loops [23]. Although a few forms of the Duhem model have been proposed in the literature to overcome these limitations, these require adding conditions limit the model's application in control system design.

2.4 Hysteresis compensation

Owing to undesirable effects of smart material hysteresis, considerable efforts have been made towards design of controllers for compensation of hysteresis in smart actuators. Alternatively, a number of model-based hysteresis compensation methods have also been proposed. The methods-based on controller design are generally not concerned with the hysteresis model, while the model-based methods rely on inverse hysteresis model to cancel the hysteresis effect.

A number of control methods have been proposed to compensate for smart actuator hysteresis such as robust adaptive [7], sliding-mode [53,54] and other nonlinear control algorithms [1,56]. Su et al. [55] proposed an adaptive controller to control a nonlinear system preceded by unknown Prandtl-Ishlinskii hysteresis nonlinearities. In this study, the proposed controller leading to the desired output and global stability was presented. Smith [56] coupled a nonlinear differential equation with an LQR controller designed to compensate for hysteresis in a magnetostrictive actuator described by the Jiles-Atherton physics-based hysteresis model. The study employed the model along with an inverse magnetization model involving solutions of the partial differential equations using numerical techniques. This approach could yield errors from two sources

associated with modelling inaccuracies of the numerical inverse. In general, the physics-based hysteresis models [1,19] are not invertible, and control of hysteresis employing such models necessitates design of complex nonlinear controllers in a closed-loop manner, inherently dependent on initial conditions, which requires adaptive or more robust control techniques [1].

The inverse model-based hysteresis compensation methods employ the inverse of the hysteresis model as a feedforward compensator in a cascade arrangement of the hysteresis model and its inverse. These methods are considered to be effective and convenient for real-time compensation and control [16,34,35, 42,57]. The inverse model-based compensation, however, necessitates the formulation of the hysteresis inverse model, which is often a challenging task. An open-loop inverse model-based compensation method, shown in Figure 1.8, has been widely proposed in the literature to reduce the effects of the rate-independent hysteresis nonlinearities. In this figure, ψ^{-1} is the inverse hysteresis model, ψ represents the hysteresis model and $v^*(t)$ is the desired output. This method was suggested by Tao and Kokotovic [27], and involves the formulation of the inverse model of the hysteretic system. Their study developed a control algorithm to compensate for the hysteresis nonlinearities of a system comprising a linear plant proceeded by a hysteresis block representing a hysteretic actuator.

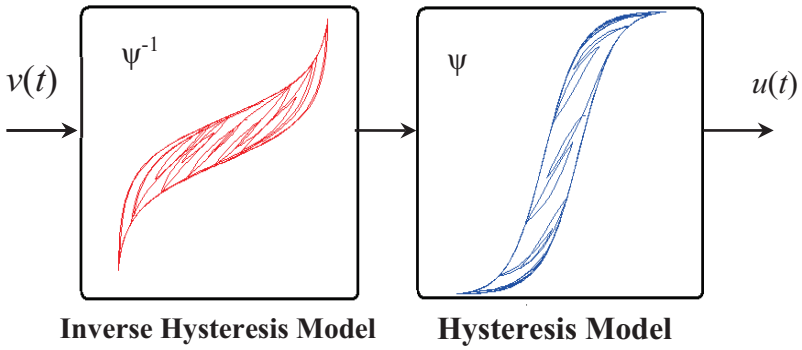

Figure 1.8: Open-loop hysteresis compensation using inverse hysteresis model.

The implementation of an inverse model-based compensation method, however, involves complexities associated with formulation of the inverse of the proposed model. The Preisach and Krasnosel'skii-Pokrovskii models are not analytically invertible. Consequently, different numerical methods have been developed to obtain inversions of these models. Schafer and Janocha [58] proposed a numerical method to compensate for rate-independent hysteresis nonlinearities of magnetostrictive actuators represented by the classic Preisach model. In another study, Ge and Jouaneh [57] employed inverse Preisach model, derived based on a numerical algorithm, as a feedforward compensator coupled with a PID feedback control system to reduce the hysteresis nonlinearities in a piezoceramic actuator. A numerical inverse of the Krasnosel'skii-Pokrovskii model was also applied by Galinaitis [28] in an open-loop manner to compensate for hysteresis of a piezoceramic actuator. In this study, the compensation of the hysteresis nonlinearities was demonstrated for three different sinusoidal inputs at a frequency of 0.01 Hz. With regards to magnetostrictive actuators, Iyer and Tan [16] proposed two different methods to seek compensation of major hysteresis loops. Both the methods have been employed to derive an inverse for the Preisach model for characterizing hysteresis nonlinearities of the actuator. Both the methods, however, revealed certain errors that could be attributed to two primary factors:

- Modeling inaccuracies and uncertainty of the Preisach density function; the Preisach plane requires many refinements to formulate hysteresis model to describe the hysteresis properties more accurately [16].

- The second source of error is attributed to the discontinuity of the relay operator, which permits for evaluation of only a numerical inversion of the model.

Tan and Baras [7] applied the inverse Preisach model in an adaptive control system to compensate for hysteresis nonlinearities of a magnetostrictive actuator. The classic Preisach model was coupled with a second order system to quantify the rate-dependent hysteresis nonlinearities, which implied the same two sources of errors described in the rate-independent case [16]. Moreover, the proposed compensator would be effective under low frequency inputs and could not be applied for inputs at different frequencies. The compensation of rate-dependent hysteresis effects using the inverse rate-independent hysteresis models could thus yield high compensation errors at higher excitation frequencies since hysteresis effects increased with the excitation frequency.

Aljanaideh et al. [59] proposed hysteresis compensation for a piezoceramic actuator using a stop operator based Prandtl-Ishlinskii (SPI) model. The proposed compensator was derived based on the principle of employing an inverse of the play operator-based Prandtl-Ishlinskii (PPI) model in a feedforward manner to compensate for hysteresis nonlinearities of the actuator. The application of the proposed model as a feedforward compensator resulted in significant reduction in the positioning error due to hysteresis of the actuator.

Unlike the Preisach and Krasnosel'skii-Pokrovskii models, the Prandtl-Ishlinskii model offers a unique advantage, as its inverse can be obtained analytically. Krejci and Kuhnen [42] derived and applied the analytical inverse of the Prandtl-Ishlinskii model for compensation of hysteresis nonlinearities of a piezoceramic actuator. The analytical inverse, however, is applicable only for rate-independent symmetric hysteresis nonlinearities that are observed in piezoceramic actuators. Kuhnen [12] compensated the rate-independent asymmetric hysteresis nonlinearity of a magnetostrictive actuator using inverses of a free memory function and a rate-independent Prandtl-Ishlinskii model. In another study, Kuhnen and Krejci [44] employed a play operator of a deadzone

function in order to characterize and compensate for complex hysteresis and creep effects in a piezoceramic actuated system designed with extended operating range. A numerical inverse was derived and applied in order to compensate for hysteresis nonlinearities of the actuator, which showed an error of only 4.4% in the input-output compensation.

A generalized Prandtl-Ishlinskii model and its analytical inverse has been suggested in [60] to compensate for asymmetric hysteresis nonlinearities of magnetostrictive and SMA actuators. The study proposed envelope functions for the classic play operator based Prandtl-Ishlinskii model for characterization of asymmetric hysteresis nonlinearities. The analytical inverse of the play operator-based Prandtl-Ishlinskii model together with the inverse of the envelope functions were formulated for compensation of rate-independent asymmetric hysteresis nonlinearities of the proposed model. However, the suggested method could not be applied for compensation of rate-dependent asymmetric hysteresis, which is mainly attributed to the discontinuity in the envelope functions that might be observed under high rates of input.

The Prandtl-Ishlinskii model based on play operators offers attractive properties attributed to continuity of the play operators which permits the formulation of an analytical inverse for real-time implementations [42]. The classic Prandtl-Ishlinskii model, however, is limited to characterization of smart material actuators that exhibit rate-independent symmetric input-output characteristics, such as those observed for piezoceramic actuators. A few studies have reported alternate Prandtl-Ishlinskii models to describe asymmetry and saturation of the output. For example, a Prandtl-Ishlinskii model cascaded with a memoryless hyperbolic tangent function was proposed in [31] to formulate a hysteresis model for describing saturated hysteresis nonlinearities of a superconductor. A generalized Prandtl-Ishlinskii has been recently reported for characterization of asymmetric hysteresis nonlinearities by employing a generalized play operator

instead of the classic play operator [45]. The suggested play operator employed different loading and unloading hyperbolic tangent envelope functions, which relaxes the symmetry in the output of the Prandtl-Ishlinskii model. In [61], the generalized model reported in [60] was applied for characterizing the butterfly-shaped hysteresis nonlinearity of a Terfenol-D magnetostrictive actuator considering identical envelope functions of the play operators. Kuhnen [12], characterized asymmetric hysteresis nonlinearity of a magnetostrictive actuator using the rate-independent Prandtl-Ishlinskii model coupled with a superposition of weighted deadband operators.

Although the above studies have proposed a number of alternate Prandtl-Ishlinskii models to describe asymmetric hysteresis nonlinearities, the strong effects of the input rate on the hysteresis nonlinearities have been mostly ignored. The hysteresis nonlinearities of magnetostrictive actuators, similar to the other smart material actuators, invariably, increase with increasing excitation frequency of the applied input [7,62], which limits the application of these models to a narrow range of excitation frequency. Moreover, the applications of the inverse of these models would yield considerable compensation errors under excitations at higher frequencies.

A recent study [63] developed an analytical inverse of the rate-dependent play operator-based Prandtl-Ishlinskii model for compensation of rate-dependent hysteresis nonlinearities. According to this study, an analytical inverse of the rate-dependent Prandtl-Ishlinskii model Π can be obtained under the threshold dilation condition, which implies that the difference between two consecutive dynamic thresholds $r_{i+1}(\dot{v}(t))$ and $r_i(\dot{v}(t))$ does not decrease in time, such that $\forall\, i = 1, \ldots, n\text{-}1$:

$$\frac{d}{dt}\left(\Delta r_i(\dot{v}(t))\right) \geq 0 \tag{1.23}$$

where $\Delta r_i(\dot{v}(t)) = r_{i+1}(\dot{v}(t)) - r_i(\dot{v}(t))$.

The study provided analytical formulations for characterizing and compensating the rate-dependent symmetric hysteresis nonlinearities of smart material actuators. The method, however, could also be extended for describing and compensation of rate-dependent asymmetric and saturated hysteresis nonlinearities that is observed in magnetostrictive actuators, under wide ranges of input amplitudes and rates.

2.5 Scope and objectives

Considerable efforts have been made to characterize hysteresis properties of smart material actuators in order to study the effects of these nonlinearities and to seek methods for enhancing micropositioning precision and tracking performance of these actuators. These efforts have resulted in a number of hysteresis models for describing hysteresis nonlinearities of piezoceramic, SMA and magnetostrictive actuators. These models have proven effective for characterization and compensation of hysteresis observed at lower frequency excitation and for actuators with symmetric output-input properties.

The magnetostrictive actuators, however, exhibit output-input characteristics that are strongly dependent upon the input. Furthermore, such actuators exhibit output saturation and asymmetric output-input characteristics. Developments in alternate methods are thus vital not only for characterizing the asymmetric and rate-dependent hysteresis but also for compensating the hysteresis effects. These need to address two major challenges associated with characterization of

hysteresis nonlinearities under a wide range of inputs through effective model development and formulations of model inverse for compensation of rate-dependent and asymmetric hysteresis nonlinearities.

Owing to the continuous nature of the play operators, a rate-dependent Prandtl-Ishlinskii model could be formulated for characterizing the rate-dependent hysteresis nonlinearities of a magnetostrictive actuator. This model could also be applied in a cascade configuration with a memoryless function of weighted deadband operators to describe asymmetry in the output together with output saturation under inputs over a wide frequency range. The resulting may provide accurate predicts of minor as well as major rate-dependent hysteresis loops under a wide range of inputs. Furthermore, such a model could also be applied to describe rate-independent as well as rate-dependent asymmetric hysteresis nonlinearities of magnetostrictive actuators provided that the threshold dilation condition is satisfied. A stop-operator based Prandtl-Ishlinskii model may also be considered to seek compensation of hysteresis effects using the cascade arrangement of the play and stop-operator based models.

2.5.1 Objectives of the dissertation research

The proposed dissertation research aims at characterization and compensation of hysteresis nonlinearities of smart material actuators for enhancement of their micro-positioning and tracking performance. The primary objective is to develop methodologies for characterization and compensation of rate-dependent and asymmetric hysteresis of smart material actuators over a wide range of input rates and amplitudes in an open-loop feedforward manner. The specific objectives of the dissertation research are summarized below:

1. Develop an analytical method for compensation of rate-independent symmetric hysteresis nonlinearities described by a play-operator based Prandtl-Ishlinskii model through formulation and application of a stop-operator based Prandtl-Ishlinskii model. Investigate the effectiveness of the compensator through simulations as well as hardware-in-the-loop experiments on a smart material actuator.

2. Characterize the output-input properties of a Terfenol-D type magnetostrictive actuator in the laboratory under a wide range of input amplitudes, rates, and magnetic bias levels, as well as under the effect of a mechanical load.

3. Develop a methodology, based on the experimental observations, for describing rate-dependent symmetric hysteresis nonlinearities of a magnetostrictive actuator through formulation of a rate-dependent Prandtl-Ishlinskii model.

4. Formulate an inverse rate-dependent Prandtl-Ishlinskii model for open-loop compensation of rate-dependent symmetric hysteresis nonlinearities of a magnetostrictive actuator over a wide range of input frequency, and investigate the effectiveness of the compensator through simulations and as well as experimentally.

5. Formulate an integrated Prandtl-Ishlinskii model, based on the experimental observations, that employs a rate-dependent Prandtl-Ishlinskii model along with a superposition of deadband operators, for describing rate-dependent asymmetric hysteresis nonlinearities of magnetostrictive actuator at different levels of input amplitudes applied over a wide frequency range.

6. Develop an integrated inverse rate-dependent Prandtl-Ishlinskii model for compensation of rate-dependent asymmetric hysteresis nonlinearities of the magnetostrictive actuator, and explore its effectiveness through simulations and as well as through hardware-in-the loops laboratory tests.

2.5.2 Organization of the manuscript-based thesis

This dissertation has been written according to the manuscript-based format, as described in "Thesis Preparation and Thesis Examination Regulation" booklet of the School of Graduate Studies of Concordia University. This dissertation research is organized into 7 chapters, including a literature review chapter (Chapter 1) summarizing the state-of-the-art review of reported studies

relevant to modeling and compensation of hysteresis in smart material actuators. Chapter 2 presents a detailed description of experiment design and methods used to characterize output-input characteristics of a magnetostrictive actuator under wide ranges of inputs. These included different levels of excitation amplitudes and frequencies, magnetic bias and mechanical loading.

Chapter 3 presents a primary study on modeling and compensation of rate-independent symmetric hysteresis nonlinearities. This chapter presents the theory of stop operator-based Prandtl-Ishlinskii model as a compensator for the rate-independent symmetric hysteresis nonlinearities represented by the play operator-based Prandtl-Ishlinskii model. The results obtained have been published in the following article:

> "Compensation of Play Operator-based Prandtl-Ishlinskii Model Using Stop Operator with Application to Piezoceramic Actuators", *International Journal of Advanced Mechatronic Systems*, vol. 4, no. 1, 2012.

This article presents a new methodology for compensation of rate-independent symmetric hysteresis nonlinearities of smart material actuators. The initial loading curves of the play operator-based Prandtl-Ishlinskii (PPI) and the stop operator-based Prandtl-Ishlinskii (SPI) models were first used to explore the hysteresis properties of both the PPI and SPI models. The results illustrate that the PPI model exhibits convex counter-clockwise hysteresis loops while that of the SPI model were concave clockwise hysteresis loops. An SPI model could thus be utilized for compensation of rate-independent symmetric hysteresis nonlinearities described by the PPI model. The thresholds and the weights of the SPI model were analytically derived based on known parameters of the PPI model. The effectiveness of the compensator was demonstrated through experimental results attained with a piezoceramic micro-positioning stage. The experimental results showed that the SPI model can serve as an effective feedforward compensator for the rate-independent hysteresis nonlinearities of a piezoceramic actuator.

In Chapter 4, a comprehensive experimental study on the characterization and modeling of hysteresis nonlinearities of magnetostrictive actuator is presented. The experimental measurements, model and the simulation results have been published in the *Journal of Smart Materials and Structures*.

"Experimental Characterization and Modeling of Asymmetric and Saturated Hysteresis of Magnetostrictive Actuators", *Smart Materials and Structures,* vol. 23, no. 3, 2014.

In this paper, hysteresis nonlinearities of a magnetostrictive actuator were characterized under different amplitudes of simple and complex harmonic excitations over a wide range of frequencies (10-200 Hz) and magnetic bias levels (35-75 kA/m), as described in details in Chapter 2. The measured data revealed asymmetric output-input characteristics and strong dependence on the magnetic bias, amplitude and frequency of the input. Output saturation was also observed under moderate to high amplitude excitations. The area bounded by the hysteresis loop showed a nonlinear dependence on the amplitude of the input, while this dependence was linear on the excitation frequency of the applied input, irrespective to the input amplitude. A rate-dependent model employing a rate-dependent Prandtl-Ishlinskii model integrating a memoryless function was proposed for the characterization of rate-dependent asymmetric hysteresis nonlinearities of the actuator. Following the experimental observations, a linear rate-dependent threshold function was employed to formulate the rate-dependent Prandtl-Ishlinskii model, while an asymmetric deadband function was incorporated to add asymmetry to the symmetric output of the rate-dependent Prandtl-Ishlinskii model. Comparisons of the integrated Prandtl-Ishlinskii model responses with the measured data suggested that the proposed model could effectively describe the nonlinear hysteresis properties of the magnetostrictive actuator over a broad range of excitation amplitudes and frequencies.

The relative significance of the proposed rate-dependent and asymmetric integrated model was explored by evaluating its performance in relation to the Prandtl-Ishlinskii models suggested in the literature for characterization of hysteresis nonlinearities of magnetostrictive actuators. The results revealed that neglecting either the rate effect in the threshold of the Prandtl-Ishlinskii model or the asymmetry attributed to the memoryless function yields significant errors in the displacement responses of the magnetostrictive actuator model.

In an attempt to design a compensator for the rate-dependent symmetric hysteresis nonlinearities of smart actuators, the data obtained under simple and complex harmonic excitations over a wide range of frequencies (10-200 Hz) were employed to define a rate-dependent Prandtl-Ishlinskii model. The inverse rate-dependent model was subsequently formulated and applied for compensation of rate-dependent symmetric hysteresis of the magnetostrictive actuator. The results of this segment of the study have been published in the following article, which is presented in Chapter 5.

"Compensation of Rate-Dependent Hysteresis Nonlinearities in a Magnetostrictive Actuator Using Inverse Prandtl-Ishlinskii Model", *Smart Materials and Structures,* vol. 22, no. 2, 2012.

This chapter suggests a new inverse rate-dependent compensator for compensation of rate-dependent symmetric hysteresis nonlinearities of magnetostrictive actuator in an open-loop manner. The hysteresis nonlinearities of the magnetostrictive actuators were first explored under an input amplitude of 2.3 A applied over a wide frequency range up to 200 Hz. A rate-dependent threshold, as a linear function of the rate of input, was employed to formulate a symmetric rate-dependent Prandtl-Ishlinskii model considering the threshold dilation condition that ensures the analytical invertability of the model. The inverse rate-dependent Prandtl-Ishlinskii model was then formulated on the basis of the rate-dependent Prandtl-Ishlinskii model. The effectiveness of the inverse model compensator for mitigating the rate-dependent hysteresis nonlinearities was

demonstrated through simulation results and hardware-in-the-loop laboratory measurements with a magnetostrictive actuator. Both the simulation and experimental results revealed reduction in the peak hysteresis from 4.7 μm to 0.645 μm, when the proposed inverse rate-dependent model was applied as a feedforward hysteresis compensator. The peak error occurred only under excitations at the lowest frequency of 1 Hz. The results suggested that the inverse Prandtl-Ishlinskii model could provide hysteresis compensation under different rates of inputs in a simple and effective manner.

Employing the inverse model suggested in Chapter 5 for compensation of rate-dependent hysteresis nonlinearities of magnetostrictive actuator at high input current amplitudes (e.g., 5 and 6 A) resulted in substantial errors in the output. This was attributed to significant output asymmetry observed under medium to high inputs. Consequently, Chapter 6 describes a methodology for compensation of rate-dependent asymmetric hysteresis nonlinearities of smart material actuators. An integrated Prandtl-Ishlinskii model and its inverse model are presented. The model and its inverse together with the simulation and experimental results have been submitted to the *Sensors and Actuators: A Physical*.

> "Feedforward Compensation of Asymmetric Rate-Dependent Hysteresis Nonlinearities of a Magnetostrictive Actuator", under review, *Sensors & Actuators A: Physical* (Submitted, Nov. 2013).

In this chapter, an inverse model is formulated to seek real-time compensation of rate-dependent and asymmetric hysteresis nonlinearities of a Terfenol-D magnetostrictive actuator. The inverse model was formulated by integrating the inverse of the rate-dependent Prandtl-Ishlinskii model, satisfying the threshold dilation condition, together with the inverse of the deadband function. The integrated inverse model was subsequently applied to the nonlinear hysteresis model

as a feedforward compensator. The simulation results were attained under different harmonic and complex harmonic excitations of varying current amplitudes in the 1-250 Hz range, which suggested that the integrated inverse model can effectively compensate for the hysteresis, and output asymmetry and saturation effects over a wide range of excitations. The proposed compensator was subsequently implemented to the actuator hardware in the laboratory to study its potential for rate-dependent and asymmetric hysteresis compensation on a real-time basis. The experimental results obtained under harmonic and complex harmonic excitations further revealed that the integrated inverse compensator can substantially suppress the hysteresis and output asymmetry nonlinearities in the entire frequency range considered in the study.

CHAPTER 2

EXPERIMENTAL AND ANALYTICAL STUDY ON HYSTERESIS OF SMART ACTUATORS

3.1 General

The output-input properties of a magnetostrictive actuator invariably exhibit hysteresis, output saturation and asymmetry in the output. These nonlinearities are known to strongly depend on the design and operating conditions of the actuator, particularly, the input amplitude and frequency, magnetic bias, mechanical loading and type of the input. Although a number of physical and phenomenological models have been proposed to describe hysteresis nonlinearities of such actuators [e.g.,11,17], relatively fewer studies have attempted to characterize the hysteresis

nonlinearities through measurements. A few studies have reported measured output-input properties of magnetostrictive actuators under limited ranges of inputs [7,11,13,17], which show hysteresis dependence on the magnitude, bias and rate of the input.

A few studies have also shown asymmetric output-input of the magnetostrictive actuators, particularly under high amplitude inputs [7,12] and inputs with bias [13]. The output-input properties, in-general, suggest coupled effects of input amplitude, bias and rate on the hysteresis and output saturation nonlinearities. The reported studies, however, have been generally limited to the study of only one of factors such as input amplitude [5,12,64], bias [13] or frequency [7,29]. Only limited data thus exists to describe coupled effects of different inputs. Furthermore, the majority of the experimental studies have been performed on actuators without a mechanical load, which could also be expected to contribute to nonlinear output-input characteristics of the actuators. In this study, a laboratory experiment was designed to characterize the output-input characteristics of a magnetostrictive actuator under simple and complex harmonic inputs of different amplitudes over a wide frequency and magnetic bias levels as well as mechanical loads. The output-input properties of a magnetostrictive actuator were measured under different inputs up to 10 A over the frequency range up to 250 Hz, in order to fully characterize hysteresis nonlinearities as a function of the input amplitude and frequency. The measured data are further analyzed to describe major and minor hysteresis loops under harmonic excitations under different rate of inputs, magnetic bias and mechanical loads. This chapter also represents a short background about the magnetostriction phenomenon, followed by a description for the magnetostrictive actuators and the experimental set-up that was used in the study.

3.2 Magnetostriction and magnetostrictive actuators

Magnetostriction was first observed by James Joule in 1842. It concerns coupling between the magnetic and mechanical properties of some ferromagnetic materials, where strain is generated in response to an applied magnetic field. The strain in the ferromagnetic materials is a result of the rotations of small magnetic domains within the material, which cause internal expansion, ΔL. For a ferromagnetic material of length L_o, the magnetostriction is defined in terms of strain, as [1]:

$$\lambda = \frac{\Delta L}{L_o} \tag{2.1}$$

The magnetostriction in ferromagnetic materials arises from the rotation of magnetic domains under a magnetic field H. Each of these domains represents a region of uniform magnetization, when the applied magnetic field forces the domains boundaries (also called domain walls) resulting in shifting and motion of the domain walls. Both the rotation of the magnetic domains and the shift of domain walls yield changes in the magnetostrictive material shape and dimension (Figure 2.1), which is referred to as the magnetostriction that can be used for actuation purposes.

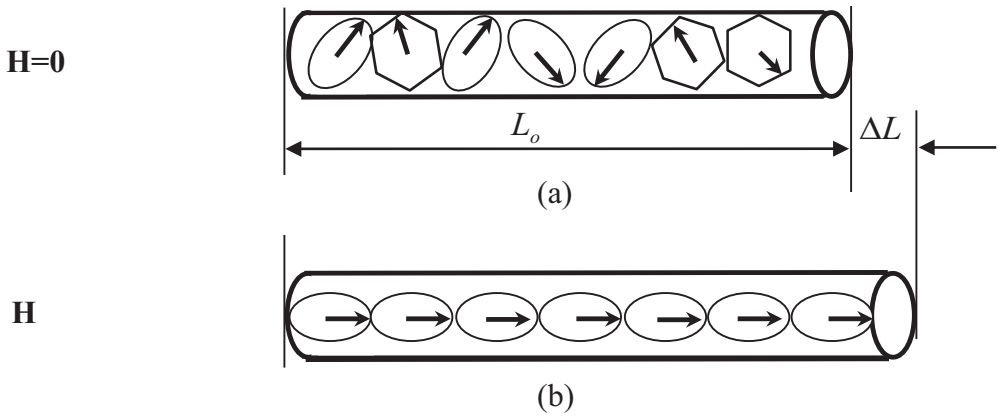

Figure 2.1: Magnetic domain orientations: (a) in the absence of a magnetic field, H=0 [1]; and (b) in the presence of a magnetic field [1].

Magnetostrictive actuators are built using a smart magnetostrictive material, such as "Terfenol-D", which consists of Terbium (Ter), Iron (Fe) and Dysprosium (D) [40]. This material is known to exhibit highest magnetostriction among the various known magnetostrictive alloys at room temperature [1]. Furthermore, the Terfenol-D possesses high energy density. A small size material could convert magnetic field intensity into mechanical energy at a high speed leading to a high magnitude force over a broad frequency band up to 15 kHz [1]. Such actuator designs do not contain moving parts and thus are not expected to encounter mechanical failures related to mechanical fatigue. Unlike piezoceramic materials, Terfenol-D materials are also known to be thermally robust. The smart materials in general tend to lose their properties when heated beyond the Curie temperature, the magnetostrictive materials, however, regain their properties when cooled [1,40]. These properties make Terfenol-D actuators attractive for numerous applications including all micropositioning tasks in environments where thermal and mechanical robustness are necessary. The main components of a typical Terfenol-D actuator include the following:

- **Terfenol-D rod** is the key component of a magnetostrictive actuator, which provides the actuation when exposed to a magnetic field. The rod yields predominantly axial deformations with minimal shear and radial stresses.

- **Drive coil**, encapsulates a Terfenol-D rod of length L_o and imposes alternating magnetic field H on the Terfenol-D rod. The ratio of number of the turns in the coil (n_c) to the rod length is referred to as the coil factor.

- **A permanent magnet** provides the Terfenol-D rod with a direct magnetic bias field H_{bias} to provide nearly linear bidirectional motion of the rod under an alternating input current.

- **A compression bolt** causes a residual stress in the Terfenol-D rod to align magnetic domains in the radial direction and thereby permits greater displacement attributed to rotation of the domains.

3.3 Characterization of output-input properties of a magnetostrictive actuator

Compared to piezoceramic micro actuators, the output-input hysteresis properties of magnetostrictive actuators have addressed in a relatively fewer studies. Most of the reported studies have focused on synthesizing a model and a compensator on the basis of either measured or reported output-input properties under selected operating conditions [7,10,11,12]. The proposed models and compensators may thus yield errors under different operating conditions. In particular, the influences of frequency, bias and magnitude of the excitation current, and the mechanical loading have not been fully characterized. Consequently, the primary goal of this chapter is to characterize input-output characteristics of a magnetostrictive actuator under a wide range of operating conditions involving input amplitude, rate and bias, and mechanical loads.

3.3.1 Experimental set-up

A magnetostrictive actuator (Etrema Inc; model MFR OTY77) was acquired for the experimental study. The magnetostrictive actuator comprised two 60.3 mm long and 12.3 mm diameter Terfenol-D rods, and three permanent magnets that provided a magnetic bias (≈ 44.1 kA/m) to permit the actuator to operate in the linear region. This actuator also houses a coil

surrounding the Terfenol-D rods, which are preloaded by a compression bolt and a spring washer. The Terfenol rods serve as the active component, which provide the output displacement when excited by a magnetic field. The coil factor of the coil encapsulating the drive rod of the actuator was specified the manufacturer as 5.09×10^3/m. The actuator, within the recommended operating range, provided a 100 μm stroke under 7.07 A recommended peak excitation current over a frequency range up to 1250 Hz.

The reported experimental studies on characterization of output-input properties of a magnetostrictive actuators have generally employed an LVDT for measurement of the actuator displacement [e.g.,11,65]. In [65], the author observed a lack of repeatability of measurement, which was believed to be caused by a drift either in the LVDT sensor fixture or in the material. In this study, a capacitive non-contacting position sensor (Lion Precision-model C23-C 250 μm range) was acquired for accurate measurement of the actuator displacement. The sensitivity of the sensor was 80 mV/μm with bandwidth of 15000 Hz and resolution of 35.53 nm. The sensor was calibrated considering 250 μm static gap with respect to the actuator head, where 125 μm was considered as the near gap and 375 μm as the far gap. The default output voltage of the sensor within the calibrated range was ± 10 VDC corresponding to the extreme near and far positions, while the output corresponding to the static position of 250 μm was 0 V.

A fixture was designed to ensure adequately aligned actuator and the sensor. Figure 2.2 illustrates pictorial views of the fixture designed to facilitate measurement of output displacement of the actuator. The capacitive displacement sensor is installed within a fixed block (3), while the actuator is supported on two pillow blocks (2). All these components were fixed to a flat aluminum plate (1), as illustrated in Figure 2.2. A power amplifier (model LVC 2016, AETECHRON) was employed to generate the desired input currents of various amplitudes and frequencies. The

excitation signal was synthesized in the ControlDesk platform and applied to the power amplifier in order to generate the desired excitation current to the drive coil of the actuator (Figure 2.3). The actuator displacement response and the applied input current were acquired in the ControlDesk platform at a sampling frequency of 50,000 Hz to evaluate output displacement-input current characteristics of the actuator.

3.3.2 Experiment design

An experiment was designed to study the effects of main factors on the hysteresis properties of the actuator, including the mechanical load, input bias, excitation frequency and magnitude, and type of excitation current. The experiment design involved four series of measurements with an objective to study: (i) the effects of input amplitude; (ii) the effects of magnetic bias; (iii) the influence of the input waveform; and (iv) the effect of mechanical load on the output-input characteristics. The experiment was designed to characterize the effects of these input parameters over a range of input frequencies up to 250 Hz. Inputs at higher frequencies up to 3,200 Hz were also applied to study the frequency response characteristics of the actuator and the effects of a mechanical load. Under a harmonic input current, the magnetic field is directly related to the applied current I such that:

$$H(t) = k_o \cdot (I_o \sin(2\pi ft) + I_{bias}) + H_{PM} \tag{2.2}$$

where I_o is amplitude of input current, f is frequency of the input, $k_o = n_c/L_o$, is the coil factor and I_{bias} is the bias in the input current, when considered. H_{PM} in the above equation is the magnetic field bias attributed to permanent magnets used in the actuator design. For the selected actuator, H_{PM} was estimated experimentally as 44.1 kA/m.

A complex harmonic waveform was also synthesized upon superposition of two harmonic signals, to study the major and minor hysteresis loops, such that:

$$I(t) = I_{AC1}\sin(2\pi f_o t) + I_{AC2}(6\pi f_o t) + I_{bias} \tag{2.3}$$

where I_{AC1} is the amplitude of the harmonic input at the chosen fundamental frequency f_o, and I_{AC2} is the amplitude corresponding to the frequency 3 times the fundamental frequency. Both the applied input current and output displacement data were acquired for subsequent analysis to fully characterize the minor and major hysteresis loops under different inputs. As an example, Figure 2.4 shows the measured output-input properties of the magnetostrictive actuator under an input current of 7 A amplitude at an excitation frequency of 10 Hz and 44.1 kA/m magnetic field bias. The results clearly show strong presence for asymmetric hysteresis nonlinearity as well as output displacement saturation. The hysteresis loops will be quantified either by the peak percent hysteresis, the peak hysteresis magnitude H_P normalized by peak-to-peak displacement M_P (Figure 2.4), or by the area bounded by the hysteresis loop.

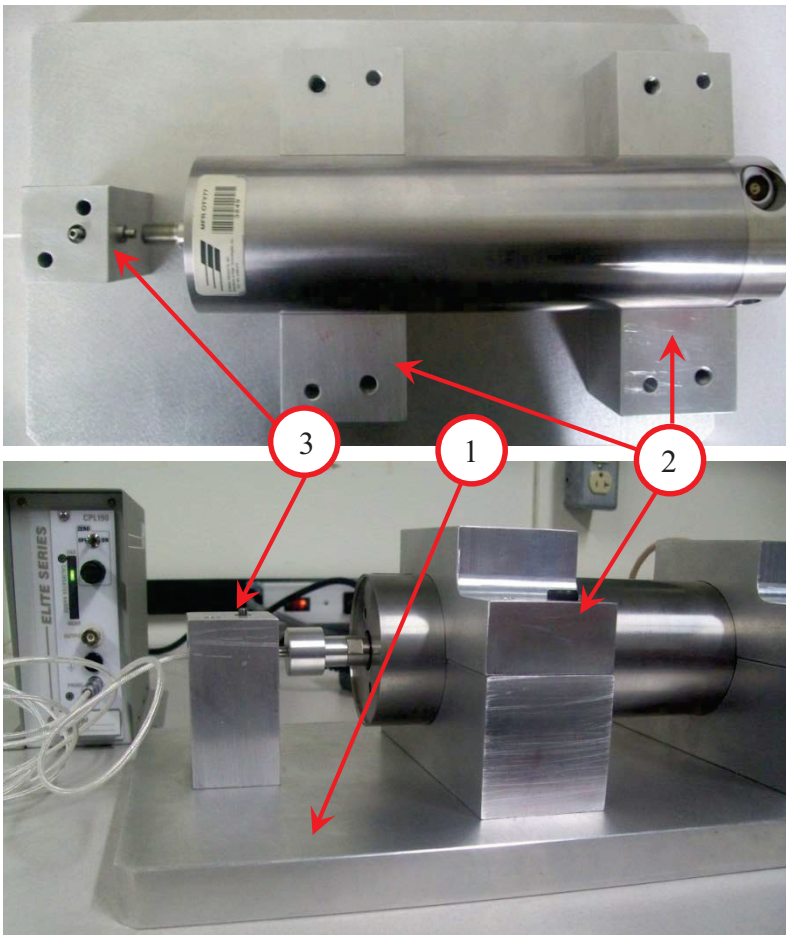

Figure 2.2: Pictorial views of the magnetostrictive actuator and sensor support fixture.

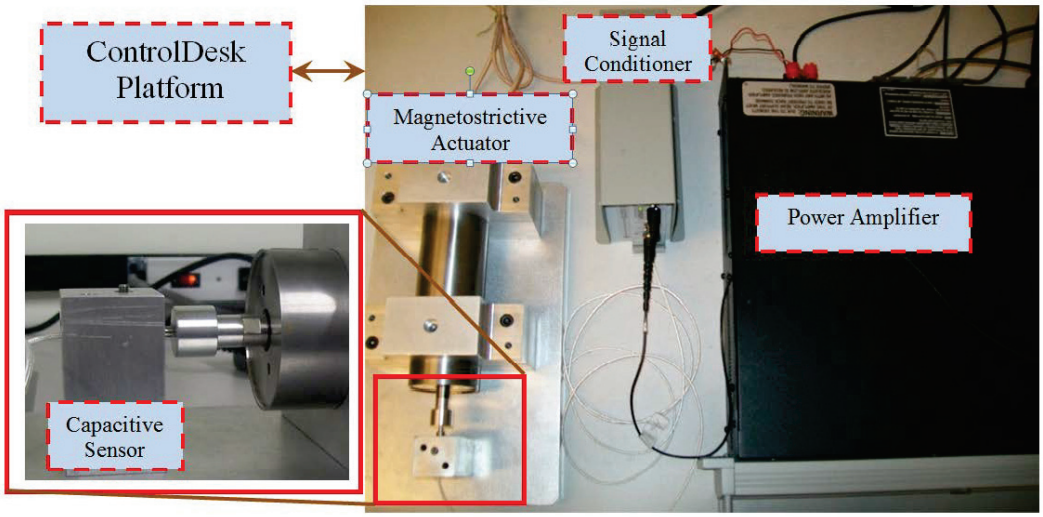

Figure 2.3: Experimental platform.

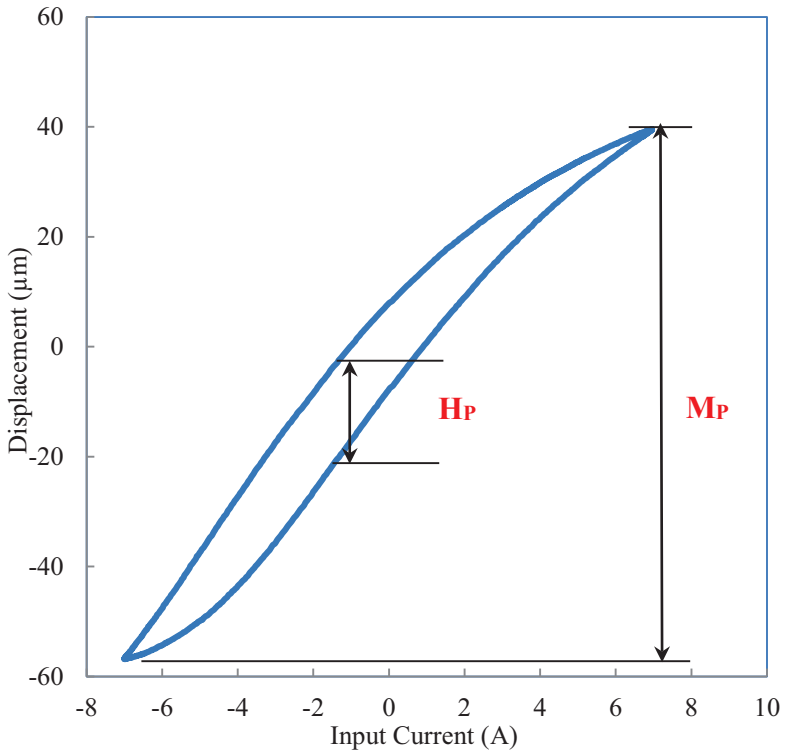

Figure 2.4: Measured output-input characteristics of the magnetostrictive actuator, displaying hysteresis, and output asymmetry ad saturation (I_o=7 A, f=10 Hz, H_{bias}=44.1 kA/m).

3.4 Measured output-input characteristics

The measured output displacement and input current data are analyzed to study the effects of input current amplitude, frequency, input bias and mechanical loads. These are discussed in the following subsections.

3.4.1 Input current amplitude and rate effects

Figure 2.5 illustrates the output-input characteristics and the major and minor hysteresis loops of the actuator. The data were acquired under a harmonic current with amplitude increasing gradually to 7 A within a duration of 1 s, as shown in Figure 2.6 (a). The input current was applied

at a constant frequency of 10 Hz. The figure also shows the time-history of the actuator displacement.

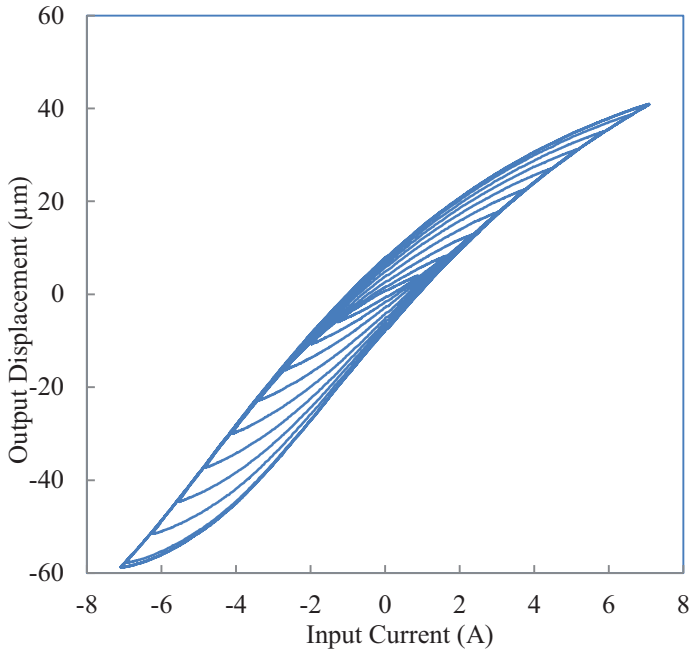

Figure 2.5: Measured output-input characteristics of the magnetostrictive actuator under a harmonic current excitation with linearly increasing current (f=10 Hz).

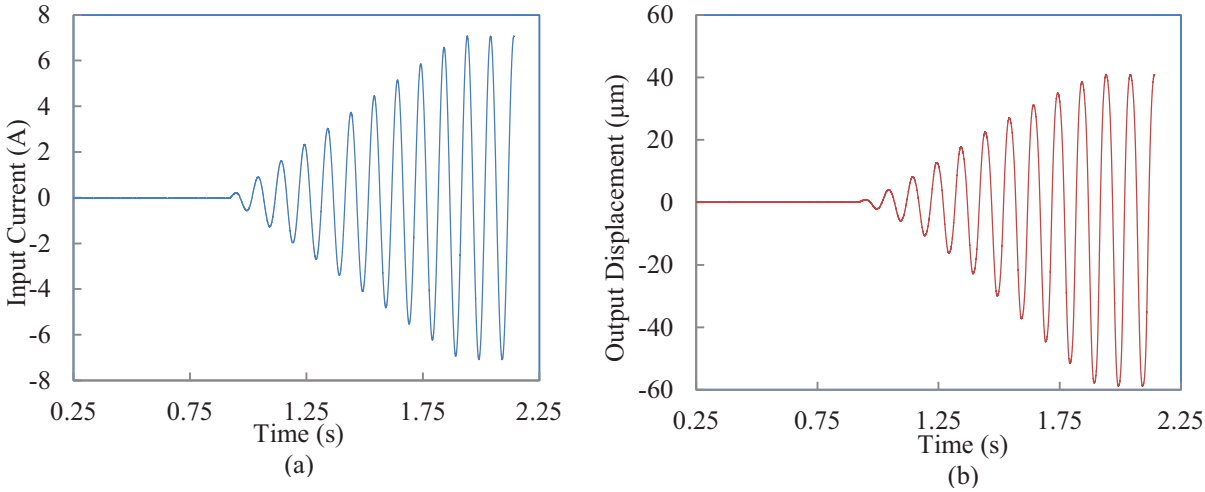

Figure 2.6: Time histories of: (a) Excitation current; and (b) Actuator displacement (f=10 Hz).

The output-input characteristics of the actuator were subsequently acquired under different constant amplitude currents (1, 2, 3, 4, 5, 6, 7, and 8 A) at a frequency 10 Hz and a magnetic bias

of 44.1 kA/m ($H_{bias}=H_{PM}$). The results are presented in Figure 2.7. Asymmetry of the hysteresis loops and output saturation are evident under excitations exceeding 2 A. The output asymmetry becomes significant at amplitudes exceeding 5 A. The time histories of the output displacement are also illustrated in Figure 2.8 over 1 complete cycle under different amplitudes of the input current.

Subsequent measurements were performed under harmonic inputs at different discrete frequencies in the 10 to 250 Hz frequency range. The output-input characteristics of the actuator subject to 5 different input amplitudes (2, 4, 5, 6 and 8 A) in the 10 to 250 Hz frequency range are illustrated in Figure 2.9. The results are presented for the constant magnetic bias of 44.1 kA/m, and different discrete excitation frequencies, namely, 10, 25, 50, 100, 200 and 250 Hz. The results show that the actuator hysteresis increases with increase in the excitation frequency of the applied input current, which has also been reported in other studies [7,8]. The responses within the frequency range considered in the measurements illustrate symmetric output-input loops under current amplitude of 2 A, while the output exhibits significant asymmetry at current of 4 A or greater.

The measurements acquired under the two extreme amplitudes, 2 A and 8 A, were selected to study the effects of the input rate on the hysteresis nonlinearities of the actuator. The area bounded by the hysteresis loops corresponding to these two amplitudes applied in the 10 to 250 Hz frequency range are evaluated and presented in Figures 2.10 (a) and 2.10 (b), as a function of the input frequency. Although, the output-input characteristics under the higher amplitude of 8 A are highly asymmetric, the area bounded the hysteresis loops shows nearly linear relation with the excitation frequency. Davino et al. [66] has also shown nearly linear energy loss of the actuator with the excitation frequency.

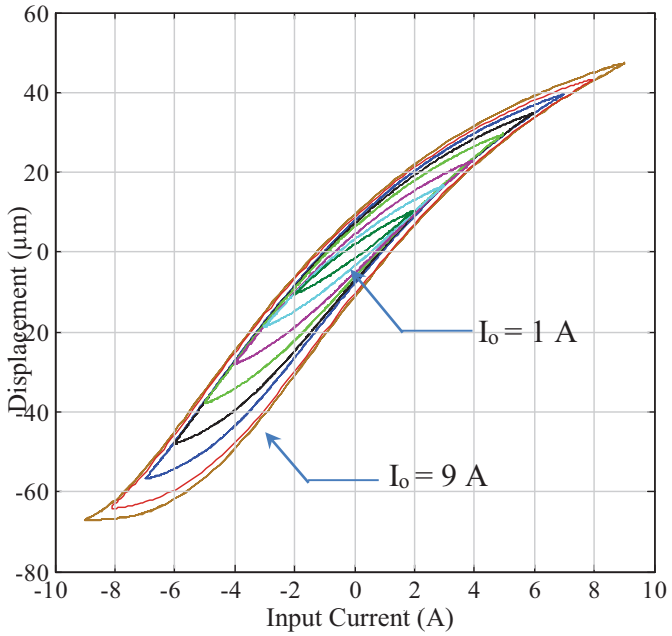

Figure 2.7: Measured hysteresis loops illustrating output asymmetry and saturation nonlinearities of the magnetostrictive actuator under different current amplitudes ranging from 1 to 9 A.

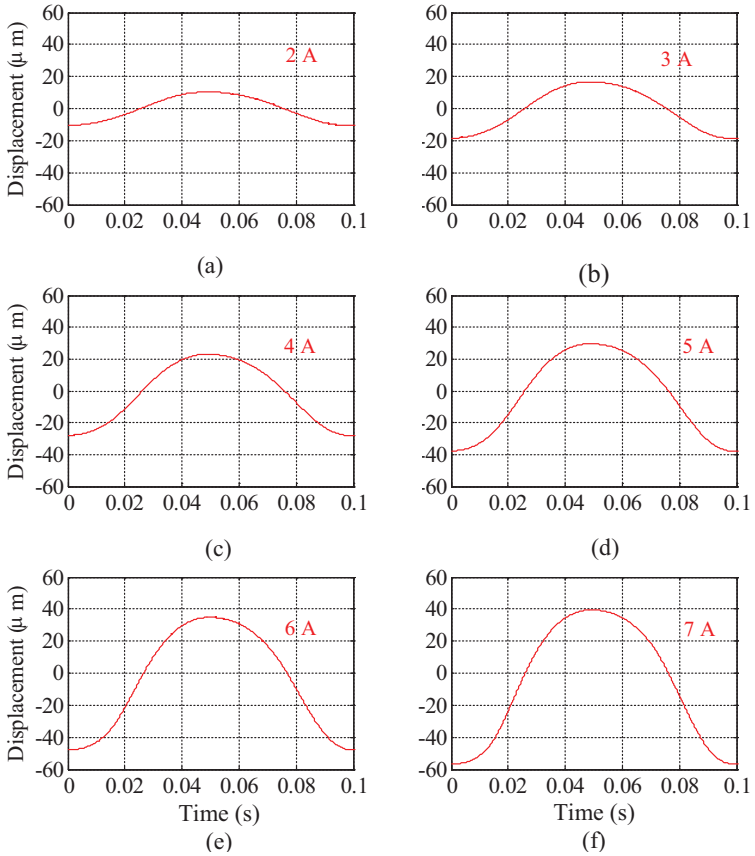

Figure 2.8: Time histories of output displacement measured under different amplitudes of applied current at frequency of 10 Hz (H_{bias}=44.1 kA/m).

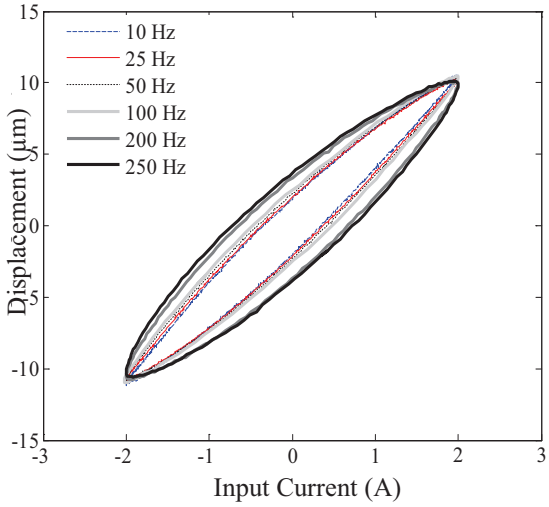
10 Hz
25 Hz
50 Hz
100 Hz
200 Hz
250 Hz
Displacement (μm)
Input Current (A)

(a)

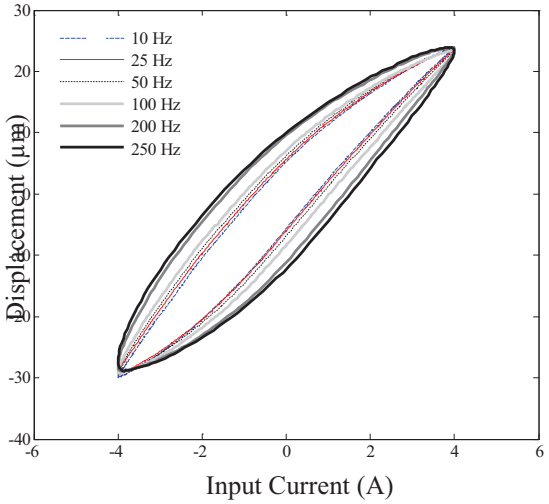
10 Hz
25 Hz
50 Hz
100 Hz
200 Hz
250 Hz
Displacement (μm)
Input Current (A)

(b)

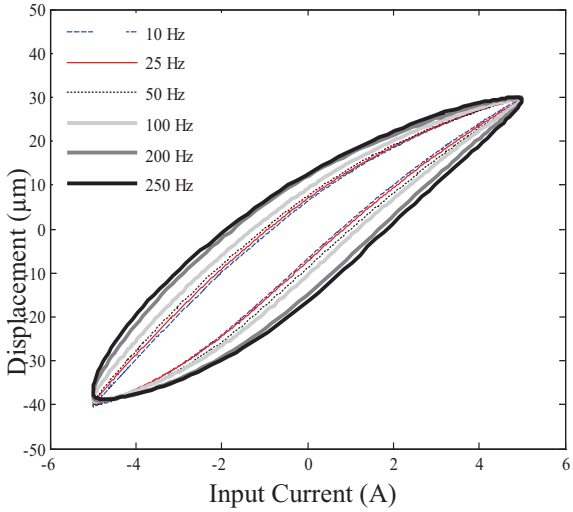
10 Hz
25 Hz
50 Hz
100 Hz
200 Hz
250 Hz
Displacement (μm)
Input Current (A)

(c)

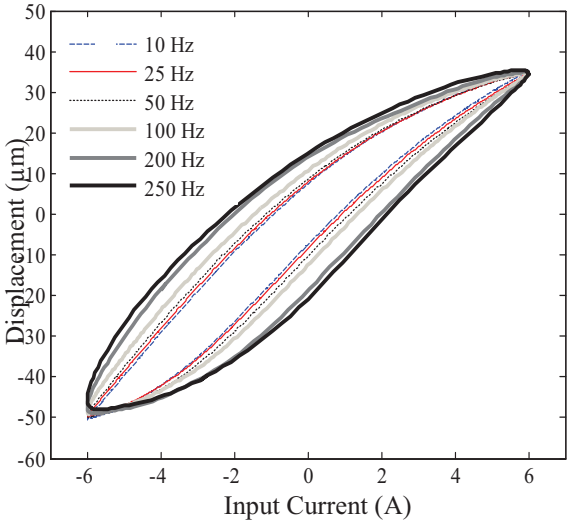
10 Hz
25 Hz
50 Hz
100 Hz
200 Hz
250 Hz
Displacement (μm)
Input Current (A)

(d)

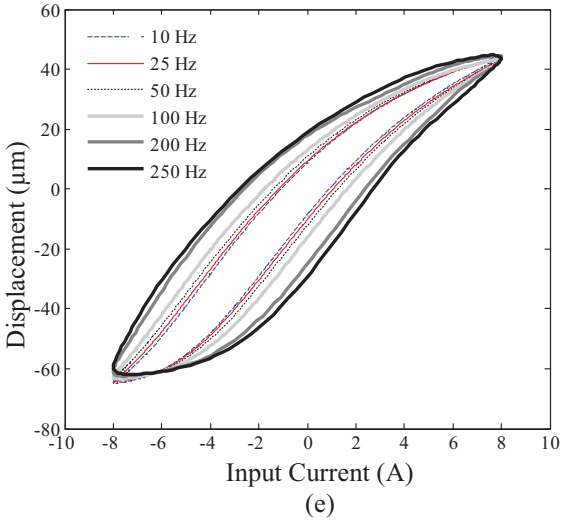
10 Hz
25 Hz
50 Hz
100 Hz
200 Hz
250 Hz
Displacement (μm)
Input Current (A)

(e)

Figure 2.9: Measured hysteresis loops relating output displacement response of the magnetostrictive actuator to the harmonic input current at different frequencies in the 10 to 250 Hz range: (a) I_o=2 A; (b) I_o = 4 A; (c) I_o = 5 A; (d) I_o = 6; and (e) I_o = 8 A (H_{Bias}=44.1 kA/m).

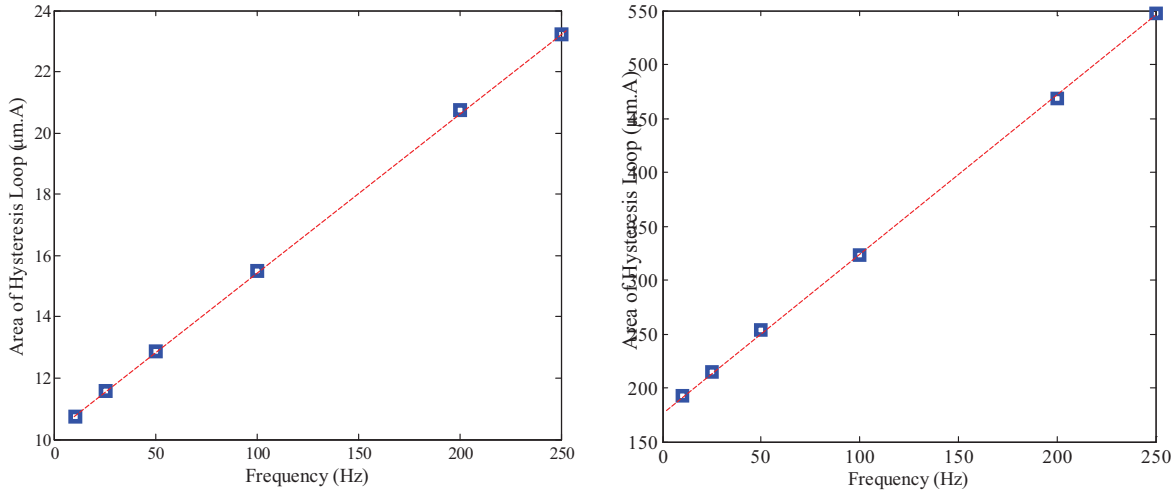

Figure 2.10: Area bounded by the hysteresis loops of the magnetostrictive actuator under harmonic excitations at different frequencies in the 10 to 250 Hz range: (a) I_o =2 A; and (b) I_o = 8 A (Bias=44.1 kA/m).

3.4.2 Minor and major hysteresis loops

The data acquired under the complex harmonic waveform are analyzed to obtain the major and minor hysteresis loops. Figure 2.11 illustrates the actuator output displacement versus the applied input current, $I(t) = I_{AC1} \sin(2\times f_o t)+I_{AC2} \sin(3\times 2f_o t)$, where the fundamental frequency f_o= 20 Hz, and I_{AC1}=4 and I_{AC2}=3 A. The applied input current was synthesized so as to characterize two minor hysteresis loops under peak-to-peak input current of 4.25 A. As the results demonstrate, the hysteresis minor loops show widely different peak-peak output displacement responses in the order of 18 and 26 μm, although both were characterized under identical peak-to-peak current of 4.25 A. This is attributed to the saturation of the output displacement.

The characterization was also performed considering alternate amplitudes of the complex harmonic waveforms (I_{AC1}=5 A, I_{AC1}= 2 A) and (I_{AC1}=3 A, I_{AC1}= 4 A), while the same fundamental excitation frequency was retained. Figure 2.12 presents the measured output displacement and

input current under both the complex harmonic waveforms. The results show substantial differences in the peak-peak displacement amplitudes of the minor loops under the two excitations, which is attributed to the output saturation.

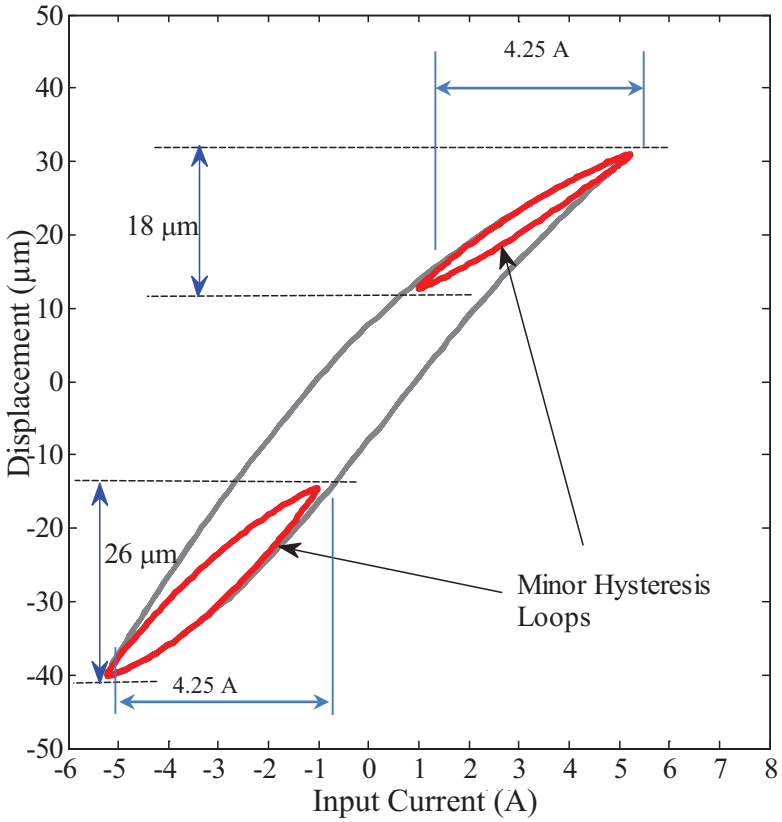

Figure 2.11: Measured output-input characteristics under the complex harmonic input current of the form, $I(t) = 4\sin(2\pi f_o t) + 3\sin(6\pi f_o t)$, illustrating major and minor hysteresis loops.

The measurements were repeated by letting f_o= 100 Hz, while three different sets of current amplitudes were considered: (I_{AC1}, I_{AC2}) = (3, 4), (4, 3) and (5, 2). Figure 2.13 illustrates the output-input characteristics of the actuator subject to three different complex harmonic currents with f_o= 100 Hz. The results clearly show significantly greater widths of the minor hysteresis loops compared to those observed under inputs with f_o= 20 Hz. The results thus suggest increase in the minor hysteresis loop with increase in the input rate, as it was observed for the major loops under simple harmonic inputs (Figure 2.9).

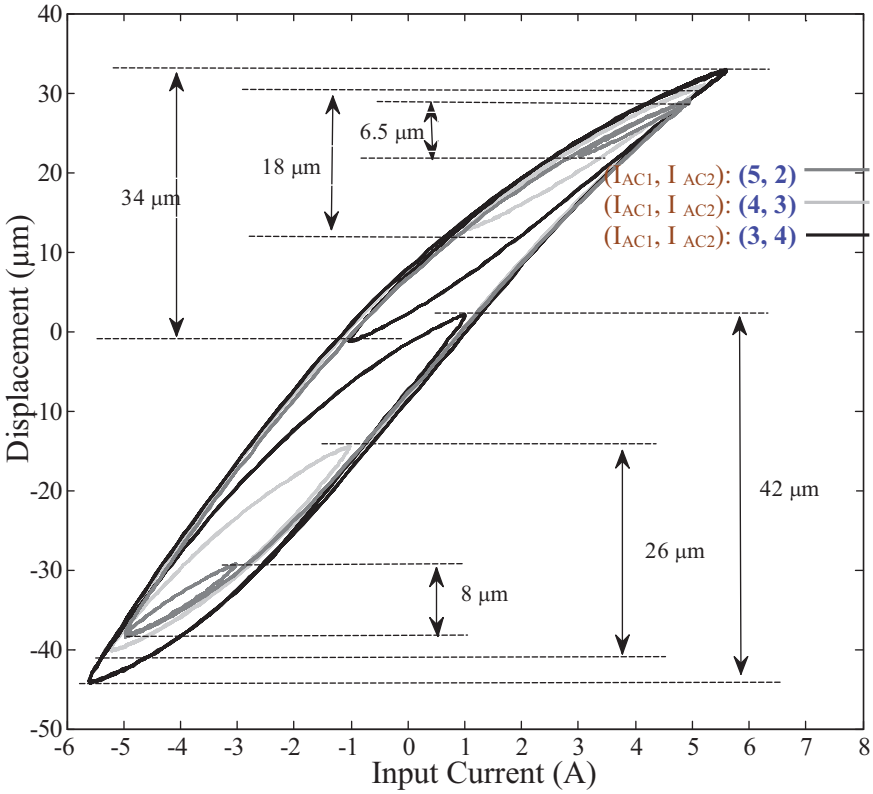

Figure 2.12: Output-input characteristics of the magnetostrictive actuator illustrating different minor hysteresis loops under three different complex harmonic inputs of the form: $I(t)= I_{AC1}\sin(2\pi f_o t)+ I_{AC2}\sin(6\pi f_o t)$, with ($I_{AC1}$, I_{AC2} = 3, 4 A), (I_{AC1}, I_{AC2} = 5, 2 A) and (I_{AC1}, I_{AC2} = 4, 3 A).

The displacement response obtained under the complex harmonic input, $I(t)= 3\sin(2f_o\pi t)+4\sin(3\times f_o\pi t)$, was selected for characterization of input rate effect on the output-input of the actuator. For this purpose, complex harmonic input was applied considering three different fundamental frequencies f_o=20, 50 and 100 Hz. The measured output-input characteristics, presented in Figure 2.14 (a), show two sets of minor hysteresis loops, labeled as 'A' and 'B'. The figure also shows variations in the major hysteresis loops attributable to changes in the input rate. The peak-peak displacements corresponding to both the minor loops remain constant in the order of 42 and 34 μm, respectively, irrespective of variations in f_o, which is due to identical input amplitudes. The

peak hysteresis of the minor loops, however, differs for different fundamental frequencies of the input. The peak percent hysteresis for each hysteresis loop was evaluated as illustrated in Figure 2.14 (b), as a function the fundamental input frequency f_o. The results show that the peak percent hysteresis corresponding to the minor loops increases nearly linearly with the excitation frequency for a given input amplitude, as it was observed for the major hysteresis loops (Figure 2.9).

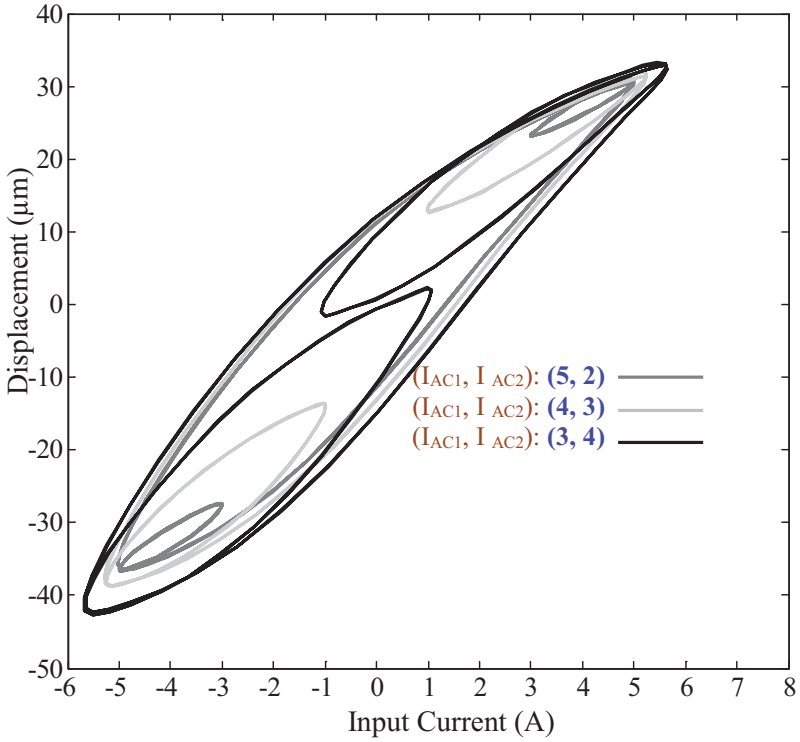

Figure 2.13: Measured hysteresis loops relating output displacement response of a magnetostrictive actuator with the complex harmonic input current, $I(t)=I_{AC1}\sin(2\pi f_o t)+ I_{AC2}\sin(6\pi f_o t)$, with three different amplitudes, $(I_{AC1}, I_{AC2})=(5, 2)$, $(4, 3)$, and $(3, 4)$, and fundamental frequency $f_o=20$ Hz.

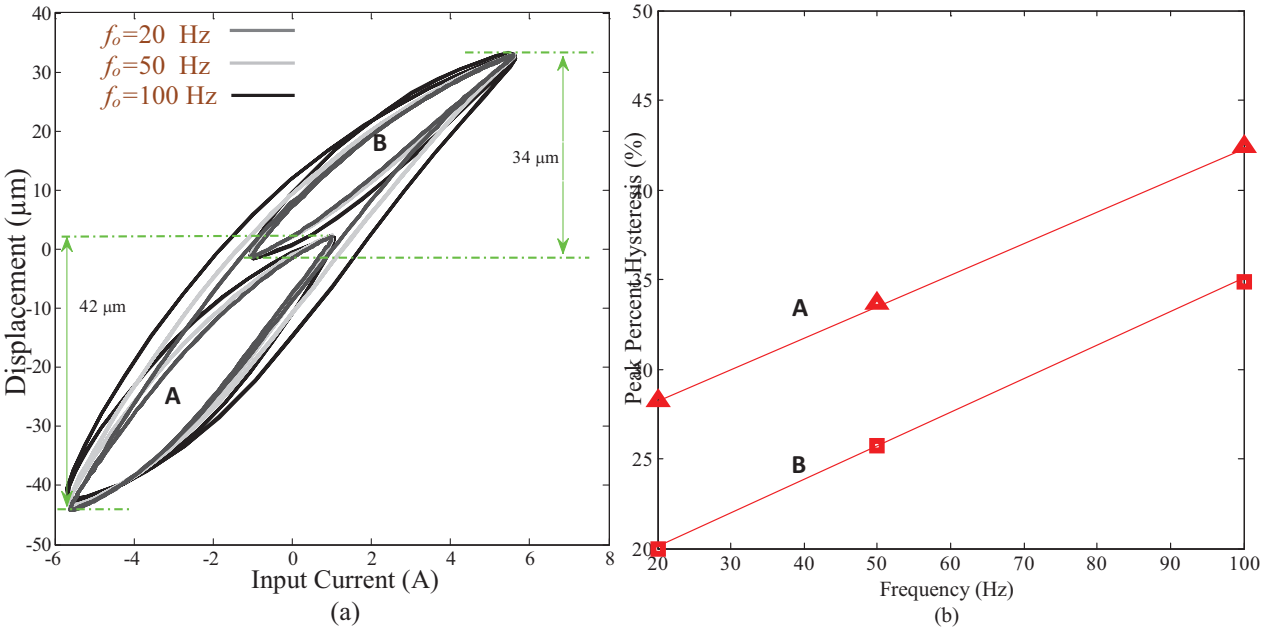

Figure 2.14: (a) Measured output-input characteristics of the actuator under complex harmonic input at different fundamental frequencies (f_o=20, 50 and 100 Hz) illustrating two sets of minor hysteresis loops 'A' and 'B'; and (b) The peak percent hysteresis of the minor hysteresis loops as a function of the fundamental frequency, f_o (set A; set B).

3.4.3 Input magnetic bias and rate effects

The saturation and asymmetry of the actuator output is strongly affected by the magnetic bias. The experiments were thus performed to study the effects of magnetic bias on the actuator displacement response. For this purpose, the current excitation with a bias (I_{bias}) was applied such that $I_b(t)= I_o\sin(2\pi ft)+ I_{bias}$. This resulted in a bias in the magnetic field strength in addition to that caused by the permanent magnets, H_{PM}, such that:

$$H(t) = k_o(I_o \sin(2\pi ft) I_{bias}) + H_{PM} \tag{2.4}$$

The total bias realized during the experiments can be directly related to the bias current, as [7]:

$$H_{bias}(t) = k_o I_{bias} + H_{PM} \tag{2.5}$$

The experiments were conducting considering three different levels of total magnetic bias, H_{bias}=30, 45 and 60 kA/m and four different excitation frequencies=10, 50, 100 and 150 Hz. The selected bias levels also include the bias of 44.1 kA/m due to permanent magnets.

The output-input characteristics of the actuator subject to different combinations of bias and excitation frequencies are illustrates in Figure 2.15(a), (b) and (c). The results show that peak-peak displacement and the output asymmetry are strongly affected by the magnetic bias. Increasing the magnetic bias limits the peak actuator displacement and yields greater output saturation, as seen in Figure 2.15(d). Both the peak displacement and the asymmetry, however, are not affected by variations in the input rate, which tends to yield greater hysteresis, as seen in Figure 2.16. The results suggest that increasing the bias can help reduce the hysteresis of the actuator. Selection of input bias would thus involve a compromise between the peak hysteresis and actuator displacement.

3.4.4 Mechanical load effect

The output-input properties of a magnetostrictive actuator have been invariably characterized in the absence of a mechanical load. In this study, an experiment is designed to study the effect of actuator load on the output-input characteristics. A compact loading fixture (mass=3.7 kg) was designed with four guiding rods, placed between two aluminum plates. The loading fixture could be easily fixed to the main fixture to facilitate measurement of output displacement of the actuator under the influence of different mechanical loads. For this purpose, the actuator fixture was oriented vertically, as shown in Figure 2.17. The figure shows the load-support fixture attached to the main fixture. The figure also shows an accelerometer attached to the load for measurement of acceleration.

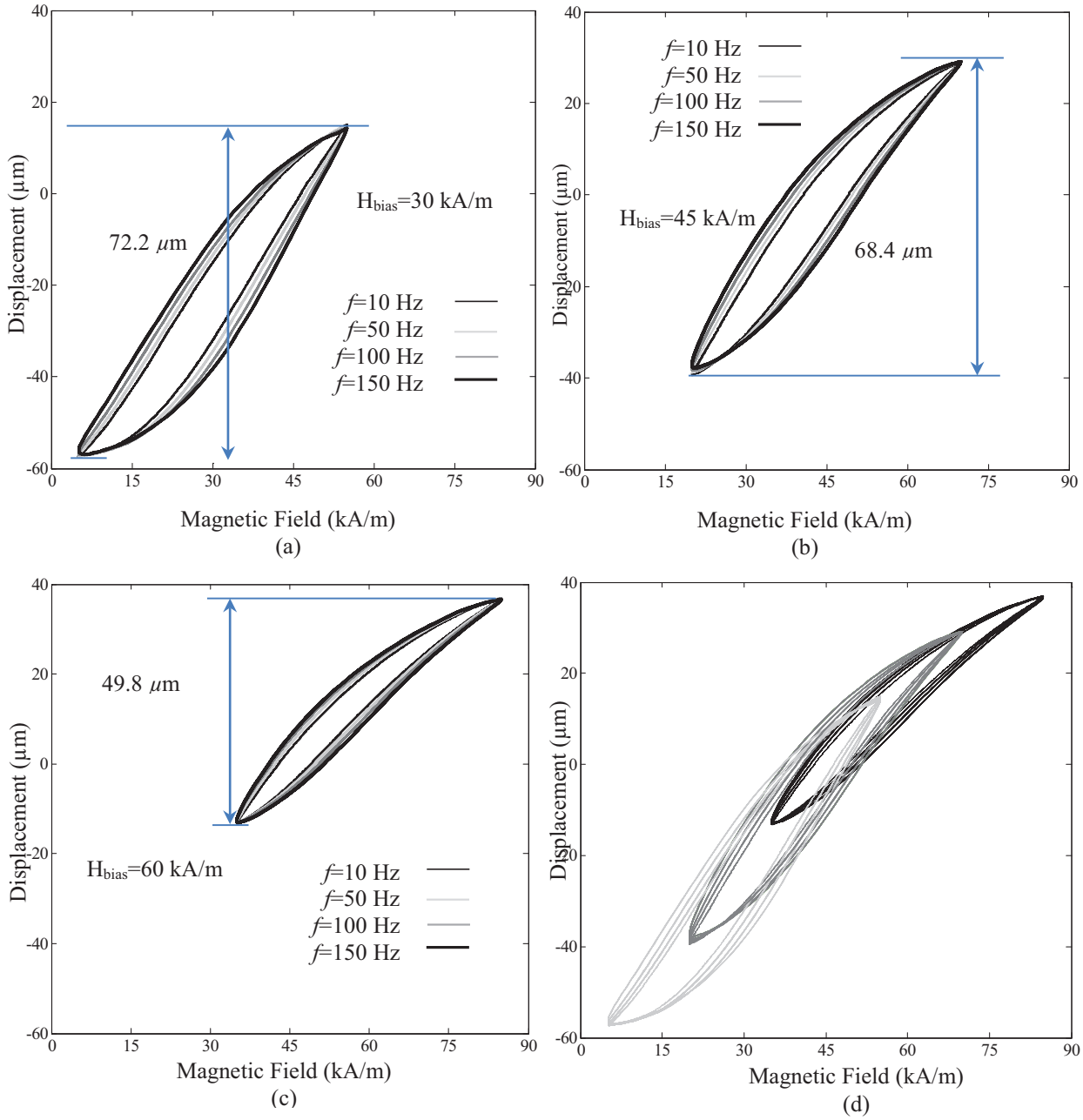

Figure 2.15: Influence of variations in the excitation frequency *f* on the output-input characteristics of the magnetostrictive actuator under different levels of magnetic bias (H_{bias}): (a) 30 kA/m; (b) 45 kA/m; (c) 60 kA/m; and (d) Comparison of the measured responses under three bias levels.

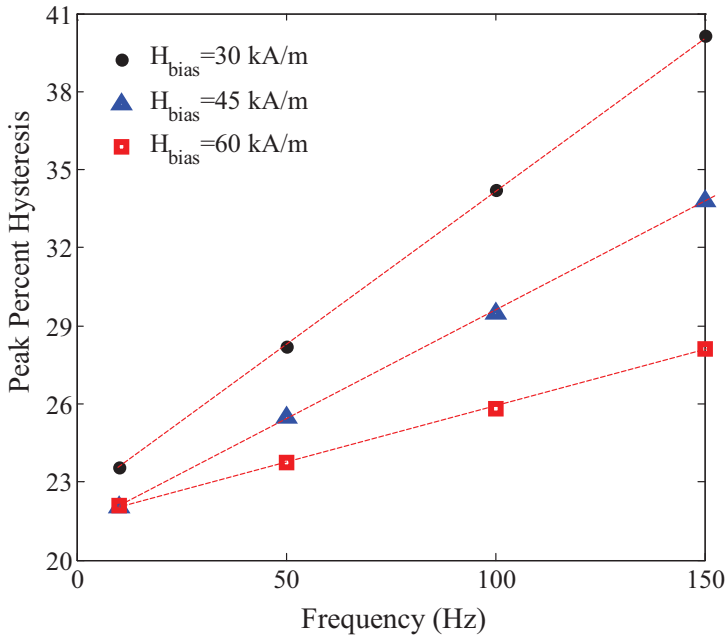

Figure 2.16: Variations in peak percent hysteresis in the displacement responses as a function of frequency of the applied input at three different levels of magnetic bias.

Different blocks of lead were added to the fixture to achieve desired loads. Each block was positioned within the load-support fixture constrained by the four guiding rods so as ensure pure vertical motion of the loaded actuator. In order to investigate the effective stiffness, the actuator was loaded with three different lead blocks weighting 5.5, 11 and 16.5 kg, while the static position of the actuator was measured with load-support fixture fastened to the drive rod of the actuator. The static stiffness of the actuator was subsequently obtained from the static load-deflection characteristics, shown in Figure 2.18. The measured data shows linear stiffness of 33.597 MN/m of the actuator. Considering the Terfenol-D rods mass of 112.2 g (specified by the manufacturer), the natural frequency of the actuator was obtained as 2756.2 Hz.

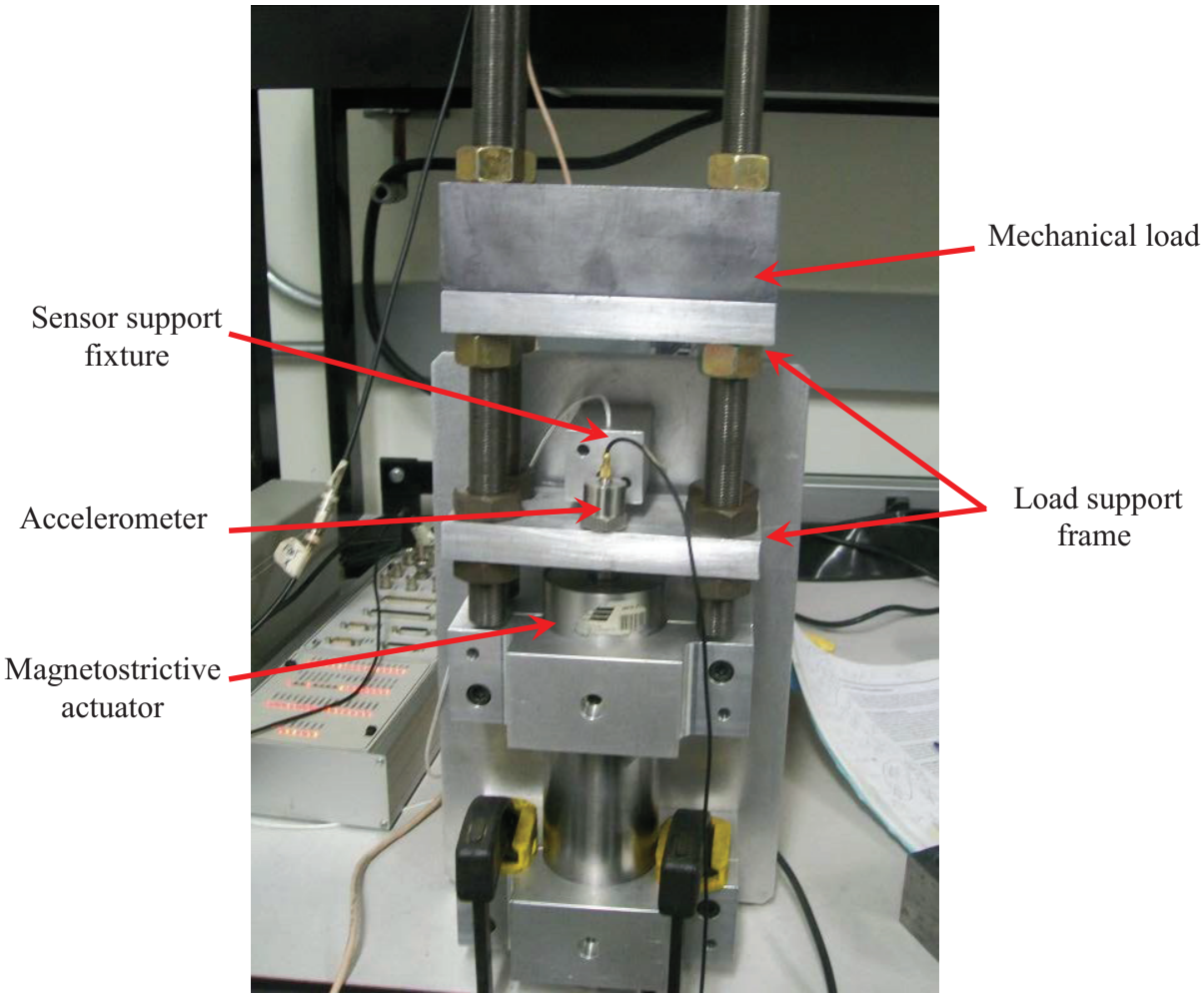

Figure 2.17: A pictorial view of magnetostrictive actuator with the mechanical loads.

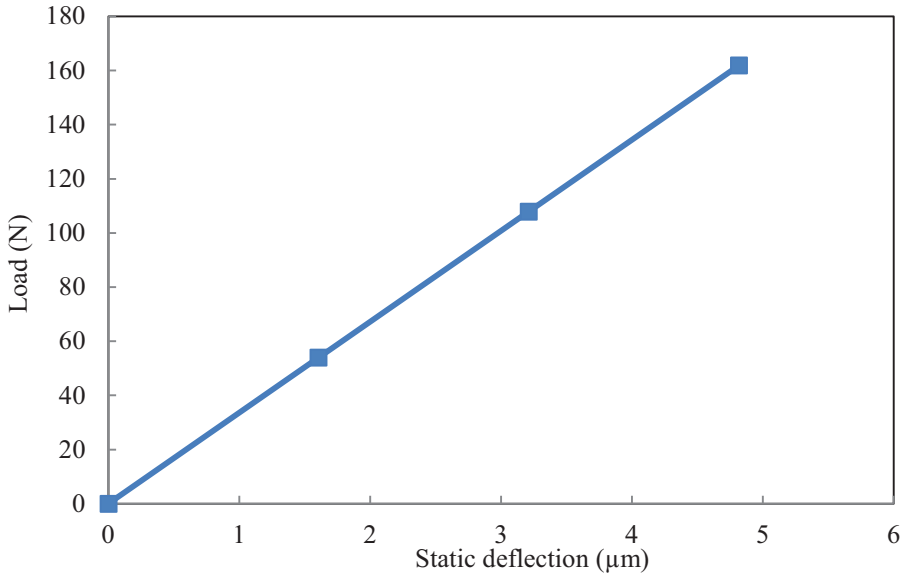

Figure 2.18: Static load-deflection characteristic of the magnetostrictive actuator.

The effective damping ratio of the actuator was also estimated through measurements of its response to a step change in the current. The measured displacement responses revealed nearly exponential decay, as seen in Figure 2.19 under a 1 A step input. The effective damping was subsequently, estimated using the logarithmic decrement method [67]. It should be noted that the measurement were initially performed with unloaded actuator, although the actuator rod was coupled to an aluminum head (11 g) with a nut (39 g). The effective damping ratio of the unloaded actuator was estimated as, ζ=0.12, while the measured data revealed an oscillation frequency of 14.362 kHz. The actuator natural frequency was subsequently obtained as 2,300 Hz. This frequency would correspond to Terfenol-D rods mass 112.45, which is quiet close to that specified by the manufacturer (111.2 g). The measurements were repeated under 0.5, 0.75 and 1.5 A step inputs. The analysis of the measured data revealed very similar values of damping coefficients and natural frequency.

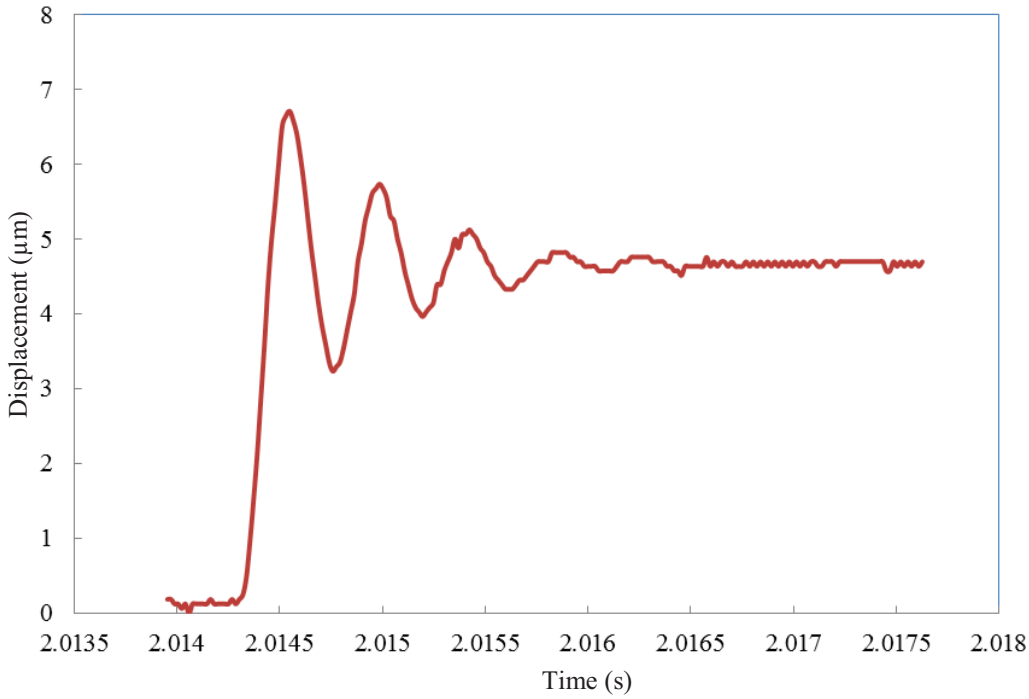

Figure 2.19: Time history of the displacement response of the unloaded actuator to 1 A step current.

The displacement responses of the unloaded as well as loaded actuator were measured under different amplitudes of harmonic currents. The measurements were performed over a wide frequency range, up to 3,100 Hz in order to characterize frequency response of the actuator with and without the mechanical loads. Figure 2.20 illustrates the output-input characteristics of the unloaded actuator as well as loaded actuator under 1.0 A harmonic current at different frequencies. The results are presented for the actuator without the load, where the effective mass on the actuator is due to Terfenol-D rods, the head and the nut (162 g), as shown in Figure 2.20 (a). Figure 2.20 (b), (c) and (d) illustrate the output-input properties under additional mechanical loads of 3.7, 9.2 and 14.7 kg, respectively. The results clearly show higher displacement amplitude at higher frequencies for all the load conditions. Furthermore, the area bounded by the output-input loops increases with the frequency and tends to be substantially high at higher frequencies. The peak displacement response also tends to be higher with increasing mass.

From the results, it is evident that the output-input characteristics of the actuator are most substantially affected by the actuator load. This is attributable to dynamic properties of the actuator. Increasing the mass reduces the actuator natural frequency and alters its dynamic response, as seen from the measured frequency responses of the unloaded as well as the loaded actuators in Figure 2.21. The figures show the variation in the peak displacement response, normalized with respect to that measured at a low frequency of 40 Hz, with the excitation frequency. The output-input loops in Figure 2.20 show substantial rotations of the loops, at higher frequencies, which are attributed to the phase between the displacement response and the excitation current.

The effects observed in Figure 2.20 cannot be attributed to hysteresis of the Terfenol-D rod actuator but to the inertia. These results suggest that output-input relations of the actuator need to be characterized considering the inertia effect apart from the material hysteresis. This would also hold for an unloaded actuator, where the effective mass of the rod also contributes to the perceived hysteresis.

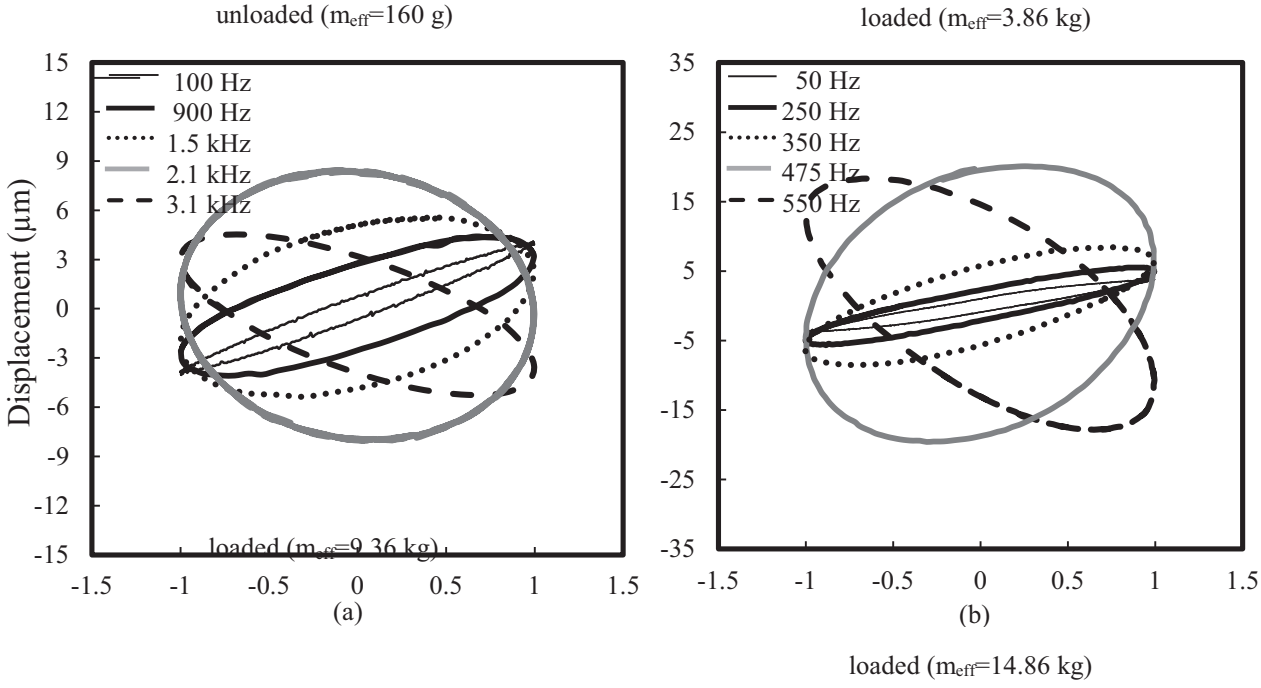

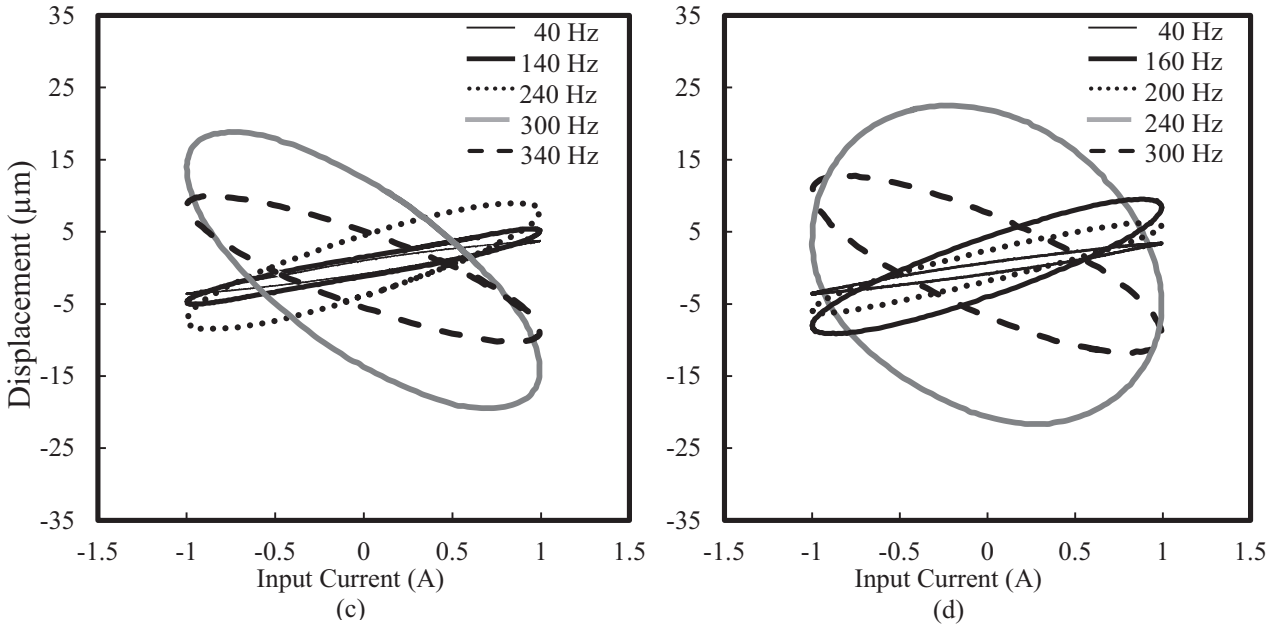

Figure 2.20: The output-input characteristics of the unloaded and the loaded actuator under 1.0 A harmonic current at different frequencies.

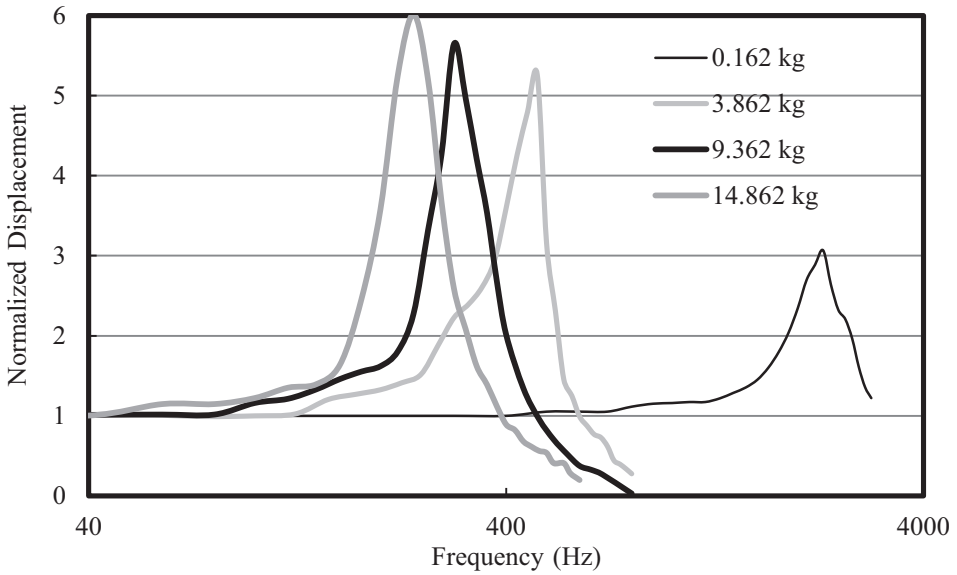

Figure 2.21: The normalized output displacement of the unloaded and loaded actuator under 1.0 A harmonic current at different frequencies.

3.5 Summary and conclusions

The output-input characteristics of the magnetostrictive actuator were explored under a wide range of input current and actuator loads. These included the input current amplitude, excitation frequency, bias in the input current and different mechanical loads. The output-input characteristics of the unloaded actuator suggested substantial output asymmetry and saturation under medium to high amplitude excitations, and increasing hysteresis with increasing excitation frequency. The area bounded by the hysteresis loop increased nonlinearly with the input amplitude but nearly linearly with the excitation frequency. The variations in the magnetic field bias mostly affected the output asymmetry and saturation, and the displacement response.

An increase in the magnetic bias could help limit the peak hysteresis at the expense of reduced displacement response of the actuator, however, was not affected by the frequency of input, in the range considered in the study. The displacement response of the actuator, however, increased at substantially higher frequencies, particularly when the excitation frequency approached the actuator natural frequency. Increasing the actuator load resulted in substantially lower natural frequency of the actuator, and thereby considerably higher displacement response at higher frequencies. From the results, it is deduced that the inertia effect strongly alters the output-input characteristics of the actuator. The modelling effects thus need to incorporate the inertia effect. The inertia effect due to mass of the actuator load alone may also contribute to actuator hysteresis and the rate effect, which has not yet been addressed.

CHAPTER 3

COMPENSATION OF PLAY OPERATOR-BASED PRANDTL-ISHLINSKII MODEL USING STOP OPERATOR WITH APPLICATION TO PIEZOCERAMIC ACTUATOR

4.1 Introduction

Piezoceramic actuators have the advantages of producing large force, fast response and high precision [1,57,68] and have been widely used in nano-positioning systems [69], such as AFM [70], SPM [71], dual-stage servo system for HDDs [68] and active aperture [72]. However, piezoceramic actuators exhibit limited tracking performance in precision control due to their inherent hysteresis non-linearity, which can severely limit the system positioning performance by giving rise to undesirable inaccuracy or oscillations, even leading to an instability of the closed-loop system [57,73]. Therefore, considerable efforts have been made towards design of controllers

for compensating the hysteresis effect. The majority of the reported approaches are inversion based compensation approaches [57,42].

There are several models available for describing hysteresis behaviour, such as the Preisach model, the Prandtl-Ishlinskii (PI) model, the Bouc-Wen model and the Duhem model. Among them, the PI model is attractive due to its simplicity and suitability to construct feedforward compensator for the purpose of mitigating the hysteresis effect. A PI model could be constructed through superposition of two different operators. One is the stop operator-based Prandtl-Ishlinskii (SPI) model, and another is the play operator-based Prandtl-Ishlinskii (PPI) model. The SPI model, which was formulated for describing elastoplasticity hysteresis behavior of materials [26], yields concave clockwise hysteresis loops. However, the PPI model yields convex counterclockwise hysteresis loops. Thus, it makes the SPI model a potential feedforward compensator if proper weights and thresholds can be analytically derived. Kuhnen and Janocha [74] attempted a SPI model to compensate for hysteresis described by a PPI model, where the thresholds and weights of the SPI model were calculated in an adaptive manner based on an error function. In this paper, the PPI model is utilized to describe the hysteresis behavior of the piezoceramic actuator. The thresholds and the weights of the SPI model are subsequently analytically derived for the first time in the literature, which constitutes the main contribution of the paper. The effectiveness of the SPI model in compensating the hysteresis non-linearity is investigated in the laboratory by implementing the SPI model with a piezo micro-positioning stage in a feedforward manner. It should be noted that because the inverse of the PPI model and the derived SPI model serve the same role as a compensator of the PPI model, the derived SPI model can be thought as an alternative to the inverse compensation.

4.2 The Prandtl-Ishlinskii model

4.2.1 The PPI model

The PPI model integrates the play operator together with a weight function to characterize the hysteresis non-linearity. The properties of the PPI model have been described in details in [26]. The PPI model is defined as:

$$\overline{\Phi} = \int_0^R \overline{p}(r) F_r\,[v](t).dr \tag{3.1}$$

where $\overline{p}(r)$ is weighting function, satisfying $\overline{p}(r) > 0$ with $\int_0^\infty r\overline{p}(r) < \infty$, R is a constant so that the weight function p(r) vanishes for large value of R. $F_r[v]$ is the play operator defined by [26]:

$$\begin{aligned} F_r[v](t) &= f_r(v(0),0) \\ F_r[v](t) &= f_r(v(t), F_r[v](t_i)) \end{aligned} \tag{3.2}$$

for $t_i < t \le t_{i+1}$; $0 \le i \le l+1$, with

$$f_r(v, F_r[v]) = \max\{v(t) - r, \min\{v(t) + r, F_r[v](t)\}\} \tag{3.3}$$

where $0 = t_0 < t_1 < \ldots < t_l = T$ is a partition of $[0,T]$ such that the function $v(t) \in C[0,T]$, $C[0,T]$ denotes the space of continuous function on [*0*, *T*], is monotone on each of the subintervals [t_i, t_{i+1}]. The input-output relationship of a play operator is shown in Figure 3.1. The play operator is rate-independent, Lipchitz-continuous and monotone.

The PPI model can also be formulated in the discrete form as:

$$\Phi[v](t) = \sum_{i=0}^{n_p} p(r_i) F_{r_i} \tag{3.4}$$

where n_p is the number of the play operators of thresholds, $0 = r_0 < r_1 < \ldots < r_n = R$, and $p(r_i)$ are the weights of the density function, defined as:

$$p(r_i) = \overline{p}(r_i)(r_{i+1} - r_i) \tag{3.5}$$

For $r_0 = 0$, the output of the PPI model can be expressed as:

$$\Phi[v](t) = qv(t) + \sum_{i=1}^{n_p} p_r(r_i) F_{r_i}[v](t) \tag{3.6}$$

where $q = p(0) = p_0$.

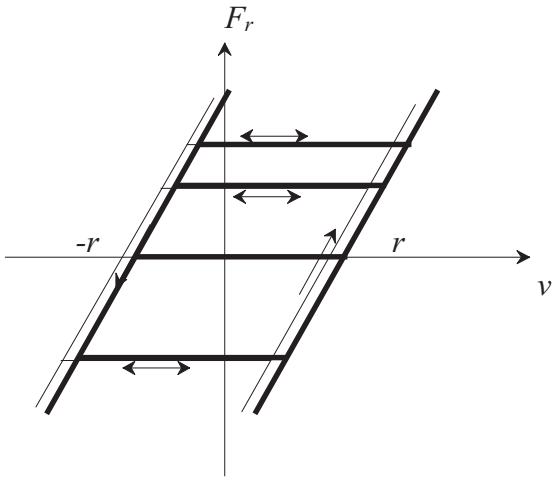

Figure 3.1: Input-output relationship of the play hysteresis operator.

4.2.2 The SPI model

The Prandtl-Ishlinskii model has also be constructed using the stop operators for describing hysteresis nonlinearity in materials [26]. Unlike the PPI model, the stop operator-based Prandtl-Ishlinskii (SPI) model exhibits clockwise hysteresis loops, attribute to the properties of the stop operator. Similar to the play operator, the output of a stop operator is a function of its threshold *s* and the input *v*. The input-output relationship of a stop operator is illustrated in Figure 3.2. The output of the stop operator for the input $v(t) \epsilon C$ [0, *T*] can be expressed as:

$$E_s[v](0) = e_s(v(0))$$
$$E_s[v](t) = e_s(v(t) - v(t_i) + E_s[v](t_i)) \tag{3.7}$$

for $t_i < t \le t_{i+1}$; $0 \le i \le l+1$, with:

$$e_s = \min(s, \max(-s, v)) \tag{3.8}$$

where $0 = t_0 < t_1 < \ldots < t_l = T$ is a partition of $[0, T]$ such that the function $v(t) \in C[0,T]$, $C[0,T]$ denotes the space of continuous function on [*0*, *T*], is monotone on each of the subintervals [t_i, t_{i+1}].

Some of the essential properties of the stop operator can be described as follows:

- **Clockwise operator:** The stop operator yields clockwise input-output curves, while the play operator results in counter-clockwise input-output curves;

- **Monotonicity:** The stop operator E_s is a monotone operator. For a given input $v(t) \epsilon C[0, T]$, the following property holds [16] :

$$(E_s[v](T) - E_s[v](0))(v(T) - v(0)) \ge 0 \tag{3.9}$$

- **Lipschitz-continuity:** For a given input $v(t) \epsilon C[0, T]$, the stop operator is Lipschitz continuous [26].

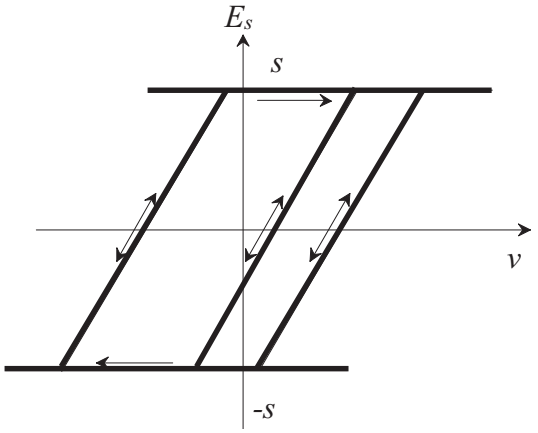

Figure 3.2: Input-output relationship of the play hysteresis operator.

The output of the SPI model is formulated upon integration of the stop operator corresponding

to different thresholds s in conjunction with the positive and integrable density function $\overline{w}_s(s)$, such that [26]:

$$\overline{\Psi}[v](t) = \int_0^S \overline{w}_s(s) E_s[v](t) dr \tag{3.10}$$

The output of the SPI can also be described by n stop operators, $0 = s_0 < s_1 < ... < s_n = S$, such that:

$$\Psi[v](t) = \sum_{i=1}^{n_s} w_s(s_i) E_{s_i}[v](t) \tag{3.11}$$

where $w_s(s)$ represents the weights of the density function as:

$$w_s(s_i) = \overline{w}_s(s_i)(s_{i+1} - s_i) \tag{3.12}$$

Owing to the Lipschitz continuous stop operator E_s and integrable density function, it can be concluded that the stop-operator based Prandtl-Ishlinskii (SPI) model is Lipschitz-continuous for a given input $v(t) \epsilon C[0, T]$. It can be further concluded that the SPI model is monotone operator and the weight function is integrable and positive.

4.3 Compensation of hysteresis via SPI model

4.3.1 Feedforward compensation

The feedforward compensation, shown in Figure 3.3, was used in this paper to obtain identity mapping between the desired input $v(t)$ and the output $u(t)$ as:

$$u(t) = \Phi[\Psi[v]](t) \tag{3.13}$$

As shown in section 3.2.2, the SPI model yields clockwise hysteresis loops, which is essential to introduce the SPI model as a compensator to mitigate the hysteresis effects described by the PPI model.

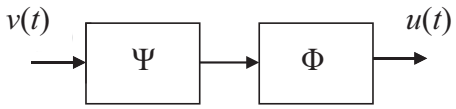

Figure 3.3: Open-loop control system.

Lemma 3.1: SPI model Ψ is a compensator of the PPI model Φ if, for any initial output Φ(0), there exists a Ψ(0), such that the series connection of the compensator and the model yields identity transformation starting from the initial states Φ(0) and Ψ(0). And v=Ψ[Φ(v)]=Id[v]= v (v>0).

Figure 3.4 shows the inner structure for SPI model and the PPI model. The two parameter, thresholds s_i and the weights w_i of the SPI model can be analytically derived based on the initial loading curve and the given thresholds r_i and the weights p_i of the PPI model.

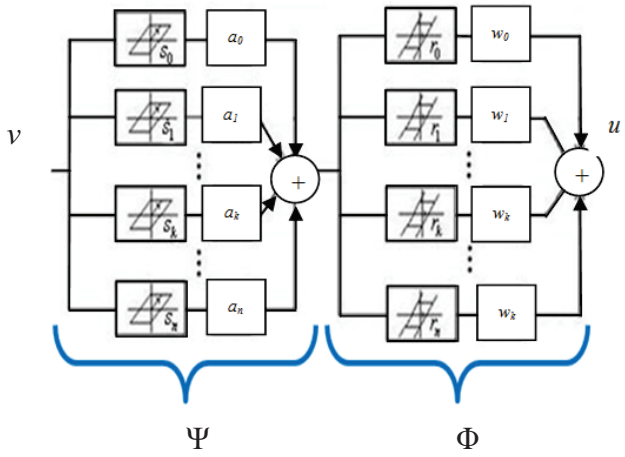

Figure 3.4: Inner structure of the stop-operator based Prandtl-Ishlinskii model (SPI) and play-operator based Prandtl-Ishlinskii model (PPI).

4.3.2 Analytical implementation of the feedforward compensator by using SPI model

In this section, the initial loading curve of the PPI model is presented as a tool to analytically calculate the thresholds and weights of the SPI model. This curve describes the possible hysteresis

loops generated by the Prandtl-Ishlinskii model. The initial loading curve of the PPI model can be expressed as:

$$\phi_p(r) = \sum_{i=0}^{n_p} \max(0, r - r_i) p_i \tag{3.14}$$

where $r \in [r_0, r_{n_p}]$, and r_0=0, n_p is the number of the play operator. The function $\phi_p : \mathrm{R}^+ \rightarrow \mathrm{R}^+$ is convex and increasing function. In order to obtain the parameters of the compensator, the initial loading curve ϕ_s of the stop-operator based Prandtl-Ishlinskii model is defined as:

$$\phi_s(r) = \sum_{i=0}^{n_s} \min(s, s_i) w_i \tag{3.15}$$

where $\phi_s : \mathrm{R}^+ \rightarrow \mathrm{R}^+$ is concave and increasing function, and n_s is the number of the stop operator. $s \in [0, s_0]$, s_0 is set to be a large positive real number, satisfying $s_0 > \max(v(t))$, to ensure strict monotonicity of the SPI model.

As shown in Figure 3.5 (a) and (b), the initial loading curve of the SPI model ϕ_s is concave, while the initial loading curve of the PPI model ϕ_r is convex. Owing to the convex initial loading curve the hysteresis loops resulting from the PPI model would be counter clockwise loops. On the other hand, hysteresis loops resulting from the SPI model is clockwise loops. This denotes that a composition between the SPI and PPI models could yield identity in input-output curves with proper thresholds and weights and the initial loading curve of them should be also symmetric about the line $y = x$, shown in Figure 3.5 (c).

Figure 3.6 shows the relationship of the initial loading curves between the SPI model and the PPI model. In order to obtain the proper weights and thresholds of the SPI model which can effectively

mitigate the hysteresis non-linearity described by the PPI model, the thresholds and the initial loading curve of the SPI model must satisfy:

$$s_i = \phi_r(r_i) \tag{3.16}$$

$$\phi_s(s_i) = r_i \tag{3.17}$$

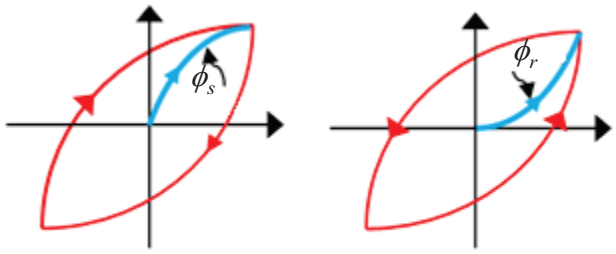

(a) (b)

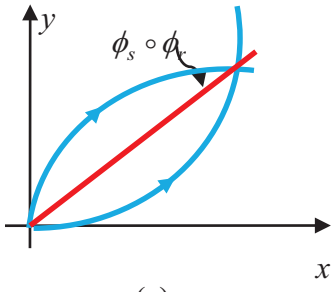

(c)

Figure 3.5: (a) Initial loading curve of the stop operator based Prandtl-Ishlinskii (SPI) model SPI, (b) Initial loading curves of the stop operator based Prandtl-Ishlinskii (PPI) model, (c) Composition of the initial loading curves of the SPI and PPI models to achieve perfect compensation.

ϕ_s
ϕ_r

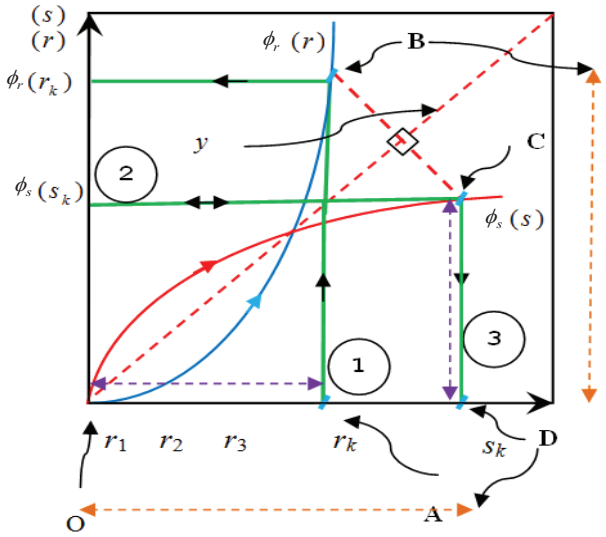

Figure 3.6: The initial loading curves of the SPI and PPI models.

According to equations (3.16) and (3.17) for any point $B(r_k, \phi_r)$ on the initial loading curve of the PPI, it can always find a point $C(s_k, \phi_s)$ on the initial loading curve of the SPI model. Furthermore, points C and B are symmetric about the line y=x, and OA=CD and AB=OD. The thresholds of the SPI model may be related to those of the PPI model in the following manner:

$$\begin{aligned} s_1 &= r_1 p_0 \\ s_2 &= (r_2 - r_1)p_1 + r_2 p_0 \\ s_3 &= (r_3 - r_1)p_1 + (r_3 - r_2)p_2 + r_3 p_0 \\ s_n &= (r_n - r_1)p_1 + (r_n - r_2)p_2 + \ldots + r_n p_0 \end{aligned} \tag{3.18}$$

Then the weights if the SPI model w_i can be calculated according to (3.17) as:

$$\begin{aligned} & s_1 w_0 + s_1 w_1 + s_1 w_2 + s_1 w_3 + \ldots + s_1 w_k + \ldots + s_1 w_n = r_1 \\ & s_2 w_0 + s_1 w_1 + s_2 w_2 + s_2 w_3 + \ldots + s_2 w_k + \ldots + s_2 w_n = r_2 \\ & s_3 w_0 + s_1 w_1 + s_2 w_2 + s_3 w_3 + \ldots + s_3 w_k + \ldots + s_3 w_n = r_3 \\ & \vdots \\ & s_k w_0 + s_1 w_1 + s_2 w_2 + s_3 w_3 + \ldots + s_k w_k + \ldots + s_k w_n = r_k \end{aligned} \tag{3.19}$$

$$\vdots$$

$$s_n w_0 + s_1 w_1 + s_2 w_2 + s_3 w_3 + ... + s_k w_k + ... + s_n w_n = r_n$$

Equation set (3.19) includes n +1 unknown variable, while the number of equations is n. In order to solve Equation (3.19) and to obtain the weights w_n, the weight w_0 should be solved first. For this purpose, an additional point is taken on the initial loading curve of the SPI model as (s_{n+1}, ϕ_s (s_{n+1})). By letting $s_{n+1} = \bar{\rho} + s_n$ with $\bar{\rho}$ being a positive real number, it can be shown that $\xi = \phi_s$ (s_{n+1}).

According to (3.16) and (3.17):

$$\xi p_0 + (\xi - r_1) p_1 + ... + (\xi - r_k) p_k + ... + (\xi - r_n) p_n = s_n + \bar{\rho} \tag{3.20}$$

$$(s_n + \bar{\rho}) w_0 + s_1 w_1 + ... + s_k w_k + ... + s_n w_n = \xi \tag{3.21}$$

Equations (3.19) and (3.21):

$$\bar{\rho} w_0 = \xi - r_n \tag{3.22}$$

Equation (3.20) can be expressed as:

$$(\xi - r_n) p_0 + r_n p_0 + (\xi - r_n) p_1 + (r_n - r_1) p_1 + ... + (\xi - r_n) p_k + (r_n - r_k) p_k + (\xi - r_n) p_n = s_n + \bar{\rho} \tag{3.23}$$

Then it can be concluded from (3.22) and (3.23) yields w_0:

$$w_0 = \frac{1}{p_0 + p_1 + ... + p_k + ... p_n} \tag{3.24}$$

Then weights w_i of the SPI model can be easily obtained by solving Equation (3.19).

Remark: It should be noted that an inverse Prandtl-Ishlinskii model formulation was proposed in [12] on the basis of the initial loading curve. The proposed stop-based model is comparable with the inverse model. Considering that the inverse and SPI models serve as compensators to cancel the effect of hysteresis, the initial loading curve of the SPI model must be same as that of the

inverse of the PPI model. Because of the uniqueness of the inverse initial loading curve, it explains why Figure 3.6 is similar to Figure 4 in [12]. To make the initial loading curve of the SPI model as shown in Figure 3.6, two parameters, the thresholds and the weights, have to be formulated. From the above results, the thresholds of the SPI model (3.18) are the same as those of the inverse PPI model [see the expression (12) in [12] because of the uniqueness of the initial loading curve. However, the weights calculated from (3.19) and (3.24) are completely different. As for the question whether to use the inverse or the SPI as a compensator, there is no clear answer and it needs to be further investigated.

4.4 Experimental verification

4.4.1 Experimental setup

In order to validate the effectiveness of the SPI model in compensating the hysteresis behavior of the piezoceramic actuator, an experimental platform is established as shown in Figure 3.7. It consists of the following elements:

1. **Piezoceramic actuator**: P-753.31C Piezoceramic actuator manufactured by Physik Instrumente Company was considered for measurements of the hysteresis properties. The actuator provided a maximum displacement of 38 μm from its static equilibrium position. The excitation voltage to the actuator ranged from 0 to 100 V.

2. **Capacitive sensor**: An integrated capacitive sensor was used for measurements of the actuator displacement response with a sensitivity of 2.632V/μm.

3. **Voltage amplifier**: The excitation voltage to the actuator was applied through a voltage amplifier (LVPZT, E-505), with a fixed gain of 10.

4. **Data acquisition system**: The actuator displacement response signal was acquired in the dSpace Control Desk, together with the input signal.

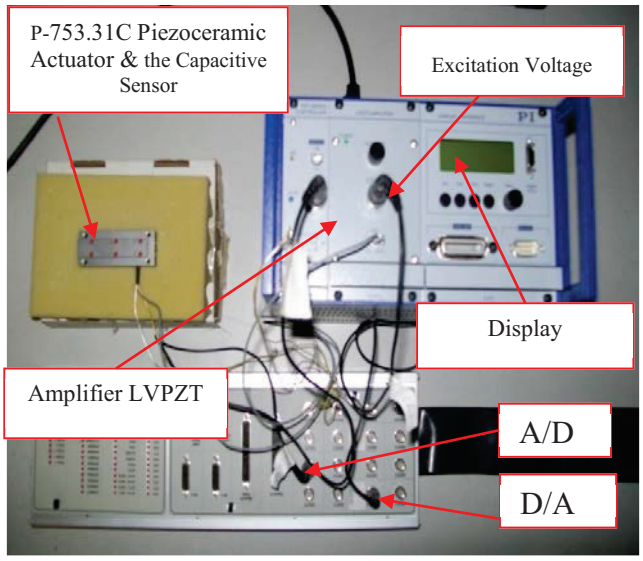

Figure 3.7: The experimental platform.

The measurements of the actuator displacement response were performed under two different excitations. These included:

1. A harmonic excitation at a low frequency of 1 Hz, $v(t) = 30\sin(2\pi t) + 40$

2. A complex harmonic excitation, $v(t) = 4.16\sin(\pi t) + 29.11\sin(2\pi t) + 37.9$.

The measured signals were analysed to characterise the hysteresis effects of the actuator, where the first excitation was selected to identify the major loop input-output property of the actuator, while the complex harmonic excitation was chosen to measure the major as well as minor hysteresis loops.

4.4.2 Hysteresis modeling

The hysteresis non-linearity of the piezoceramic actuator can be described by the PPI model. The model is formulated using the threshold and density function of the following forms:

$$r_i = \overline{\sigma}\, i \tag{3.25}$$

$$p(r_i) = \overline{\alpha}\, e^{-\overline{\beta}\, i} \tag{3.26}$$

where $\bar{\alpha}$, $\bar{\beta}$ and $\bar{\sigma}$ are positive constants. Ten play operators (n_p = 10) were chosen to formulate the PPI model. The model parameters, $X = \{\bar{\alpha}, \bar{\beta}, \bar{\sigma}, p_0\}$, were identified through minimization of an error sum-squared function by using MATLAB optimization toolbox, subject to the following constrains:

$$\bar{\alpha}, \bar{\beta}, \bar{\sigma}, p_0 > 0 \tag{3.27}$$

The identified parameters of the PPI model by using the input-output data of the piezoceramic actuator were found to be: $\bar{\sigma} = 3.548$, $\bar{\alpha} = 0.0383$, $\bar{\beta} = 0.1206$ and $p_0 = 0.2567$. The validity of the PPI model is investigated by comparing the model responses and the laboratory-measured data of the piezoceramic actuator. These comparisons under the chosen input voltages are shown in Figure 3.8 (a) and (b). The results clearly show that the PPI model can effectively characterize the minor as well as major hysteresis loops of the piezoceramic actuator.

4.4.3 Compensation of hysteresis nonlinearity using SPI model

In this section, the SPI model is utilised as a feedforward compensator to compensate for the hysteresis non-linearity. The parameters of the SPI model are derived based on the obtained thresholds (3.25) and weights (3.26) of the PPI model that were presented in the previous section. The weights a_i and the thresholds s_i of the SPI model are obtained using (3.18) and (3.19), , and (3.24) as: 2.146, 0.4544, 0.3230, 0.2397, 0.1831, 0.1444, 0.1156, 0.0941, 0.0774, 0.0642, 0.0543 and 100, 0.9108, 1.9418, 3.0797, 4.3122, 5.6285, 7.0194, 8.4762, 9.9915, 11.5587, 13.1716. Figure 3.9 (a) and Figure 3.9 (b) show the outputs of the SPI model applied to the input amplifier of the piezoceramic actuator through the output board and D/A converter. It should be noted that this output is further amplified by the voltage amplifier (gain = 10). The measured input-output characteristics of the piezoceramic actuator with the SPI model are illustrated in Figure 3.10 for

the two selected inputs. The figures show inputs in terms of the desired input displacement, *v*, as seen in Figure 3.3. The experimental results illustrate that the SPI model can serve as an effective feedforward hysteresis compensator for the piezoceramic actuator.

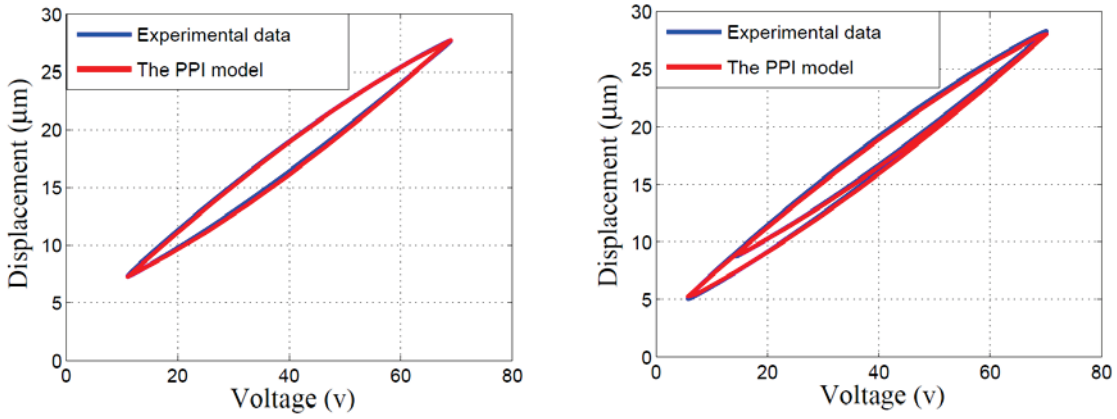

(a) (b)

Figure 3.8: Comparisons between the measured displacement responses with the results derived from the PPI model under two selected inputs, (a) sinusoidal excitation (b) complex harmonic excitation.

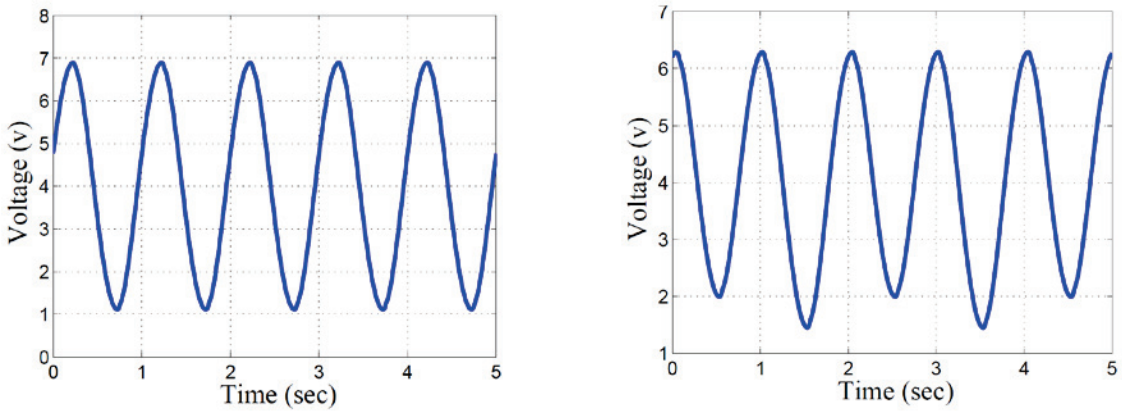

(a) (b)

Figure 3.9: The outputs of the SPI model under two selected inputs, (a) sinusoidal excitation (b) complex harmonic excitation.

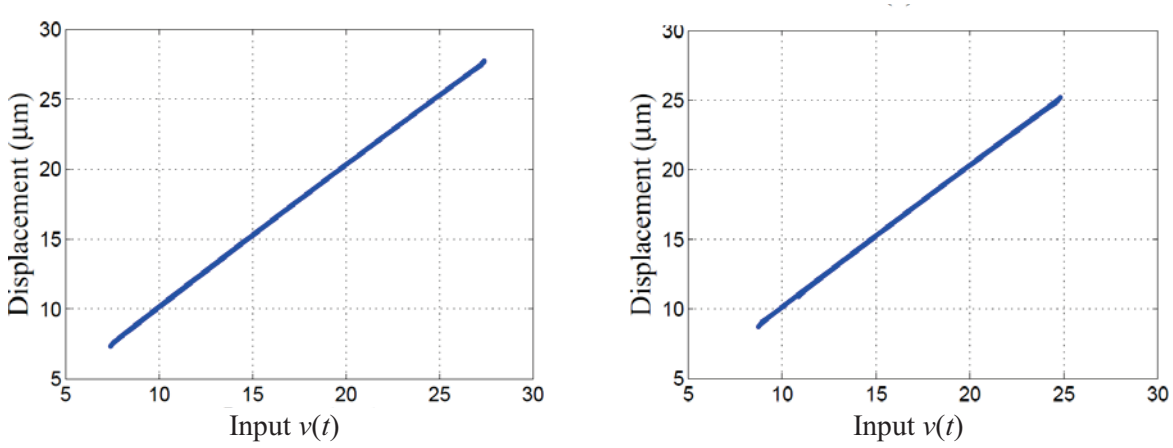

Figure 3.10: Input-output characteristics of the piezoceramic stage with the SPI model compensator under two selected inputs, (a) sinusoidal excitation (b) complex harmonic excitation.

4.5 Conclusions

This paper formulates an SPI model as a feedforward compensator to compensate for the hysteresis non-linearity in a piezoceramic actuator. The thresholds and the weights of the SPI model are analytically derived for the first time in the literature, which constitutes the main contribution of the paper. The results attained from laboratory experiments performed with a piezoceramic micro-positioning stage showed that the SPI model can serve as an effective compensator for the hysteresis nonlinearities. The effectiveness of the SPI model as the feedforward compensator is demonstrated under harmonic and complex harmonic inputs involving both major as well as minor loop hysteresis nonlinearities.

CHAPTER 4

EXPERIMENTAL CHARACTERIZATION AND MODELING OF ASYMMETRIC AND SATURATED HYSTERESIS OF A MAGNETOSTRICTIVE ACTUATOR

5.1 Introduction

Magnetostrictive materials are increasingly being explored for micro/nano scale actuations attributed to material deformations in the presence of an external magnetic field, known as the magnetostriction. Among the available magnetostrictive materials, Terfenol-D alloy is known to yield significant magnetostriction, which is well-suited for both actuation and sensing applications. Terfenol-D alloys, preloaded through mechanical springs together with a compression bolt, have been used with permanent magnets to design fast response, high resolution and high force capacity magnetostrictive actuators for varied applications such as high speed precision milling machines, hydraulic valves and active vibration attenuation [1,2,3,75, 76,77]. The magnetostrictive material actuators, however, exhibit considerable hysteresis nonlinearities between the input current and the output displacement, as observed in other smart material actuators such as piezoceramic [2,6]. Furthermore, the output-input properties of magnetostrictive actuators exhibit asymmetry about the input, and output saturation under moderate to high amplitude excitations [1,2,5,76]. Such

nonlinearities further depend upon the excitation bias, amplitude and frequency in a highly complex manner.

The presence of hysteresis nonlinearities poses challenges in realizing precise micro/nano positioning performance for such actuators. The oscillations in the actuators' responses and thus the positioning errors, and potential instabilities of the closed-loop actuation systems have been widely attributed to the hysteresis nonlinearity [5]. The characterization of output-input properties of smart actuators is thus considered vital for enhancing the understanding of hysteresis nonlinearities and for developing effective model-based hysteresis compensation methods [5,78]. The response properties of the magnetostrictive actuators have been characterized in a few studies under different inputs. These have shown that the hysteresis and output-input properties of such actuators are strongly dependent upon amplitude, bias and frequency of the input.

The output-input properties of magnetostrictive actuators tend to be asymmetric, and exhibit greater hysteresis and output saturation under moderate to high amplitude excitations [11,12,79,80]. For example, Calkins et al. [11] characterized the hysteresis nonlinearities of a magnetostrictive actuator comprising a 115 mm long and 12.7 mm diameter Terfenol-D rod, subject to different magnetic fields up to 5.6 kA/m. The results of the study revealed significant output saturation nonlinearity under large amplitude excitations compared to that observed under low amplitude excitations. Studies reporting measured output-input characteristics of magnetostrictive actuators have shown that hysteresis nonlinearities are strongly dependent on the rate of input beyond 5-10 Hz [7,8]. Tan and Baras [7] characterized the hysteresis of a magnetostrictive actuator comprising a 51.3 mm long Terfenol-D rod and permanent magnets, causing a bias of 1.54×10^4 A/m, under inputs in the 10-300 Hz frequency range. The measured

data obtained under harmonic excitations (amplitude = 0.8A; bias = -0.1A) revealed asymmetry in the output about the input and increase in hysteresis with increasing rate of the applied input.

Stuebner et al. [13] measured the effect of the input bias on the hysteresis properties of a magnetostrictive actuator by applying inputs of identical amplitude (12.5 kA/m) but three different bias levels (25, 50 and 75 kA/m). The amplitudes of output displacement were observed to be 50% and 75% lower, respectively, in the presence of 50 and 75 kA/m bias compared to that measured under the lower bias of 25 kA/m. The measured data revealed not only substantially lower output displacement in the presence of input bias but also lower hysteresis and higher asymmetry in the output-input characteristics with increasing bias. The reported studies suggest coupled effects of input bias, amplitude and frequency on the hysteresis and output saturation nonlinearities of the magnetostrictive actuators, although most of the reported studies have mostly investigated the effects of only one of the factors, namely, the input amplitude [5,12,64], bias [13] or frequency [7,8]. A study of the output-input properties of the magnetostrictive actuator under varying amplitude, bias and frequency of the input may provide a better understanding of the hysteresis and saturation nonlinearities of the actuator.

A thorough characterization of the hysteresis and saturation nonlinearities is vital for developing hysteresis models that may be applied for compensation of the nonlinear effects so as to achieve enhanced micro-positioning and tracking performance of the actuation system. A number of hysteresis models have been proposed to characterize hysteresis of smart material actuators, which could be classified into physics-based and phenomenological hysteresis models. The physics-based models employ fundamental stress-strain and energy principles to describe hysteresis behavior of piezoceramic and magnetostrictive actuators [17,79,81,82,83]. The phenomenological models such as Preisach and Prandtl-Ishlinskii models employ a summation of

weighted hysteresis operators to describe hysteresis of smart materials and actuators. The classical Preisach and Prandtl-Ishlinskii models, however, ignore the effects of input bias and rate on the hysteresis [89,84,83]. A number of such operator based models, however, have evolved over the past two decades that can effectively account for both rate-dependency and asymmetry effects in hysteresis. The dependence of the hysteresis on the rate of input has been widely characterized through formulations and application of dynamic density functions in the classical Preisach and Prandtl-Ishlinskii models. For instance, Mayergoyz [30] and Ben Mrad et al. [47] proposed Preisach models with dynamic density functions to describe rate-dependent hysteresis of magnetostrictive materials and piezoceramic actuators. Davino et al. [8] and Tan and Baras [7] proposed different linear time-invariant dynamic systems coupled with the classical Preisach model to describe the rate-dependent hysteresis properties of magnetostrictive actuators as well as asymmetric output-input characteristics of the actuator.

Output saturation and asymmetry effects are widely observed in magnetostrictive actuators under moderate and high amplitude inputs or under inputs with a bias. Smith [64] employed a Preisach model to describe saturation and hysteresis nonlinearities observed in a magnetostrictive actuator mounted on a cantilever beam. In [5], Visone characterized the output saturation and asymmetry effects of a magnetostrictive actuator using the Preisach model under a complex harmonic input. A modified Prandtl-Ishlinskii model was suggested by Kuhnen [12] to describe asymmetric major and minor hysteresis loops of a magnetostrictive actuator by applying a complex harmonic input current.

A few studies have proposed generalized Prandtl-Ishlinskii models to describe symmetric as well as asymmetric rate-independent and rate-dependent hysteresis of different smart material actuators. Drinčić et al. [61] employed an alternate envelope function in the play operators to

formulate a generalized Prandtl-Ishlinskii model to account for saturated symmetric hysteresis nonlinearity of a magnetostrictive actuator. Al Janaideh et al. [9,85] proposed a rate-dependent play operator and a dynamic density function for the Prandtl-Ishlinskii model to describe the input rate effect on the hysteresis nonlinearity of a piezoceramic actuator. Dissimilar envelope functions of the play operators during increasing and decreasing inputs were further proposed to describe output asymmetry and saturation nonlinearities of a magnetostrictive actuator [86]. The implementation of two different envelope functions corresponding to increasing and decreasing inputs, however, could cause a discontinuity in the output. Unlike the Preisach model, the Prandtl-Ishlinskii model is analytically invertible due to continuity of the play operators. The Prandtl-Ishlinskii model is thus considered meritorious for formulating an analytical inverse model that could be applied to achieve real-time hysteresis compensation in an efficient manner [63].

The primary aim of this study is to develop a Prandtl-Ishlinskii model capable of describing the hysteresis nonlinearities under a broad range of excitation amplitudes and frequencies. A laboratory experiment was thus designed to characterize the output-input characteristics of a magnetostrictive actuator under simple and complex harmonic inputs of different amplitudes over a wide range of frequencies. A memoryless function is proposed and integrated to a rate-dependent Prandtl-Ishlinskii model in order to describe the output asymmetry and saturation nonlinearities together with rate-dependent hysteresis. The effectiveness of the proposed model in predicting the asymmetric output-input properties of the actuator together with output saturation and hysteresis is demonstrated through comparisons with the measured data under a wide range of inputs. The output of the suggested model is continuous in time and permits the formulation of an analytical inverse model that could be applied for compensation of rate-dependent asymmetric hysteresis nonlinearities.

5.2 Output-input characteristics of a magnetostrictive actuator

5.2.1 Experimental setup and methods

An experimental setup was designed in the laboratory to characterize the output-input characteristics of a magnetostrictive actuator under a wide range of simple and complex harmonic inputs. The experiments were conducted on a magnetostrictive actuator, manufactured by Etrema (model MFR OTY77; stroke= 100 μm). The actuator comprised two 60.3 mm long and 12.3 mm diameter Terfenol-D rods, and three permanent magnets that provided a magnetic bias (≈ 44.1 kA/m) to permit the actuator to operate in the linear region (Figure 4.1 (a)). The coil factor of the coil encapsulating the drive rod of the actuator was specified as 5.09×10^3/m. This actuator provided peak-peak output displacement of 100 μm within the recommended operating conditions (peak input current = 7.07 A, 1250 Hz frequency range). A capacitive sensor (Lion Precision, C23-C250) with sensitivity of 80 *m*V/μm and 35.53 *n*m resolution was used to measure the output displacement of the actuator from its static position. The excitation input signal was synthesized in the ControlDesk platform and applied to a power amplifier (LVC 2016, AE TECHRON) in order to generate the desired excitation current to the drive coil of the actuator. The actuator displacement response together with the applied input were acquired in the ControlDesk platform. A schematic of the experimental set-up is shown in Figure 4.1(b).

Three series of experiments were conducted, which involved factorial designs of two of the three primary input factors, namely, the input frequency, amplitude and bias. The first series involved measurements under different combinations of 9 input current amplitudes (I_o=1 to 9 A) and 6 levels of input frequencies (f=10, 25, 50, 100, 150 and 200 Hz). It should be noted that the

amplitudes exceeding the recommended peak current of 7.07 A were used so as to capture the actuator properties under extreme inputs.

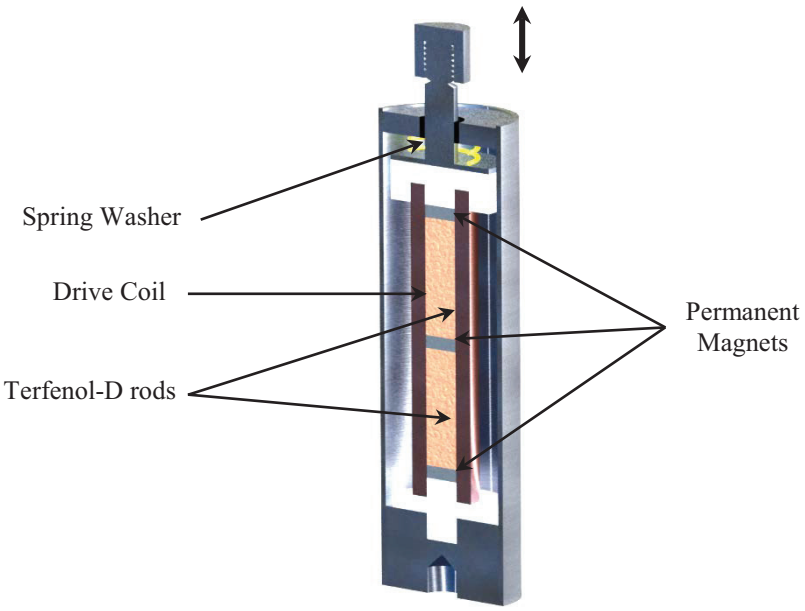

(a)

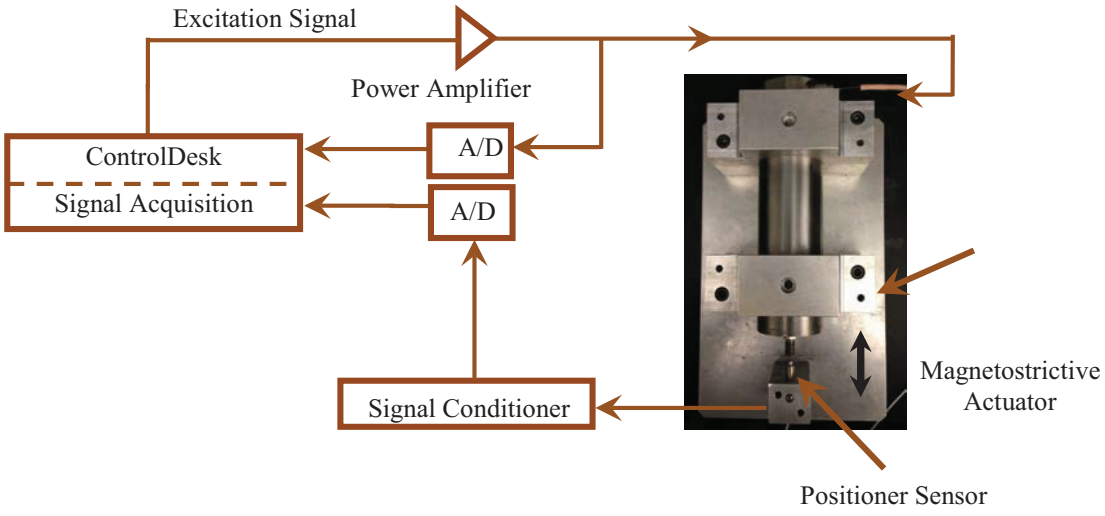

(b)

Figure 4.1: Schematic of the (a) Terfenol-D magnetostrictive actuator used in the study; and (b) experimental setup.

The second series considered 6 magnetic bias levels in the 25 to 75 kA/m range together with 2.965 A harmonic excitation at the above-stated input frequencies. The selected range of the bias corresponds to -3.96 to 5.89 A bias in the current excitation. In the final series, a complex harmonic input of the form, $I(t)=A_1 \sin(2\pi n_1 f_o t)+A_2 \sin(2\pi n_2 f_o t)$, was applied for characterizing the major- and minor-loop hysteresis, where f_o is the fundamental frequency, A_1 = 2 A and A_2 = 3 A are the magnitudes of the two harmonic components, and n_1=2.5 and n_2=1 are the respective frequency factors. The measured data were analyzed to study the effects of each input factor on the peak-peak output displacement, output saturation and the hysteresis.

5.2.2 Influence of input amplitude

The output-input characteristics of the actuator corresponding to different amplitudes of input current are illustrated in Figure 4.2. The results are presented for excitations at a constant frequency of 10 Hz, and a constant magnetic bias of 44.1 kA/m. Asymmetry of the hysteresis loops and output saturation are evident under excitations exceeding 2 A. The actuator responses to excitations exceeding 3 A show substantial degree of asymmetry and output saturation. While the displacement response is nearly symmetric under increasing and decreasing inputs up to 2 A, the peak displacement under increasing input tends to be lower than that under decreasing input at current inputs exceeding 2 A. The results suggest that the asymmetry in the output increases with the excitation magnitude. The difference between the peak displacement under increasing and decreasing inputs with respect to peak-peak output displacement is near 6.4 % at 3 A and it increases to 17.31 % at 9 A. The results also show greater degree of output saturation under higher

excitation current. A few reported experimental studies on magnetostrictive actuators and transducers, have also shown output asymmetry and saturation under moderate to high inputs [5,12,79,78].

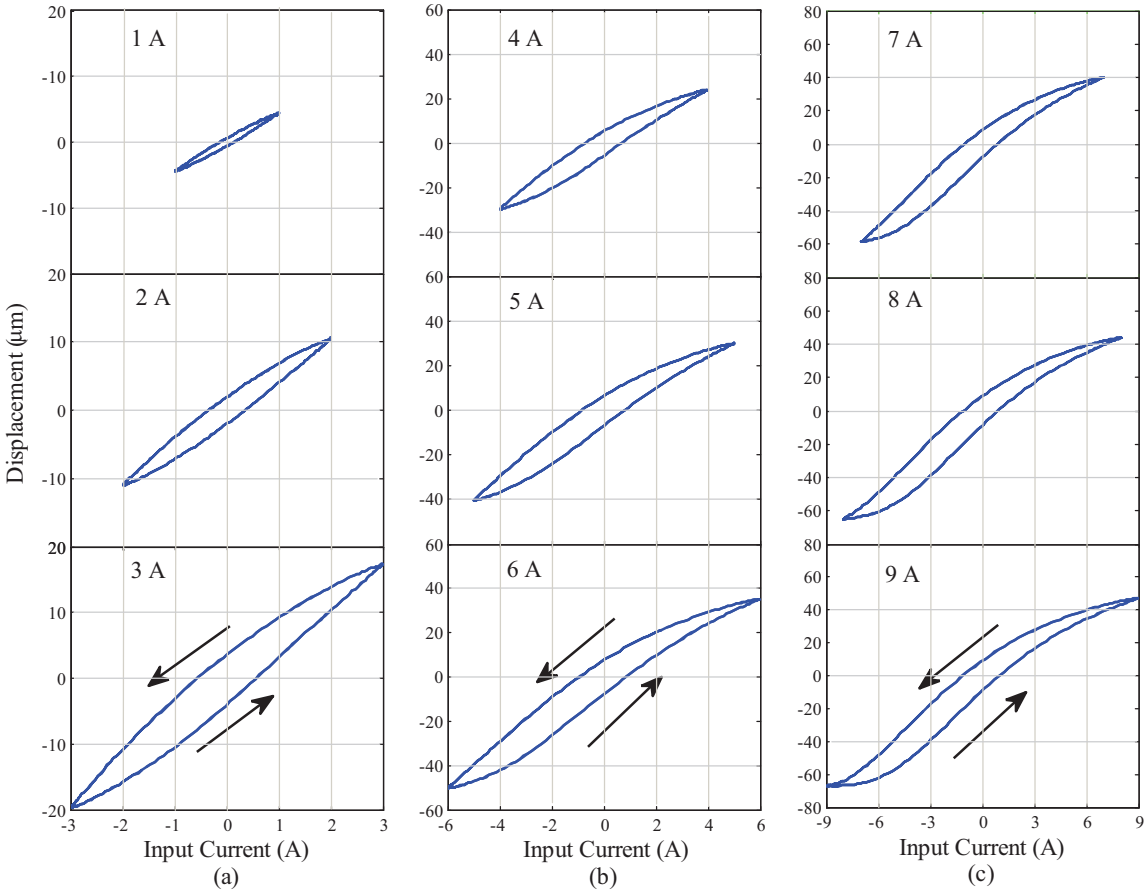

Figure 4.2: Variations in the actuator displacement response under different amplitudes of harmonic current excitation: (a) 1, 2 and 3 A; (b) 4, 5 and 6 A; and (c) 7, 8 and 9 A (*f*= 10 Hz; magnetic bias= 44.1 kA/m).

The measured data were further analyzed to study the influence of the input amplitude on the output-input characteristics in terms of peak-to-peak output displacement and the area bounded by the hysteresis loop, as shown in Figure 4.3 (a) and (b). Figure 4.3 (a) also illustrates the rate of change of peak-peak displacement with respect to the peak-peak input current, which defines the mean displacement sensitivity of the actuator. The results suggest nearly linear increase in the

displacement with current in the 3 to 6 A range. The displacement sensitivity, however, is lower at currents exceeding 5 A, which can be mostly attributed to the output saturation of the actuator. Low current excitations also yield lower sensitivity that is attributed to lower permeability of the Terfenol-D material at these levels [1,66,76]. Similar trend is also evident in variations the area of the hysteresis loop with increasing current, as shown in Figure 4.3 (b), which relates to the energy loss attributed to hysteresis of the magnetostrictive material [76]. The results suggest increasing hysteresis with increasing current amplitudes, as it is also seen in Figure 4.2.

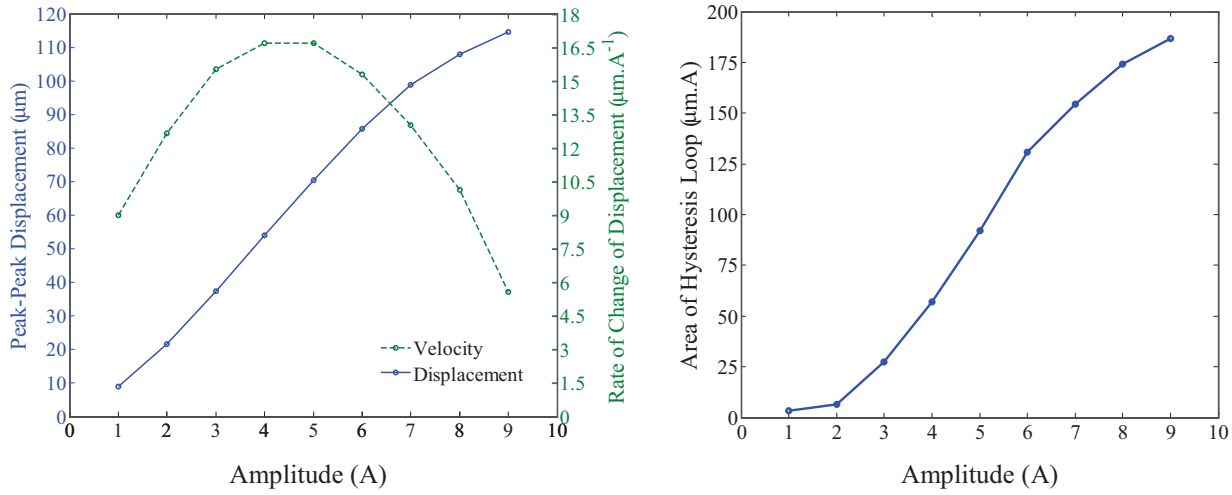

Figure 4.3: Influence of variations in the applied current amplitude on: (a) peak-peak output displacement and rate of change of the peak-peak displacement with respect to peak-peak current; and (b) the area bounded by the hysteresis loop (f=10 Hz).

5.2.3 Influence of rate of input

The output-input characteristics of the actuator corresponding to two different input amplitudes (3 A and 7 A) in the 10 to 200 Hz frequency range are illustrated in Figure 4.4 (a) and (b), respectively. The results are presented for the constant magnetic bias of 44.1 kA/m and different discrete excitation frequencies, namely, 10, 25, 50, 100, 150 and 200 Hz. The results show

increasing hysteresis with increasing excitation frequency for both the input amplitudes, which has also been reported in other studies [7,12]. The responses to 3 A excitation show relatively lower output asymmetry and saturation, while those under 7 A excitation show significantly greater asymmetry and saturation. The peak displacement amplitude in each excitation case, however, remains nearly constant, irrespective of the excitation frequency, as seen in Figure 4.5(a).

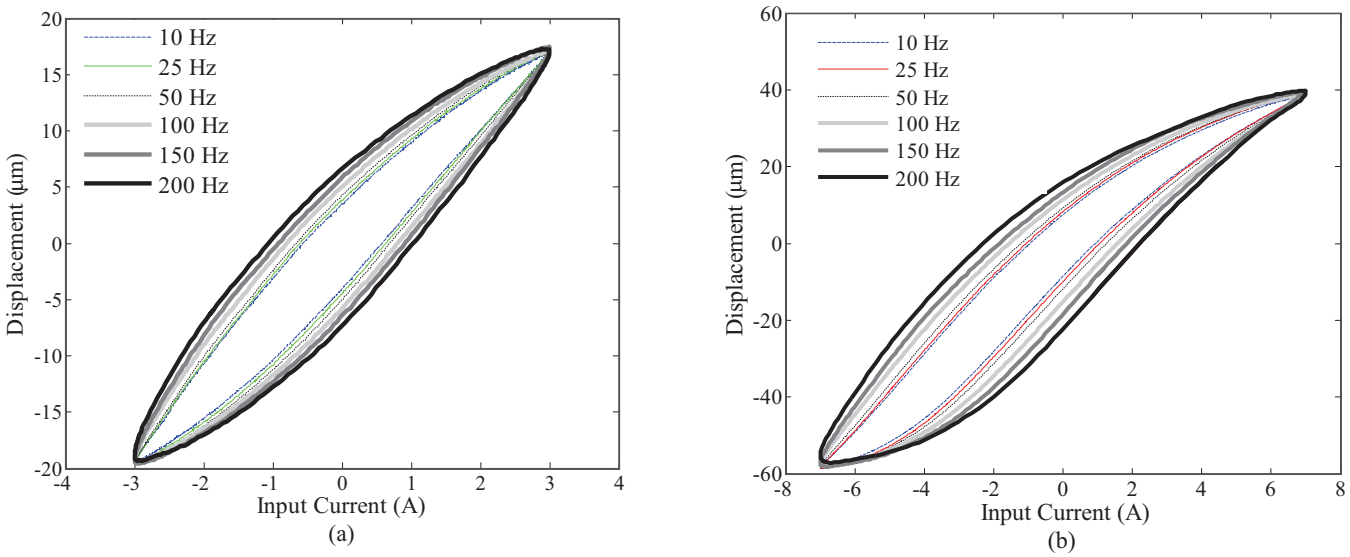

Figure 4.4: Measured hysteresis loops relating output displacement response of the magnetostrictive actuator under harmonic excitations at different frequencies in the 10-200 Hz range: (a) input current=3 A; and (b) input current = 7 A (Bias=44.1 kA/m).

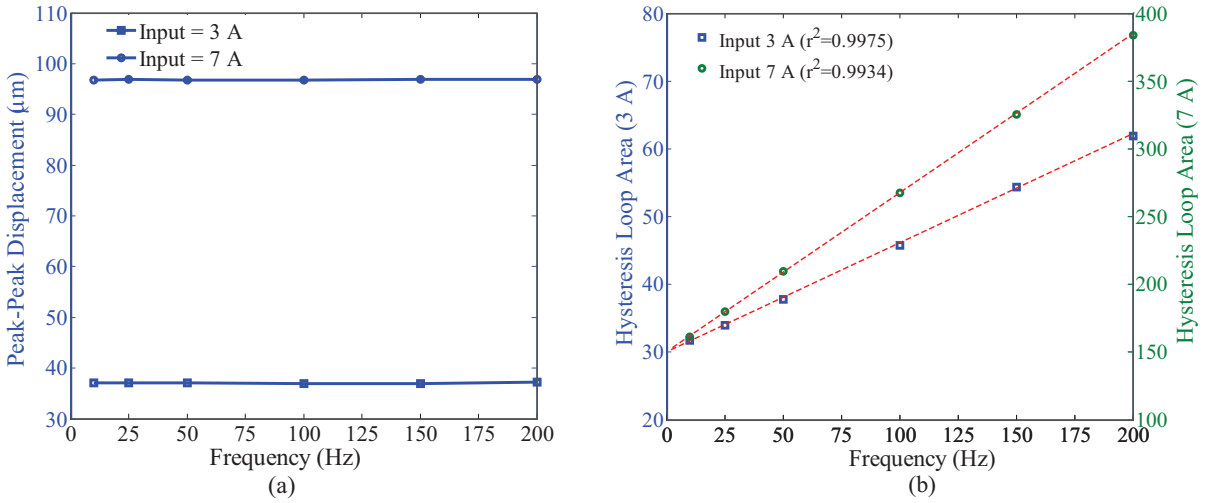

Figure 4.5: Effects of excitation frequency on: (a) the peak-peak displacement response; and (b) the area bounded by the hysteresis loop.

The results in Figure 4.3 and Figure 4.4 suggest that for the given bias level, the output asymmetry and saturation are mostly affected by the input amplitude, while the effect of input frequency is nearly negligible. The hysteresis of the material, however, is strongly dependent upon the excitation frequency, as seen from the variations in the area of the hysteresis loop in Figure 4.5 (b), apart from the input amplitude. Unlike the input amplitude effect, the hysteresis loop area increases nearly linearly with the excitation frequency (r^2=0.99) for a given input amplitude, while it tends to be higher under the higher input current. These suggest strong dependence of the hysteresis on both the excitation magnitude and the frequency.

5.2.4 Influence of input bias

The effect of input bias on the actuator response is investigated by applying biased input currents, such that $I_b(t)=I_o \sin(2\pi ft)+I_{bias}$, where I_{bias} is the input bias. The bias levels are selected by considering the bias in the magnetic field strength H applied to the actuator coils, which is related to the applied current in the following manner [7]:

$$H(t) = k_o I_b(t) + H_{PM} \tag{4.1}$$

where k_o=5.09×10^3 m^{-1} is the coil factor and H_{PM} =44.1 kA/m is the magnetic field bias attributed to permanent magnets used in the actuator design. Application of the biased current permits variations in the magnetic field bias, such that:

$$H(t) = k_o I_o \sin(2\pi ft) + H_{bias} \tag{4.2}$$

In the above $H_{bias} = k_o I_{bias} + H_{PM}$, where $k_o I_{bias}$ relates to the additional magnetic bias applied to the actuator. The range of total bias used in the experiment (25 to 75 kA/m) range, which correspond to I_{bias} in the -3.75 to 6.07 A range. The input current amplitude I_o of 2.95 A at a frequency of 25 Hz was considered in this series of experiments, which corresponds to field strength $k_o I_o$ of 15 kA/m.

Figure 4.6 (a) illustrates the output-input characteristics of the actuator subject to different input bias. Variations in the peak-peak displacement response and the area of the hysteresis loops with varying H_{bias} are presented in Figure 4.6 (b) and (c), respectively. It is evident that a magnetic bias tends to shift the equilibrium position of the actuator in the direction of bias, while the magnitude of the shift is nonlinearly dependent upon the H_{bias}. Increasing the H_{bias} yields relatively lower shift compared to that observed under the lower bias, which is again attributable to saturation under higher current. Decreasing the H_{bias} also yields greater displacement amplitude and hysteresis, as shown in Figure 4.6 (b) and (c), receptively. The permanent magnets bias (H_{PM}) in the actuator designs is generally chosen to achieve a compromise between greater displacement and lower hysteresis [1,2]. The results also suggest that the hysteresis characteristics of a magnetostrictive actuator are dependent on the H_{bias} apart from the input current amplitude and the frequency.

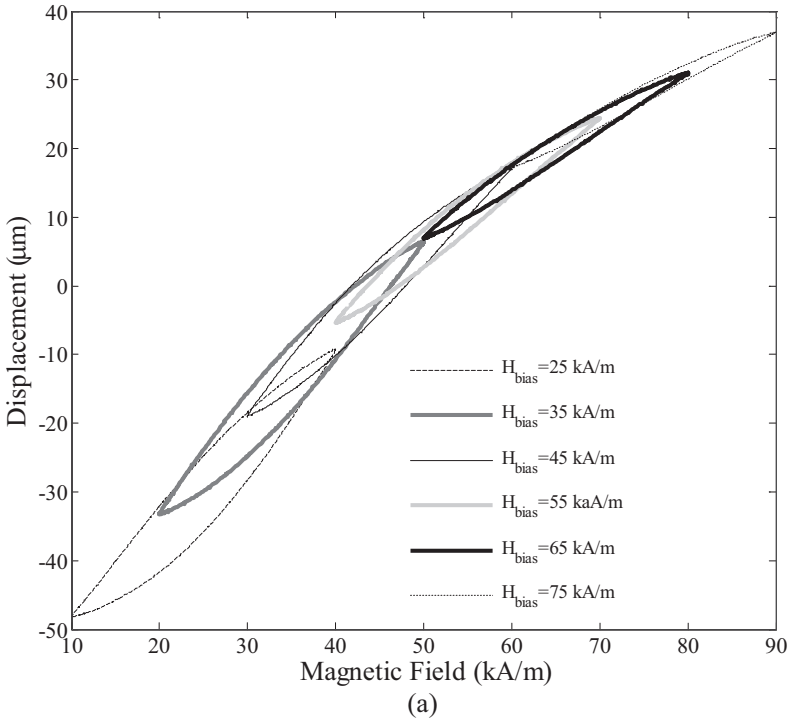
Displacement (μm)
Magnetic Field (kA/m)
H_{bias}=25 kA/m
H_{bias}=35 kA/m
H_{bias}=45 kA/m
H_{bias}=55 kaA/m
H_{bias}=65 kA/m
H_{bias}=75 kA/m

(a)

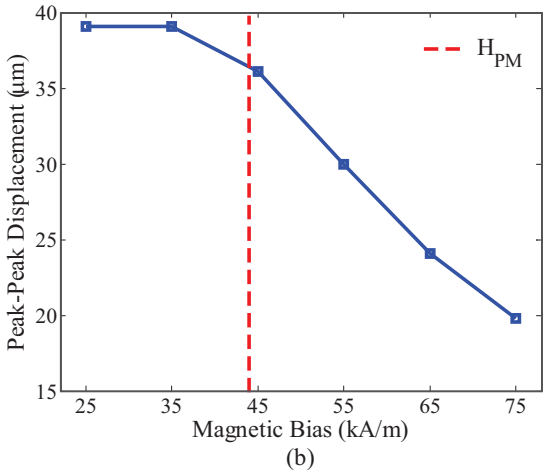
Peak-Peak Displacement (μm)
Magnetic Bias (kA/m)
H_{PM}

(b)

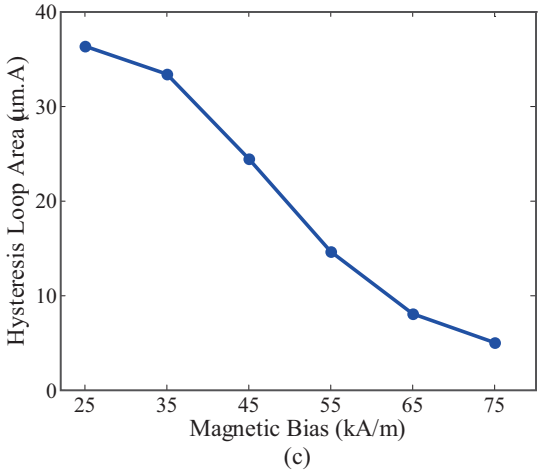

Figure 4.6: Influence of variations in the magnetic bias (H_{bias}) on: (a) the output-input characteristics of the magnetostrictive actuator, (b) peak-peak output displacement; and (c) area of the hysteresis loop (harmonic magnetic field amplitude = 15 kA/m and f=25 Hz).

5.3 Minor hysteresis loops

Figure 4.7 (a) illustrates the output-input characteristics of the actuator subject to the complex harmonic input (f_o=20 Hz) and magnetic bias of 44.1 kA/m. The results show the minor hysteresis loops at moderate and low amplitude excitations. The minor hysteresis loop labeled as 1 corresponds to the input oscillation during loading, as seen in Figure 4.7(b). In a similar manner, minor loops 2 and 3 correspond to input oscillations during unloading. The minor hysteresis loops were also obtained under the fundamental frequency f_o=40 Hz, and compared with those obtained for f_o=20 Hz in Figure 4.8. The figure shows the output-input characteristics zoomed around the oscillations in the loading and unloading inputs, labeled as 2 and 3 . The comparisons suggest that change in fundamental frequency of the input, from 20 to 40 Hz, yields only slight variations in the amplitudes of secondary oscillations during loading and unloading inputs. The

change in the rate of applied input, however, produces a notable effect on the minor loops hysteresis.

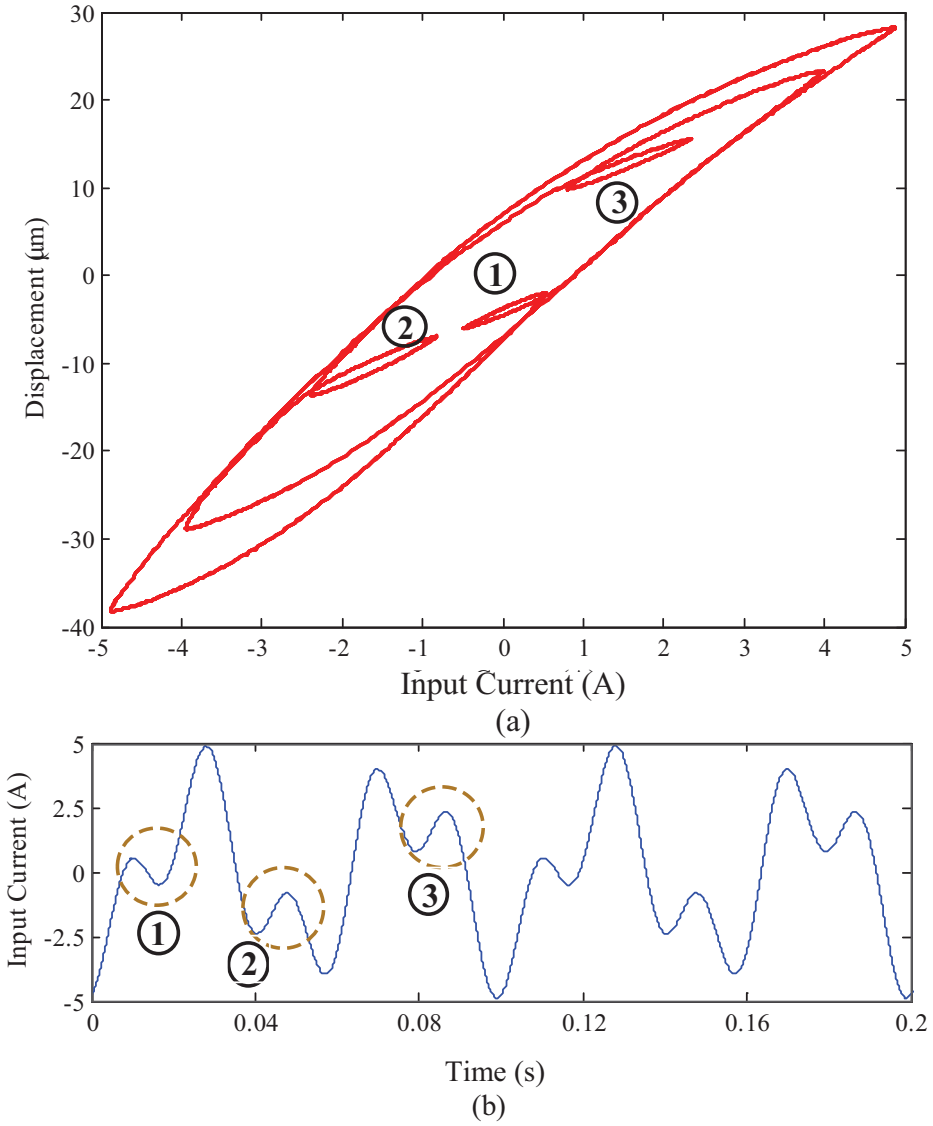

Figure 4.7: (a) The output-input characteristics of the actuator illustrating minor as well as major hysteresis loops (f_o=20 Hz; magnetic bias = 44.1 kA/m); and (b) time history of the complex harmonic input, $I(t)$=2 sin(2.5×2π$f_o t$)+ 3 sin(2π$f_o t$) applied to characterize minor hysteresis loops.

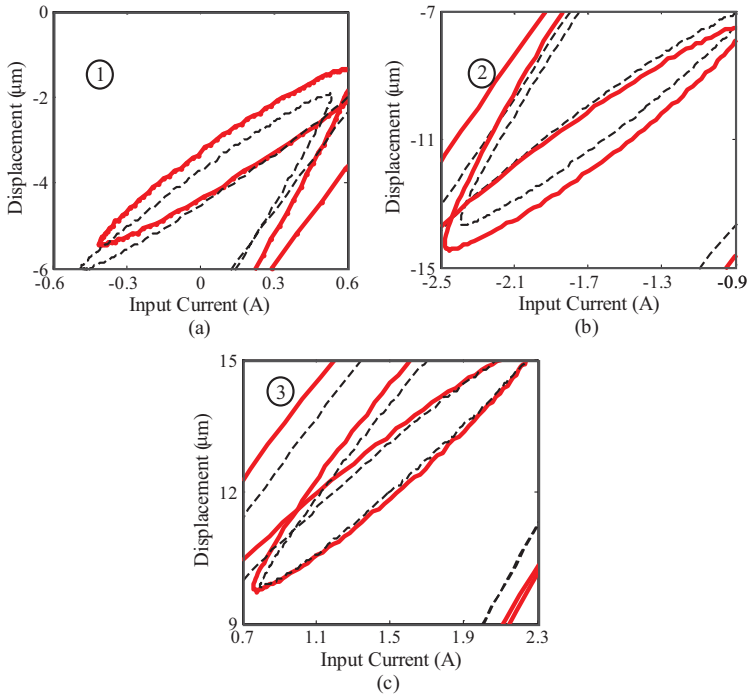

Figure 4.8: Output-input characteristics of the actuator zoomed around the minor hysteresis loops under a complex harmonic input current $I(t)=2\sin(2.5\times2\pi f_o t)+3\sin(2\pi f_o t)$ (- - -, ~~f_o~~= 20 Hz; and ~~f_o~~=40 Hz.

5.4 Formulation of an integrated hysteresis model

The rate-dependent hysteresis nonlinearities of smart material actuators have been widely described by different phenomenological models incorporating dynamic threshold, weighting or density functions. Among these, the Prandtl-Ishlinskii model offers a unique property of being analytically invertible, which is attributed to continuous nature of the play operator functions. An analytical inverse of the Prandtl-Ishlinskii model could thus be formulated to facilitate real-time compensation of the hysteresis nonlinearities [6,42,49, 63]. Owing to the symmetry of the rate-dependent play operators, a rate-dependent Prandtl-Ishlinskii model, however, could yield only symmetric hysteresis properties, as observed in a class of smart material actuators such as piezoceramic actuators [9]. A generalized rate-dependent play operator with dissimilar hyperbolic

tangent envelop functions has been proposed, in conjunction with a rate-dependent Prandtl-Ishlinskii model, to describe asymmetric hysteresis nonlinearities of a magnetostrictive actuator under increasing and decreasing inputs [87]. The proposed hyperbolic tangent functions could effectively describe asymmetric hysteresis and saturation effects in smart material actuators, a discontinuity in the output, however, may occur near input peaks due to lack of convergence of the envelope functions. This was observed particularly under high frequency inputs and would impede the formulation of an analytical inverse of the model. Alternatively, Kuhnen [12] proposed a memoryless function, a superposition of an array of deadband operators, to describe rate-independent asymmetric hysteresis nonlinearity of a magnetostrictive actuator.

The memoryless function proposed in [5,12,88] could be applied in conjunction with a rate-dependent Prandtl-Ishlinskii model to describe rate-dependent saturated and asymmetric hysteresis nonlinearities, which were evident from the measured data. Figure 4.9 (a) illustrates a cascade arrangement of the rate-dependent Prandtl-Ishlinskii model Π and the memoryless function Λ. Analytically, the integrated Prandtl-Ishlinskii hysteresis model Ω is expressed as a composition of Π and Λ, such that:

$$\rho(t) = \Omega[v](t) = (\Lambda \circ \Pi)[v](t) = (\Lambda \ (\Pi))[v](t) \tag{4.3}$$

where $\rho(t)$ is the output of the integrated hysteresis model Ω.

In the above formulation, the Prandtl-Ishlinskii model Π is formulated considering superposition of rate-dependent play operators $\Gamma_{r_i(\dot{v}(t))}$, which are real and continuous over the interval $(0,T)$. For an input $v(t) \in AC(0,T)$, where AC represents real absolute continuous functions, the output $\delta(t)$ of the model $\Pi(t)$, which is symmetric about the input, is expressed as [63]:

$$\delta(t) = \Pi[v](t) = a_0 v(t) + \sum_{i=1}^{n} a_i \Gamma_{r_i(\dot{v}(t))}[v](t) \tag{4.4}$$

where a_i are weighting constants. The input function $v(t)$ is considered monotone over each sub-interval $[t_{j-1},\ t_j]$, and $0 = t_0 < t_1 < \ldots < t_l = T$ define the intervals. The model employs rate-dependent play operators to characterize the rate-dependent hysteresis. The output of the rate-dependent play operator over the interval $t \in [t_{j-1},\ t_j]$ may be expressed as:

$$\Gamma[v](t_j) = \max\{v(t_j) - r_i(\dot{v}(t_j)), \min\{v(t_j) + r_i(\dot{v}(t_j)), \Gamma[v](t_{j-1})\}\} \tag{4.5}$$

where $i = 0,\ 1,\ 2,\ \ldots,\ n$, and $n \in \mathrm{N}$ is an integer, and $r_i(\dot{v}(t)) \in AC(0,T)$ is the rate-dependent threshold function defined such that: $0 \le r_0(\dot{v}(t)) \le r_1(\dot{v}(t)) \le r_2(\dot{v}(t)) \le \ldots \le r_n(\dot{v}(t))$.

The memoryless function Λ in (4.3) is formulated as a summation of weighted deadzone operators J_{d_i} of different threshold d_i and weighting constants g_i, as shown in Figure 4.9 (b) [12]. The weightings provide a varying slope character of the resulting function so as to characterize the asymmetric outputs during loading and unloading inputs together with output saturation. The composition of symmetric output $\delta(t)$ of the rate-dependent Prandtl-Ishlinskii model, which is monotone over each of the interval $[t_{j-1},\ t_j]$, with the memoryless function Λ yields the output $\rho(t)$, as:

$$\rho(t) = \Lambda\ [\delta](t) = \sum_{i=-m}^{m} c_i J_{d_i}[\delta](t) \tag{4.6}$$

where J_{d_i} (i=-k,…0,…k) are the deadzone operators, described as [12]:

$$J_{d_i}[\delta](t) = \begin{cases} \max\{\delta(t) - d_i, 0\} & for \quad d_i > 0, \\ \delta(t) & for \quad d_i = 0, \\ \min\{\delta(t) - d_i, 0\} & for \quad d_i < 0. \end{cases} \tag{4.7}$$

Formulating a memoryless function from a large number of deadzone operators with different thresholds d_i and weightings g_i provides greater flexibility in describing asymmetry in the outputs between the ascending and descending inputs, as well as output saturation. The integrated hysteresis model Ω would reduce to rate-dependent Prandtl-Ishlinskii model Π with symmetric rate-dependent hysteresis loops, when d_i =0 and g_i =1.

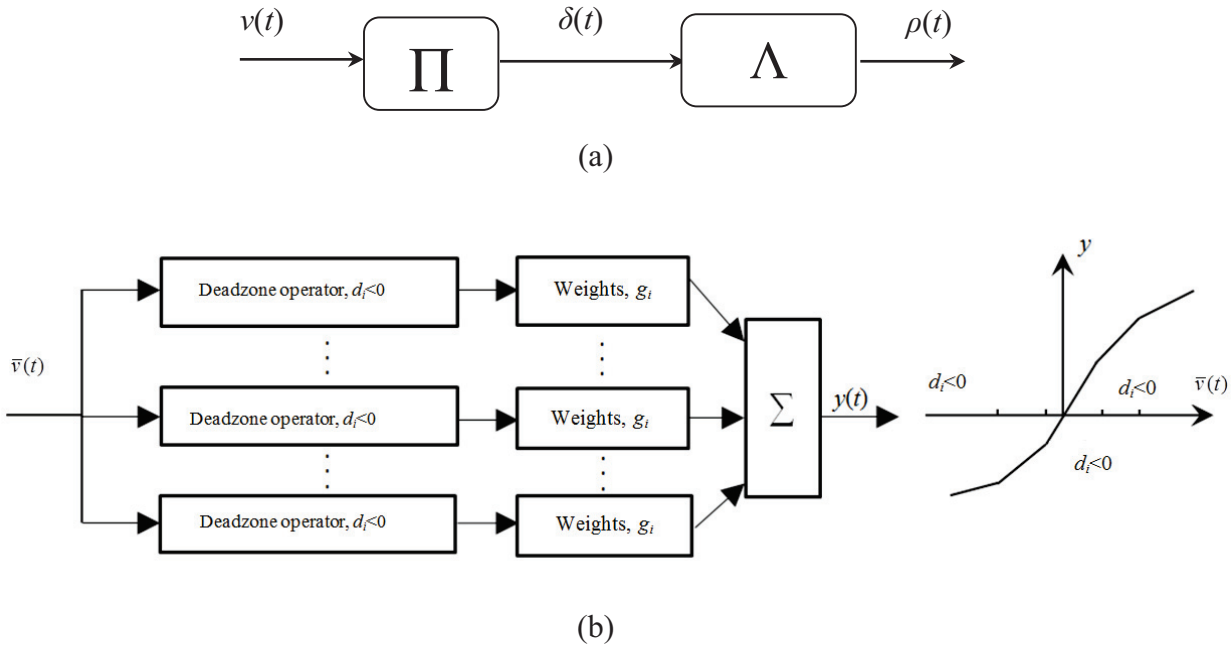

Figure 4.9: (a) A memoryless function Λ_d introduced to the output of the rate-dependent Prandtl-Ishlinskii Π model to observe saturation and asymmetry effects; and (b) structure of the memoryless function Λ_d, as a superposition of weighted deadband operators.

5.4.1 Parameters identification

The effectiveness of the integrated hysteresis model Ω in describing major and minor rate-dependent hysteresis loops with asymmetry and saturation of the output is investigated considering simple and complex harmonic current inputs in the (10-200) Hz range. For this purpose, the parameters of the rate-dependent Prandtl-Ishlinskii model Π and the memoryless function Λ are identified on the basis of the laboratory-measured data. The measured data revealed that the area bounded by the output displacement-input current hysteresis loop of the magnetostrictive actuator is nearly linearly dependent on the excitation frequency of the applied input current [66], as illustrated in Figure 4.5 (b). Consequently, the play operator with a threshold function that is linearly related to the rate of input current would be appropriate for describing rate-dependent hysteresis nonlinearity, such that:

$$r_i\left(\dot{v}(t)\right) = \gamma\ \left|\dot{v}(t)\right| + \alpha i\,; \quad i = 1,\ 2,..,\ n \tag{4.8}$$

where γ and α are positive constants. The constant α relates to the rate-independent hysteresis effect that is observed at low excitations frequencies. The above threshold function has been implemented with a Prandtl-Ishlinskii model (4.4) to describe rate-dependent symmetric hysteresis nonlinearities of a magnetostrictive actuator.

The parameter vector, $\overline{X} = \{d_i,\ g_i,\ a_i,\ \alpha,\ \gamma\}$, of the integrated Prandtl-Ishlinskii model Ω is identified from the measured data through minimization of the sum-squared error function $\overline{\Theta}$:

$$\overline{\Theta}(\overline{X}) = \sum_{\bar{c}=1}^{\bar{C}} \sum_{\bar{b}=1}^{\bar{B}} \sum_{m=1}^{M} \left(\Omega(t, m, f_{\bar{b}}, I_{o\ell}) - Y(t, m, f_{\bar{b}}, I_{o\bar{c}})\right)^2 \tag{4.9}$$

where $\Omega(t, m, f_{\bar{b}}, I_{o\bar{c}})$ is the displacement response of the model under a given excitation frequency $f_{\bar{b}}$ and input current $I_{o\bar{c}}$ and $Y(t, m, f_{\bar{b}}, I_{o\bar{c}})$ is the measured output displacement of

the magnetostrictive actuator under identical input current. The index m (m = 1, ...,M) in the error function refers to the number of discrete data points considered in computing the error over one complete hysteresis loop, while indices $\overline{B}$ and L denote the number of discrete frequencies and current amplitudes considered. The error minimization problem was solved considering 200 data points for each hysteresis loop (M=200), and two input amplitudes ($I_{o\bar{c}}$ = 3 and 7 A) applied at three different excitations of frequencies ($f_{\bar{b}}$ = 10, 100 and 200 Hz). The solution of the optimization problem was solved considering n=10 rate-dependent play operators and 17 deadband operators.

At first, the error minimization problem was solved considering different numbers of rate-dependent play operators (n ranging from 2 to 15) and different starting values of the parameter vector. For each chosen n, different starting values of the parameters converged to similar model parameters. The sum-squared error, however, decreased with increasing value of n but saturated for $n \geq 8$, as shown in Figure 4.10. Consequently, the model parameters were obtained using n =10. The validity of the resulting model was subsequently examined by comparing the model results with the measured data obtained under different inputs. Figure 4.11 compares the model results with the measured data obtained under I_o= 3 A and 7 A at different frequencies (10, 100 and 200 Hz). The model results under current of 3, 5 and 7 A, at 10 Hz are compared with the measured data in Figure 4.12 (a). The model response to the complex harmonic input current (f_o=20 Hz) is also compared with the corresponding measured data in Figure 4.12 (b) to examine the model ability to describe minor loop hysteresis.

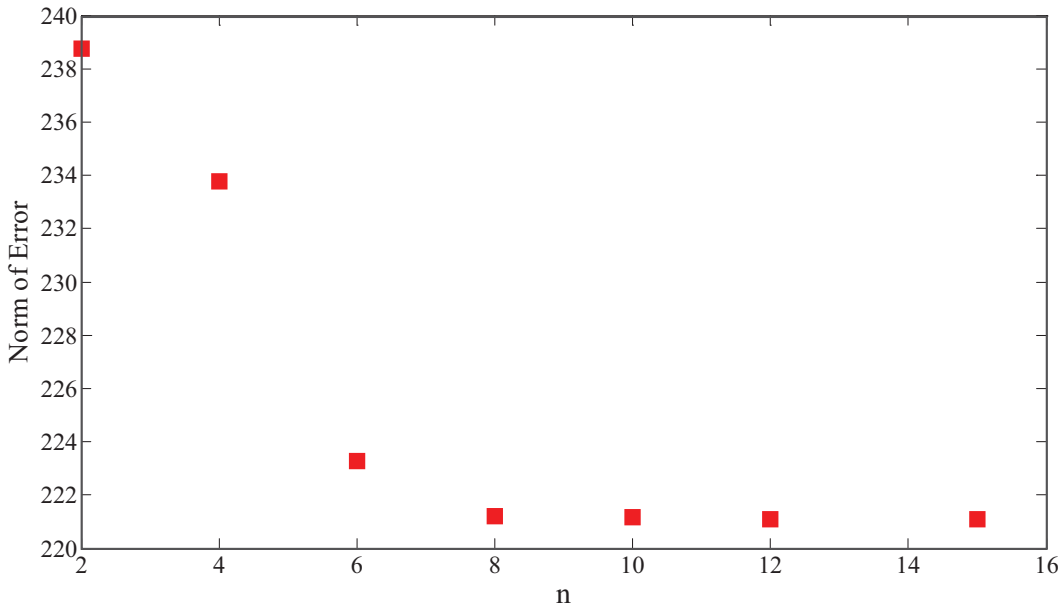

Figure 4.10: Variations in the norm of error with the number of the rate-dependent play operators (n).

The comparisons suggest that the proposed rate-dependent asymmetric Prandtl-Ishlinskii model can effectively characterize the hysteresis of the magnetostrictive actuator over a wide range of input amplitudes and frequencies. The model effectively describes the asymmetry and saturation tendencies of the actuator output under input current exceeding 2 A (Figure 4.12(a)), as it was observed from the measured data (Figure 4.2).

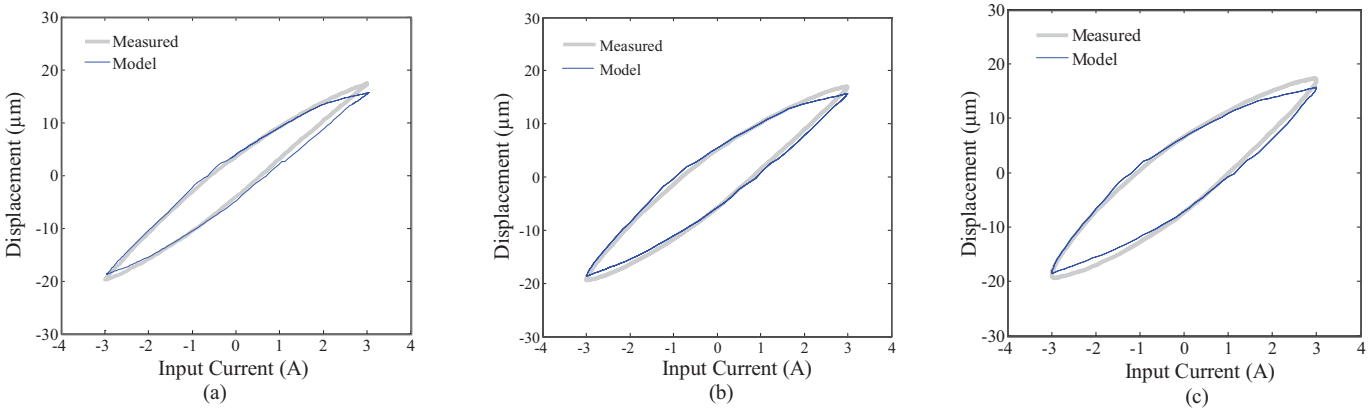

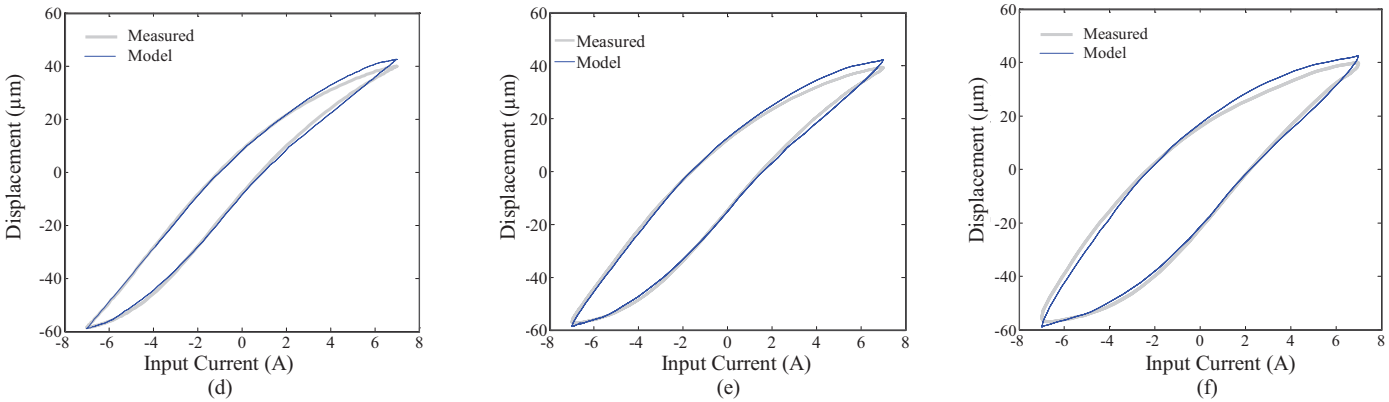

Figure 4.11: Comparisons of measured responses of the magnetostrictive actuator with those of the integrated Prandtl-Ishlinskii model Ω under: (a) I_o=3 A at 10 Hz; (b) I_o=3 A at 100; (c) I_o=3 A at 200 Hz; (d) I_o=7 A at 10 Hz; (e) I_o=7 A at 100 Hz; and (f) I_o=7 A at 200 Hz

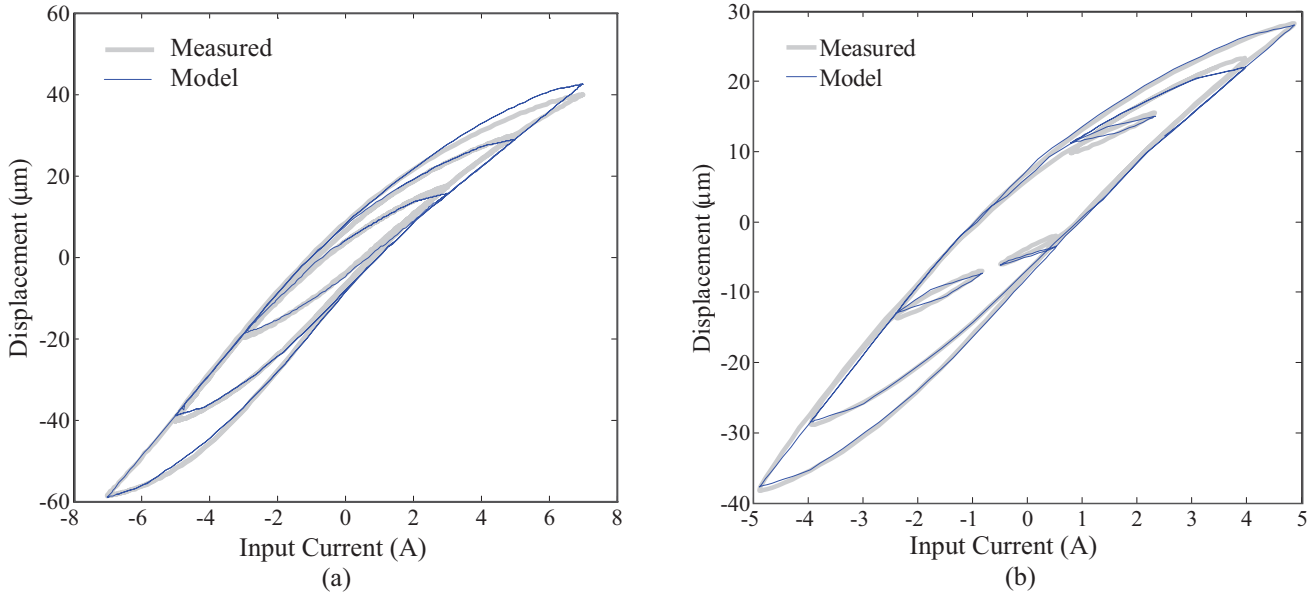

Figure 4.12: Comparisons of measured responses of the magnetostrictive actuator with those of the integrated Prandtl-Ishlinskii model under: (a) current of 3, 5 and 7 A at 10 Hz excitation frequency; and (b) complex harmonic input $I(t)$=2 sin(2.5×2π$f_o t$)+3 sin(2π$f_o t$) (f_o=20 Hz; magnetic bias = 44.1 kA/m).

The model also illustrates the effect of rate of input current on major hysteresis loops, irrespective of the current amplitude (Figure 4.11), although some errors between the model responses and measured data are evident under higher current excitations. The area bounded by the major hysteresis loop is further derived from the model response and compared with the measured data under I_o = 7 A at different excitation frequencies. The percent error between the area obtained from the model and the measured data ranged from a low of 0.12% at 10 Hz to maximum of 0.96% at

200 Hz. The peak percent error between the displacement response of the model and the measured displacement over the entire frequency range was 3.72%, which occurred at 200 Hz.

5.4.2 Relative significance of the proposed integrated hysteresis model

The relative significance of the proposed rate-dependent and asymmetric integrated model is explored by evaluating its performance in relation to: (i) the rate-independent and asymmetric hysteresis model proposed in [12]; and (ii) the rate-dependent Prandtl-Ishlinskii model alone. Consequently, the error minimization problem Figure 4.9 was solved for each model in order to identify the corresponding parameters. The output-input characteristics of the resulting models are compared in Figure 4.13 with those of the measured data obtained for the magnetostrictive actuator under 5 and 7 A excitations at 10, 50 and 200 Hz. The percent peak displacement error of each model is also obtained under 5 and 7 A inputs, as shown in Figure 4.14 (a) and (b), respectively. The results clearly show that the rate-independent asymmetric hysteresis model with the memoryless function, proposed in [12], yields substantial errors at high excitation frequencies. The peak error exceeds 13.5 % at 200 Hz excitation frequency. The rate-dependent Prandtl-Ishlinskii model, on the other hand, yields only symmetric hysteresis loops, while the peak displacement errors approach 9.6 % under inputs at 200 Hz.

Neglecting either the rate effect in the threshold of the Prandtl-Ishlinskii model or the asymmetry attributed to the memoryless function yields significant errors in the displacement responses of the magnetostrictive actuator model. It is clearly evident that implementation of the memoryless function to the rate-dependent Prandtl-Ishlinskii model enhances its ability to describe rate dependence of the asymmetric hysteresis effects in addition to the output saturation.

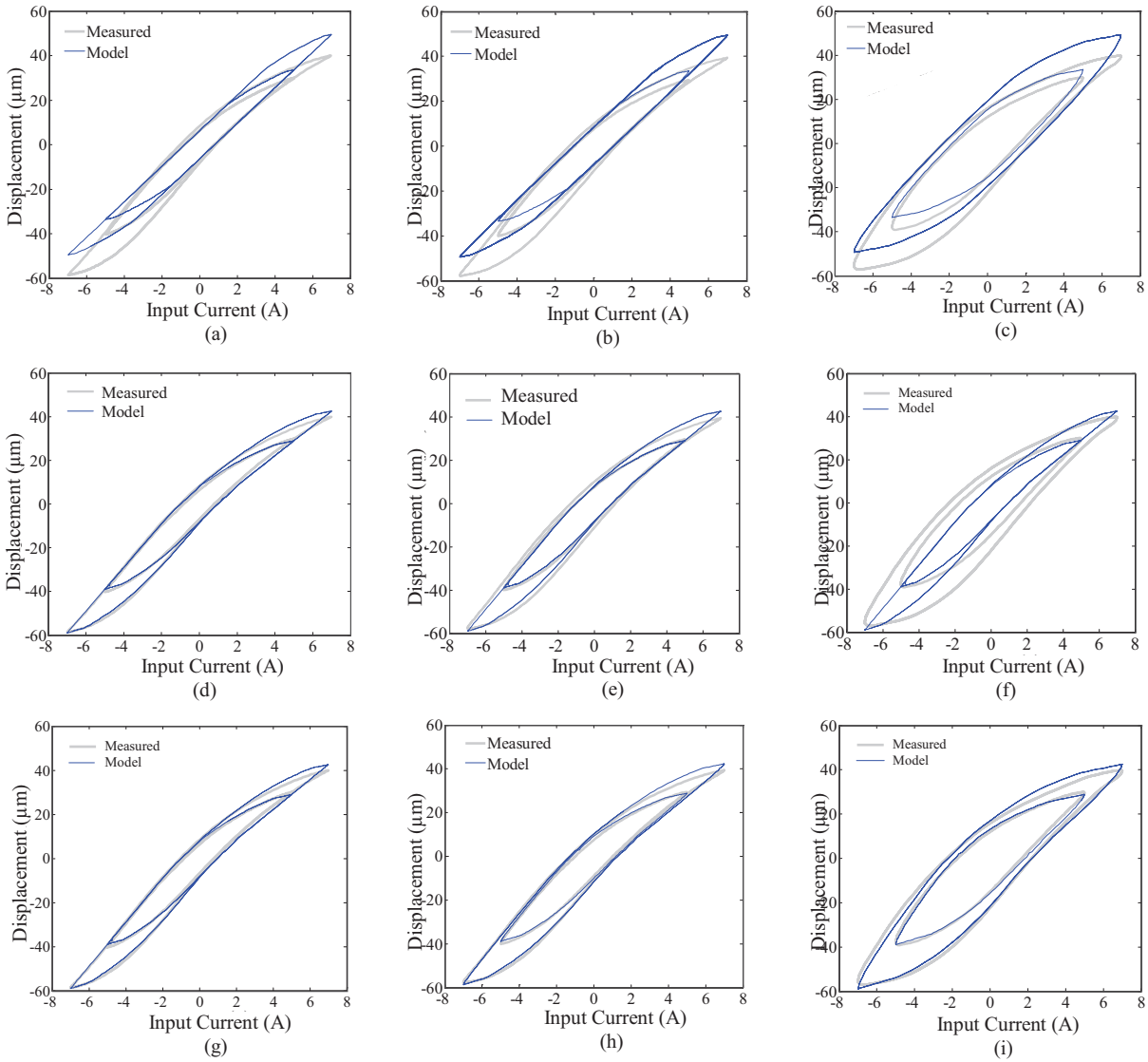

Figure 4.13: Measured responses at amplitudes of 5 and 7 A under 10, 50 and 200 Hz compared with those predicted from the: (a)-(c) rate-dependent symmetric Prandtl-Ishlinskii model, (d)-(f) asymmetric rate-independent Prandtl-Ishlinskii model [12]; and (g)-(i) the integrated Prandtl-Ishlinskii model Ω.

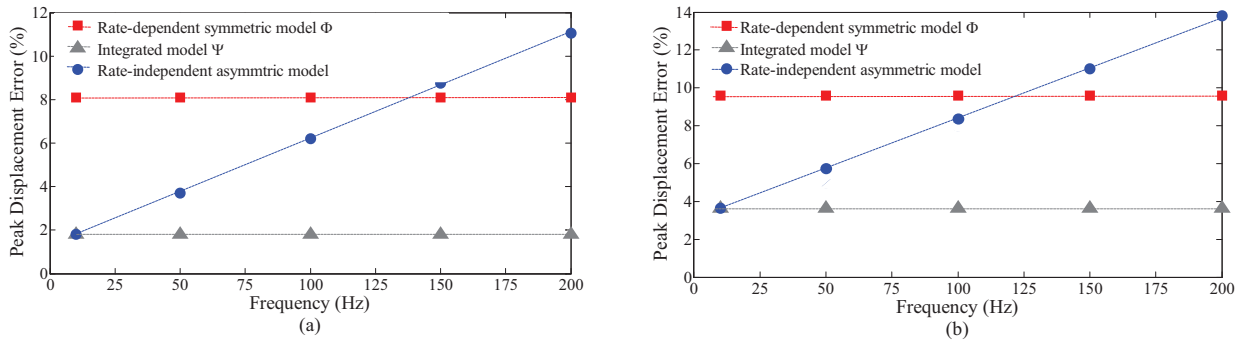

Figure 4.14: Comparisons of percent peak displacement error between the measured response from the actuator and the observed from the rate-dependent symmetric model Π, rate-independent

asymmetric model [12], and the integrated Prandtl-Ishlinskii model Ω at 10, 50 and 200 Hz applied under: (a) 5 A; and (b) 7 A.

5.5 Conclusions

The measured output-input characteristics of a magnetostrictive actuator suggested output asymmetry and saturation under medium to high amplitude excitations, and increasing hysteresis with increasing excitation frequency. The area bounded by the hysteresis loop increased nonlinearly with the input amplitude but nearly linearly with the excitation frequency. The variations in the magnetic field bias also showed substantial effects on output asymmetry and saturation, peak-to-peak displacement and the area bounded by the major hysteresis loop. The proposed rate-dependent Prandtl-Ishlinskii model integrating a memoryless function of dead-band operators could effectively describe the rate-dependent and asymmetric hysteresis properties of the actuator together with output saturation over wide ranges of input amplitudes and frequencies considered in the study. The peak error between the model displacement response and the measured data was 3.72 %, which occurred under the extreme excitation frequency of 200 Hz. It is further shown that the applications of reported rate-dependent Prandtl-Ishlinskii model, and the rate-independent Prandtl-Ishlinskii model with the memoryless function, would yield substantial response errors. It is thus concluded that neglecting either the rate effect in the threshold of the Prandtl-Ishlinskii model or the asymmetry attributed to the memoryless function would yield significant errors in the displacement response of the magnetostrictive actuator model.

CHAPTER 5

COMPENSATION OF RATE-DEPENDENT HYSTERESIS NONLINEARITIES IN A MAGNETOSTRICTIVE ACTUATOR USING INVERSE PRANDTL-ISHLINSKII MODEL

6.1 Introduction

Magnetostrictive actuators are increasingly being explored for various micro- and nano-positioning, and vibration control applications due to their fast response, and relatively large stroke and force capacity [1-4]. Such actuators, however, may yield limited positioning and tracking performance due to presence of hysteresis nonlinearities between the input current and the output

displacement [e.g.,1,7,8]. The hysteresis nonlinearities tend to be far more significant under high rates of inputs, which are known to cause inaccuracies and oscillations in the actuator's response, poor tracking performance and potential instabilities of the closed-loop system [5,7,8]. It is generally agreed that the tracking performance of such actuators could be significantly enhanced through compensation of hysteresis effects. Consequently, considerable efforts have been made towards accurate characterizations of hysteresis nonlinearities of different smart material-based actuators such as piezoceramic, magnetostrictive and shape memory alloys [8,45,85,89] and design of controllers for compensation of the hysteresis effects [5,7,35,42,49,90-93].

Different controller designs have been proposed to achieve effective compensation of hysteresis in smart material actuators including the magnetostrictive actuators. The size together with limited accuracy of the feedback devices, however, may pose challenges in realizing desirable micro-and nano-positioning precision, particularly under higher rates of inputs [85]. From a practical point of view, it has been suggested that hysteresis compensation of smart material-based actuators without a feedback device would be highly desirable [5,6]. A number of studies have proposed open-loop compensation of hysteresis nonlinearities of different smart material-based actuators [42,89]. Compensations of hysteresis effects of smart material actuators, particularly the piezoceramic and magnetostrictive have been attempted through applications of inverse hysteresis models or stop-operator based models as feedforward compensators [e.g.,12,44,94]. Such methods generally do not account for the strong dependence of the hysteresis nonlinearities on the rate of the applied input. The magnetostrictive actuators, similar to other smart material-based actuators, invariably, show increasing hysteresis with increasing excitation frequency [7,31,95]. The applications of inverse rate-independent hysteresis models would thus yield considerable

compensation errors under excitations at higher frequencies. It is thus desirable to formulate an accurate hysteresis model and its inverse considering a broad range of rates of the input.

The hysteresis nonlinearities of smart material-based actuators have been widely characterized using different phenomenological models [5,6,7,8,45,85,89]. Among these, the Prandtl-Ishlinskii model offers an attractive and unique property of being analytically invertible, attributed to continuity of the play operators. The Prandtl-Ishlinskii model would thus facilitate the formulation of the inverse rate-dependent hysteresis model and its real-time implementations for effective compensation of hysteresis [42,63,85]. In this study, a Prandtl-Ishlinskii model is formulated to characterize hysteresis nonlinearities of a magnetostrictive actuator under inputs at different frequencies. The model validity is demonstrated using the laboratory-measured output-input characteristics of the magnetostrictive actuator over a wide range of excitation frequencies. An inverse model is formulated on the basis of the hysteresis model incorporating the influence of the rate of input. Subsequently, the inverse rate-dependent model is applied in a cascade configuration with the rate-dependent hysteresis model to study its effectiveness as an open-loop feedforward hysteresis nonlinearity compensator under inputs in the 1 to 200 Hz range. The effectiveness of the proposed rate-dependent feedforward compensator is demonstrated through simulation results and laboratory tests.

6.2 Rate-dependent Prandtl-Ishlinskii model and its inverse

A Prandtl-Ishlinskii model is formulated to describe the hysteresis nonlinearity of a magnetostrictive actuator over a wide range of input frequencies. The Prandtl-Ishlinskii model is selected considering its many desirable properties including the abilities to obtain an analytical inverse and to incorporate the rate effect for predicting rate-dependent hysteresis nonlinearity [42,63,85]. The model employs a superposition of rate-dependent play operators with a rate-

dependent threshold function and positive weighting coefficients for characterizing hysteresis nonlinearities in smart actuators [9]. The model formulations have been described in [42,63] together with the condition that ensures analytic invertability of the rate-dependent Prandtl-Ishlinskii model. The rate-dependent Prandtl-Ishlinskii model is subsequently applied to formulate its inverse, which is applied to seek compensation of the rate-dependent hysteresis nonlinearity of a magnetostrictive actuator.

The rate-dependent Prandtl-Ishlinskii model is formulated considering rate-dependent play operators, which are real and continuous functions over the interval $(0,T)$. The space of such functions is denoted by $AC(0,T)$. For an input $v(t) \in AC(0,T)$, the thresholds of the play operators are defined such that:

$$0 \le r_0(\dot{v}(t)) \le r_1(\dot{v}(t)) \le r_2(\dot{v}(t)) \le \ldots \le r_n(\dot{v}(t)) \tag{5.1}$$

where $r_i(\dot{v}(t)) \in AC(0,T)$ is the rate-dependent threshold function; $i = 0, 1, 2, \ldots, n$, and $n \in \mathrm{N}$ is an integer.

The output $\bar{h}(t)$ of the rate-dependent play operator, $\Gamma[v](t)$, is given by:

$$\bar{h}_i(t) = \Gamma_{r_i(\dot{v}(t))}[v](t) \tag{5.2}$$

For any input $v(t) \in AC(0,T)$, the function v is considered monotone over each sub-interval $[t_{j-1}, t_j]$, and $0 = t_0 < t_1 < \ldots < t_l = T$ define the intervals. The output of the rate-dependent play operator may thus be expressed over a discrete interval, $t \in (t_{j-1}, t_j]$, as:

$$\bar{h}_i(t_j) = \max\{v(t_j) - r_i\left(\dot{v}(t_j)\right), \min\{v(t_j) + r_i\left(\dot{v}(t_j)\right), \bar{h}_i(t_{j-1})\}\} \tag{5.3}$$

with initial condition:

$$\bar{h}_i(0) = \max\{v(0) - r_i(\dot{v}(0)), \min\{v(0) + r_i(\dot{v}(0)),\ 0\}\} \tag{5.4}$$

The rate-dependent Prandtl-Ishlinskii model is constructed as a superposition of weighted rate-dependent play operators. The output $\Pi[v](t)$ of this model can be expressed as:

$$\Pi[v](t) = a_0 v(t) + \sum_{i=1}^{n} a_i \Gamma_{r_i(\dot{v}(t))}[v](t) \tag{5.5}$$

where a_0 and a_i are the positive weights.

The open-loop compensation employs the model inverse and the model in a cascade manner, as shown in Figure 5.1, so as to obtain an identity mapping between the input $v(t)$ and the output $u(t)$. The output of the inverse rate-dependent Prandtl-Ishlinskii model $\Pi^{-1}[v](t)$ is applied as a feedforward compensator of the rate-dependent Prandtl-Ishlinskii model $\Pi[v](t)$, such that the compensator and model yield identity transformation starting from the initial states, $\Pi^{-1}(0)$ and $\Pi(0)$. The output of the compensation can thus be expressed as:

$$\Pi \circ \Pi^{-1}[v](t) = u(t) \tag{5.6}$$

The formulation of the inverse model $\Pi^{-1}[v](t)$, however, holds under the condition that the differences between consecutive dynamic thresholds, $r_{i+1}(\dot{v}(t))$ and $r_i(\dot{v}(t))$, do not decrease in time [63]. Analytically for $\forall\, i = 1, \ldots, n\text{-}1$:

$$\frac{d}{dt}\left(\Delta r_i(\dot{v}(t))\right) \geq 0 \tag{5.7}$$

where $\Delta r_i(\dot{v}(t))$ is the difference between two consecutive thresholds.

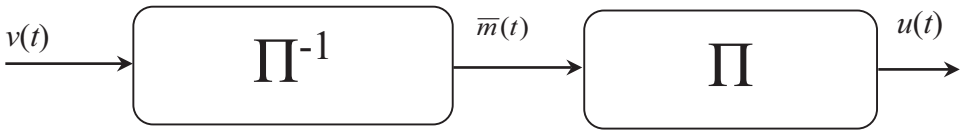

Figure 5.1: A cascade arrangement of the rate–dependent inverse Prandtl-Ishlinskii model Π^{-1} and the hysteresis model Π.

The output $\overline{m}(t)$ of the inverse rate-dependent Prandtl-Ishlinskii model can be expressed as [63]:

$$\overline{m}(t) = \Pi^{-1}[v](t) = \hat{a}_0 v(t) + \sum_{i=1}^{n} \hat{a}_i \Gamma_{\hat{r}_i(\dot{v}(t))}[v](t) \tag{5.8}$$

The rate-dependent thresholds of the inverse model $\hat{r}_i(\dot{v}(t))$ are related to those of the model itself, $r_i(\dot{v}(t))$, in the following manner [63]:

$$\begin{aligned} \hat{r}_1(\dot{v}(t)) &= a_0 \; r_1(\dot{v}(t)) \\ \hat{r}_{i+1}(\dot{v}(t)) &= \hat{r}_i(\dot{v}(t)) + \sum_{j=0}^{i} a_j \left(r_{i+1}(\dot{v}(t)) - r_i(\dot{v}(t)) \right) \end{aligned} \tag{5.9}$$

The weights of the inverse model $\hat{a}_0$, $\hat{a}_1$,…, $\hat{a}_n$ are also related to those of the Prandtl-Ishlinskii model $\Pi[v](t)$, as:

$$\hat{a}_i = \frac{1}{\sum_{j=0}^{i} a_j} - \frac{1}{\sum_{j=0}^{i-1} a_j} \; ; \; \textit{and} \; \hat{a}_0 = \frac{1}{a_0} \tag{5.10}$$

6.3 Characterization of hysteresis of a magnetostrictive actuator

The developments of the rate-dependent Prandtl-Ishlinskii model and the inverse necessitate accurate descriptions of the output-input characteristics of the smart-material actuator over a wide range of inputs. In this study, experiments were performed on a magnetostrictive actuator (Etrema Inc; model MFR OTY77) to measure its rate-dependent hysteresis nonlinearities under harmonic excitations in the 1-200 Hz frequency range. The actuator consisted of a wound wire solenoid surrounding two Terfenol-D rods, which are preloaded by a compression bolt and a spring washer.

Three permanent magnets are installed along the Terfenol-D rods to provide a magnetic field with a bias. Figure 5.2 illustrates the primary components of the actuator. The actuator provides a peak-to-peak output displacement of 100 μm under excitations at frequencies up to 1250 Hz. A capacitive sensor (Lion Precision; model $C23-C250$) with sensitivity of 80 mV/μm, bandwidth of 15 KHz, and a resolution of 35.53 nm was used to capture the output displacement of the actuator with respect to the static position. The excitation signals, $v_0(t)$, of different magnitudes and frequencies were synthesized in the ControlDesk platform and applied to a power amplifier (AE TECHRON; model LVC 2016). The current output of the power amplifier was subsequently applied to the actuator, as shown in Figure 5.3. The actuator displacement response, measured by the capacitive sensor, was also acquired in the dSpace ControlDesk together with the applied input signal $v(t)$ in order to generate the output-input hysteresis loops.

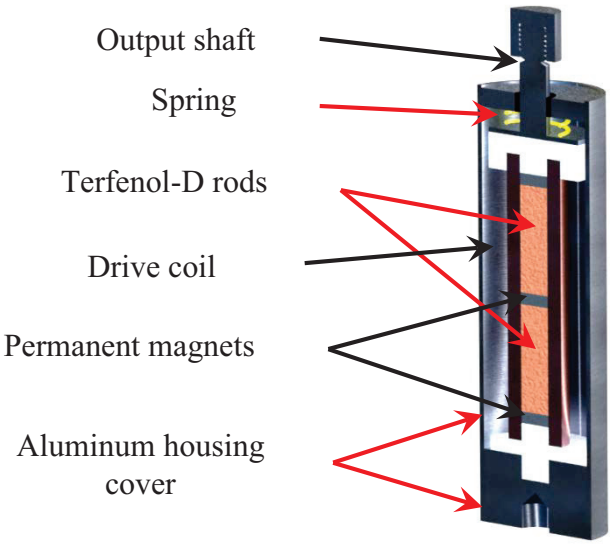

Figure 5.2: Construction of a Terfenol-D magnetostrictive actuator.

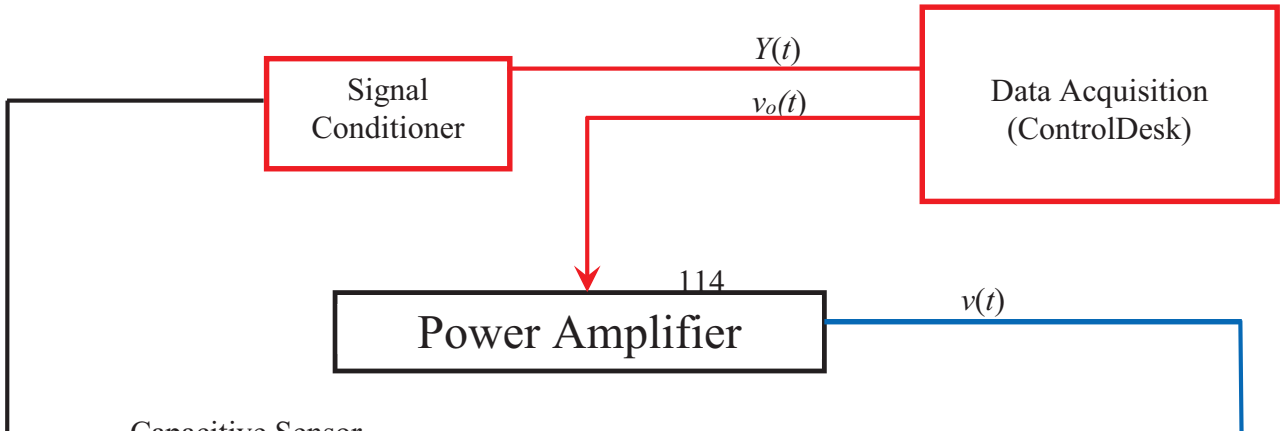

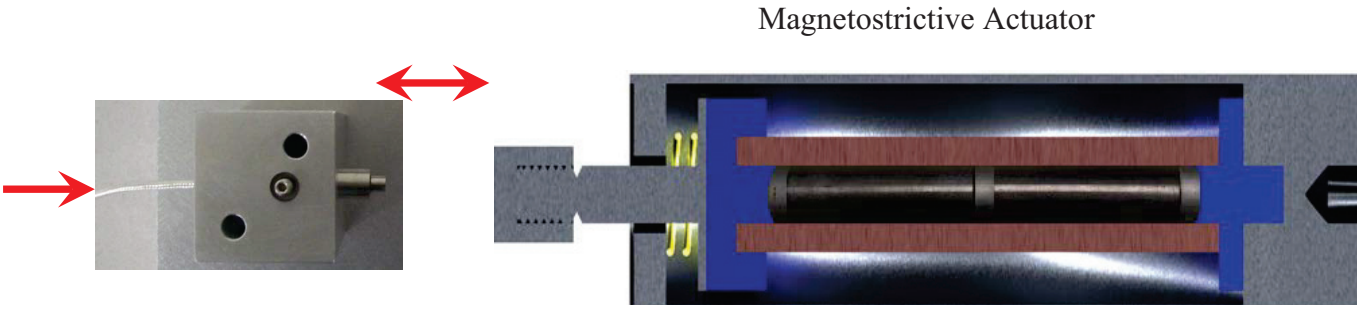

Figure 5.3: Experimental setup for characterization of hysteresis nonlinearities of a magnetostrictive actuator.

The response characteristics of the actuator were measured to characterize hysteresis loops at different discrete frequencies in the 1-200 Hz frequency range. The measurements were carried out under a harmonic input current of 2.3 A amplitude at different frequencies (1, 50, 100, 150, and 200 Hz). The major and minor hysteresis loops were also characterized under a complex harmonic input of the form: $v(t) = 1.0 \sin(100\pi ft)+1.3 \sin(90\pi ft)$. Figure 5.4(a) displays the output-input properties of the actuator under excitations at 1, 50 and 200 Hz. The figure illustrates considerably higher hysteresis at a higher frequency. The output-input characteristics under the complex harmonic input are illustrated in Figure 5.4 (b), which show the major as well as minor hysteresis loops. The data were further analyzed to derive peak normalized hysteresis, ratio of maximum difference in the outputs under decreasing and increasing input and the peak-to-peak output, as a function of the input frequency. Figure 5.5 depicts variations in percent peak normalized hysteresis as a function of the frequency of the applied input current. The results suggest nearly linear increase in the normalized hysteresis with the frequency (r^2= 0.9993) over the frequency range considered in the study.

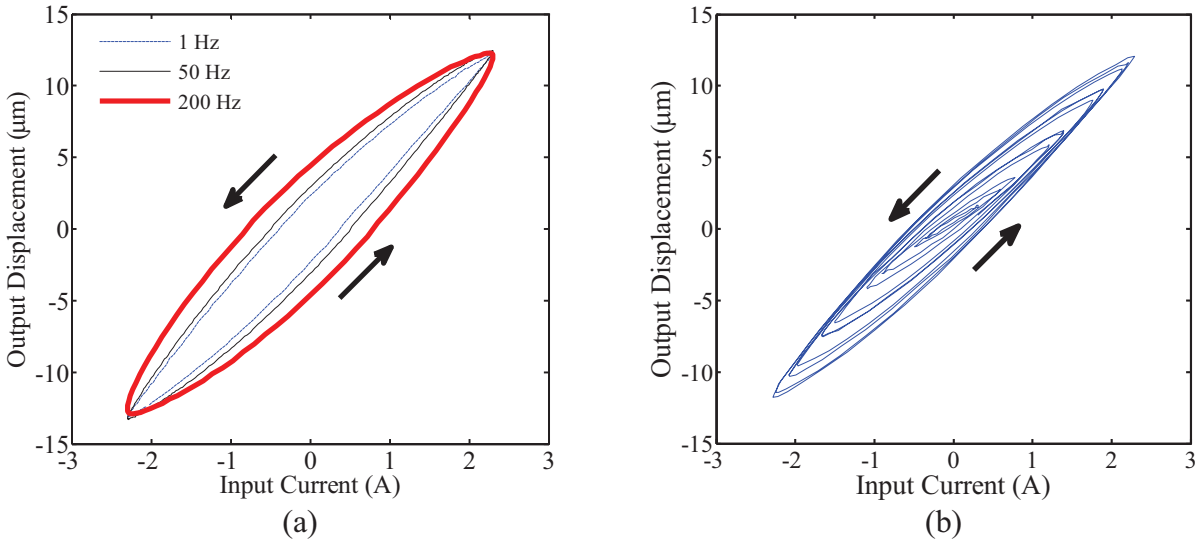

Figure 5.4: Measured hysteresis nonlinearities of the magnetostrictive actuator under different inputs: (a) $v(t) = 2.3 \sin(2\pi f\, t)$, f=1 Hz, 50 Hz and 200 Hz; and (b) $v(t) = 1.0\sin(100\pi t) + 1.3 \sin(90\pi t)$ A.

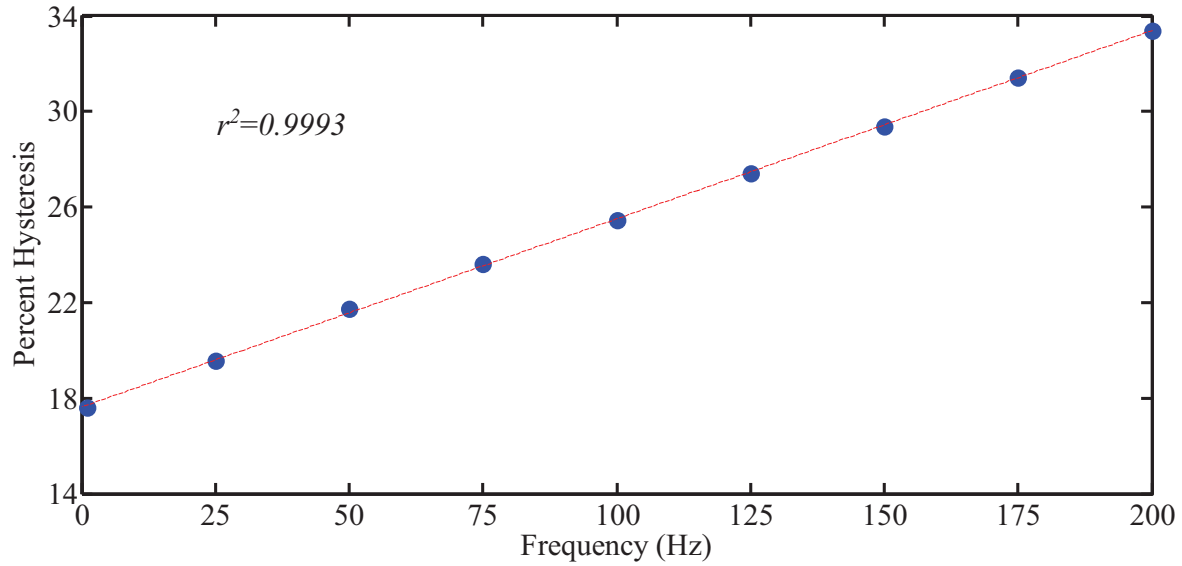

Figure 5.5: Percent peak normalized hysteresis of current-to-displacement loops of the magnetostrictive actuator at different excitation frequencies.

6.3.1 Model parameters identification

The laboratory-measured data suggests that a threshold function that is linearly related to the rate of input would be most appropriate to describe the rate-dependent Prandtl-Ishlinskii model of the

magnetostrictive actuator considered in the study. The measured responses suggest that a rate-dependent threshold as a linear function of the rate of input may thus be considered:

$$r_i\left(\dot{v}(t)\right) = \alpha\ i + \gamma\ \left|\dot{v}(t)\right| \tag{5.11}$$

where α and γ are positive constants. The difference between the two consecutive thresholds, $\Delta r_i(\dot{v}(t))$, is thus a positive constant:

$$\Delta r_i(\dot{v}(t)) = \alpha \tag{5.12}$$

and

$$\frac{d}{dt}\left(\Delta r_i(\dot{v}(t))\right) = 0 \tag{5.13}$$

The above satisfies the condition for inverse rate-dependent Prandtl-Ishlinskii model. Furthermore, the threshold function can be approximated as $r_i\left(\dot{v}(t)\right) \cong \alpha\ i$ at low excitation frequencies, suggesting that the Prandtl-Ishlinskii model can also characterize the rate-independent hysteresis nonlinearities. The parameter vector, $X = \{\alpha, \gamma, a_0, a_1, a_2, \ldots, a_n\}$ of the rate-dependent Prandtl-Ishlinskii model Π, was identified through minimization of the error function Θ over the range excitation frequencies, given by:

$$\Theta(X) = \sum_{\bar{b}=1}^{\bar{B}} \sum_{m=1}^{M} A_{\bar{p}} \left(\Pi(v(t,m,f_{\bar{b}})) - Y(t,m,f_{\bar{b}})\right)^2 \tag{5.14}$$

where $\Pi(v(t,m,f_{\bar{p}}))$ is the displacement response of the rate-dependent Prandtl-Ishlinskii model under a given excitation frequency $f_{\bar{p}}$ and $Y(t,m,f_{\bar{p}})$ is the measured displacement under the same excitation frequency. The index m ($m = 1, \ldots, M$) refers to the number of data points considered in computing the error function for one complete hysteresis loop. The error minimization problem in this study was formulated considering $M = 400$ for each measured hysteresis loop. The index $\bar{b}$ (

$\bar{b}$ = 1, 2, 3, and $\bar{B}$) denotes the number of discrete frequencies considered in the error function over the 1 to 200 Hz frequency range. Owing to the higher hysteresis at higher excitation frequencies, a weighting constant $A_{\bar{b}}$ was introduced to emphasize the error minimization at higher excitation frequencies. The weighting at a frequency $f_{\bar{b}}$ was taken as the ratio of peak normalized hysteresis at $f_{\bar{b}}$ to that under excitation at a low frequency, e.g., 1 Hz. The error minimization problem (5.14) was solved using the MATLAB constrained optimization toolbox, subject to following constraints:

$$\{\alpha, \gamma, a_0, a_1, \ldots, a_n\} > 0$$

The solutions were obtained considering different number of operators, ranging from 4 to 35. In each case, the repeated solutions of the minimization problem were obtained using different values of the starting vector, which converged to very similar model parameter vector.

The validity of the resulting models was examined by comparing the model responses with the measured data in terms of output-input loops and peak normalized hysteresis over the entire frequency range. The results revealed that model with as few as 4 play operators (n=4) could yield reasonably accurate characterization of the hysteresis nonlinearities. The error minimization considering only 4 operators resulted in parameter vector: α = 0.309, γ= 2.73×10^{-4}, a_0 = 0.4870, a_1 = 0.4261, a_2 = 0.0134, a_3 =0.0638 and a_4 = 0.1996. As an example, Figure 5.6 (a) to (c) compare the output-input hysteresis predicted from the model comprising only 4 operators with the measured data under harmonic excitations at 1, 50 and 200 Hz, respectively. The minor and major hysteresis loops obtained from the model under the complex harmonic excitation, considered in experimental characterization, are also compared with the measured data in Figure 5.6 (d). The

percent peak normalized hysteresis, derived from the predicted responses, is also compared with the measured data in Figure 5.7 which suggests very close agreement in the entire frequency range.

The responses of model comprising 25 play operators are also compared with the measured data in Figure 5.8 under same excitations. The results in Figure 5.6 and Figure 5.8, suggest that the model with only 4 operators would provide sufficiently accurate characterization of hysteresis of the actuator considered in the study under inputs up to 200 Hz in a highly efficient manner. Moreover, the model with fewer operators would be beneficial in formulating the model inverse with only fewer model parameters and facilitate its hardware implementation.

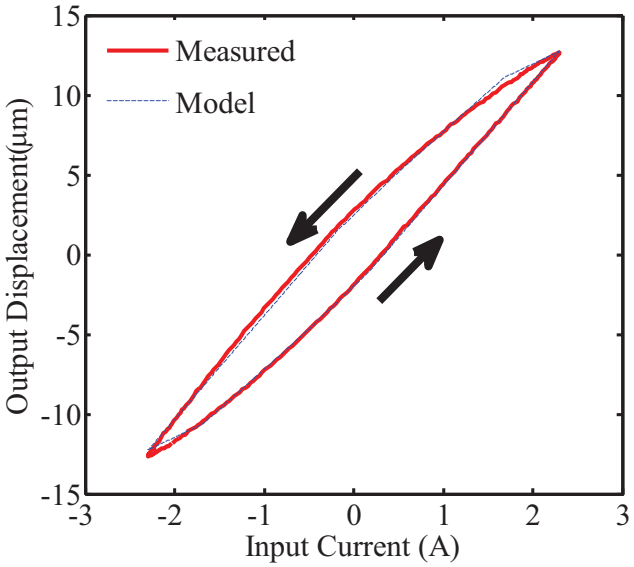

(a)

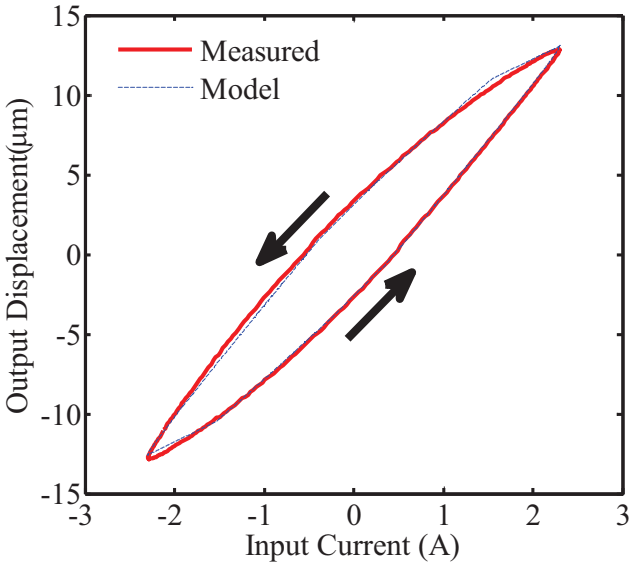

(b)

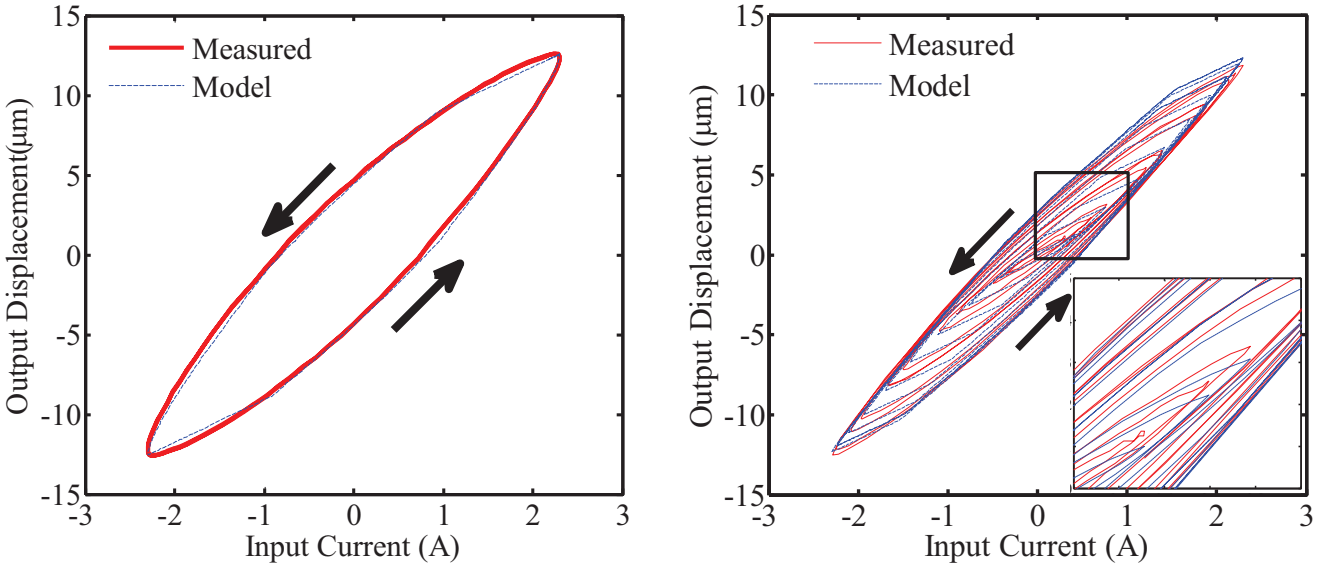

Figure 5.6: Comparisons of measured responses of the magnetostrictive actuator with those of the Prandtl-Ishlinskii model Π, formulated using *4* rate-dependent play operators, under 2.3 A harmonic input at different frequencies: (a) 1 Hz, (b) 50 Hz, (c) 200 Hz; and (d) the complex harmonic input, $v(t) = 1.0 \sin(100\pi t) + 1.3 \sin(90\pi t)$ A.

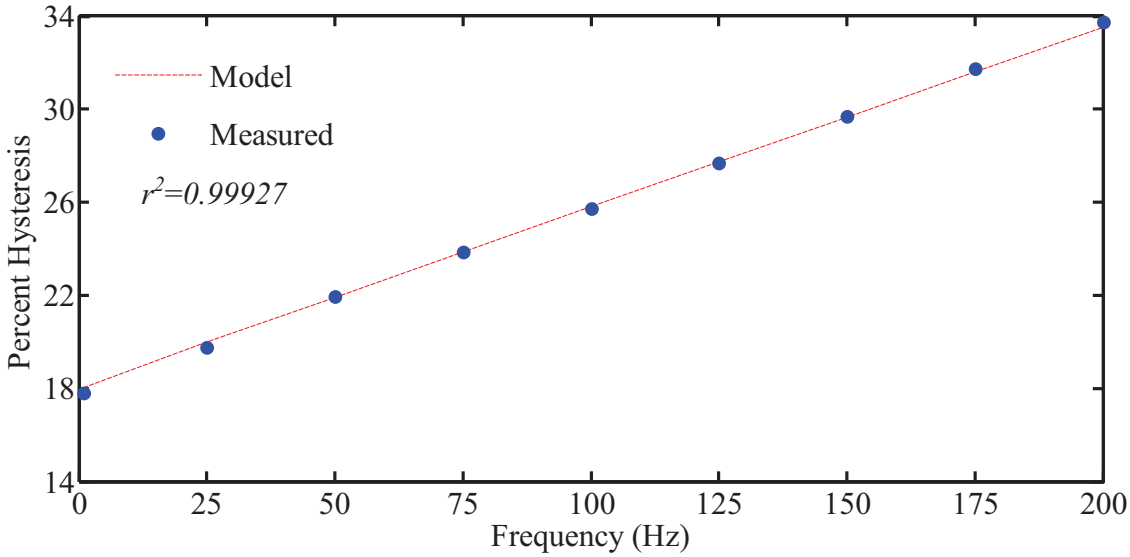

Figure 5.7: Comparisons of the percent peak normalized hysteresis obtained from the Prandtl-Ishlinskii model, formulated using *4* rate-dependent play operators, with the measured data under harmonic excitations at different frequencies.

6.4 Feedforward compensation of rate-dependent hysteresis nonlinearities

The inverse rate-dependent Prandtl-Ishlinskii model was formulated using the identified model parameters and relations (5.9) and (5.10). The output of the inverse rate-dependent Prandtl-Ishlinskii model can be expressed as:

$$\Pi^{-1}[v](t) = \hat{a}_0 v(t) + \sum_{i=1}^{n} \hat{a}_i \Gamma_{\hat{r}_i(\dot{v}(t))}[v](t) \tag{5.15}$$

The output-input characteristics of the inverse rate-dependent Prandtl-Ishlinskii model (n=4) under harmonic inputs (amplitude = 2.3 A) at 1, 50 and 200 Hz are shown in Figure 5.9, along with those attained under the complex harmonic input, $v(t)$= sin(100πft)+1.3sin(90πft). The results show hysteresis loops in the clockwise direction opposed to the counter-clockwise loops obtained from the hysteresis model (Figure 5.6 Figure 5.8). The results further show that the loops are not smooth, which is partly attributed to consideration of only 4 operators.

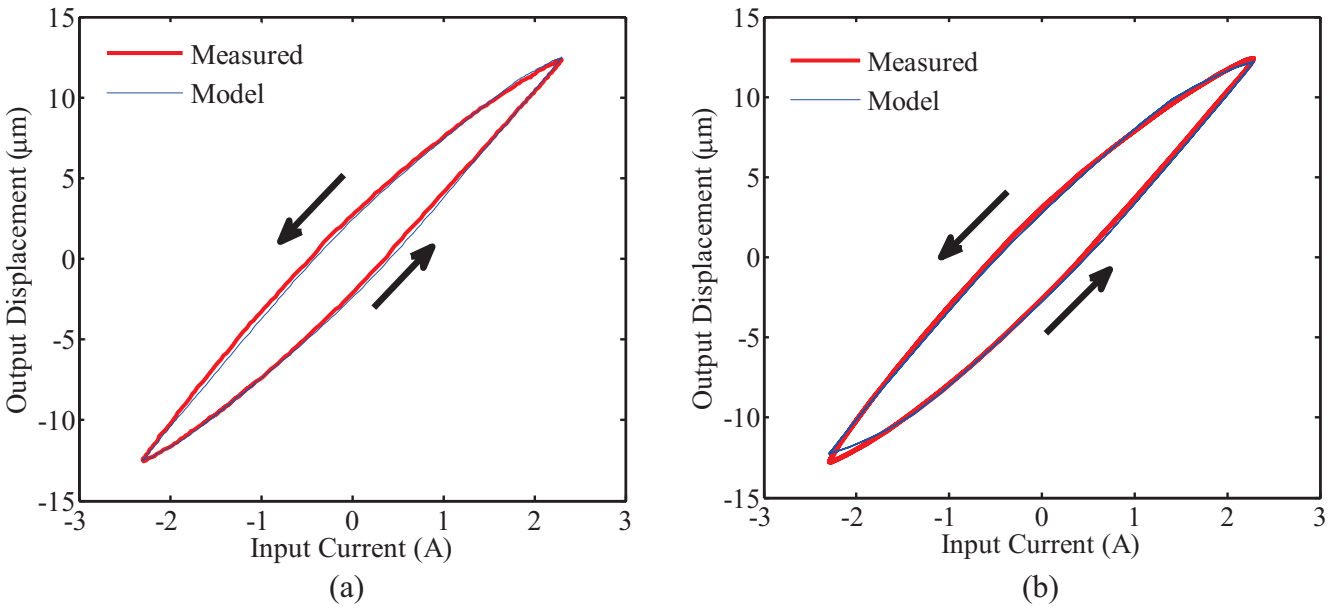

(a) (b)

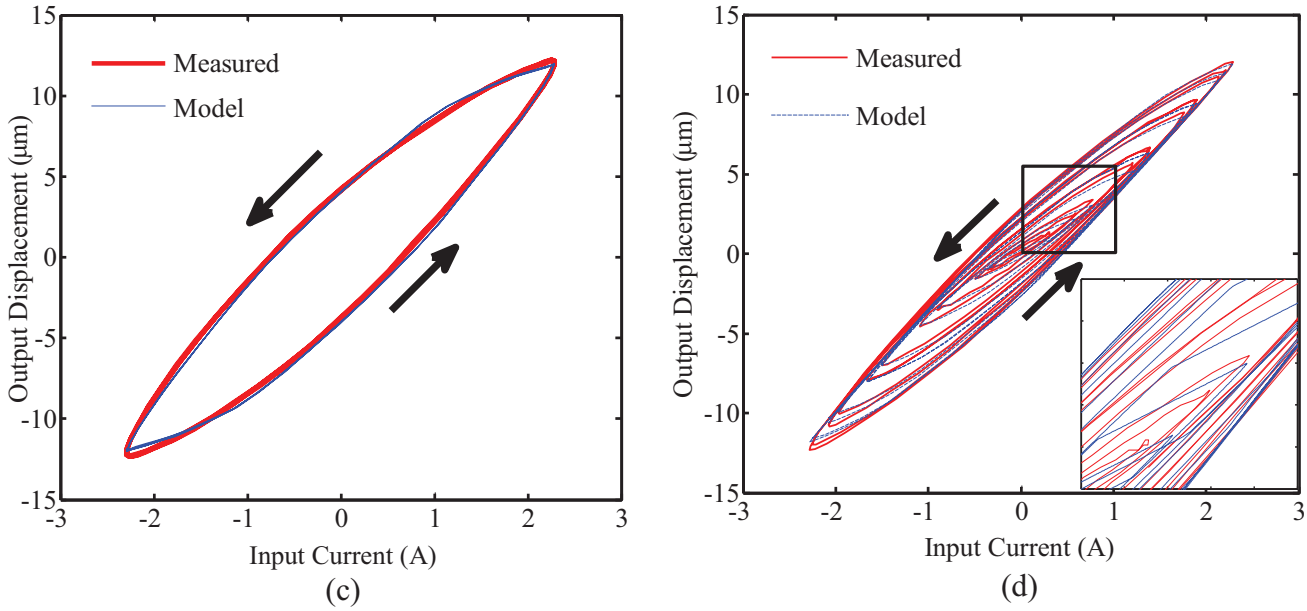

Figure 5.8: Comparisons of measured responses of the magnetostrictive actuator with those of the Prandtl-Ishlinskii model Π, formulated using *25* rate-dependent play operators, under 2.3 A harmonic input at different frequencies: (a) 1 Hz, (b) 50 Hz, (c) 200 Hz; and (d) the complex harmonic input, $v(t)$ =1.0 sin(100πt)+1.3 sin(90πt) A.

6.4.1 Simulation results

The simulations were performed to obtain the outputs of the cascade arrangement of the inverse rate-dependent Prandtl-Ishlinskii model and the Prandtl-Ishlinskii model. The magnetostrictive actuator gain of 0.1803 A/μm is applied to the inverse model output, which serves as input $v(t)$ to the Prandtl-Ishlinskii model. The outputs of the two models, Π^{-1} and Π, together with the compensated output $u=\Pi\circ\Pi^{-1}[v]$ under harmonic inputs at different frequencies (1, 50 and 200 Hz) are illustrated in Figure 5.10 (a) to 10(c). The results clearly show effective mitigation of the hysteresis effects by the inverse model-based feedforward compensator, irrespective of the excitation frequency within the range considered. The effectiveness of the rate-dependent feedforward compensator in compensating for the minor hysteresis loops is also evident from the results attained under the complex harmonic input, shown in Figure 5.10(d). Since the rate-dependent Prandtl-Ishlinskii model Π satisfies the necessary condition (5.7) in rate-dependent

thresholds for the inverse rate-dependent Prandtl-Ishlinskii model to be exact [63] the error in the compensated output $u=\Pi \circ \Pi^{-1}$ is zero. This is particularly true in the simulation results where the characterization errors of the model are absent.

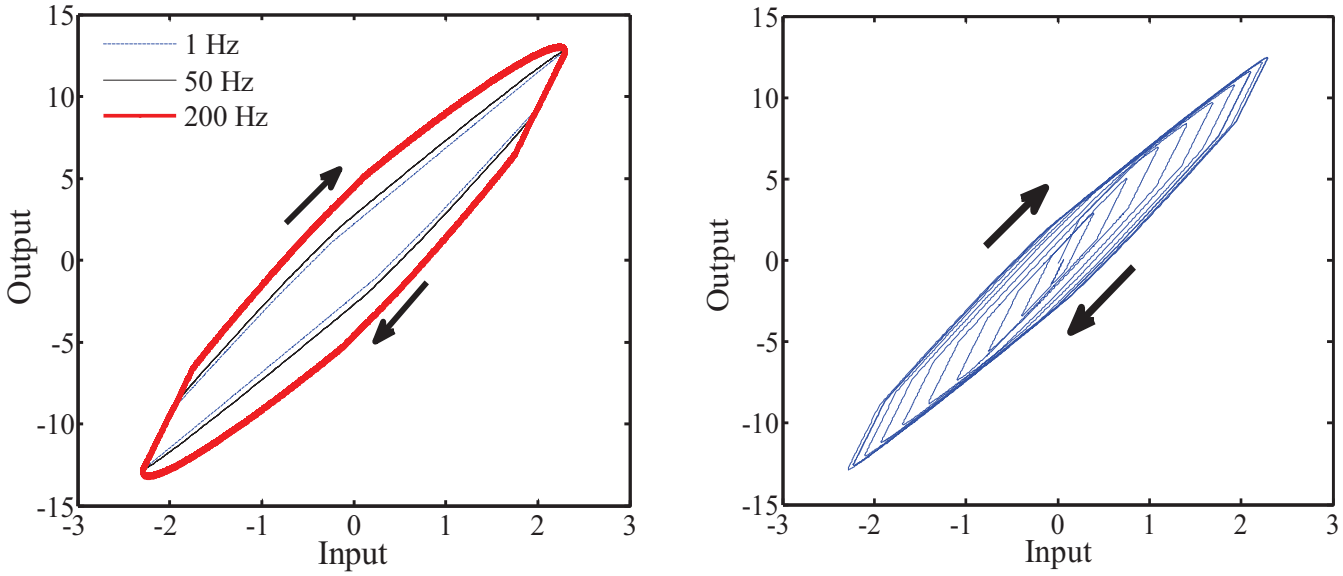

Figure 5.9: The output-input characteristics of the inverse Prandtl-Ishlinskii model, formulated using 4 rate-dependent play operators, under harmonic and complex harmonic inputs: (a) $v(t) = 2.3 \sin(2 \pi ft)$, $f = 1$, 50 and 200 Hz ; and (b) $v(t) = 1.0\sin(100\pi t) + 1.3 \sin(90\pi t)$.

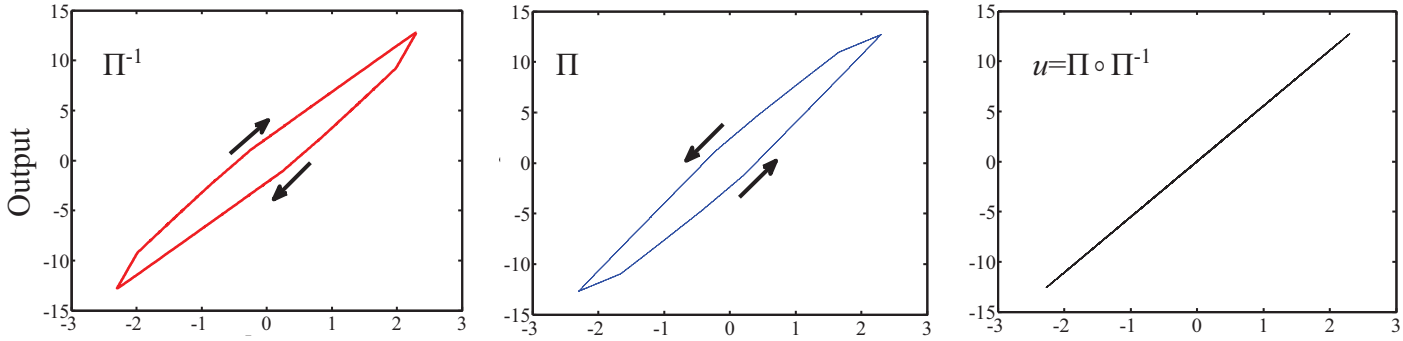

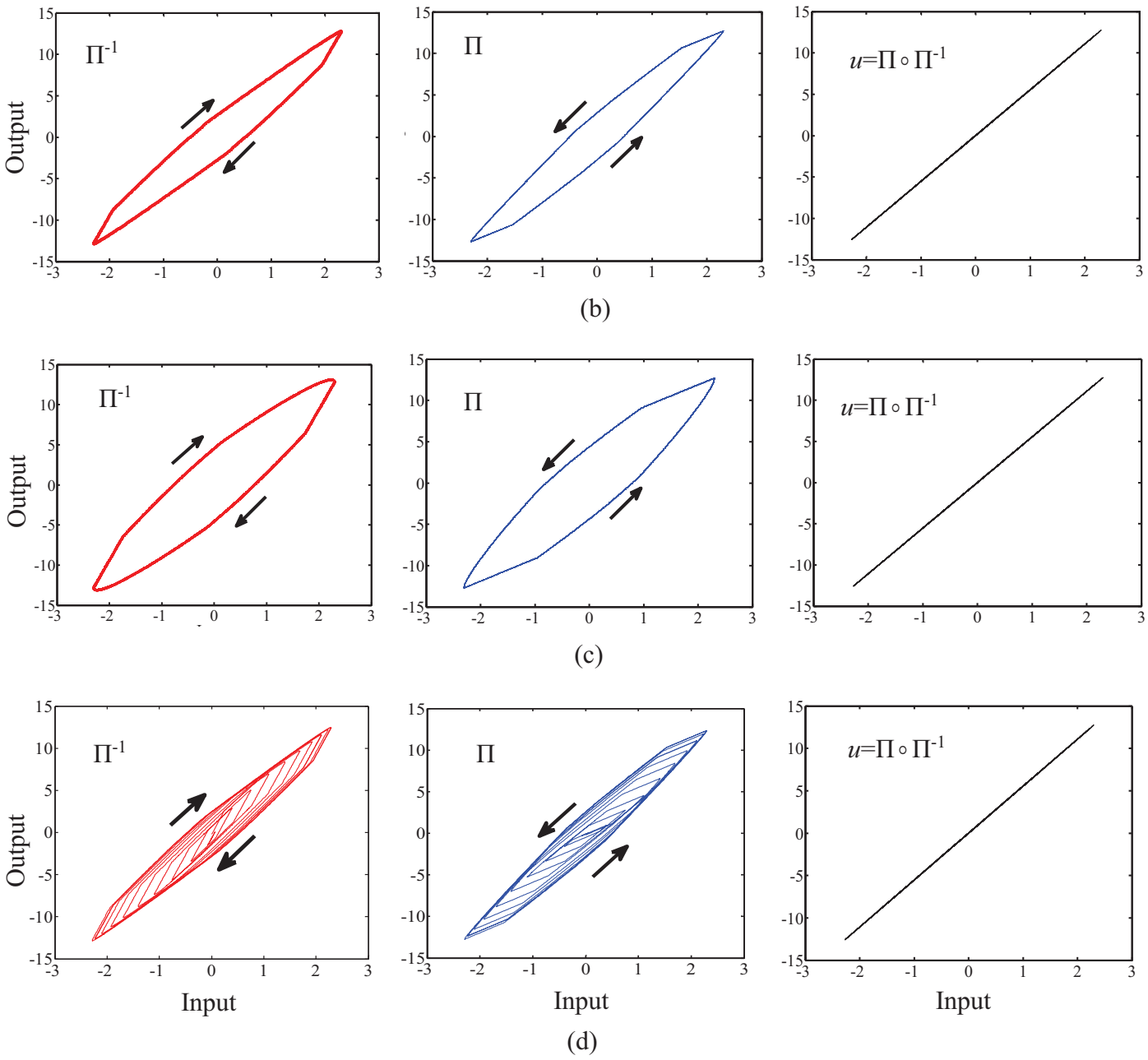

Figure 5.10: Output-input characteristics of the inverse rate-dependent Prandtl-Ishlinskii model Π^{-1}, rate-dependent Prandtl-Ishlinskii model Π, and the compensated output $u=\Pi \circ \Pi^{-1}$, where $v(t)=2.3\sin(2\pi ft)$, (a) f =1 Hz, (b) f =50 Hz, and (c) f =200 Hz, and (d) $v(t)=1.0\sin(100\pi t)+1.3\sin(90\pi t)$.

6.4.2 Experimental results

The effectiveness of the inverse rate-dependent Prandtl-Ishlinskii model as a feedforward hysteresis compensator is further investigated in the laboratory. A hardware-in-the-loop experiment was designed, where the inverse model was used as the feedforward hysteresis compensator in the ControlDesk platform. The inverse rate-dependent model based on only 4 rate-dependent play operators was applied in the experiment so as to assess its effectiveness in a simple and efficient manner. Harmonic inputs at different frequencies were applied to the compensator, and the output together with the actuator gain (0.1803 A/μm) was applied to the magnetostrictive actuator through the power amplifier. The measured actuator displacement response was subsequently acquired in the ControlDesk. The variations in measured actuator displacement with the input current applied to the feedforward compensator are illustrated in Figure 5.11(a) for different excitation frequencies. Figure 5.11(b) shows the response under the complex harmonic input. The results show that the inverse rate-dependent model can effectively compensate for the hysteresis effects, major as well as minor loops, of the actuator at different excitation frequencies in the 1-200 Hz range. Some deviations, however, are evident in the compensated output, which are mostly attributed to the characterization errors and prediction errors of the rate-dependent Prandtl-Ishlinskii model.

The peak hysteresis error was further computed from the measured data corresponding to each excitation frequency. As an example, Figure 5.12 (a) illustrates the time-history of the error under the harmonic excitation at 100 Hz, which suggests peak error of nearly 0.621 μm (4.77% of the peak displacement). The peak error is significantly lower than that obtained without the compensator (nearly 25.7%). The peak errors, expressed in percent of the peak displacement, under inputs at different frequencies are further summarized in Figure 5.12 (b). The results suggest

comparable error at frequencies above 75 Hz but slightly large error, in the order of 4.96%, at very low frequencies. The results suggest that the inverse rate-dependent Prandtl-Ishlinskii model can effectively compensate for positioning error due to hysteresis in the entire frequency range considered in the study. The slightly higher error at low frequencies is attributable to rate dependency of the threshold function employed in the Prandtl-Ishlinskii model.

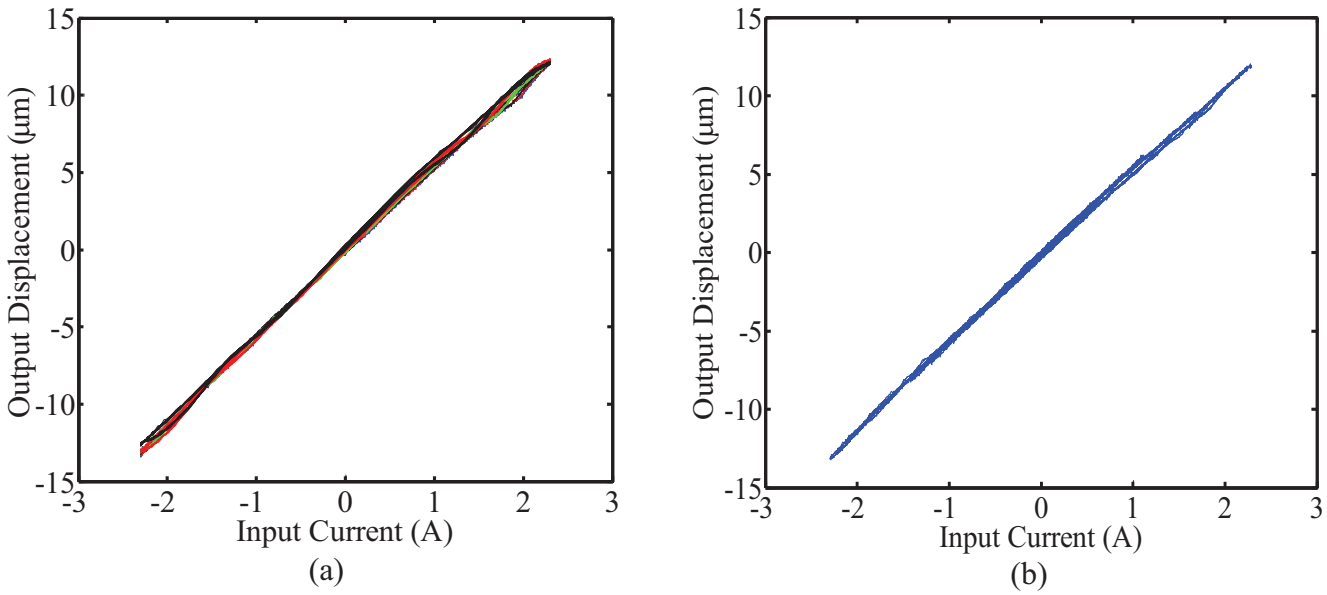

Figure 5.11: The output-input characteristics of the magnetostrictive actuator employing the inverse rate-dependent Prandtl-Ishlinskii model as a feedforward compensator under different inputs: (a) $v(t)=2.3\sin(2\pi ft)$ A, f =1, 25, 50, 75, 100, 125, 150, 175 and 200 Hz; and (b) $v(t)=1.0\sin(100\pi t)+1.3\sin(90\pi t)$ A.

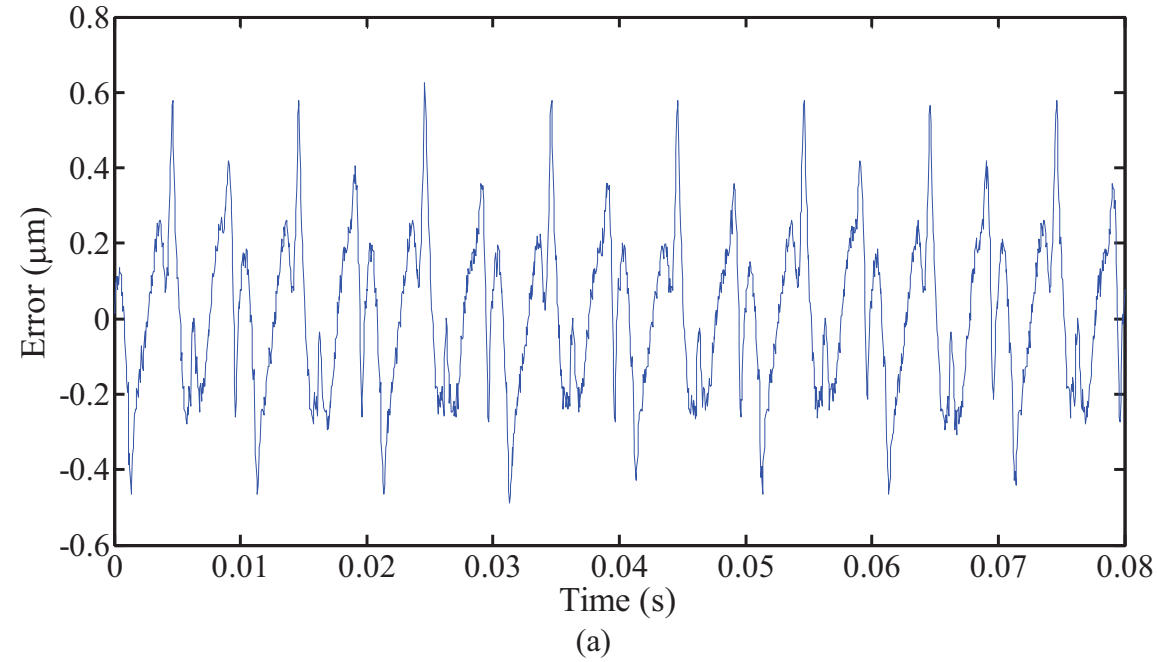

(a)

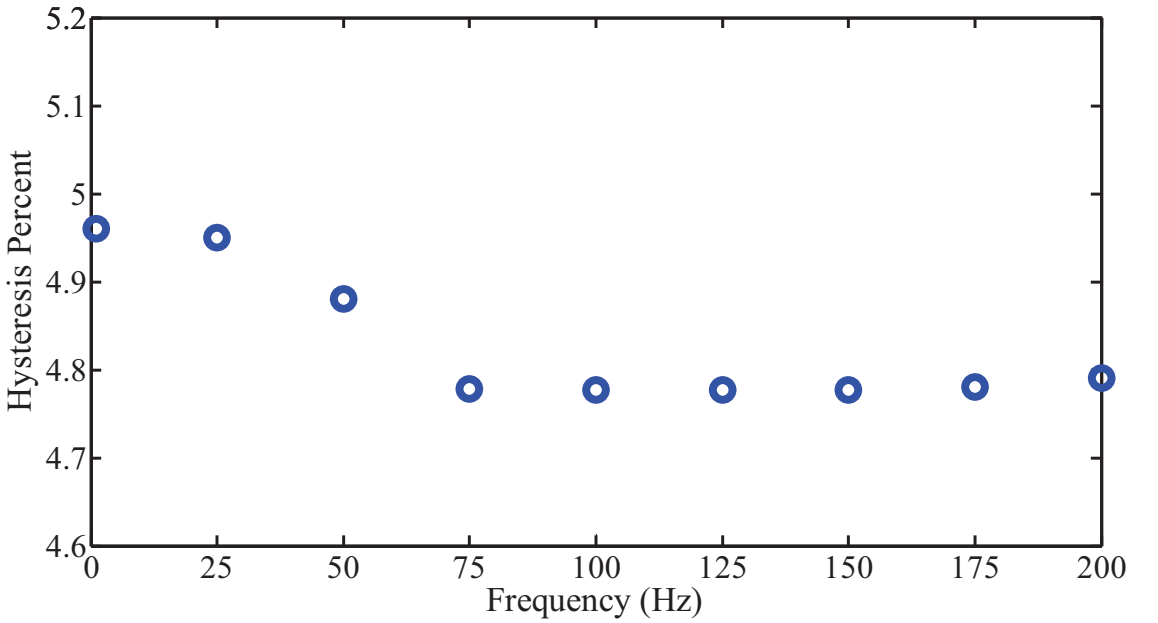

(b)

Figure 5.12: (a) The time-history of the error with the inverse rate-dependent Prandtl-Ishlinskii model under the harmonic excitation at 100 Hz, (b) Percent peak normalized hysteresis of current-to-displacement loops of the magnetostrictive actuator with the inverse rate-dependent Prandtl-Ishlinskii model at different excitation frequencies.

6.5 Conclusions

The results suggest that the inverse rate-dependent Prandtl-Ishlinskii model can provide effective compensation for hysteresis nonlinearities under inputs applied over a wide frequency range. The simulation and experimental results further showed that an inverse model based on only a few operators (n=4) could suppress the hysteresis errors effectively in a highly efficient manner. Consideration of larger number of play operators would yield even lower positioning error although at the expense of relatively higher implementation complexity. The simulations and laboratory implementations in the study, however, are limited only to symmetric hysteresis loops. The proposed compensator can thus be considered valid under inputs within the linear operating range of the magnetostrictive actuator. Smart-material actuators generally exhibit asymmetric loops and output saturation nonlinearities under moderate to high drive levels [1]. A magnetostrictive actuator will also yield asymmetric hysteresis loops in the presence of bias in the applied current or the pre- compression of the Terfenol-D rods. The hysteresis compensation under a wide range of drive amplitudes would necessitate formulations of inverse rate-dependent of a more generalized Prandtl-Ishlinskii model capable of characterizing rate-dependent asymmetric hysteresis nonlinearities. The formulation of this inverse could be attempted considering the Prandtl-Ishlinskii model with generalized play operators with asymmetric loading-unloading properties.

CHAPTER 6

FEEDFORWARD COMPENSATION OF ASYMMETRIC RATE-DEPENDENT HYSTERESIS NONLINEARITIES OF A MAGNETOSTRICTIVE MICRO-ACTUATOR

7.1 Introduction

Smart material actuators are increasingly being explored for micro-positioning applications requiring fast response, relatively higher forces, miniaturization in size and high resolution. Magnetostrictive actuators based on Terfenol-D materials are considered particularly attractive for applications involving relatively large stroke and high force capacity [1,2,3]. Such actuators have been explored for various micro-positioning and vibration control applications [4,96,97]. However, like other smart material actuators, magnetostrictive actuators show strong input rate-dependent hysteresis nonlinearities that tend to limit their positioning and tracking performance. Furthermore, the hysteresis nonlinearities tend to be significant under high rates of inputs, and asymmetric under moderate and high input magnitudes [5,7,8,98]. Such actuators may thus cause

greater tracking inaccuracies and oscillatory responses under inputs of high magnitudes and higher frequencies [1,2,5,6].

The realization of accurate positioning performance of magnetostrictive actuators under different rates and magnitudes of inputs thus requires designs of additional controllers to compensate for the effects of hysteresis nonlinearity as well as the output-input asymmetry. Several studies have reported different controller synthesis for systems with hysteresis [e.g., 90, 98,99,100]. Alternatively, hysteresis compensation methods, employing inverse hysteresis models in a cascade arrangement with the hysteresis model of the actuator, have also been proposed for effective real-time compensation. A number of inverse model based compensators have been reported for compensation of rate-independent hysteresis effects of different smart material actuators [5,7,12,44,57,101]. These have employed different phenomenological hysteresis models such as Preisach and Prandtl-Ishlinskii models. The majority of the reported methods, however, are limited to compensation of symmetric hysteresis effects, such as those observed for piezoceramic actuators [e.g.,42,49,57,78,102,103]. Furthermore, the vast majority of these do not consider the strong dependence of hysteresis nonlinearity on the rate of the applied input. Only a few studies have proposed input rate-dependent inverse models for compensation of hysteresis effects under inputs at different frequencies [102]. The Terfenol-D material of magnetostrictive actuators, invariably, exhibits output-input hysteresis together with output saturation and asymmetry with respect to the input that strongly depend upon the rate and magnitude of the input [5,7,62,90,98,101,104]. The applications of reported inverse compensation models to magnetostrictive actuators would thus yield substantial tracking errors.

A few studies have reported alternate Prandtl-Ishlinskii models to describe output asymmetry and output saturation. Visone and Sjostrom [89] proposed a Prandtl-Ishlinskii model coupled with

a memoryless hyperbolic tangent function to formulate a Preisach-like hysteresis model for describing saturated hysteresis nonlinearities of a superconductor, while the input rate effect on the hysteresis was not considered. Al Janaideh et al. [60] constructed a Prandtl-Ishlinskii model using generalized play operators with dissimilar envelope functions to characterize asymmetric hysteresis nonlinearities of magnetostrictive actuators and shape memory alloys. Drinčić et al. [61] applied the generalized model reported in [60] for characterizing the butterfly-shaped hysteresis nonlinearity of a Terfenol-D magnetostrictive actuator considering identical envelop functions of the operators. Kuhnen [12] characterized asymmetric hysteresis nonlinearity of a magnetostrictive actuator using the rate-independent Prandtl-Ishlinskii model coupled with a superposition of weighted dead-band operators.

The above-stated hysteresis models do not consider the effect of rate of input on the hysteresis. Formulation of an accurate hysteresis model and its inverse considering a broad range of input magnitudes and rates is vital for achieving effective compensation of hysteresis nonlinearities of a magnetostrictive actuator. Among the reported phenomenological hysteresis models, the Prandtl-Ishlinskii model may be preferred since it is analytically invertible owing to continuous nature of the play operators [42,63]. The effectiveness of the inverse Prandtl-Ishlinskii model for compensating symmetric as well as asymmetric rate-independent hysteresis effects has been illustrated in a few studies [5,6,12].

In this study, the asymmetric hysteresis characterization and compensation potentials of a symmetric rate-dependent Prandtl-Ishlinskii model coupled with a deadband function and their inverse are explored. The inverse model feed-forward compensator is applied for compensation of asymmetric and rate-dependent hysteresis nonlinearity of a magnetostrictive actuator. The

effectiveness of the proposed compensator is demonstrated through simulations and hardware-in-loop real-time implementation in the laboratory.

7.2 An integrated Prandtl-Ishlinskii model and its inverse

Compared to the available phenomenological hysteresis models, the Prandtl-Ishlinskii model is considered an attractive choice for modeling and compensation of hysteresis nonlinearities considering its simplicity and flexibility to include the rate-dependent hysteresis effects. Furthermore, the Prandtl-Ishlinskii model is analytically invertible.

The rate-dependent Prandtl-Ishlinskii model describing the rate-dependent but symmetric hysteresis nonlinearity could be combined with deadband function to characterize output asymmetry and saturation of a Terfenol-D magnetostrictive actuator. The validity of the resulting model, referred to as the integrated Prandtl-Ishlinskii model, was demonstrated in a recent study using the laboratory-measured output-input characteristics under different magnitudes of inputs in the 1-250 Hz frequency range. In this study, integrated model is briefly described, and its inverse is formulated to seek compensation of the rate-dependent and asymmetric hysteresis nonlinearity of a magnetostrictive actuator in an open-loop manner. Figure 6.1 illustrates a cascade arrangement of the integrated rate-dependent Prandtl-Ishlinskii model Ω and its inverse Ω^{-1}, as the feed-forward hysteresis compensator.

For an input $v(t)$, the integrated rate-dependent model Ω employs a composition of both the rate-dependent Prandtl-Ishlinskii model Π and the deadband function Λ, such that:

$$\Omega[v](t) = \Lambda(\Pi[v](t)). \tag{6.1}$$

The rate-dependent Prandtl-Ishlinskii model Π employs a superposition of weighted rate-dependent play operators, which are real and absolute continuous functions over the interval [*0*,

T], as described in [63,85]. The output $\delta(t)$ of the rate-dependent Prandtl-Ishlinskii model $\Pi[v](t)$ can also be expressed in the discrete form, as:

$$\delta(t) = \Pi[v](t) = a_0 v(t) + \sum_{i=1}^{n} a_i \Gamma_{r_i(\dot{v}(t))}[v](t), \tag{6.2}$$

where a_0 and a_i are the weights.

Each rate-dependent play operator $\Gamma_{r_i(\dot{v}(t))}$ is defined using the input $v(t) \in AC(0,T)$, and a rate-dependent threshold function $r_i(\dot{v}(t)) \in AC(0,T)$, $i = 0, 1, 2, \ldots, n$, where $n \in \mathrm{N}$ is an integer. The threshold function is defined, such that:

$$0 = r_0(\dot{v}(t)) \le r_1(\dot{v}(t)) \le r_2(\dot{v}(t)) \le \ldots \le r_n(\dot{v}(t)) \tag{6.3}$$

The input $v(t)$ is considered monotone over each sub-interval $[t_{j-1}, t_j]$, and $0 = t_0 < t_1 < \ldots < t_l = T$ define the intervals. The output of the rate-dependent play operator $\Gamma[v](t)$ over an interval, $t \in [t_{j-1}, t_j)$, can be expressed as

$$\Gamma_{r_i(\dot{v}(t))}[v](t) = \max\{\, v(t_j) - r_i\left(\dot{v}(t_j)\right), \min\{\, v(t_j) + r_i\left(\dot{v}(t_j)\right), \Gamma_i(t_{j-1})\}\}. \tag{6.4}$$

The integrated rate-dependent Prandtl-Ishlinskii model is subsequently formulated using the deadband function Λ so as to describe asymmetric output-input characteristics and output saturation. The output of the integrated model Ω can be expressed as [104]:

$$\Omega[v](t) = \Lambda[\Pi[v]](t) = \sum_{i=-k}^{k} g_i J_{d_i}[\Pi[v]](t), \tag{6.5}$$

where function Λ is a summation of weighted deadband operators J_{d_i}, d_i (i=-k, -k+1,...,k-1, k) are the thresholds of the deadband operators, k is a positive integer, and g_i are the weighting constants [12]. The output of the deadband operator J_{d_i} is given by:

$$J_{d_i}[\delta](t) = \begin{cases} \max\{\delta(t) - d_i, 0\} & for \quad d_i > 0, \\ \delta(t) & for \quad d_i = 0, \\ \min\{\delta(t) - d_i, 0\} & for \quad d_i < 0. \end{cases} \tag{6.6}$$

Figure 6.1: Feedforward Compensation using the cascade arrangement of inverse model Ω^{-1} and the hysteresis model Ω.

7.2.1 Inverse of the integrated Prandtl-Ishlinskii model

The inverse of the integrated Prandtl-Ishlinskii model Ω^{-1} is obtained from the inverses of both the rate-dependent Prandtl-Ishlinskii model Π^{-1} and the deadband function Λ^{-1}. An identity mapping between the applied input $v(t)$ and the compensated output $u(t)$ can be achieved by applying the resulting inverse model as a feed-forward compensator together with the integrated Prandtl-Ishlinskii model Ω. The output $\Omega \circ \Omega^{-1}[v](t)$ yields identity mapping between the input $v(t)$ and the output $u(t)$.

The inverse model of the integrated Prandtl-Ishlinskii model Ω^{-1} can be expressed as:

$$\Omega^{-1}[v](t) = \Pi^{-1}(\Gamma^{-1}[v])(t). \tag{6.7}$$

The inverse of rate-dependent Prandtl-Ishlinskii model Π^{-1} can be formulated on the basis of the model Π itself. The formulation of Π^{-1}, however, holds under the threshold dilation condition, which implies that the differences between two consecutive dynamic thresholds $r_{i+1}(\dot{v}(t))$ and $r_i(\dot{v}(t))$ of Π do not decrease in time $\forall\, i = 1, \ldots, n\text{-}1$, [63], such that:

$$\frac{d}{dt}\left(\Delta r_i(\dot{v}(t))\right) \geq 0 \tag{6.8}$$

where

$$\Delta r_i(\dot{v}(t)) = r_{i+1}(\dot{v}(t)) - r_i(\dot{v}(t)) .$$

The rate-dependent thresholds $\hat{r}_i(\dot{v}(t))$ of the inverse rate-dependent Prandtl-Ishlinskii model Π^{-1} are related to those of the model itself, $r_i(\dot{v}(t))$, in the following manner [63]:

$$\begin{aligned} \hat{r}_1(\dot{v}(t)) &= a_0 \; r_1(\dot{v}(t)), \\ \hat{r}_{i+1}(\dot{v}(t)) &= \hat{r}_i(\dot{v}(t)) + \sum_{j=0}^{i} a_j \left(r_{i+1}(\dot{v}(t)) - r_i(\dot{v}(t)) \right). \end{aligned} \tag{6.9}$$

The output of the inverse rate-dependent Prandtl-Ishlinskii model Π^{-1} can be derived from the rate-dependent thresholds $\hat{r}_i(\dot{v}(t))$ and weights $\hat{a}_i$, as:

$$\Pi^{-1}[v](t) = \hat{a}_0 v(t) + \sum_{i=1}^{n} \hat{a}_i \Gamma_{\hat{r}_i(\dot{v}(t))}[v](t). \tag{6.10}$$

The inverse model of the deadband function Λ^{-1} is also formulated using a superposition of weighted deadband operators $J_{\hat{d}_i}$ [12]:

$$\Lambda^{-1}[v](t) = \sum_{i=-k}^{k} \hat{g}_i J_{\hat{d}_i}[v](t), \tag{6.11}$$

where $\hat{g}_i$ are constant weights and $\hat{d}_i$ are the thresholds of the inverse deadband function, which are related to those of Λ.

The weights of the inverse model $\hat{a}_0$, $\hat{a}_1$, ..., $\hat{a}_n$ are also related to those of the Prandtl-Ishlinskii model Π, as [42,63]

$$\hat{a}_0 = \frac{1}{a_0},$$

$$\hat{a}_i = -\frac{a_i}{(a_0 + \sum_{i=1}^{j} a_i)(a_0 + \sum_{i=1}^{j-1} a_i)}. \tag{6.12}$$

The constants $\hat{g}_i$ and thresholds $\hat{d}_i$ of the inverse deadband function corresponding to positive and negatives solutions of the deadband operators are related to thresholds $\hat{d}_i$ and constants $\hat{g}_i$, respectively. The thresholds and weights of the inverse corresponding to positive solutions are obtained from [12]:

$$\hat{d}_j = \sum_{i=0}^{j} g_i (d_j - d_i); j = 0, \ ..., k \tag{6.13}$$

and

$$\hat{g}_0 = \frac{1}{g_0},$$

$$\hat{g}_j = -\frac{g_i}{(g_0 + \sum_{i=1}^{j} g_i)(g_0 + \sum_{i=1}^{j-1} g_i)}; \ j= 1, ..., k \tag{6.14}$$

Similarly, the thresholds and weights of the inverse leading to negative solutions are obtained from [12] for j=-k, …, -1 as:

$$\hat{g}_j = \sum_{i=j}^{0} g_i (d_j - d_i), \tag{6.15}$$

$$\hat{g}_j = -\frac{g_i}{(g_0 + \sum_{i=j}^{-1} g_i)(g_0 + \sum_{j=i+1}^{-1} g_i)}. \tag{6.16}$$

Then, the output of inverse model $\Omega^{-1}[v](t)$ can be expressed as:

$$\Omega^{-1}[v](t) = \Pi^{-1}[\Lambda^{-1}[v]](t). \tag{6.17}$$

7.3 Characterization of hysteresis of a magnetostrictive actuator

Formulation of an inverse model for compensation of rate-dependent asymmetric hysteresis of smart actuators necessitates an effective model that can accurately describe the rate-dependent asymmetric hysteresis properties of these actuators over a broad range of inputs. For this purpose, the output-input properties of a magnetostrictive actuator (model MFR OTY77; Etrema Inc.) were characterized in the laboratory. The experiment design has been described in details in Chapter 2. Figure 6.2 illustrates a schematic of the experimental setup, where the actuator displacement was measured using a capacitive sensor (model C23–C250; Lion Precision). Briefly, the measurements were undertaken under: (i) harmonic inputs of different magnitudes, ranging from 3 to 6 A, and frequencies, f = 10, 50, 150 and 250 Hz; and (ii) complex harmonic excitations of the form, $v(t)$= $\sin(2\pi\times 50 f_o t)+5\sin(2\pi\times 100 f_o t)$; f_o=1 and 2 Hz.

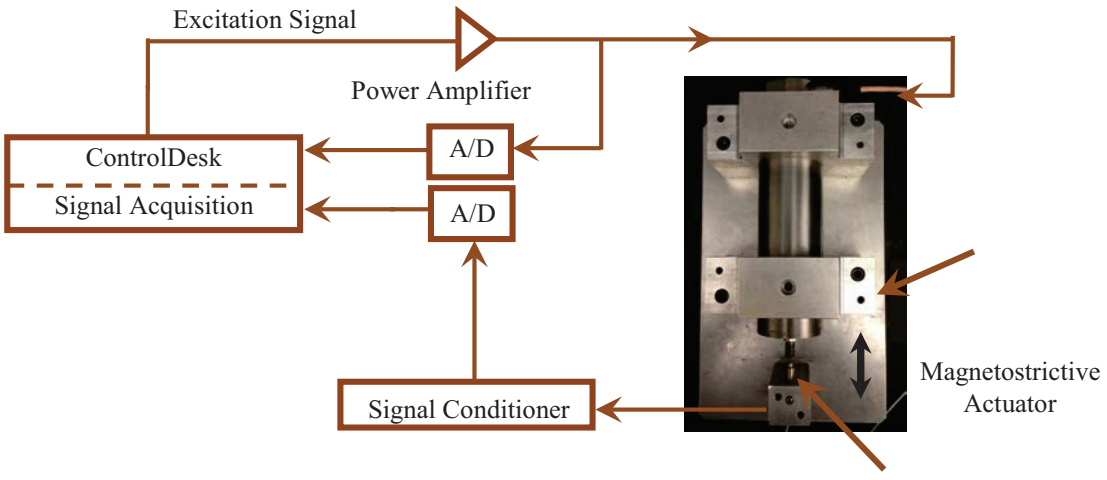

Figure 6.2: Experimental setup for characterization of hysteresis nonlinearities of a magnetostrictive actuator.

Figure 6.3, as an example, illustrates the measured output displacement-input current characteristics of the actuator under 6 A harmonic excitations at different frequencies, and both the complex harmonic excitations. The results clearly show an increase in hysteresis loop width with the excitation frequency for both the harmonic and complex harmonic excitations. The results revealed nearly linear increase in peak hysteresis with increasing excitation frequency, suggesting strong input rate dependence of the hysteresis. The area bounded by the hysteresis loop also increased nearly linearly with the excitation frequency, as seen in Figure 6.4 (r^2=0.99), which further suggests linear dependence of hysteresis on the excitation frequency. A similar linear relationship between the excitation frequency and the hysteresis loss of a magnetostrictive actuator has been illustrated by Davino et al. [66]. Furthermore, at low excitation amplitudes, the magnetostrictive actuators revealed nearly symmetric hysteresis loops with only minimal output saturation. However, at moderate and high excitation amplitudes, the outputs were observed to be highly asymmetric and saturated, irrespective of the excitation frequency.

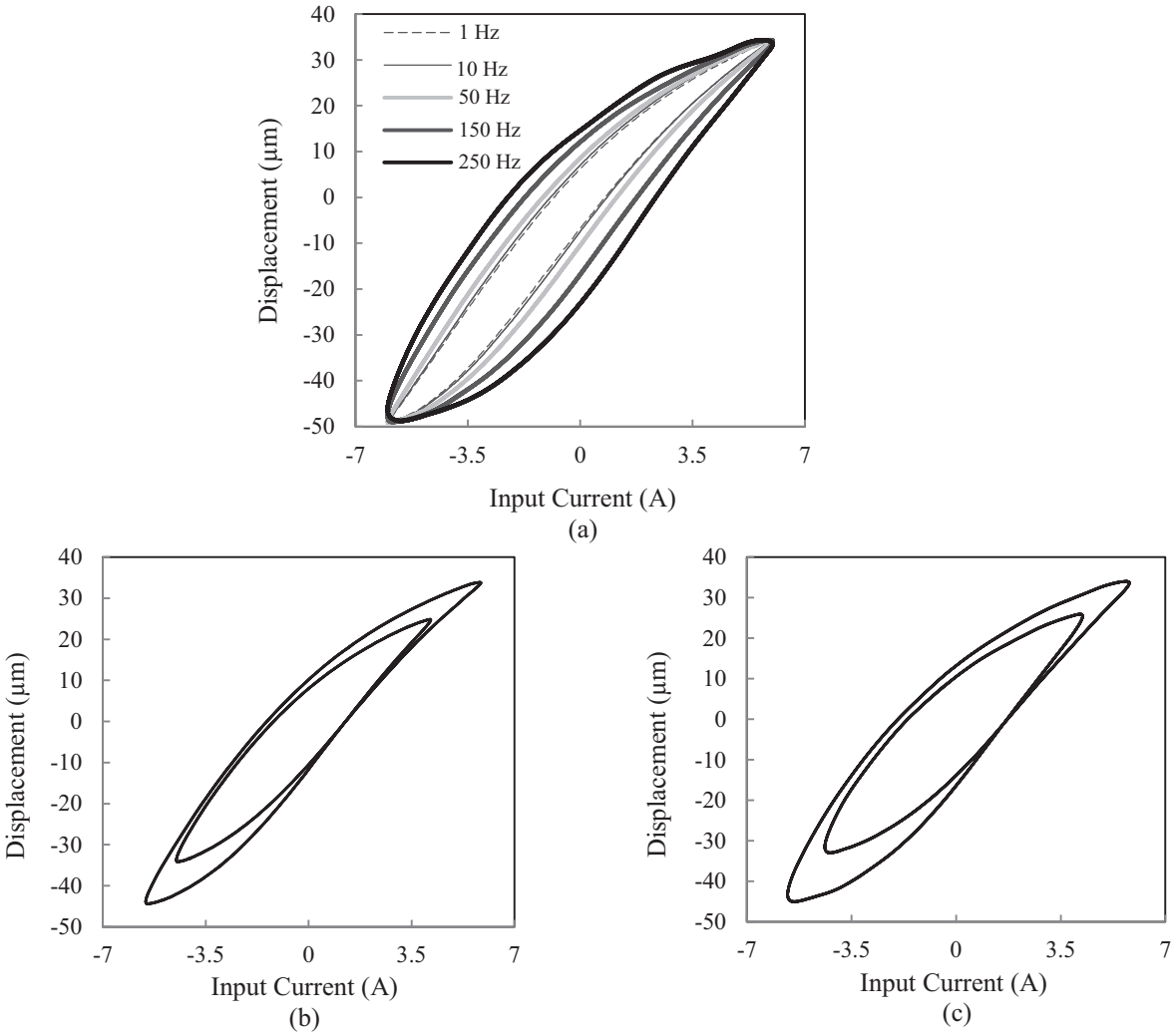

Figure 6.3: Output displacement-input current of the magnetostrictive actuator under different inputs: (a) $v(t) = 6.0 \sin(2\pi f t)$, f=10, 50, 150 and 250 Hz; and $v(t)$=1.0 $\sin(2\pi\times 50 f_o t)$+ 5.0 $\sin(2\pi\times 100 f_o t)$ A, (b) f_o=1 and, (c) f_o=2.

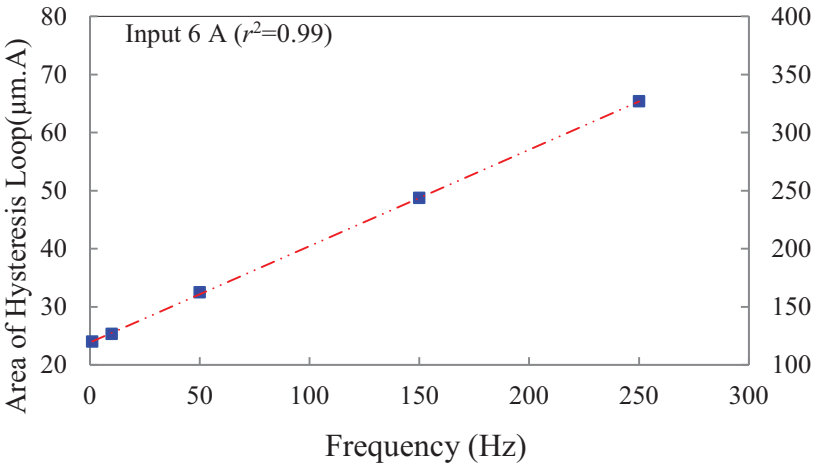

Figure 6.4: Area bounded by hysteresis of displacement-to-current loops of the magnetostrictive actuator under 6 A harmonic excitation at different frequencies.

The laboratory-measured data were employed to identify parameters of the integrated rate-dependent Prandtl-Ishlinskii model Ω (6.5), which was subsequently applied to formulate its inverse Ω^{-1}. Owing to the linear dependence of the hysteresis on the rate of input, the threshold function was defined as a linear function of the input frequency, such that:

$$r_i\left(\dot{v}(t)\right) = \gamma \ \left|\dot{v}(t)\right| + \alpha i, \tag{6.18}$$

where α and γ are positive constants. The above formulation yields, $\Delta r_i(\dot{v}(t)) = \alpha$, which satisfies the threshold dilation condition for inversion of the rate-dependent Prandtl-Ishlinskii model, as described in (6.8). The above threshold function can also describe rate-independent hysteresis nonlinearity at low excitation frequencies [7], where it can be approximated as $r_i\left(\dot{v}(t)\right) \cong \alpha \ i$. The output asymmetry and saturation effects, on the other hand, are described by the deadband function Λ .

The weighting constants of the Prandtl-Ishlinskii model were chosen using the following function:

$$a_i = \alpha_o e^{-\beta_o i} \tag{6.19}$$

The thresholds and the weighting functions corresponding to positive solutions of the deadband function are selected for $i = 0, 1, \ldots, k$ as:

$$d_i = d_p \ i, \tag{6.20}$$

and

$$g_i = -\alpha_1 e^{-\beta_1 i}. \tag{6.21}$$

In a similar manner, the thresholds and weighting functions corresponding to negative solutions are selected for $i = -k, -k+1, \ldots, -1$ as:

$$d_i = d_n \; i, \tag{6.22}$$

and

$$g_i = \alpha_2 e^{\beta_2 i}. \tag{6.23}$$

where d_n, d_p, α_1, α_2, β_1, β_2 and a_0 ($i=0$) are constants.

The parameters vector, $\overline{X} = \{\alpha, \gamma, q_0, \alpha_o, \beta_o, g_0, \alpha_1, \beta_1, \alpha_2, \beta_2, d_p, \text{ and } d_n\}$, of the integrated rate-dependent Prandtl-Ishlinskii model Ω, was identified through minimization of the error function $\overline{\Theta}$ under different excitation amplitudes and frequencies, given by:

$$\overline{\Theta}(\overline{X}) = \sum_{\overline{c}=1}^{\overline{C}} \sum_{f_{\overline{b}}=1}^{f_{\overline{B}}} \sum_{m=1}^{M} \left(\Omega(v(t,m,f_{\overline{p}},I_{ol})) - Y(t,m,f_{\overline{b}},I_{o\overline{c}})\right)^2, \tag{6.24}$$

where $\Omega(v(t,m, f_{\overline{b}}, I_{o\overline{c}}))$ is the response of the integrated rate-dependent Prandtl-Ishlinskii model under a given excitation frequency $f_{\overline{b}}$ ($\overline{b}$ =1, 2, ..., $\overline{B}$) and amplitude $I_{o\overline{c}}$ ($\overline{c}$ =1, ..., $\overline{C}$), and $Y(t,m, f_{\overline{p}}, I_{o\overline{c}})$ is the measured output displacement under the same input. The index m (m = 1,...,M) refers to the number of data points considered in computing the error function for one complete hysteresis loop. The error minimization problem in this study was formulated considering M=300 data points for each measured hysteresis loop, five frequencies ($\overline{B}$ = 5; $f_{\overline{b}}$ =10, 50, 100, 150 and 250 Hz) and two excitation amplitudes ($\overline{C}$ =2; I_{ol} $I_{o\overline{c}}$ = 3 A and 6 A), subject to following constrains

$$\alpha, \gamma, a_o, b_o, g_0, \alpha_1, \alpha_2, d_p, d_n, \beta_1 \text{ and } \beta_2 \geq 0.$$

The error minimization problem was solved considering different combinations of rate-dependent play operators (n = 4, 8, 12 and 16) and deadband operators (k=*4* and k=*8*). Moreover, the error minimization problem was solved using different initial values of the parameters. The solutions converged to nearly similar parameter values for the different starting values considered. From the results, it was concluded that the integrated model with 12 play operators and 17 deadband operators would yield good agreements between the model results and the measured data.

The validity of the integrated rate-dependent Prandtl-Ishlinskii model was thus subsequently examined under different input amplitudes and frequencies considering 12 rate-dependent play operators and 17 deadband operators. Figure 6.5 and Figure 6.6, as examples, illustrate comparisons of the output-input responses of the model with the measured data corresponding to selected inputs, including: (i) simple harmonic current excitations of 3, 5 and 6 *A* amplitude at different frequencies (10, 150 and 250 Hz); and (ii) two complex harmonic inputs, $v(t)$= sin(100πt)+5 sin(100πt) A and $v(t)$= sin(200πt)+5 sin(400πt) A. The results clearly suggest that the model can effectively predict the major as well as minor hysteresis loops and asymmetric output properties of the magnetostrictive actuator under a wide range of harmonic inputs. The effectiveness of the integrated rate-dependent Prandtl-Ishlinskii model is further illustrated through comparisons of the area bounded by the hysteresis loops predicted by the model with those of the measured data obtained under 3 and 6 A excitations at different frequencies in the 1-250 Hz range, as shown in Figure 6.7. The comparisons in Figure 6.5 and Figure 6.6, and Figure 6.7 suggest that the proposed rate-dependent Prandtl-Ishlinskii model integrating the deadband operators can effectively describe the rate-dependent asymmetric hysteresis nonlinearities of the magnetostrictive actuator under the range of inputs considered in the study.

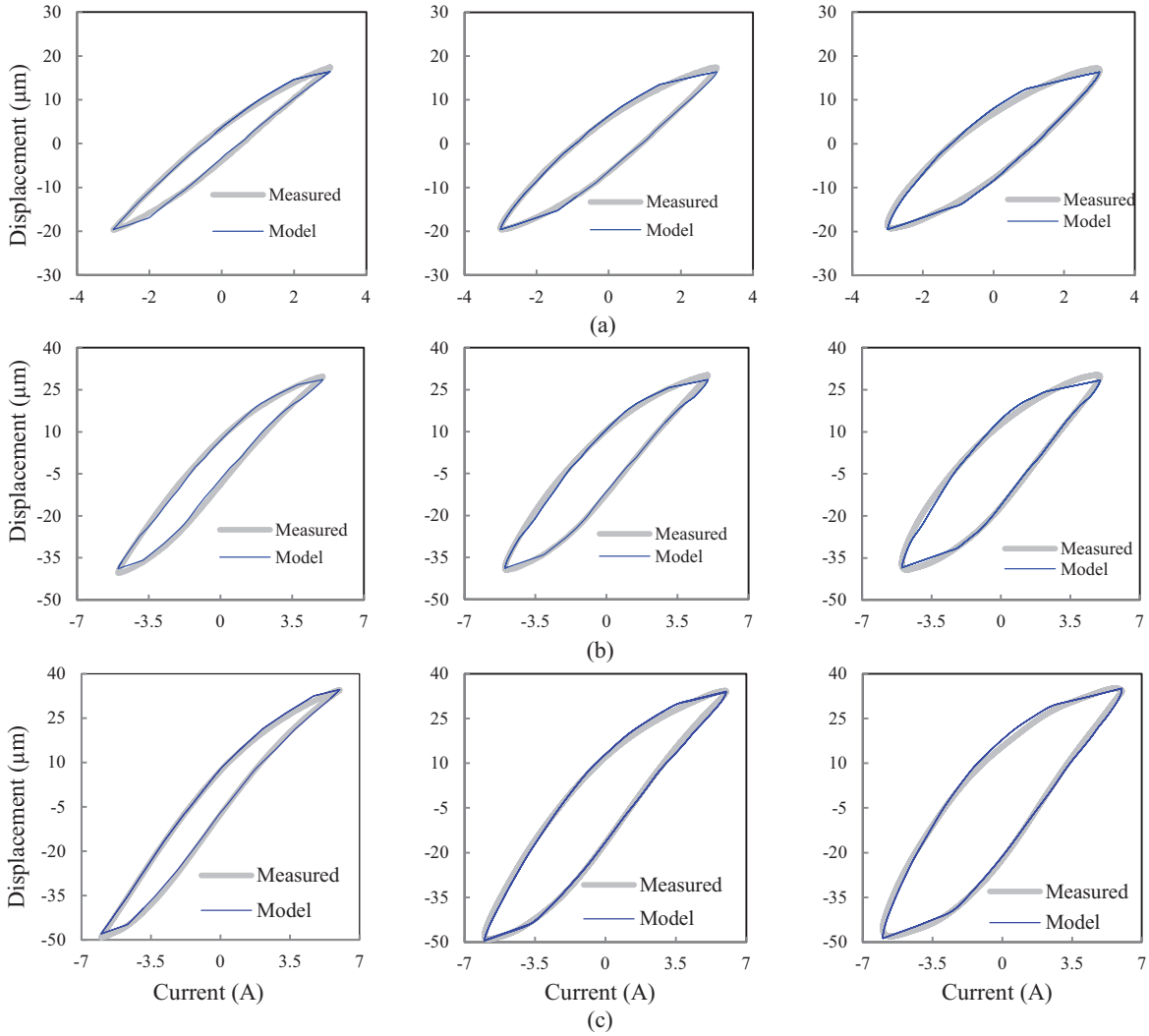

Figure 6.5: Comparisons of measured responses of the magnetostrictive actuator with those of the integrated rate-dependent Prandtl-Ishlinskii model Ω formulated using 12 rate-dependent play operators and 17 deadband operators, at different frequencies 10, 150 and 250 Hz applied under amplitudes of : (a) 3 A, (b) 5 A, and (c) 6 A.

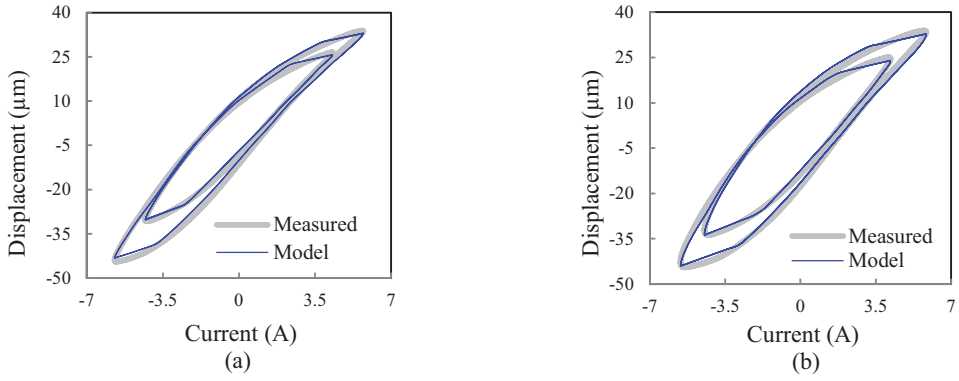

Figure 6.6: Comparisons of measured responses of the magnetostrictive actuator with those of the integrated rate-dependent Prandtl-Ishlinskii model Ω formulated using 12 rate-dependent play operators and 17 deadband operators, under the complex harmonic inputs: (a) 1.0 sin(100πt) +5.0 sin(200πt) A, and (b) 1.0 sin(200πt) +5.0 sin(400πt).

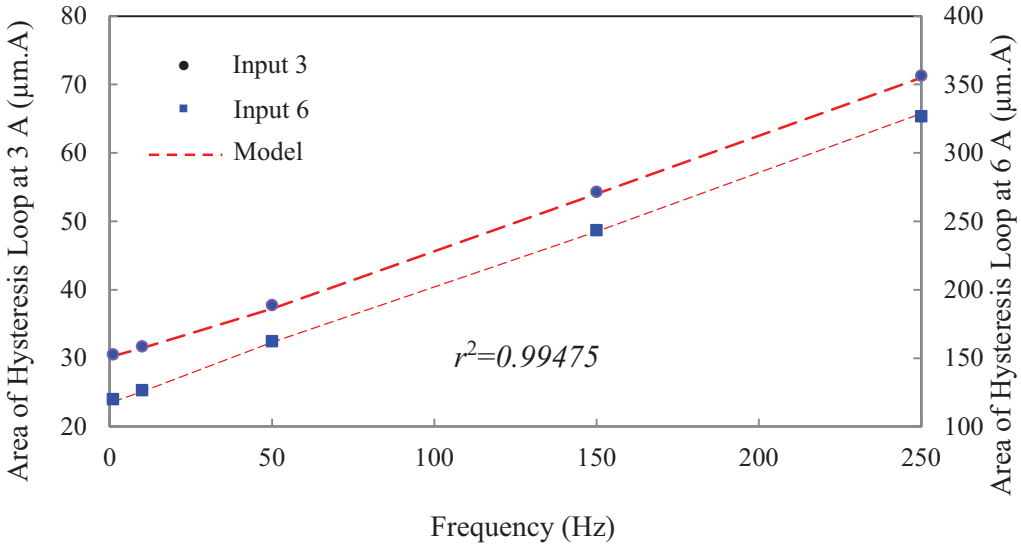

Figure 6.7: Comparisons of the area bounded by the hysteresis loops obtained from the integrated rate-dependent Prandtl-Ishlinskii model, with the measured data under 3 and 6 A harmonic excitations at different frequencies.

The accuracy of the model could be further enhanced by considering greater number of operators. Figure 6.8 illustrates comparisons of output-input responses of the proposed model using 36 rate-dependent play operator (n=36) with those of the measured data under 3 and 6 A harmonic excitations, and two complex harmonic excitations. The results revealed slightly smaller deviations between the model results and the measured data compared to those obtained with the model with n=12. The peak deviations for the models with n=36 and n=12 with respect to the measured data were obtained as 3.27% and 3.68%, respectively, under the 6 A excitation at 250 Hz. The results thus suggest that consideration of greater number of play operators yields only minimal beneficial effect. The integrated model with fewer play operators, however, would be

desirable for hardware implementations. Consequently, the model with 12 rate-dependent play operators and 17 deadband operators was considered adequate for deriving model inverse and for hardware implementations, as described in the subsequent sections.

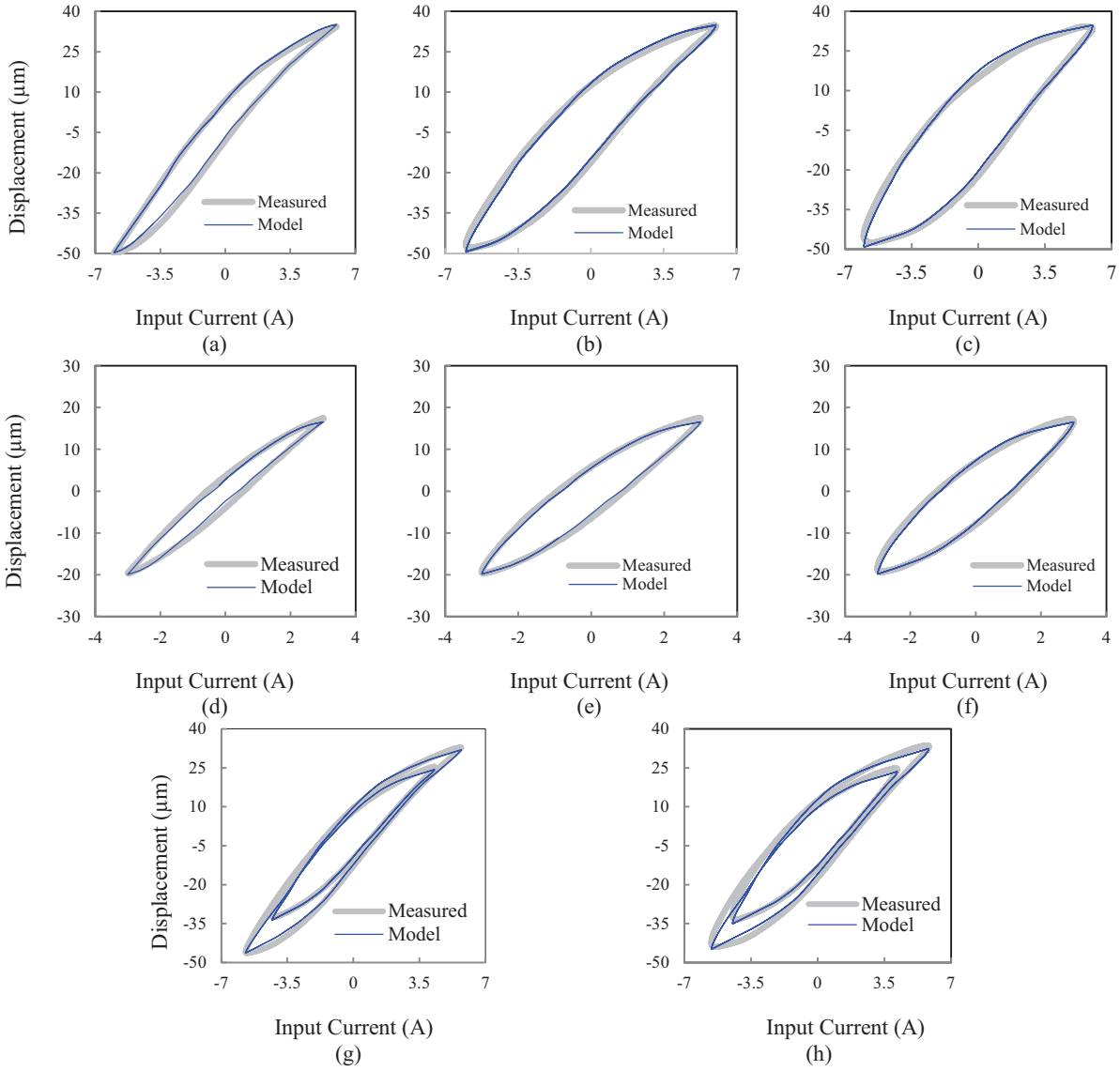

Figure 6.8: Comparisons of measured responses of the magnetostrictive actuator with those of the integrated rate-dependent Prandtl-Ishlinskii model Ω formulated using 36 rate-dependent play operators and 17 deadband operators: 6 A harmonic input at different frequencies-(a) 10 Hz, (b) 150 Hz and (c) 250 Hz; 3 A harmonic input at different frequencies-(d) 10 Hz, (e) 150 Hz, (f) 250 Hz; (g) $\sin(100\pi t) + 5\sin(200\pi t)$ A; and (h) $\sin(200\pi t) + 5\sin(400\pi t)$.

7.4 Compensation of rate-dependent asymmetric hysteresis

The inverse of the integrated rate-dependent Prandtl-Ishlinskii model Ω^{-1}, formulated using (6.10) and (6.11) , was applied as a feedforward rate-dependent hysteresis compensator in an open-loop manner, as seen in Figure 6.1. The parameters of the inverse rate-dependent Prandtl-Ishlinskii Π^{-1} were obtained using equations (6.9) and (6.12), while relations (6.13) to (6.16) were used to attain the parametres of the inverse of the deadband function Λ^{-1}. The effectiveness of the inverse for compensating the asymmetric and rate-dependent hysteresis nonlinearities of the integrated rate-dependent Prandtl-Ishlinskii model Ω is investigated through both simulations and hardware-in-the-loop tests in the laboratory.

7.4.1 Simulation results

Figure 6.9 and Figure 6.10 illustrate the output-input characteristics of the integrated rate-dependent Prandtl-Ishlinskii model Ω and its inverse Ω^{-1} together with their composition $u(t) = (\Omega \circ \Omega^{-1})[v](t)$ under 3 and 6 A harmonic excitations respectively, at different frequencies (f =10, 150 and 250 Hz). Figure 6.11 shows the simulation results attained under the two complex harmonic excitations: $v(t)$= sin(100πt)+5 sin(200πt); and $v(t)$= sin(200π t)+5 sin(400πt). The simulation results suggest that the inverse of the integrated Prandtl-Ishlinskii model Ω^{-1} can effectively compensate for both the rate-dependent hysteresis and output asymmetry nonlinearities described by the integrated rate-dependent Prandtl-Ishlinskii model Ω, irrespective of the excitation amplitude and frequency.

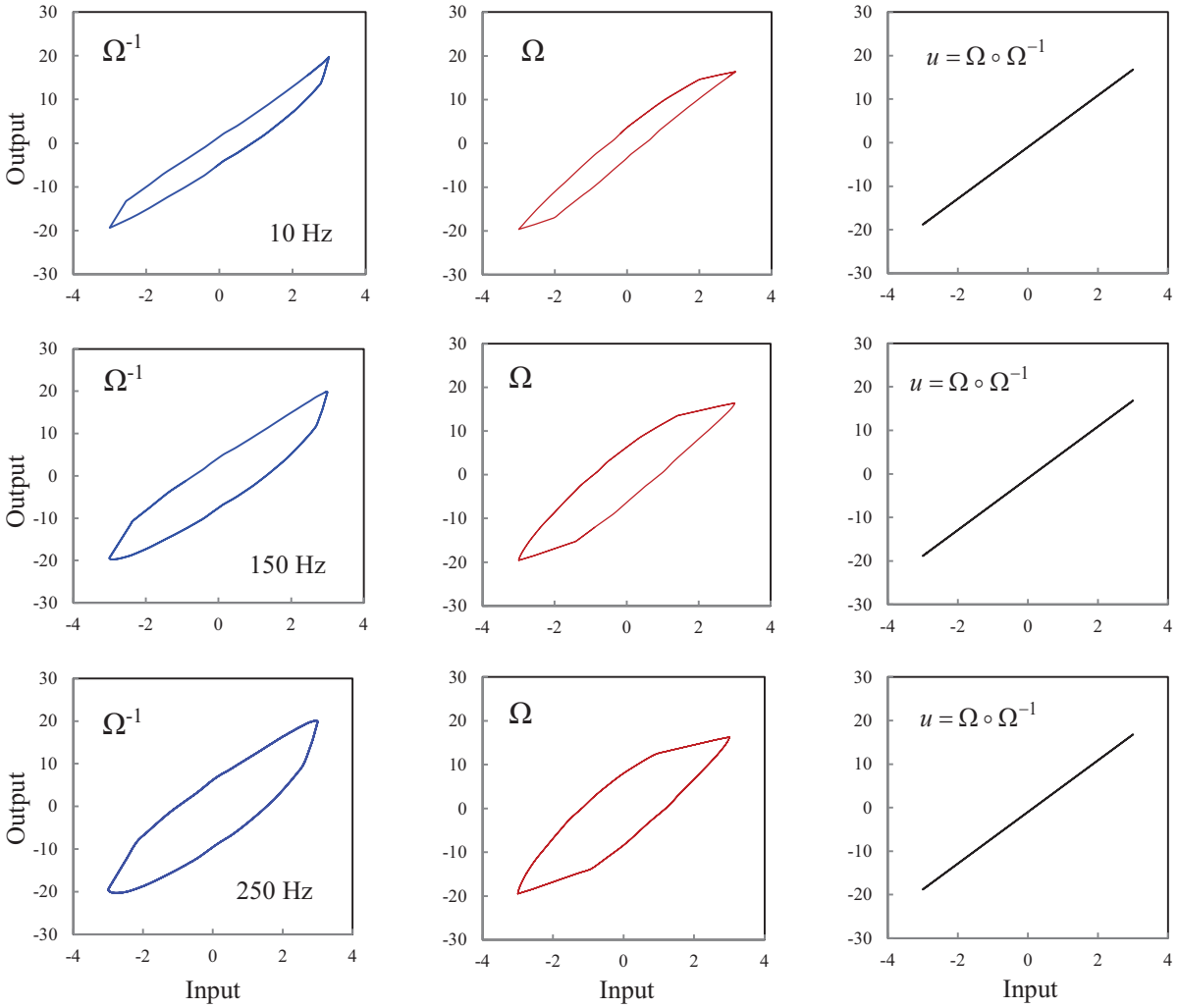

Figure 6.9: Output-input characteristics of the inverse of the integrated rate-dependent Prandtl-Ishlinskii model Π^{-1} formulated using 12 rate-dependent play operators and 17 deadband operators, the integrated rate-dependent Prandtl-Ishlinskii model Ω, and the composition $u = (\Omega \circ \Omega^{-1})$, under 3 A excitation at different frequencies (10, 150, 250 Hz).

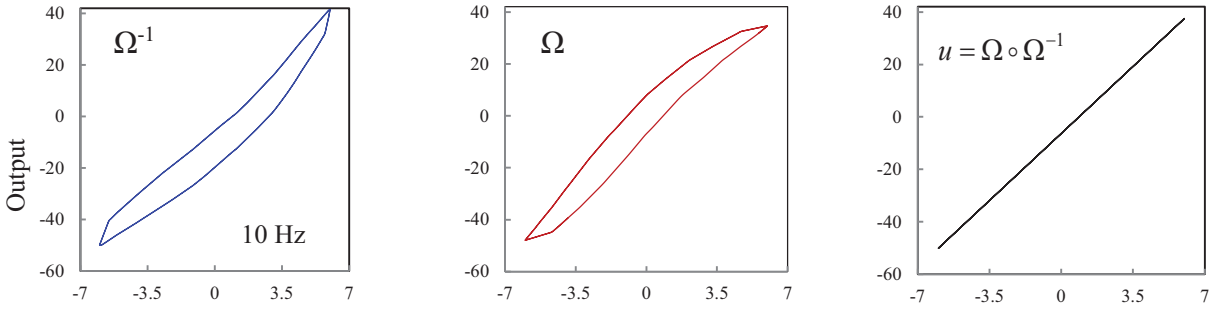

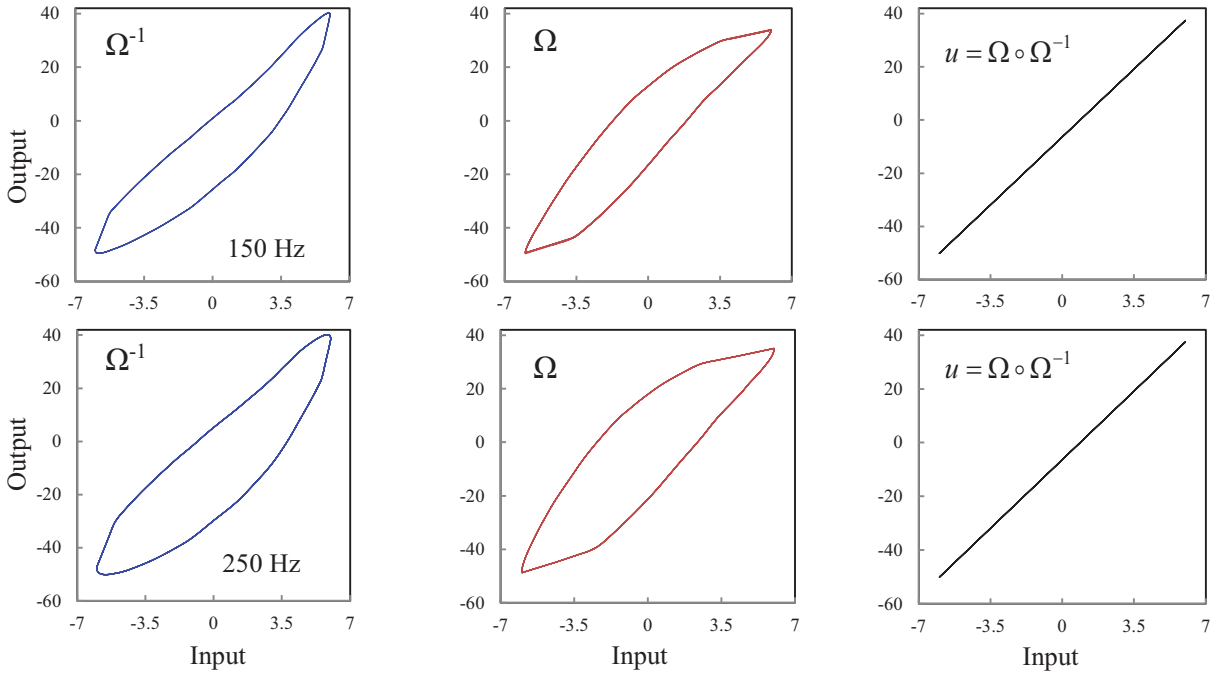

Figure 6.10: Output-input characteristics of the inverse of the integrated rate-dependent Prandtl-Ishlinskii model Ω^{-1} formulated using 12 rate-dependent play operators and 17 deadband operators, the integrated rate-dependent Prandtl-Ishlinskii model Ω, and the composition $u = \Omega \circ \Omega^{-1}$, under 6 A excitation at different frequencies (10, 150, 250 Hz).

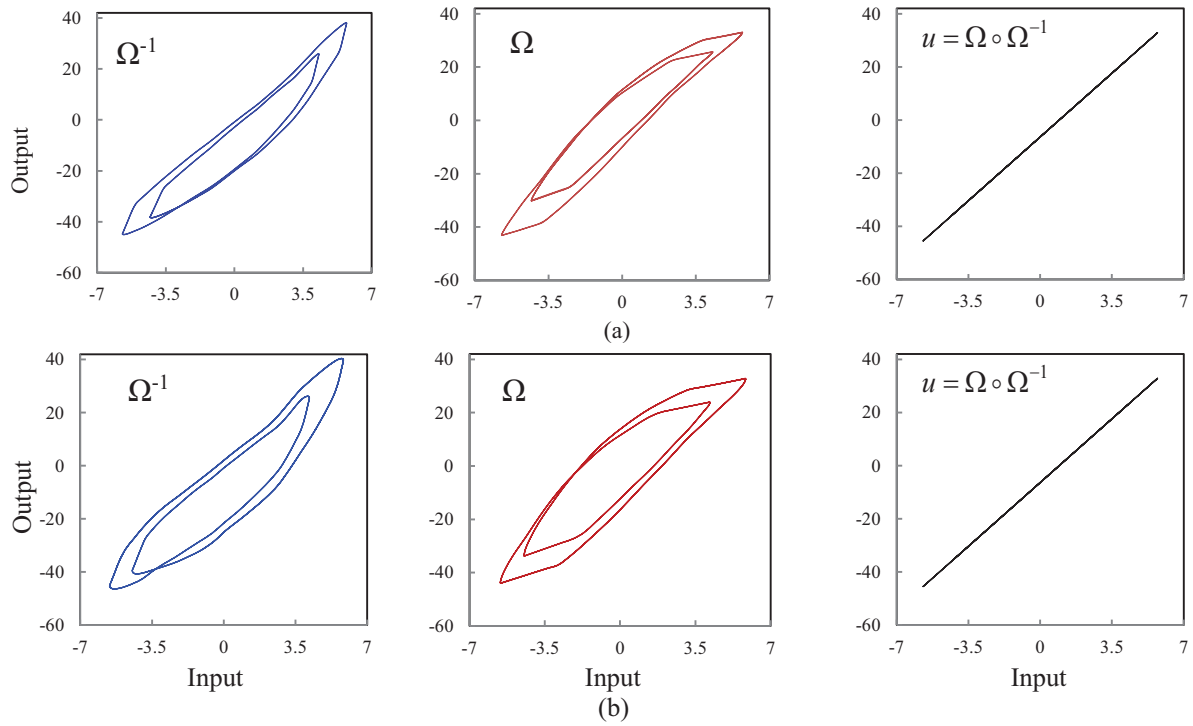

Figure 6.11: Output-input characteristics of the inverse of the integrated rate-dependent Prandtl-Ishlinskii model Ω^{-1} formulated using 12 rate-dependent play operators and 17 deadband operators,

the integrated rate-dependent Prandtl-Ishlinskii model Ω, and the composition $u = \Omega \circ \Omega^{-1}$, under complex harmonic excitations: (a) $v(t)$ = sin(100πt)+5 sin(200πt) A; and (b) $v(t)$ = sin(200πt)+5 sin(400πt).

7.4.2 Hardware-in-the-loop implementation of the inverse compensator

The effectiveness of the inverse of the integrated rate-dependent Prandtl-Ishlinskii model Ω^{-1} in compensating output asymmetry and rate-dependent hysteresis effects of was further investigated through laboratory implementations on a magnetostrictive actuator. For this purpose, a hardware-in-the-loop experiment was designed, where the inverse model Ω^{-1}, formulated using MATLAB/SIMULINK, was employed as a feedforward compensator together with the magnetostrictive actuator in the ControlDesk platform. The experiments were conducted under different amplitudes of harmonic currents at different frequencies in the 1-250 Hz range and the complex harmonic inputs used in the simulation results. The selected inputs were applied directly to the inverse compensator, while the output of the compensator was applied to the magnetostrictive actuator through D/A output board and the power amplifier. The magnetostrictive actuator displacement, measured using the capacitive position sensor, together with the applied input current were analyzed to assess the effectiveness of the inverse compensator under different inputs.

As examples, Figure 6.12 illustrates variations in the measured displacement responses of the actuator under different current inputs: (a) 6 A harmonic current at different excitations frequencies (1, 10, 50, 150 and 250 Hz); (b) complex harmonic input, $v(t)$= sin(100πt)+5 sin(100πt) A; and (c) complex harmonic input, $v(t)$= sin(200π t)+5 sin(400πt) A. Nearly identity mapping between the applied input $u(t)$ and the compensated output $v(t)$ of the actuator is evident under the excitations considered in the example results. Similar mappings were also obtained under different

inputs considered in the laboratory experiments. From the results it can be concluded that the inverse of the rate-dependent Prandtl-Ishlinskii model integrating the deadband function can not only mitigate the rate-dependent hysteresis effects but also the output asymmetry and saturation effects. Some deviations, however, are evident in the compensated output, which can be partly attributed to error associated with experimental characterization of the magnetostrictive actuator and in-part to prediction errors of the integrated model with limited number of rate-dependent play operators and deadband operators.

The peak deviation between the applied input and the actuator response was evaluated from the respective time-histories. As an example, Figure 6.13(a) compares the time histories of the desired output under the reference complex harmonic input $v(t)= \sin(100\pi t)+5 \sin(100\pi t)$ A and the measured displacement response of the magnetostrictive actuator. The time-history of the error between the two is further shown in Figure 6.13 (b), which suggests peak positioning error of the 83.1 μm stroke actuator in the order of 3.1 μm, when the proposed inverse compensator is implemented. The peak percent hysteresis error was further computed from the output-input characteristics of the actuator under different inputs. Figure 6.13 (c) compares the variations in the peak percent hysteresis response of the magnetostrictive actuator with and without the inverse compensator with the excitation frequency under the 6 A harmonic current input. The peak percent hysteresis of the actuator was 18.2% at the low frequency input of 1 Hz, which increased with input frequency and approached 49.1% corresponding to the 250 Hz input. Application of the inverse compensator, however, resulted in nearly steady peak hysteresis error in the entire frequency range, as seen in Figure 6.13 (c). The peak hysteresis error of the compensated actuator is 3.7%, which is attained under the input at 250 Hz. The experimental results thus further confirm that the inverse of the rate-dependent Prandtl-Ishlinskii model together with that of the deadband

function, Π^{-1}, can effectively mitigate the rate-dependent and asymmetric hysteresis nonlinearities of the magnetostrictive actuator, as observed from the simulation results.

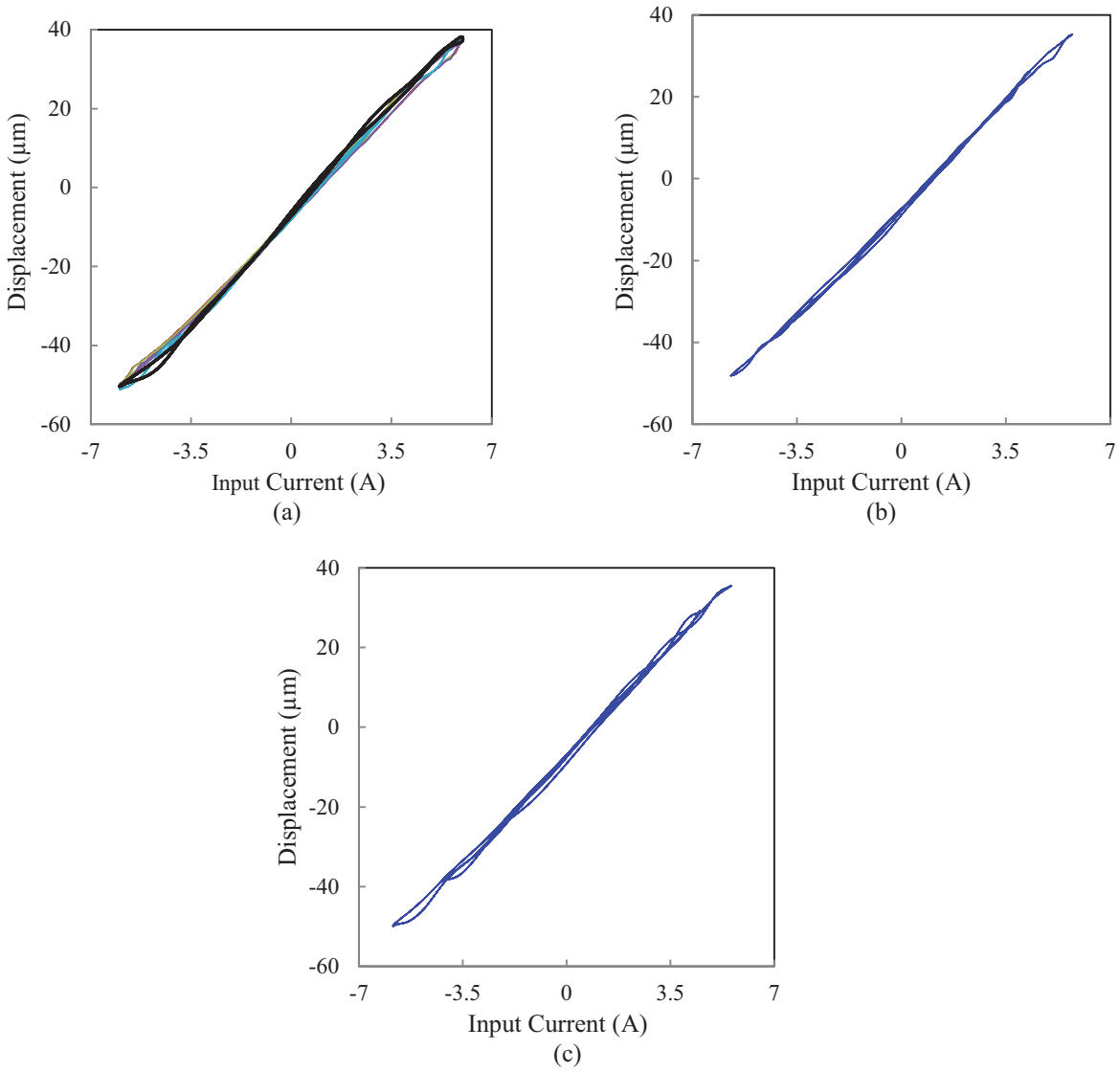

Figure 6.12: The output-input characteristics of the magnetostrictive actuator with the inverse of the integrated rate-dependent Prandtl-Ishlinskii model Ω^{-1} under different inputs: (a) $v(t)$=6.0 sin(2πft) A, f =1, 10, 50, 150, and 250 Hz; (b) $v(t)$=1.0 sin(100π t)+5.0 sin(100πt) A; and (c) $v(t)$=1.0 sin(200π t)+5.0 sin(400πt) A.

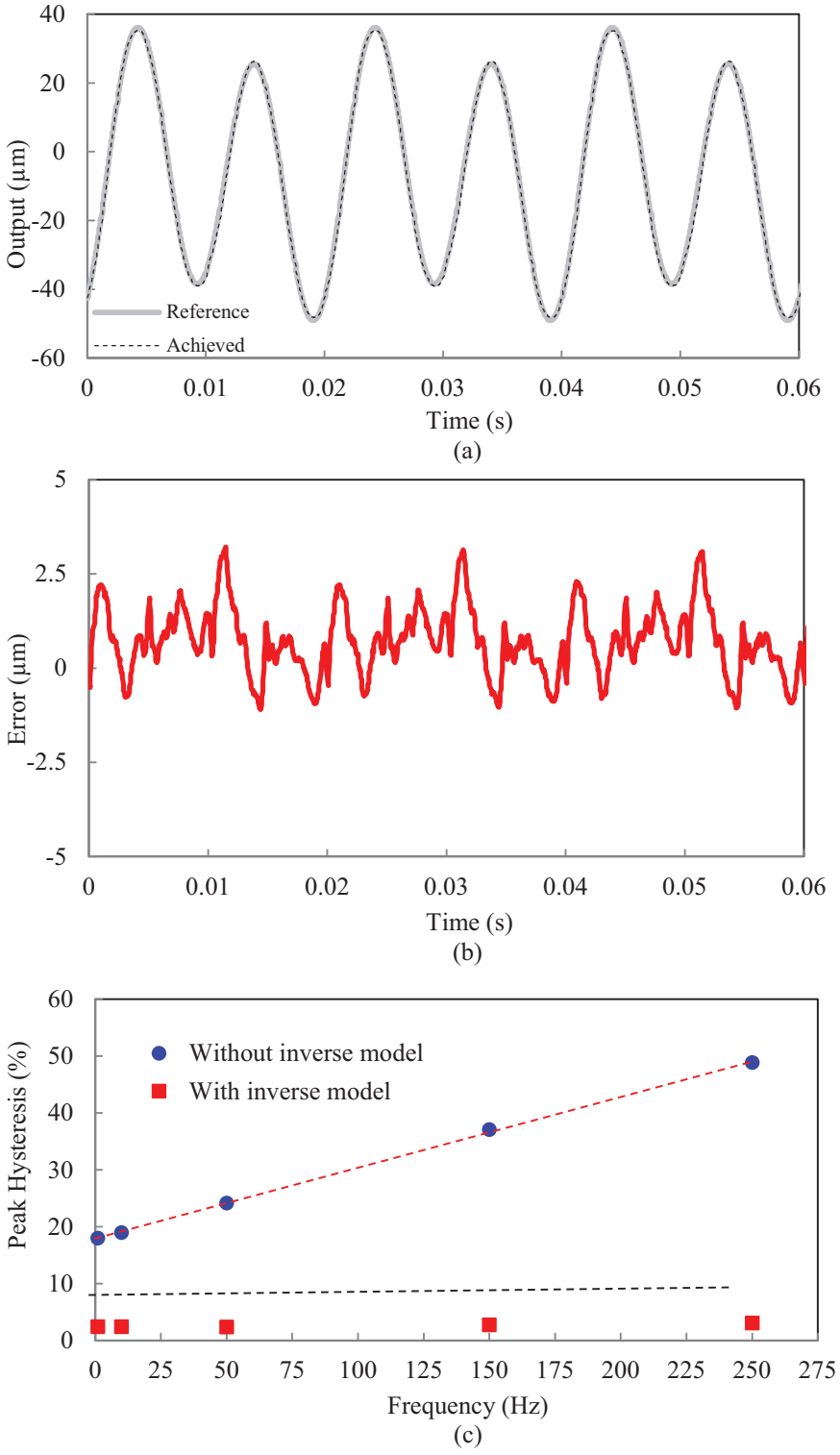

Figure 6.13: (a) The time-history of desired output and the achieved output displacement of the magnetostrictive actuator with the inverse model Ω^{-1} under the harmonic input $v(t)$=1.0 sin(100πt)+5.0 sin(100πt) A; (b) The time-history of error between the desired and the achieved output displacement under the harmonic input $v(t)$=1.0 sin(100πt)+5.0 sin(100πt) A; and (c)

percent peak normalized hysteresis of displacement-to-current loops of the magnetostrictive actuator with the inverse model Ω^{-1} at different excitations of frequency under amplitude of 6 A.

7.5 Conclusions

A rate-dependent Prandtl-Ishlinskii model coupled with a function of deadband operators can accurately describe the rate-dependent and asymmetric hysteresis nonlinearities of a magnetostrictive actuator over a wide range of excitations. The measured output displacement-input current characteristics revealed asymmetric hysteresis nonlinearities under medium and high amplitude excitations, which are further dependent on excitation frequency. An inverse of the integrated Prandtl-Ishlinskii model could be formulated to serve as a feedforward compensator of rate-dependent and asymmetric hysteresis nonlinearities.

The simulation results revealed that the proposed inverse model can effectively compensate for the rate-dependent and asymmetric hysteresis nonlinearities over a wide range of excitation amplitudes and frequencies. The effectiveness of the inverse model was further verified through hardware-in-the loops laboratory tests on the magnetostrictive actuator. The experimental results also suggested that the inverse model can provide an effective compensation for the rate-dependent and asymmetric hysteresis nonlinearities under inputs in the 1-250 Hz frequency range. The peak percent positioning error was reduced to nearly 3.7 % under the 6 excitation over the 1-250 Hz frequency range, which was observed in the 18.2 to 49.1 % range in the absence of the compensator. The error in the compensated output could be partly attributed to error associated with experimental characterization of the magnetostrictive actuator and in-part to prediction errors of the integrated model with limited number of rate-dependent play operators and deadband operators.

CHAPTER 7

CONCLUSIONS AND RECOMMENDATIONS FOR FUTURE WORK

8.1 Major contributions of the dissertation research

The hysteresis nonlinearities have been invariably observed in smart materials actuators such as piezoceramic and magnetostrictive actuators. These nonlinearities become particularly significant under high rates of inputs, and exhibit output asymmetry and saturation under moderate to high inputs. Such nonlinearities are known to cause oscillations in the responses of the open-loop systems, and poor tracking performance and potential instabilities in the closed-loop systems. This dissertation research has proposed a feedforward rate-dependent compensator on the basis of the inverse rate-dependent Prandtl-Ishlinskii model coupled with memoryless deadband operators to seek compensation of rate-dependent and asymmetric hysteresis nonlinearities of magnetostrictive actuators.

The major contributions of this dissertation are summarized below:

- A Stop operator based Prandtl-Ishlinskii (SPI) model has been proposed to compensate for hysteresis nonlinearities of piezoceramic actuators. A methodology is presented for identification of parameters of the SPI model on the basis of the initial loading curves of both the Play operator based Prandtl-Ishlinskii (PPI) model and the SPI model.

- An experimental was designed and executed to fully characterize the hysteresis nonlinearities of a Terfenol-D based magnetostrictive actuator, under a wide range of inputs, namely, amplitude, rate and bias of input, as well as mechanical loads. The measured data were analyzed to demonstrate the dependence of the actuator displacement on each operating factor. The measured data were further analyzed to study the effects of different factors on the area bounded by the hysteresis loop, displacement range as well as the peak hysteresis percentage.

- The output-input characteristics of the magnetostrictive actuator were expressed in terms of rate-dependent hysteresis effect, output saturation and asymmetry, as function of input amplitude, input rate, input bias and the actuator load.

- A rate-dependent Prandtl-Ishlinskii model was formulated together with its analytical inverse to describe and compensate for the rate-dependent symmetric hysteresis nonlinearities of the magnetostrictive actuator under relatively low levels of input currents. A rate-dependent threshold function was proposed on the basis of the experimental observations, which revealed that the peak hysteresis varies linearly with the excitation frequency.

- A rate-dependent Prandtl-Ishlinskii model integrating a deadband function was formulated to describe the rate-dependent asymmetric hysteresis nonlinearities of the magnetostrictive actuator obtained under medium to high current inputs in the 10-250 Hz frequency range. The rate-dependent Prandtl-Ishlinskii model was employed to account for input rate effects, while the deadband function was incorporated to describe output asymmetry and saturation.

- An analytical inverse of the model integrating the inverses of the rate-dependent Prandtl-Ishlinskii model and the memoryless function was proposed for compensation of rate-dependent and asymmetric hysteresis nonlinearities of the magnetostrictive actuator. The inverse model was employed as a feedforward rate-dependent compensator for compensation of hysteresis nonlinearities of magnetostrictive actuator in an open-loop manner under different levels of input amplitudes over a wide frequency range. The validity of the model was demonstrated through laboratory experiments using the hardware-in-the-loop methodology.

8.2 Major conclusions

The dissertation research has proposed an integrated Prandtl-Ishlinskii model and its inverse for describing and compensating the rate-dependent and asymmetric hysteresis nonlinearities of a smart actuator in an open-loop manner. The major conclusions drawn from the dissertation research are summarized below:

- Piezoceramic actuators exhibit notable hysteresis nonlinearity between the input voltage and the output displacement, which is generally symmetric about the input. The measured output-input characteristics revealed major as well as minor hysteresis loops, while the peak percentage error due to hysteresis was in the order 16% in the output. At low excitation frequencies the classic play operator based Prandtl-Ishlinskii (PPI) model could effectively characterize the major and the minor loop hysteresis nonlinearities of the piezoceramic actuator.

- The initial loading curves could be employed to build an analytical stop operator-based Prandtl-Ishlinskii (SPI) model to obtain compensation of hysteresis nonlinearities described by the PPI model. The effectiveness of the SPI model in real-time was demonstrated through laboratory measurements on a piezoceramic micropositioning stage.

- Magnetostrictive actuators show strong input rate-dependent hysteresis nonlinearities under high rates of inputs, which are nearly symmetric at low magnitudes but asymmetric under moderate and high inputs. The hysteresis of these actuators is also strongly dependent upon the rate of input, as well, on the input magnetic bias and the mechanical loads.

- The area bounded by the hysteresis loop and the peak hysteresis percentage increased nonlinearly with the input amplitude but nearly linearly with the excitation frequency up to 250 H range. The variations in the magnetic field bias as well as input amplitude showed substantial effects on output asymmetry and saturation, peak-to-peak displacement response and the area bounded by the hysteresis loop.

- An inverse rate-dependent Prandtl-Ishlinskii model could be obtained under any rate-dependent threshold functions satisfying the dilation condition.

- The inverse rate-dependent Prandtl-Ishlinskii model could provide effective compensation of rate-dependent symmetric hysteresis under inputs over a wide frequency range. The simulation results revealed near perfect compensation of the hysteresis nonlinearities under different simple and complex harmonic inputs. The experiments conducted on the magnetostrictive actuator further showed that the inverse model could suppress the hysteresis errors effectively in a highly efficient manner.

- The proposed rate-dependent Prandtl-Ishlinskii model integrating a function of deadband operators could effectively describe the rate-dependent and asymmetric hysteresis properties of the magnetostrictive actuator together with output saturation over wide ranges of inputs. The peak error between the model displacement response and the measured data was observed in the order of 3.72 %, which occurred under the extreme excitation frequency of 200 Hz.

- The inverse of the integrated Prandtl-Ishlinskii model could be formulated using the inverses of the rate-dependent Prandtl-Ishlinskii model and the deadband function, which would serve as an effective feedforward compensator of rate-dependent and asymmetric hysteresis nonlinearities. The simulation results revealed that the proposed inverse model could mostly eliminate the hysteresis nonlinearities characterized by the integrated model over a wide range of excitation amplitudes and frequencies.

- The laboratory experiments with the magnetostrictive actuator confirmed that the integrated inverse model can effectively compensate for the rate-dependent and asymmetric hysteresis nonlinearities under inputs in the 1-250 Hz frequency range. The peak percent positioning error was reduced to nearly 3.7 % under the 6 A excitation over the 1-250 Hz frequency range, which was observed in the 18.2 to 49.1 % range in the absence of the compensator. The error in the

compensated output are likely attributed to errors associated with experimental characterization of the magnetostrictive actuator, and the prediction errors of the integrated model with limited number of rate-dependent play operators and deadband operators.

8.3 Recommendations for future work

The dissertation research represents the use of the rate-dependent Prandtl-Ishlinskii model and its analytical rate-dependent inverse model to describe and compensate for rate-dependent hysteresis nonlinearities of magnetostrictive actuators for micro-positioning applications. The proposed models provided very good predictions of the symmetric and asymmetric rate-dependent hysteresis effects, while the inverse models serve the essential basis for realizing compensation of hysteresis nonlinearities in real-time applications. Following are some suggested further studies that should be undertaken to enhance the hysteresis compensation in varying smart material actuators applications:

- From the laboratory measurements, it became evident that the actuator loading strongly affects the output-input characteristics of the actuator. It is thus essential to build alternate hysteresis and output-input models incorporating the actuator load effects.

- The inertia effect of the actuator rod may also contribute to the observed hysteresis effect. A hysteresis model should therefore incorporate the actuator dynamics so as to accurately describe the material hysteresis.

- The applicability of the proposed models and their inversions should be explored for compensation of butterfly shape hysteresis nonlinearities observed in magnetostrictive actuators in the absence of the permanent magnets bias.

- The magnetic bias effect may be incorporated within the density function to accurately describe output saturation.

- Further efforts are desirable in extending the proposed methodologies for modeling and compensating bias- and amplitude- dependent hysteresis nonlinearities of magnetostrictive actuators.

- Further efforts are also desirable for compensation of hysteresis nonlinearities of magnetostrictive actuators using the inverse generalized Prandtl-Ishlinskii model as a feedforward compensator.

- Further efforts are desirable for modeling hysteresis nonlinearities of magnetostrictive actuators subjected to mechanical loads with adaptive robust control methods.

REFERENCES

1 R. Smith, Smart material system: Model development, Society for Industrial and Applied Mathematics, 2005.

2 José L. Pons, Emerging Actuator Technologies: A Micromechatronic Approach, Wiley, New York, 2005.

3 A.G. Olabi, A. Grunwald, Design and application of magnetostrictive materials, Materials & Design, 29, pp. 469-483, 2008.

4 C. Body, G. Reyne, G. Meunier, E. Quandt, K. Seemann, Application of magnetostrictive thin films for microdevices, IEEE Transactions on Magnetics, vol. 33 , no. 2, Part 2, pp. 2163-2166, 1997.

5 C. Visone, Hysteresis modelling and compensation for smart sensors and actuators, Journal of Physics Conference Series, vol. 138, 012028, 2008.

6 M. Rakotondrabe, C. Clévy, and P. Lutz, Complete open loop control of hysteretic, creeped, and oscillating piezoelectric cantilevers, IEEE Transactions On Automation Science and Engineering, vol. 7, no. 3, pp. 440-451, 2010.

7 X. Tan and J. S. Baras, Modeling and control of hysteresis in magnetostrictive actuators, Automatica, vol. 40, pp. 1469-1480, 2004.

8 D. Davino, C. Natale, S. Pirozzi, and C. Visone, Phenomenological dynamic model of a magnetostrictive actuator, Physica B, vol. 343, pp. 112-116, 2004.

9 M. Al Janaideh, S. Rakheja, and C-Y. Su, Experimental characterization and modeling of rate-dependent hysteresis of a piezoceramic actuator, Mechatronics, vol. 19, pp. 656–70. 2009.

10 C. Natale, F. Velardi, and C. Visone, Identification and compensation of hysteresis for magnetostrictive actuators, Physica B, vol. 306, pp. 161–165, 2001.

11 F. Calkins, R. Smith, and A. Flatau, An energy-based hysteresis model for magnetostrictive transducers, IEEE Transactions on Magnetics, vol. 36, pp. 429-439, 2000.

12 K. Kuhnen, Modeling, identification and compensation of complex hysteretic nonlinearities - a modified Prandtl-Ishlinskii approach, European Journal of Control, vol. 9, pp. 407-418, 2003.

13 M. Stuebner, J. Atulasimha, and R. Smith, Quantification of hysteresis and nonlinear effects on the frequency response of ferroelectric and ferromagnetic materials, vol. 18, 2009.

14 M. Dapino and R. Smith, A coupled structural-magnetics strain and stress model for magnetostrictive transducers, IEEE Transactions of Magnetics, vol. 11, pp. 135-152, 2000.

15 S. Valadkhan, Nano-positioning control using magnetostrictive actuators, Waterloo University, Ph.D. dissertation, 2007.

16 R. V. Iyer and X. Tan, Control of hysteretic systems through inverse compensation, IEEE Control System Magazine, vol. 29, pp. 83-99, 2009.

17 J. Nealis and R. Smith, Model-based robust control design for magnetostrictive transducers operating in hysteretic and nonlinear regimes, IEEE Transactions on Control Systems Technology, vol. 15, pp. 22-39, 2007.

18 X. Tan, Control of smart actuators, Ph.D. dissertation, University of Maryland, 2004.

19 R. Smith and Z. Ounaies, A domain wall model for hysteresis in piezoelectric materials, Journal of Intelligent Material Systems and Structures, vol. 11, pp. 62–79, 2000.

20 L. Grcev, Z. Tasev, and L. Kocarev, Frequency dependent model of ferromagnetic hysteresis for time domain analysis of cable shields, IEEE International Symposium on Electromagnetic, pp. 586-591, 1997.

21 R. Smith, S. Seelecke, Z. Ounais, and J. Simth, A free energy model for hysteresis in ferroelectric materials, Journal of Intelligent Materials Systems and Structures, vol. 14, pp. 719-739, 2003.

22 I.D. Mayergoyz, Mathematical models of hysteresis, Elservier, 2003.

23 J. Macki, P. Nistri, and P. Zecca, Mathematical models for hysteresis, SIAM Review, vol. 35, pp. 94-123, 1993.

24 A. Visintin, Differential models of hysteresis, Spring-Verlag, Berlin, Hiedelberg, 1994.

25 P. Ge, Modeling and control of hysteresis in piezoceramic actuator, Ph.D. dissertation, University of Rhode Island, 1996.

26 M. Brokate and J. Sprekels, Hysteresis and phase transitions, Springer, New York, 1996.

27 G. Tao and P. Kokotovic, Adaptive control of plants with unknown hysteresis, IEEE Transactions on Automatic Control, vol. 40, 1995.

28 W. Galinaities, Two methods for modeling scalar hysteresis and their use in controlling actuators with hysteresis, Ph.D. dissertation, Blacksburg, Virginia, USA, 1999.

29 M. Krasnoselskii and A. Pokrovskii, Systems with hysteresis, 1983, Springer, Moscow, 1989.

30 I. Mayergoyz, Dynamic Preisach models of hysteresis, IEEE Transactions on Magnetics, vol. 24, pp. 2925-2927, 1988.

31 D. Jiles, Introduction to magnetism and magnetic materials, second edition, CRC Press, 1998.

32 D. Hughes and J. Wen, Preisach modelling of piezoceramic and shape memory alloy hysteresis, Smart Materials and Structures, vol. 6, pp. 287–300, 1997.

33 P. Ge and M. Jouaneh, Modeling hysteresis in piezoceramic actuators, Precision Engineering, vol. 17, pp. 211-221, 1997.

34 R. Gorbet, D. Wang, and K. Morris, Preisach model identification of a two wire SMA actuator, Proc. IEEE Int. Conf. on Robotics and Automation 3, pp. 2161-2168, Leuven, May, 1998.

35 R. Gorbet, Control of hysteresis systems with Preisach representations, Ph.D. dissertation, University of Waterloo, Canada, 1997.

36 K. Ahn and N. Khan, Modeling and control of shape memory alloy actuators using Preisach model, genetic algorithm and fuzzy logic, Mechatronics, vol. 18, pp. 141-152, 2008.

37 A. Cavallo, D. Davino, G. Maria, and C. Visone., Hysteresis compensation of smart actuators under variable stress conditions, Physica B, vol. 403, pp. 261-265, 2008.

38 A. Adly, I. Mayergoyz, and A. Bergqvist, Preisach modelling of magnetostrictive hysteresis, Journal of Applied Physics, vol. 69, pp. 5777-5779, 1991.

39 H. Banks, A. Kurdilaand, and G. Webb, Identification of hysteretic control influence operators representing smart actuators, Mathematical Problems in Engineering, vol. 3, pp. 287-328, 1997.

40 H. Janocha, Adaptronics and smart structures, Springer-Verlag Berlin, 1999.

41 H. Janocha and K. Kuhnen, Real-time compensation of hysteresis and creep in piezoelectric actuators, Sensors and Actuators A: Physical, vol. 79, pp. 83-89, 2000.

42 P. Krejci and K. Kuhnen, Inverse control of systems with hysteresis and creep, IEE Proceedings Control Theory Application, vol. 148, pp. 185-192, 2001.

43 N. Nise, Control systems engineering, fifth edition, Wiley, 2007.

44 K. Kuhnen and P. Krejci, Compensation of complex hysteresis and creep effects in piezoelectrically actuated systems-A new Preisach modeling approach, IEEE Transactions on Automatic Control, vol. 54, pp. 537-550, 2009.

45 M. Al Janaideh, S. Rakheja, and C.-Y. Su, A generalized Prandtl-Ishlinskii model for characterizing the hysteresis and saturation nonlinearities of smart actuators, Smart Materials and Structures, vol. 18, no. 4, 045001, 2009.

46 W. Ang, F. Garmon, P. Khosla, and C. Riviere, Modeling rate-dependent hysteresis in piezoelectric actuators, Proc. Int. Conf. of Intelligent Robots and Systems, pp.1975-1980, Las Vegas, 2003.

47 R. Ben Mrad and H. Hu, A model for voltage-to-displacement dynamics in piezoceramic actuators subject to dynamic-voltage excitations, IEEE Transactions on Mechatronics, vol. 7, pp. 479-489, 2002.

48 F. Ikhouane and J. Rodellar, Systems with hysteresis: Analysis, identification and control using the Bouc-Wen model, Wiley-Interscience, 2007.

49 M. Rakotondrabe, Bouc-Wen modeling and inverse multiplicative structure to compensate hysteresis nonlinearity in piezoelectric actuators, IEEE Transactions on Automation Science and Engineering, vol. 8, no. 2, 428-431, 2011.

50 C. Lin and S. Yang, Precise positioning of piezo-actuated stages using hysteresis-observer based control, Mechatronics, vol. 16, pp. 417–426, 2006.

51 B. Spencer, S. Dyke, M. Sain, and J. Carlson, Phenomenological model of a magnetorheological damper, ASCE Journal of Engineering Mechanics, vol. 123, no. 3, pp. 230-283, 1997.

52 B. Coleman and M. Hodgdon, A constitutive relation for rate-independent hysteresis in ferromagnetically soft materials, International Journal of Engineering Science, vol. 24, pp. 897-919, 1986.

53 X. Chen and T. Hisayama, Adaptive sliding-mode position control for piezo-actuated stage, IEEE Transactions on Industrial Electronics, vol. 55, pp. 3927-3934, 2008.

54 H. Liaw, B. Shirinzadeh and J. Smith, Sliding-mode enhanced adaptive motion tracking control of piezoelectric actuation systems for micro/nano manipulation, IEEE Transactions on Control Systems Technology, vol. 16, pp. 826-833, 2008.

55 C. Y. Su, Q. Wang, X. Chen, and S. Rakheja, Adaptive variable structure control of a class of nonlinear systems with unknown Prandtl-Ishlinskii hysteresis, IEEE Transactions on Automatic Control, vol. 50, pp. 2069- 2074, 2005.

56 R. C. Smith, Inverse compensation for hysteresis in magnetostrictive transducers, CRSC, North Carolina State Univ., Raleigh, NC, Tech. Rep. CRSC-TR98-36, 1998.

57 P. Ge and M. Jouaneh, Tracking control of a piezoceramic actuator, IEEE Transaction on Control Systems Technology, vol. 4, pp. 209-216, 1996.

58 J. Schäfer and H. Janocha, Compensation of hysteresis in solid-state actuators, Sensors Actuators Physical: A, vol. 49, pp. 97-102, 1995.

59 O. Aljanaideh, S. Rakheja, and Chun-Yi Su, Compensation of a piezoceramic actuator hysteresis nonlinearities using the stop operator-based Prandtl-Ishlinskii model, Int. Conf. of Modelling Identification and Control (ICMIC), pp. 364-369, Okayama, 2010.

60 M. Al Janaideh, C-Yi. Su, and S. Rakheja, An analytical generalized Prandtl-Ishlinskii model inversion for hysteresis compensation in micro-positioning control, IEEE/ASME Transactions on Mechatronics, 2010.

61 B. Drinčić, X. Tan, D.S. Bernstein, Why are some hysteresis loops shaped like a butterfly?, Automatica, vol. 47 pp. 2658-2664, 2011.

62 D. Davino, C. Natale, S. Pirozzi, C. Visone, Phenomenological dynamic model of a magnetostrictive actuator, Physica B, vol. 343, pp. 112-116, 2004.

63 M. Al Janaideh and P. Krejci, An inversion formula for a Prandtl-Ishlinskii operator with time-dependent thresholds, Physica B, vol. 406, no. 8, pp. 1528-1532, 2011

64 R. Smith, Modeling techniques for magnetostrictive actuators, Proceedings of the SPIE, Smart Structures and Materials: Smart Structures and Integrated Systems, 1997.

65 R. Venkataraman, Modeling and Adaptive Control of Magnetostrictive Actuators, PhD dissertation, University of Maryland, 1999.

66 D. Davino, C. Natale, S. Pirozzi, C. Visone, Rate-dependent losses modeling for magnetostrictive actuators, Journal of Magnetism and Magnetic Materials, vols. 272–276, pp. 1781-1782, 2004.

67 S. S. Rao, Mechanical Vibrations, Prentice Hall, 2010

68 Shen, J-C., Jywe, W-Y., Chiang, H-K. and Shu, Y-L. 'Mechatronics of electrostatic microactuators for computer disk drive dual-stage servo systems'Precision Engineering, vol. 32, no. 2, pp. 71–87, 2008.

69 Devasia, S., Eleftheriou, E. and Moheimani, A survey of control Issues in nanopositioning IEEE Transactions on Magnetics, vol. 15, no. 5, pp. 802-823 (2007).

70 Leang, K., Zou, Q. and Devasia, S., Feedforward controlof piezoactuators in atomic force microscope systems: inversion-based compensation for dynamics and hysteresis, IEEE control magazine, vol. 19, no. 1, pp. 70-82, 2009.

71 A. Esbrook, M. Guibord, X. Tan, H. K. Khalil, Control of systems with hysteresis via servocompensation and its application to nanopositioning, American Control Conference, June 30 2010-July, 2010.

72 R.Granger, G. Washington, S-K Kwak, Modeling and control of a singly curved active aperture antenna using curved piezoceramic actuators, vol. 11, no. 17, pp. 225-233, 2000.

73 H. Hu and R. B. Ben Mrad, On the classic Preisach model Mechatronics, vol. 13, pp 85-94, 2003

74 K. Kuhnen, H. Janocha Adaptive inverse control of piezoelectric actuators with hysteresis operators, European control conference, pp. 6531-6536, 1999.

75 R. Greenough, M. Schulze, A. Jenner, and A. Wilkinson, Actuation with Terfenol-D, IEEE Transactions on Magnetics, vol. 27, pp. 5346 - 5348, 1991.

76 Richard M. Bozorth, Ferromagnetism, Wiley-IEEE Press, 1993.

77 Karunanidhi, M. Singaperumal, Design, analysis and simulation of magnetostrictive actuator and its application to high dynamic servo valve, Sensors and Actuators A: Physical, vol. 157, pp. 185-197, 2010.

78 M. Al Janaideh, S. Rakheja, S. Chun-Yi, An analytical generalized Prandtl-Ishlinskii model inversion for hysteresis compensation in micropositioning control, Mechatronics, IEEE/ASME Transactions on, vol. 16 pp. 734-744, 2011.

79 M.J. Dapino, R.C. Smith, A.B. Flatau, Structural magnetic strain model for magnetostrictive transducers, Magnetics, IEEE Transactions on, vol. 36, pp. 545-556, 2000.

80 D. Davino, A. Giustiniani, C. Visone, The piezo-magnetic parameters of Terfenol-D: An experimental viewpoint, Physica B: Condensed Matter, vol. 407, pp. 1427-1432, 2012.

81 W. Oates, P. Evans, R. Smith, M. Dapino, Experimental implementation of a hybrid nonlinear control design for magnetostrictive actuators, Journal of Dynamic Systems, Measurement, and Control, vol. 131, no. 4 041004, 2009.

82 D.C. Jiles, Modelling the effects of eddy current losses on frequency dependent hysteresis in electrically conducting media, Magnetics, IEEE Transactions on, vol. 30, pp. 4326-4328, 1994.

83 D. Jiles and D. Atherton, Theory of ferromagnetic hysteresis, Journal of Magnetism and Magnetic Materials, vol. 61, pp. 48–60, 1986.

84 C. Natale, F. Velardi, C. Visone, Identification and compensation of Preisach hysteresis models for magnetostrictive actuators, Physica B: Condensed Matter, vol. 306, pp. 161-165, 2001.

85 M. Al Janaideh, C-Y. Su, and S. Rakheja, Development of the rate-dependent Prandtl-Ishlinskii model for smart actuators, Smart Materials and Structures, vol. 17, no. 3, 035026, 2008.

86 M.A. Janaideh, S. Rakheja, S. Chun-Yi, A generalized rate dependent play operator for characterizing asymmetric and symmetric hysteresis nonlinearities, in: American Control Conference, pp. 1911-1916, 2008.

87 M.A. Janaideh, S. Rakheja, Chun-Yi Su, Modelling rate-dependent symmetric and asymmetric hysteresis loops of smart actuators, International Journal of advanced Mechatronic Systems, vol. 1, pp. 32-34, 2008.

88 L. Riccardi, D. Naso, B. Turchiano, H. Janocha, Adaptive Control of Positioning Systems With Hysteresis Based on Magnetic Shape Memory Alloys, Control Systems Technology, IEEE Transactions on, vol. 21, no. 6, pp. 2011-2023, 2013.

89 C. Visone, M. Sjöström, Exact invertible hysteresis models based on play operators, Physica B: Condensed Matter, vol. 343, pp. 148–152, 2004

90 William S. Oates, R. Zrostlik, S. Eichhorn, R. Smith, A Non-linear optimal control design using narrowband perturbation feedback for magnetostrictive actuators, Journal of Intelligent Material Systems and Structures, vol. 21, pp. 1681-1693, 2010.

91 Chun-Yi Su, Q. Wang, X. Chen, and S. Rakheja, Adaptive variable structure control for a class of nonlinear systems with unknown Prandtl-Ishlinskii Hysteresis, IEEE Transactions on Automatic Control, vol. 50, no. 12, pp. 2069-2074, 2005.

92 P. Nguyen and S. Choi, Compensator design for hysteresis of a stacked PZT actuator using a congruency-based hysteresis model, Smart Materials and Structures, vol. 21, 2012.

93 B. Kim, G. Washington, and H. Yoon, Hysteresis-reduced dynamic displacement control of piezoceramic stack actuators using model predictive sliding mode control, Smart Materials and Structures, vol. 21, 2012.

94 O. Aljanaideh, A Stop Operator-Based Prandtl-Ishlinskii Model For Compensation Of Smart Actuator Hysteresis Effects, Master's Dissertation, Concordia University, 2009

95 O. Bottauscio, P.E Roccato, M. Zucca, Modeling the dynamic behavior of magnetostrictive actuators," IEEE Transactions on Magnetics, vol. 46, no. 8, pp. 3022-3028, 2010

96 F. Braghin, S. Cinquemani, and F. Resta, A model of magnetostrictive actuators for active vibration control, Sensors and Actuators A: Physical, vol. 165, pp. 342-350, 2011.

97 S. Moona, C. Limb, B. Kima, and Y. Parkc, Structural vibration control using linear magnetostrictive actuators, Journal of Sound and Vibration, vol. 302, pp. 875-891, 2007.

98 K. Kuhnen and H. Janocha, Complex hysteresis modeling of a broad class of hysteretic nonlinearities, Proc. of the 8th Int. Conf. on New Actuators, Bremen, pp. 688-691, June 2002.

99 D. Davino, A. Giustiniani, V. Vacca, and C.Visone, Embedded Hysteresis Compensation and Control on a Magnetostrictive Actuator, IEEE Transactions on Magnetics, vol. 42, pp. 3443- 3445, 2006.

100 B. Kim, G. Washington, and H. Yoon, Hysteresis-reduced dynamic displacement control of piezoceramic stack actuators using model predictive sliding mode control, Smart Materials and Structures, vol. 21, 2012.

101 D. Davino, C. Natale, S. Pirozzi and C. Visone, A fast compensation algorithm for real-time control of magnetostrictive actuators, Journal of Magnetism and Magnetic Materials, vol. 290-291, pp. 1351–1354, part 2, 2005.

102 W. Ang, P. Khosla, and C. Riviere, Feedforward controller with inverse rate-dependent model for piezoelectric actuators in trajectory-tracking applications, IEEE/ASME Trans. Mechatronics, vol. 12, no. 2, pp. 134-142, 2007.

103 Y. Li and Q. Xu, A novel piezo-actuated XY stage with parallel, decoupled and stacked flexure structure for micro/nano Positioning, IEEE Trans. Ind. Electron., vol. 58, no. 8, pp. 3601–3615, 2011

104 O. Aljanaideh, S. Rakheja, and C-Y. Su, Experimental verification and modeling rate-dependent hysteresis nonlinearities of a magnetostrictive Actuator, Proc. of the 9th Int. Symp. on Hysteresis Modeling and Micro-magnetism, Taormina, May 2013.